The role of MEGF10 in skeletal muscle myopathy.

Thesis by

Ruth Elizabeth Hughes

Submitted in accordance with the requirements for the degree of Doctor of Philosophy

The University of Leeds
Faculty of Biological Sciences
School of Molecular & Cellular Biology

October 2016

The candidate confirms that the work submitted is his/her own and that appropriate credit has been given where reference has been made to the work of others.

Acknowledgements

I am indebted to the Medical Research Council for their funding, and the Faculty of Biological Sciences for making my PhD possible.

I would like to thank my supervisors Michelle Peckham and Colin Johnson for their patience, tireless enthusiasm and sage advice throughout the ups and downs of the project.

I am grateful to Sara Cruz Migoni from the Borycki lab (Sheffield) for teaching me the single fibre isolation technique and Stuart Egginton and Roger Kissane for their help in setting up the hyperplasia model. I am thankful to Clare Logan and Gabrielle Wheway for their help with setting up and analysing the RNAseq data. Protein identification by mass spectrometry was performed by James Ault in the University of Leeds Mass Spectrometry Facility. Also thanks to the University of Leeds Bio-imaging facility for use of the DeltaVision and LSM880 microscopes.

I am indebted to the past and present members of the Johnson and Peckham labs for their camaraderie and invaluable support. In particular Adriana, Alexa, Alistair, Brendan, Charlie, Fran, Glenn, Kasia, Marcin, Marta, Matt, it's been an adventure.

I am so grateful to my friends, my second family, here in Leeds for helping me to keep work and life in perspective. Finally, the support and encouragement of my family; Mum, Dad, David (Dr Geezer-Features), Rachael & Evangeline has been amazing.

Abstract

Mutations in the transmembrane protein MEGF10 (multiple epidermal growth factor-like protein 10) cause early-onset myopathy, areflexia, respiratory distress and dysphagia (EMARDD), an autosomal recessive congenital myopathy, characterized by reduced muscle fibre size. MEGF10 is reportedly expressed in satellite cells, playing a role in regulating cell proliferation and differentiation. The pattern of expression and the function of MEGF10 have not been clearly described.

Cultured myoblasts, isolated single fibres and a muscle hyperplasia model were used to investigate changes in MEGF10 expression. Western blotting, immunofluorescence and RNAseq showed that MEGF10 was expressed at low levels in cultured myoblasts, suggesting that these cells are a poor model for studying endogenous MEGF10. Overexpression of GFP-tagged wildtype MEGF10 and MEGF10 containing pathogenic mutations decreased myoblasts cell motility and fusion. Isolated single fibres showed the presence of quiescent ($Pax7^+$), committed and activated ($MyoD^+$ or $myogenin^+$) satellite cells after 2 - 4 days in culture. However, these cells did not consistently express MEGF10. A muscle hyperplasia model showed no MEGF10 expression in $CD34^+/Pax7^+$ or $MyoD^+$ positive satellite cells, but $MEGF10^+/CD34^-$ cells were present on these fibres. Finally, the expressed and purified extracellular domain (ECD) of MEGF10 was heavily post-translationally modified and facilitated myoblast attachment to a non-adherent surface. Pathogenic mutations in the ECD did not have a significant effect on myoblast fusion, whilst the wildtype ECD inhibited fusion.

In conclusion, the choice of skeletal muscle model system is important in obtaining meaningful results. The discovery of MEGF10 expression in, as yet, unidentified $CD34^-$ cells on isolated fibres requires further study. MEGF10 is likely to respond to differing cues within the complex muscle environment to regulate myogenesis through cellular changes affecting differentiation and motility. Whilst EMARDD is a rare condition, insights into MEGF10 function may give insight into mechanisms of pathogenesis in a range of skeletal muscle diseases.

Table of Contents

List of Tables

List of Figures

List of Abbreviations

AA	Amino Acid
APS	Ammonium persulfate
ATP	Adenosine-5'-triphosphate
BCA	Bicinchoninic Acid
bp	Base pair
BSA	Bovine Serum Albumin
C-	Carboxyl
CAM	Carbamidomethylation
cDNA	Complimentary DNA
CEE	Chick Embryo Extract
Da	Daltons
kDa	10^3 Daltons
DAPI	4',6'- diamidino-2-phenylindole
DSHB	Developmental Studies Hybridoma Bank
°C	Degrees Celsius
DMEM	Dulbecco's Modified Eagles Medium
DNA	Deoxyribonucleic Acid
E	Elution
ECD	Extracellular Domain
EDL	Extensor Digitorum Longus
EDTA	Ethylenediaminetetraacetic acid

EGF	Epidermal Growth Factor
eGFP	Enhanced green fluorescent protein
EMARDD	Early-onset Myopathy, Areflexia, Respiratory Distress and Dysphagia
EMI	Emilin
ER	Endoplasmic Reticulum
Ex.	Excitation
Em.	Emission
FBS	Foetal Bovine Serum
FITC	Fluorescein Isothiocyanate
FPKM	Fragments Per Kilobase of transcript per Million mapped reads
FT	Flow Through
Fwd.	Forward
X g	Acceleration of gravity
Gal	Galactose
GalNAc	N-acetylgalactosamine
Gas.	gastrocnemius
GFP	Green Fluorescent Protein
γ-IFN	Gamma Interferon
Glc	Glucose
GlcNAc	N-acetylglucosamine
GTP	Guanosine-5'-triphosphate
HA Tag	Human influenza hemagglutinin Tag

HEPES	4-(2-Hydroxyethyl)piperazine-1-ethanesulfonic acid
hr	Hour(s)
HRP	Horseradish Peroxidase
H/S	Horse Serum
IF	Immunofluorescence
Ig	Immunoglobulin
Kb	Kilobase
LDL	Low-density lipoprotein
M	Molar
Man	Mannose
Max.	Maximum
mAmp	10^{-3} ampere
ml	10^{-3} litre(s)
mm	10^{-3} meter(s)
mM	10^{-3} molar
µl	10^{-6} litre(s)
µm	10^{-6} meter(s)
µM	10^{-6} molar
MEGF	Multiple Epidermal Growth Factor-like Domains Protein
min	Minute(s)
MIM	Mendelian Inheritance in Man
MOI	Multiplicity of Infection

mRNA	Messenger RNA
Mw	molecular weight
MWCO	Molecular weight cut off
N-	Amino-
nm	10^{-9} meter(s)
nM	10^{-9} molar
Pax	Paired box
PBS	Phosphate buffered saline
PCR	Polymerase chain reaction
PFA	Paraformaldehyde
pH	Potential hydrogen. Decimal logarithm of hydrogen ion.
PS	Phosphatidylserine
P/S	Penicillin-Streptomycin
PTM	Post-Translational Modification
Rev.	Reverse
RI	Refractive Index
RNA	Ribonucleic acid
RNAseq	RNA sequencing
rpm	Revolutions per minute
rRNA	ribosomal ribonucleic acid
RTK	Receptor tyrosine kinase
S.D.	Standard deviation

SDS-PAGE	Sodium Dodecyl Sulphate- Polyacrylamide Gel Electrophoresis
sec	Second(s)
S.E.M	Standard error of the mean
SH2	Src Homology 2
siRNA	Small interfering RNA
SOC	Super Optimal broth with Catabolite repression
Sol	Soleus
TA	Tibialis Anterior
TEMED	N,N,N',N'-tetramethylethane-1,2-diamine
TF	TF
Tm	Melting temperature
TM	Transmembrane
TRITC	Tetramethylrhodamine B isothiocyanate
TTBS	Tris Tween Buffered Saline
U	Unit
UV	Ultraviolet
Vol	Volume
v/v	% volume per volume
W	Wash
WB	Western blot
w/v	% weight per volume

1 Introduction.

1.1 Early-onset Myopathy Areflexia Respiratory Distress and Dysphagia (EMARDD)

Muscular dystrophies and myopathies are a heterogeneous group of inherited conditions, which have some common clinical features and symptoms. Current care for these conditions predominantly involves monitoring and managing symptoms, and therefore a better understanding of these diverse conditions may enable an effective therapy rather than palliative management of these conditions to be developed. Myopathies and dystrophies differ in their underlying cause, with myopathies primarily being caused by mutations causing defects in the contractile apparatus of muscle as seen in muscle biopsies. Conversely, muscular dystrophies tend to be caused by defective proteins in the muscle membrane or that support the muscle and dystrophies are typically characterised by pathological muscle degeneration and regeneration (Cardamone et al., 2008).

Whilst there are more common and well-characterised muscular dystrophies, such as Duchenne and Becker muscular dystrophy, there are also a number of rare muscle wasting disorders, which have not been well described. One of these rare and under-characterized disorders is early onset myopathy, areflexia, respiratory distress and dysphagia (EMARDD), an autosomal recessive congenital myopathy (MIM number 614399), caused by compound heterozygous or homozygous mutations in the gene encoding multiple epidermal growth factor-like protein 10 (MEGF10) (MIM number 612453) on chromosome 5q23. A group of patients were identified that presented with cyanosis indicating early onset respiratory distress caused by reduced function in the diaphragm muscle, as well as areflexia and dysphagia. The severe myopathy EMARDD was named after its clinical features: early onset myopathy, areflexia, respiratory distress and dysphagia (Figure 1. A.). The absence of neurological reflexes and the difficulty in swallowing differentiates EMARDD from some other disorders such as spinal muscular

atrophy with respiratory distress (SMARD). SMARD (MIM number 604320) is also an autosomal recessive disorder but is characterised by neurogenic muscular degeneration caused by loss of α-motor neurons in the spinal cord. In contrast, EMARDD patients have normal nerve conduction speeds in both sensory and motor neurons suggesting that the muscle weakness is not due to defective transmission of motor nerve impulses. Muscle biopsies from EMARDD patients have a reduced muscle fibre diameter and fewer nuclei per myofibre compared to a control healthy individual, suggesting disruption in the assembly or maintenance of the myofibres (Figure 1. B.) (Logan et al., 2011).

Like other muscular disorders, EMARDD appears to be within a spectrum of conditions with some patients only surviving into early infancy (Logan et al., 2011), whilst other individuals with EMARDD have been reported at age 12, suggesting a milder phenotype is present (Meilleur et al., 2012). Mutations in MEGF10 have also been associated with muscle myopathy with a multi-minicore disease phenotype (Boyden et al., 2012a; Jungbluth, 2007). More recently, mutations in MEGF10 have been associated with the congenital myopathy multi-minicore disease (MIM number 255320), in which patients had the additional features of scoliosis, distal joint hyperlaxity and adult-onset respiratory insufficiency, as opposed to the infantile-onset described for EMARDD (Liewluck et al., 2016). This further implies that mutations in MEGF10 can produce a number of conditions with differing symptoms and presentations.

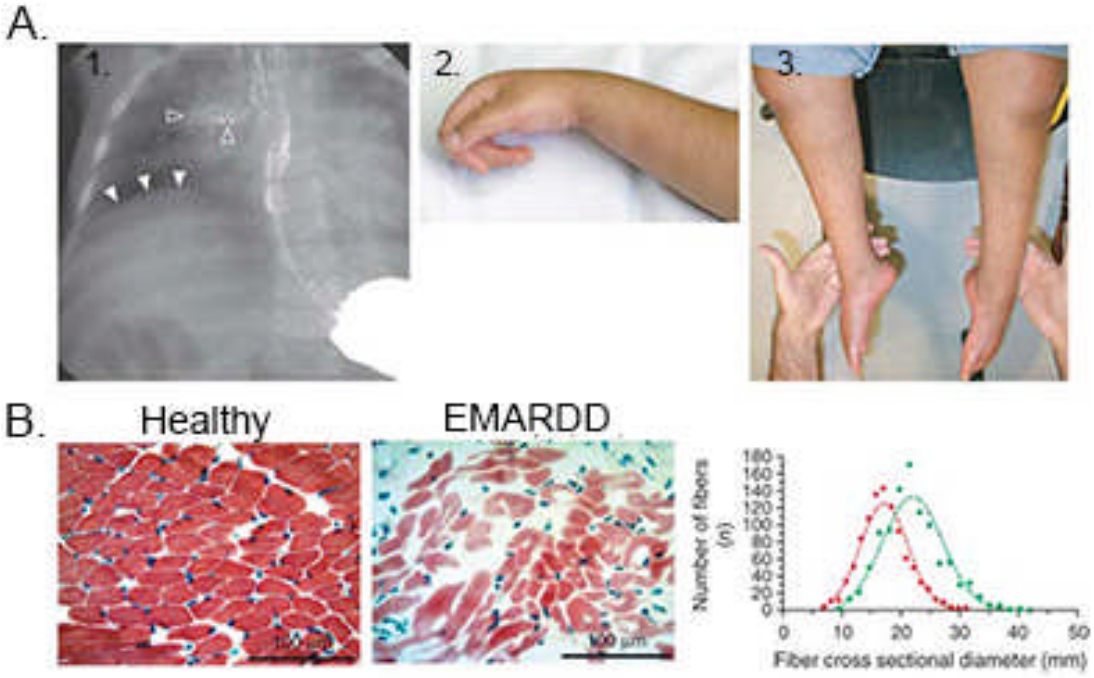

Figure 1. Clinical Presentation and muscle pathology of EMARDD.

A. Aspiration in the lung (1) (arrowheads) indicating dysphagia and distal weakness shown in the hand (2) and by thinning in the thighs (3) in EMARDD patients. **B.** Haematoxylin and eosin stained transverse sections of the deltoid muscle from healthy and EMARDD patients. The cross-sectional diameter of the fibres was measured in control (green) and EMARDD patients (red), with fibre diameter significantly reduced in EMARDD patients. Adapted from (Logan et al., 2011).

1.2 Multiple epidermal growth factor-like domains protein 10 (MEGF10)

1.2.1 **Disease mutations.**

Mutations in the gene encoding the type-1 transmembrane (TM) protein MEGF10 were identified in patients with EMARDD (Logan et al., 2011). Five mutations were initially identified within the *MEGF10 gene* for this cohort of EMARDD patients. Most of these mutations led to the introduction of a premature stop codon into the DNA sequence, including p.P442'HfsX9, p.W520X, p.C767X, p.Y1048X, of MEGF10 causing predicted nonsense mediated decay of the transcript and loss of protein expression (Figure 2. red). By contrast, the p.C774R mutation in the 16th epidermal growth factor (EGF)-like domain in MEGF10, through conversion of a cysteine to an arginine, may cause disruption to the cysteine bond in the EGF-like domain affecting interactions within the extracellular domain (ECD) of MEGF10 (Logan et al., 2011) (Figure 2. pink). Other cysteine mutations subsequently identified as being associated with minicore myopathy, p.C326R and p.C611W (Figure 2. green), may also cause disruption to the EGF-like domains and destabilization to the ECD of MEGF10 (Boyden et al., 2012a). Mutations C326R and C774R in MEGF10 associated with skeletal muscle myopathy, were shown to reduce the tyrosine phosphorylation of MEGF10. The tyrosine phosphorylation may disrupt signaling by MEGF10 that regulates myoblast proliferation (Mitsuhashi et al., 2013).

Subsequent identification of additional patients with EMARDD led to the identification, by SNP array analysis and exome sequencing, of a novel mutation comprising a deletion of exon 7 in MEGF10 (Meilleur et al., 2012; Pierson et al., 2013) (Figure 2. blue). Mutations in *MEGF10* have also been associated with a recessive congenital myopathy with minicores characterised by distal muscle weakness, scoliosis and either infantile- (Boyden et al., 2012a) or adult-onset (Liewluck et al., 2016) respiratory failure. Mutations are shown in Figure 2. Knockdown of *megf10* in zebrafish demonstrates the pathogenicity of some of these mutations (Boyden et al.,

2012a), however this study did not investigate the effect of these mutations in a mammalian muscle system.

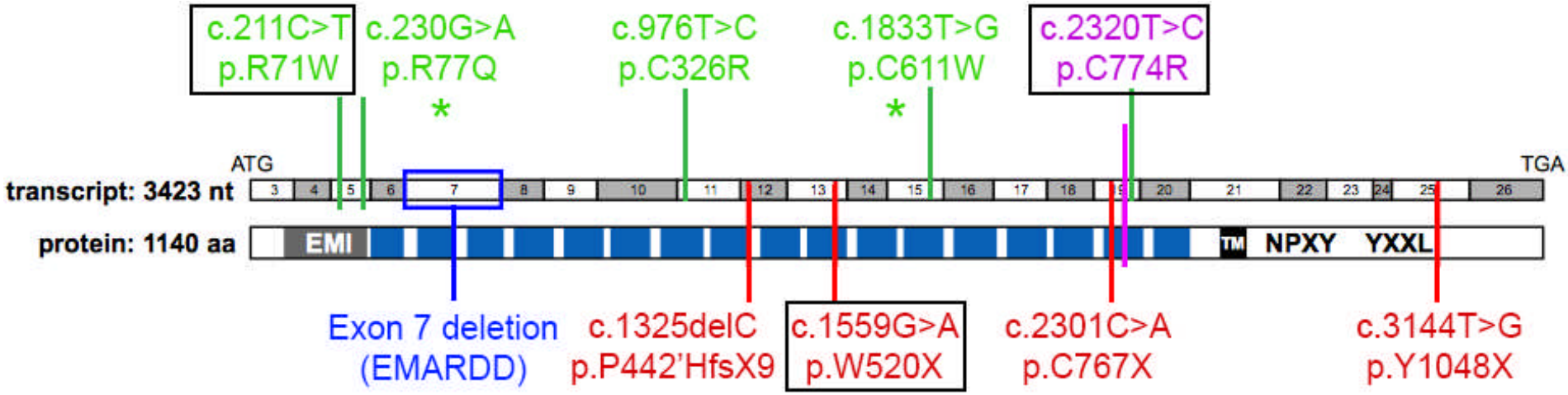

Figure 2. Pathogenic mutations in *MEGF10*.

The genomic sequence of *MEGF10* with non-coding exons is shown in grey. The protein sequence of MEGF10 showing conserved domains including EMI and EGF-like domains (blue boxes), a TM domain and two intracellular motifs. Mutations introducing a premature stop codon are shown in red, and the missense mutation identified in EMARDD patients shown in pink (Logan et al., 2011). The exon 7 deletion associated with EMARDD is shown in blue (Meilleur et al., 2012). Mutations causing minicore myopathy are shown in green (Boyden et al., 2012a), and those highlighted with an asterisk indicate mutations causing minicore myopathy with adult-onset respiratory insufficiency (Liewluck et al., 2016). Mutations highlighted with a box were used in this study.

Figure adapted from Logan et al., 2011.

1.2.2 **The MEGF Family**

MEGF10 is part of the 12-member MEGF family of TM proteins (MEGF1-12), characterized by repeating EGF-like domains in the ECD. Many of these contain an N-terminal EMI domain and typically these proteins play a role in development. Members of the MEGF family were identified by motif-trap screening, including MEGF1 composed of a large ECD and commonly expressed in cerebellum, MEGF2 and MEGF3 with seven times TM domains, MEGF4 and 5 homologues of the *Drosophila* Slit protein and MEGF7 an uncharacterized low-density lipoprotein (LDL) receptor-like protein (Nakayama et al., 2002). Novel proteins MEGF6, and MEGF8 - 12 were also identified and were subsequently studied. MEGF6 has an EMI domain and multiple EGF domains like MEGF10, but the predicted sequence lacks a TM domain. It may have a role in extracellular matrix elastic fibre assembly (Penner et al., 2002). MEGF8, contains multiple EGF domains, lacks an EMI domain, but contains several CUB (Complement C1r/C1s, Uegf, Bmp1; (Blanc et al., 2007) and PSI (Plexin, Semaphorin and Integrin; domains (Basile et al., 2007; Love et al., 2003; Xiao et al., 2004). Both of these domains contain conserved cysteine residues forming disulphide bonds and may have a role in mediating protein - protein interactions. Mutations in MEGF8 cause a subtype of Carpenter syndrome, characterised by defective left – right patterning during development, possibly through disruption of Hedgehog signalling (Twigg et al., 2012).

The shorter TM protein MEGF9 (Figure 3.) is post-translationally modified and its expression in the nervous system and has been shown to be regulated during development (Brandt-Bohne et al., 2007). MEGF11 is very similar to MEGF10 in terms of size and domain structure, and has been shown to interact with MEGF10 (Kay et al., 2012). MEGF12, also known as JEDI or Platelet endothelial aggregation receptor 1 (PEAR1), is primarily expressed in platelet cells and has a signaling role upon contact between platelet cells (Nanda et al., 2005). In *Drosophila* the genes encoding MEGF10, MEGF11 and MEGF12 in mammals have a single orthologue, Draper. Silencing of the *Draper* gene in flies cause a muscle myopathy similar to that seen in human EMARDD, as well as vacuoles to form in the

brain (Draper et al., 2014). In summary, the MEGF family of proteins share similar domain structures and appear to have a broad range of functions in tissue development and disease. However, MEGF10, 11 and 12 appear to be most closely related and may have related functions. Sequence alignment of MEGF10, MEGF11 and MEGF12 proteins showed high sequence similarity particularly within the ECDs whilst, the intracellular domains are more divergent there is some similarity in sequence surrounding conserved tyrosine residues. This led to the conclusion that these three proteins are part of a family of TM multiple-EGF like domain proteins, which differ from other EGF-like repeat proteins such as Serrate or Jagged since the MEGF proteins lack the characteristic cysteine-rich region before the TM region of Serrate/Jagged proteins (Krivtsov et al., 2007). Predicted representations of the domain structure for each of the 12 MEGF family members are depicted in Figure 3.

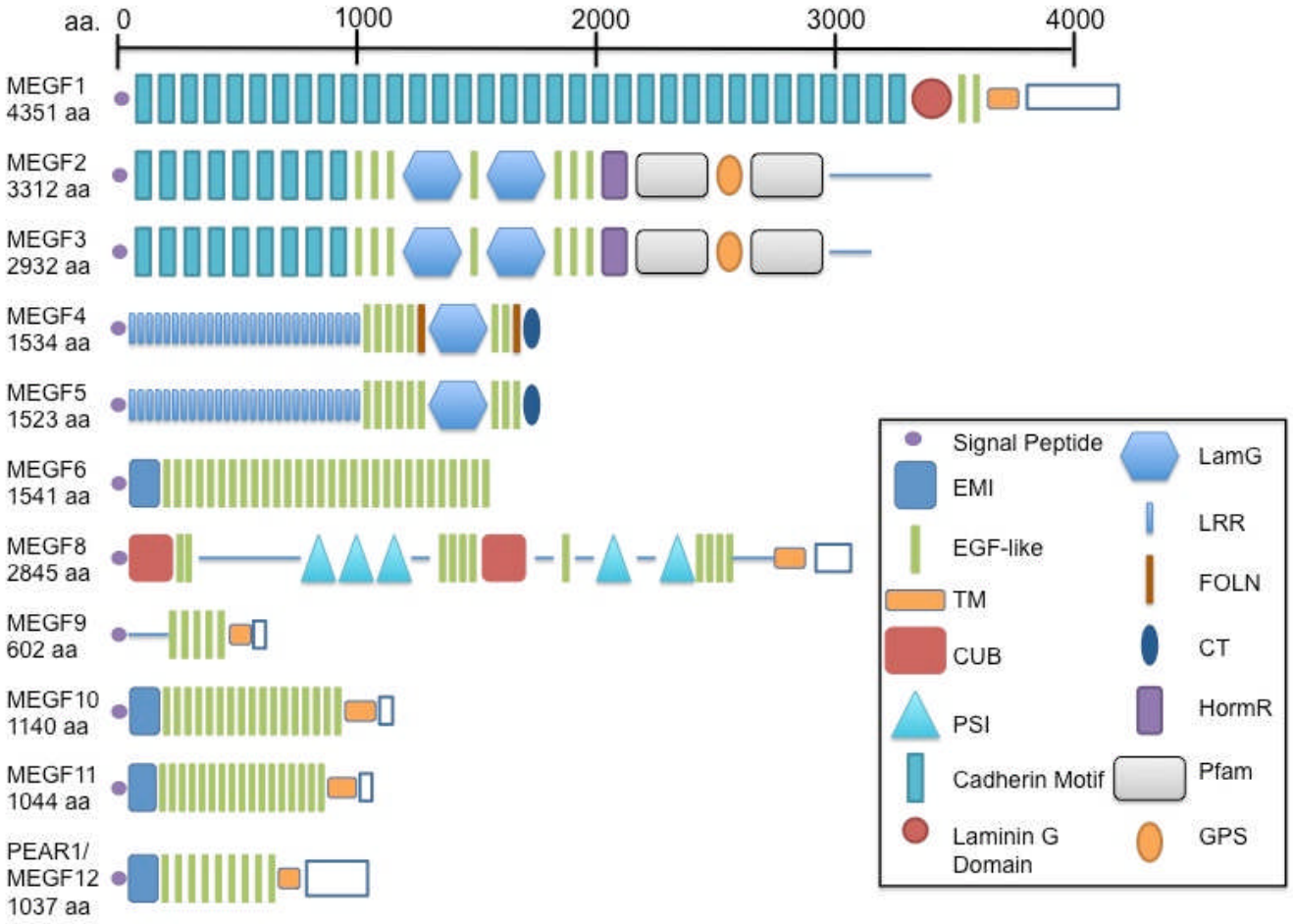

Figure 3. The protein domain structure of the MEGF family.

Comparison of the predicted domain arrangement of members of MEGF family. Domains include the EMI, EGF, TM, CUB, PSI, laminin G domain (LamG), Leucine Rich Repeat (LRR), Follistatin N-terminal domain (FOLN), C-terminal cysteine knot-like domain (CT), Hormone Receptor domain (Horm R), Protein families (Pfam), G-protein coupled receptor proteolytic site domain (GPS). Domains were predicted using Simple Modular Architecture Research Tool (SMART) (Letunic et al., 2015; Schultz et al., 1998) and InterPro (Mitchell et al., 2015).

1.3 The Structure of MEGF10

MEGF10 is a type-1 single-pass TM protein, composed of a signal peptide to mediate transportation to and orientation in the plasma membrane, an EMI domain and 17 EGF-like domains in the extracellular region of the protein (Doliana et al., 2000; Kay et al., 2012). The intracellular region contains both phosphotyrosine binding (PTB) and Src homology-2 (SH2) binding sites. Both of these domains indicate a role in receptor tyrosine kinase (RTK) signalling pathways, as discussed below. The full MEGF10 sequence and each key region are depicted in Figure 4.

1.3.1 **EMI domain**

The EMI domain is present at the N-terminus of the protein once the signal peptide has been cleaved and protein correctly inserted into the plasma membrane. This cysteine-rich domain, composed of seven conserved cysteine residues, has been associated with cell adhesion (Doliana et al., 2000). The seven cysteine residues have been proposed to interact in a similar way to EGF-like domains, forming intramolecular cross-links between pairs of residues. However, the remaining unpaired cysteine has been suggested to play a role in disulphide bond formation with other proteins or multimerisation of the protein. The EMI domain may therefore be crucial for MEGF10 extracellular interactions (Doliana et al., 2000).

1.3.2 **EGF domains**

There are two main types of the 17 EGF-like domains in the ECD: EGF-like and EGF-laminin domains (Figure 5. A.). Typical EGF-like domains have six conserved cysteine residues, which form intracellular disulphide bonds between cysteines 1 and 3, 2 and 4, and 5 and 6 (Figure 5. B.). In EGF-like domains, the disulphide bond between cysteines 2 and 4, in particular, has been shown to be critical for mediating signalling across the membrane into the cytoplasm (Benitez and Komives, 2000). The five EGF laminin domains are larger than the EGF-like domains, with eight conserved

cysteine residues that form four disulphide bonds (Figure 5. C.). This increased interaction has been predicted to reduce the flexibility in these domains. X-ray crystallography has shown that the binding of Ca^{2+} to EGF domains, in proteins such as Notch, stabilises them (Chillakuri et al., 2012), and that Ca^{2+} bound to EGF-like domains can also direct protein-protein interactions (Rao et al., 1995).

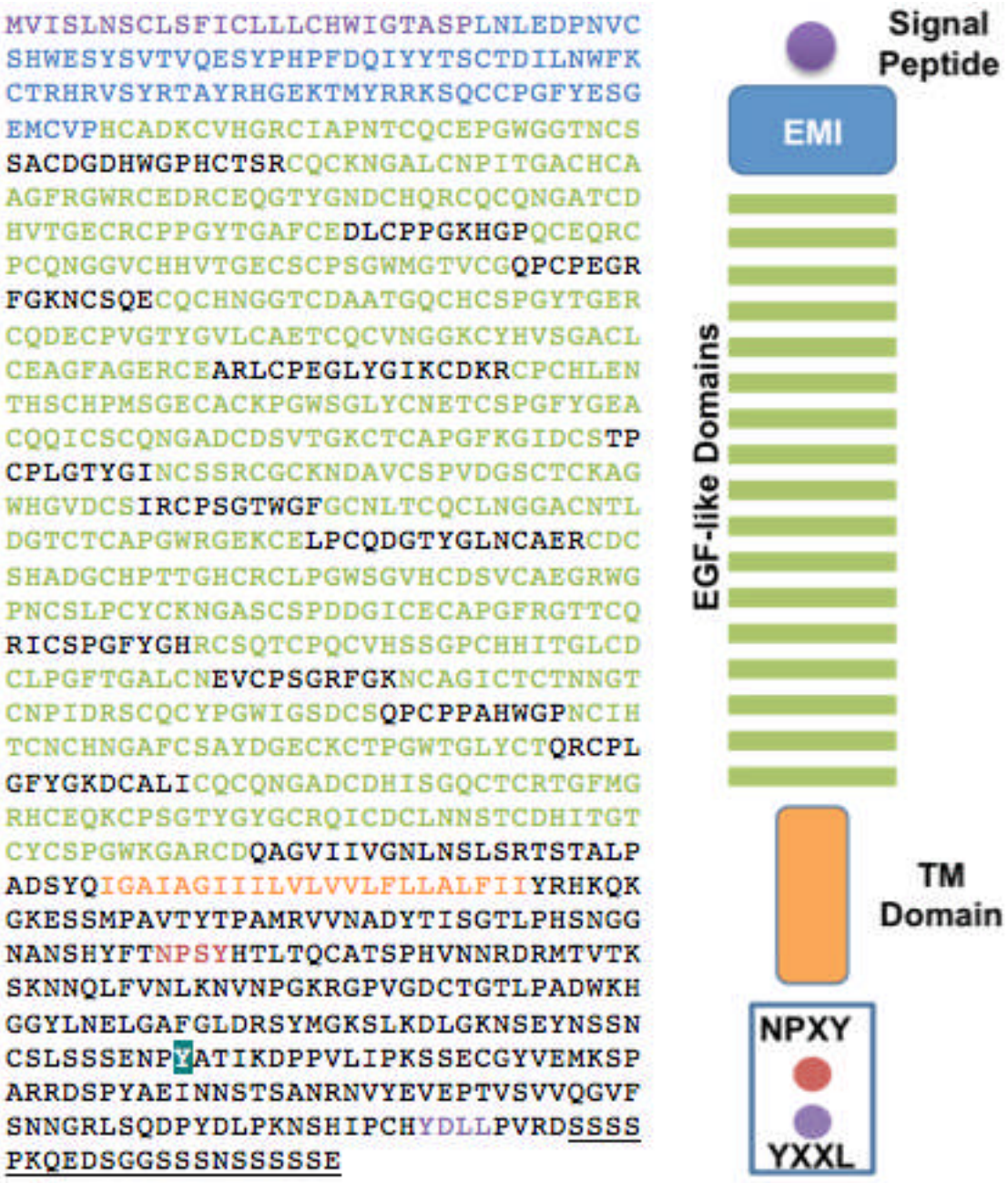

Figure 4. MEGF10 protein sequence and corresponding domain structure

Signal peptide in purple, EMI domain in blue, EGF domains in green, transmembrane (TM) domain in orange. The intracellular domain NPXY and YXXL motifs are highlighted in red and purple respectively. Tyrosine Y1030, the main site of tyrosine phosphorylation in MEGF10, is highlighted in green. A region of multiple serine residues at the C-terminus is underlined.

A. EGF-like domains

```
EGF1   HCADKCVHG-----RCIAPN-TCQCEPGWGGTNCS-----------
EGF3   DCHQRCQCQNG--ATCDHVTGECRCPPGYTGAFCE-----------
EGF4   QCEQRCPCQNG--GVCHHVTGECSCPSGWMGTVCG-----------
EGF6   LCAETCQCVNG--GKCYHVSGACLCEAGFAGERCE-----------
EGF8   ACQQICSCQNG--ADCDSVTGKCTCAPGFKGIDCS-----------
EGF9   NCSSRCGCKND--AVCSPVDGSCTCKAGWHGVDCS-----------
EGF10  GCNLTCQCLNG--GACNTLDGTCTCAPGWRGEKCE-----------
EGF12  NCSLPCYCKNG--ASCSPDDGICECAPGFRGTTCQ-----------
EGF13  RCSQTCPQCVHSSGPCHHITGLCDCLPGFTGALCN-----------
EGF14  NCAGICTCTNN--GTCNPIDRSCQCYPGWIGSDCS-----------
EGF15  NCIHTCNCHNG--AFCSAYDGECKCTPGWTGLYCT-----------
EGF17  GCRQICDCLNN--STCDHITGTCYCSPGWKGARCD-----------
```

B. EGF-laminin domains

```
EGF2   -----CQCKNG--ALCNPITGACHCAAGFRGWRCEDRCEQGTYGNDC
EGF5   -----CQCHNG--GTCDAATGQCHCSPGYTGERCQDECPVGTYGVLC
EGF7   -----CPCHLENTHSCHPMSGECACKPGWSGLYCNETCSPGFYGEAC
EGF11  -----CDCSHA--DGCHPTTGHCRCLPGWSGVHCDSVCAEGRWGPNC
EGF16  -----CQCQNG--ADCDHISGQCTCRTGFMGRHCEQKCPSGTYGYGC
```

C. Cysteine-cysteine interactions

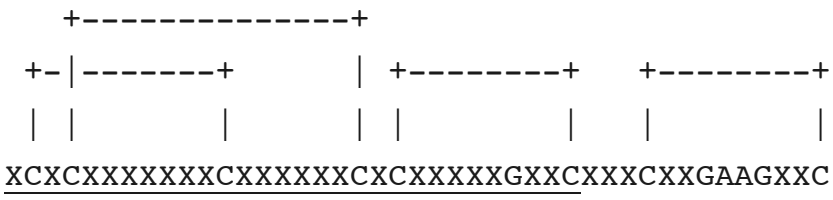

Figure 5. EGF domain alignment.

A. The EGF-like and **B.** EGF-laminin domains in MEGF10 were aligned and the conserved cysteine residues highlighted in green. Multiple protein sequence alignment was performed using Clustal W (CLUSTAL 2.1) (Larkin et al., 2007; Thompson et al., 1994) **C.** The typical interactions between conserved cysteine residues in EGF-laminin domains are shown, the underlined portion is similar to EGF-like domains. Conserved glycine (G) and aromatic (A) residues to identify EGF-like domains are shown in the sequence.

1.3.3 **Post-translational modification of EGF-like domains**

TM proteins expressed at the surface of cells typically have post-translational modification (PTM) enabling inter-cellular signaling, adhesion and migration. The most common PTM is glycosylation which involves the addition of sugar residues to the protein in the endoplasmic reticulum (ER) and Golgi. Protein glycosylation is regulated by changes in the localization of glycosylation enzymes and is important for cell signaling (Bard and Chia, 2016).

Membrane proteins, and in particular proteins containing EGF domains, are commonly post-translationally modified with N-linked glycosylation (Schwarz and Aebi, 2011) that gives high structural diversity to proteins due to branch additions and remodeling. N-glycosylation of the EGF receptor, which is composed of a similar structure as EGF-like domains, has been shown to play an important role in determining the conformation of proteins within the membrane (Kaszuba et al., 2015).

Consensus sequences have also been identified for less common *O*-linked PTMs. *O*-glucose modification of EGF-like containing proteins such as thrombospondin (Shao et al., 2002) and Notch (Matsumoto et al., 2016). EGF domains in a smaller proportion of EGF-like domain-containing proteins, such as Notch, are also modified with *O*-fucose, which is essential for Notch signaling (Haines and Irvine, 2003; Okajima and Irvine, 2002; Shi and Stanley, 2003). Less common *O*-fucose and *O*-glucose modifications on EGF-like repeats in Notch play a role in mediating both downstream and intercellular signaling (Luther and Haltiwanger, 2009a). Typical sites of PTMs in EGF-like domains are shown in Figure 6. B.

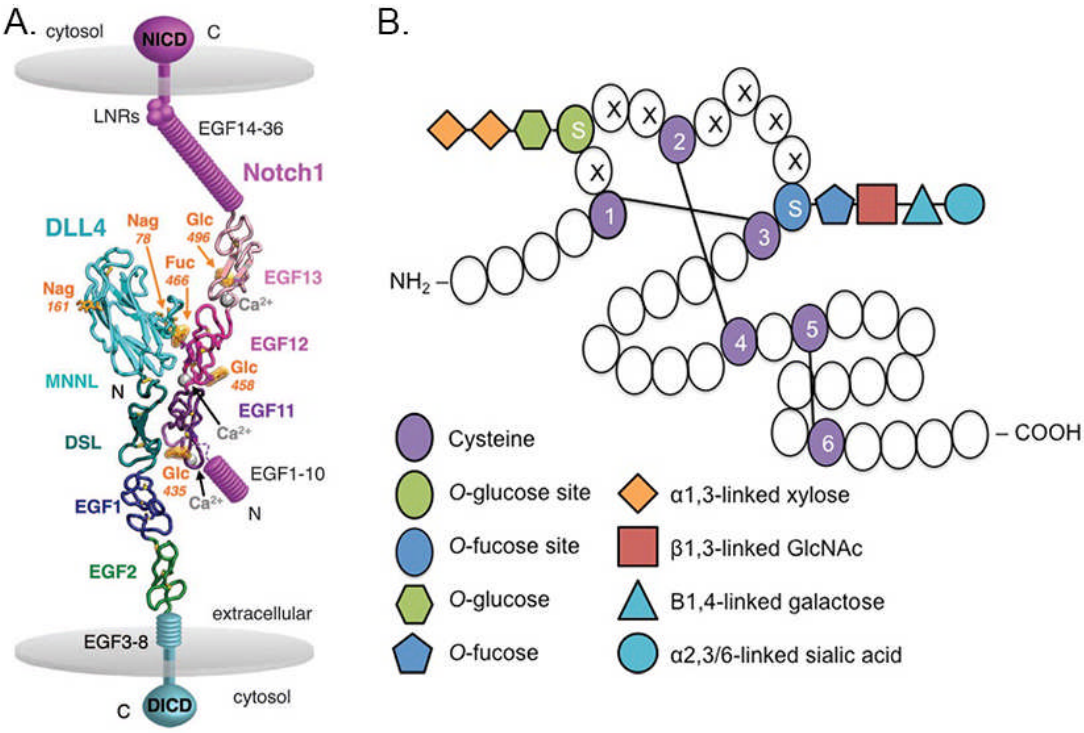

Figure 6. Notch1 and DLL4 EGF domain interactions and the typical glycosylation patterns of EGF-like domains.

A. A ribbon representation of the crystal structure of the Notch1 EGF-like domains 11 - 13 – $DLL4_{SLP}$(NEGF2) complex showing the two proteins localised in their respective cells membranes (grey discs) with Notch *O*-glycans (in orange) and bound calcium ions (in grey). A collinear, antiparallel interaction is formed between the two proteins along a narrow protein and glycan rich interface (Luca et al., 2015). **B.** A schematic of the typical structure of an EGF-like domain and its internal cysteine-cysteine interactions. Conserved sites for *O*-glucose and *O*-fucose addition are also shown (Harris and Spellman, 1993b).

The structure of the EGF-like repeats 11 and 12 of Notch bound to the Delta/Serrate/Lag-2 (DSL) domain of delta-like 4 ligands (DLL4; and related ligands), depicted in Figure 6.A., demonstrate the importance of PTMs in the modulation of binding between these two domains (Luca et al., 2015) and may give insight into interactions with the ECD of MEGF10. Specific threonine and serine residues on Notch1 are functionalised with *O*-fucose and *O*-glucose that act like amino acids forming interactions with residues on DLL4. The complex between Notch and DLL4 is formed of a collinear, antiparallel interaction between protein and glycan. EGF domains 11 – 13 are stabilised by inter-domain disulphide bonds and $Ca2^{+}$ ions at the junctions between EGF domains, however these $Ca2^{+}$ ions do not directly contribute to protein interaction (Figure 6. A.) (Luca et al., 2015). *O*-fucosylation occurs at consensus sequence C-X(4-5)-S/T-C between the second and third cysteine residues of EGF-like domain 12 in Notch (Shao et al., 2003), and this consensus sequence is present in EGF-like domains 3, 5, 12, 14, and 17 of MEGF10. *O*-glucosylation of Notch and other EGF-like repeats takes place on a serine residue at the consensus sequence (C-X-S-X-P-C) between the first and second cysteine residues (Fernandez-Valdivia et al., 2011; Harris and Spellman, 1993a; Hase et al., 1988). None of the EGF-like domains of MEGF10 have this exact sequence (Figure 5). O-fucose modification increases the affinity of Notch for its DLL ligand, whereas *O*-glucose modifications increase susceptibility to proteolysis after Notch binds to its ligand. The interaction between Notch and its ligand on another cell normally leads to proteolysis of Notch1, endocytosis of the ligand, and downstream signaling. Both mutations that disrupt the cysteine residues in the EGF domains of Jagged, together with those that interfere with these PTMs cause Alagille syndrome, characterised by abnormalities in the bile ducts, (MIM number 118450) (Luca et al., 2015).

Aside from glycosylation other PTMs have been identified in MEGF10, including mono-ubiquitination and tyrosine phosphorylation. The protein is mono-ubiquitinated, as identified by tandem mass spectrometry, and this modification is predicted to signal MEGF10 transport to lysosomes (Suzuki and Nakayama, 2007b). A tyrosine residue in the intracellular domain (Y1030) is phosphorylated by c-Src (Kauskot et al., 2012; Mitsuhashi et al.,

2013; Nanda et al., 2005). This residue is also conserved in MEGF11 and MEGF12.

1.3.4 **Intracellular domain.**

The intracellular domain of MEGF10 contains an NPXY and YXXL motifs, binding sites for phosphotryrosine binding protein (PTB) and src homology 2 (SH-2) protein domain respectively (Suzuki and Nakayama, 2007b; Wu et al., 2009) (Figure 4.). These two motifs in the cytoplasmic domain of TM receptor proteins play a role in enabling cytoplasmic adaptor proteins to interact and facilitate downstream signaling as well as tyrosine phosphorylation (Pawson and Scott, 1997). The YXXL motif, which binds SH2 domain containing adaptor proteins (Zhou et al., 1995), through phosphorylation of a tyrosine residue plays a role in signalling to facilitate the reorganization of the actin cytoskeleton (Kwiatkowska and Sobota, 1999). C-Src has been shown to interact with MEGF10 in a tyrosine-phosphorylation dependent manner (Mitsuhashi et al., 2013). In addition, Y1030 is phosphorylated in MEGF10, and this is important for neuronal cell engulfment, although it is unclear what its function is in muscle cells (Figure 4.). Two MEGF10 myopathy mutations in the EGF domains C326R and C774R, decrease tyrosine phosphorylation levels, with C774R (in the 16th EGF domain) having a major effect on muscle function (Mitsuhashi et al., 2013). The reduced levels of phosphorylation were additionally linked to a reduction in N-glycosylation, but did not change the localisation of a GFP-tagged protein when expressed in 293T cells. Phosphorylation of Y1030 is likely to be important in MEGF10 signalling, but it is not known what signalling molecules are recruited by MEGF10, or what ligand may bind to MEGF10 in order to initiate downstream signalling in human muscle. In addition, the pattern of PTMs has not been explored for MEGF10.

In *Drosophila*, the N-terminal PTB binding domain of the engulfment adaptor protein Ced-6 (mammalian orthologue of GULP, Engulfment Adaptor PTB Domain Containing 1), interacts with the NPXY motif in the cytoplasmic domain of the MEGF10 orthologue Draper (Eroglu and Barres, 2010; Hamon et al., 2006; Suzuki and Nakayama, 2007a) (Figure 7.) The *C.elegans*

orthologue Ced-1 also interacts with the NPXY motif with Ced-7 and Ced-10 also being involved in this engulfment pathway (Figure 8.). The mammalian orthologue of Ced-7 is a 12-TM ATP-binding cassette transporter protein (ABCA1) involved in engulfment, and the transport of phospholipids to the outer leaflet of the plasma membrane. ABCA1 therefore induces local changes to the phospholipid composition of the membrane (Hamon et al., 2006; Wang et al., 2001). Ced-10 is a small GTPase which, induces actin polymerisation enabling the final stages of phagocytosis (Hamon et al., 2006; Kinchen et al., 2005) (Predicted interactions are shown in Figure 8.). MEGF10 was also shown to interact with the AP50 subunit of the clathrin assembly protein complex 2 (AP2) (Chen et al., 2013; Nakayama et al., 2002; Suzuki and Nakayama, 2007b) (Figure 8). AP50 plays a role in endocytosis, sorting proteins trafficking in endosomes and is found associated with clathrin coated pits (Chen et al., 2013; Nakayama et al., 2002; Suzuki and Nakayama, 2007b). The tyrosine residue in the NPXY motif is phosphorylated by the tyrosine kinase c-Src, which activates the Erk1/2 pathway. In muscle cells, this phosphorylation is thought to result in an increase in satellite cell proliferation (Singh et al., 2010; Suzuki and Nakayama, 2007a). The NPXY and YXXL motifs may be partially redundant in function since the intracellular domain of Ced-1 is not necessary for the recognition of cell corpses however the intracellular domain has been shown to control downstream signal transduction to activate the cell corpse internalization process (Zhou et al., 2001).

MEGF10 additionally contains a short, 22 amino acid region, consisting of multiple serine residues (13 in total) close to its C-terminus (Figure 4.). This sequence is similar to that found in other 111 other ‘reviewed’ proteins in Uniprot from a Basic Local Alignment Search Tool (BLAST) search. These include FAM104A, zinc finger CCHC domain-containing protein 10, Class E basic helix-loop-helix protein 22, and E3 ubiquitin protein ligase Mdm2, and even the muscle protein obscurin. The function of this region is unknown, but it is likely to be involved in regulation mediated by phosphorylation.

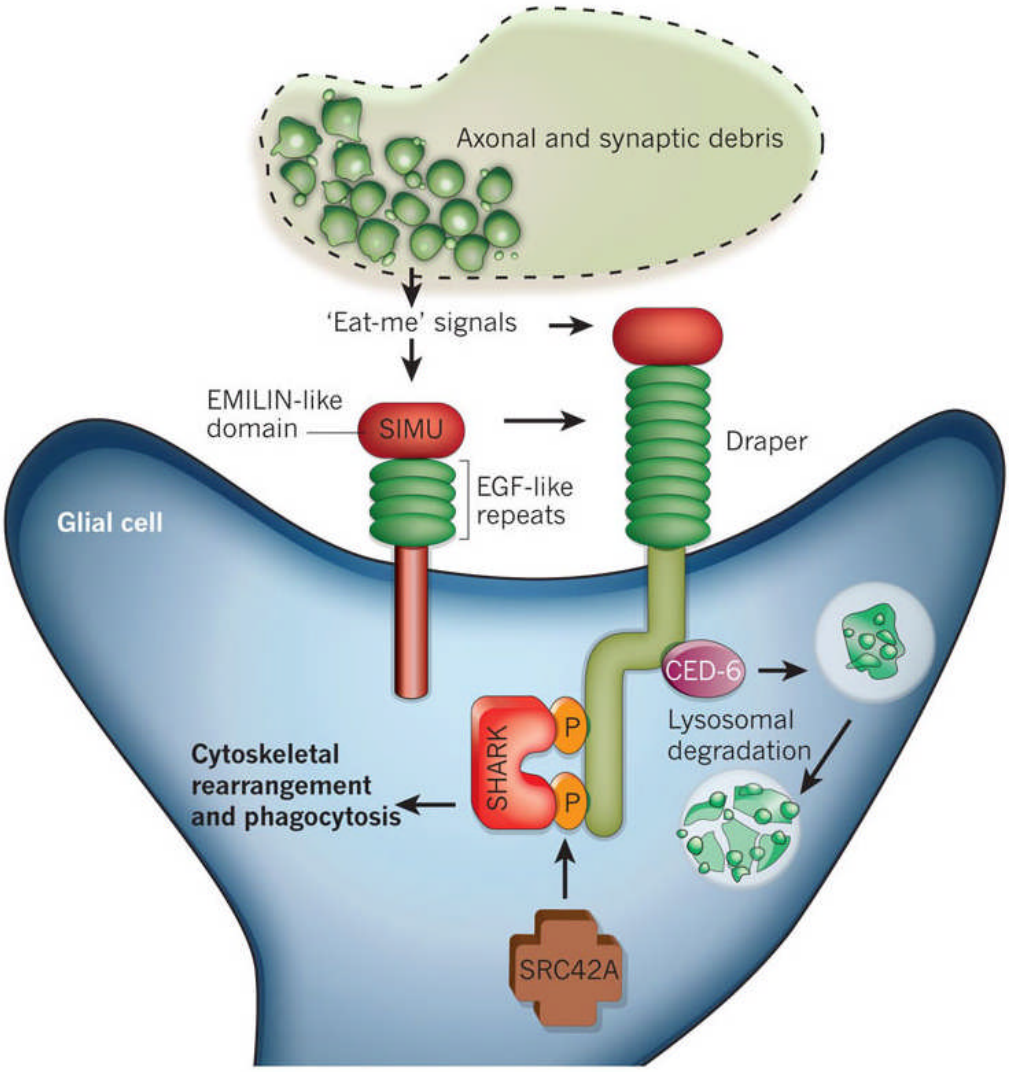

Figure 7. Role of glial cells in mediating engulfment in *Drosophila*.

A diagram depicting the interactions and pathways involved in mediating engulfment of apoptotic debris through rearrangement of the cytoskeleton mediated by the MEGF10 homologue Draper (Eroglu and Barres, 2010).

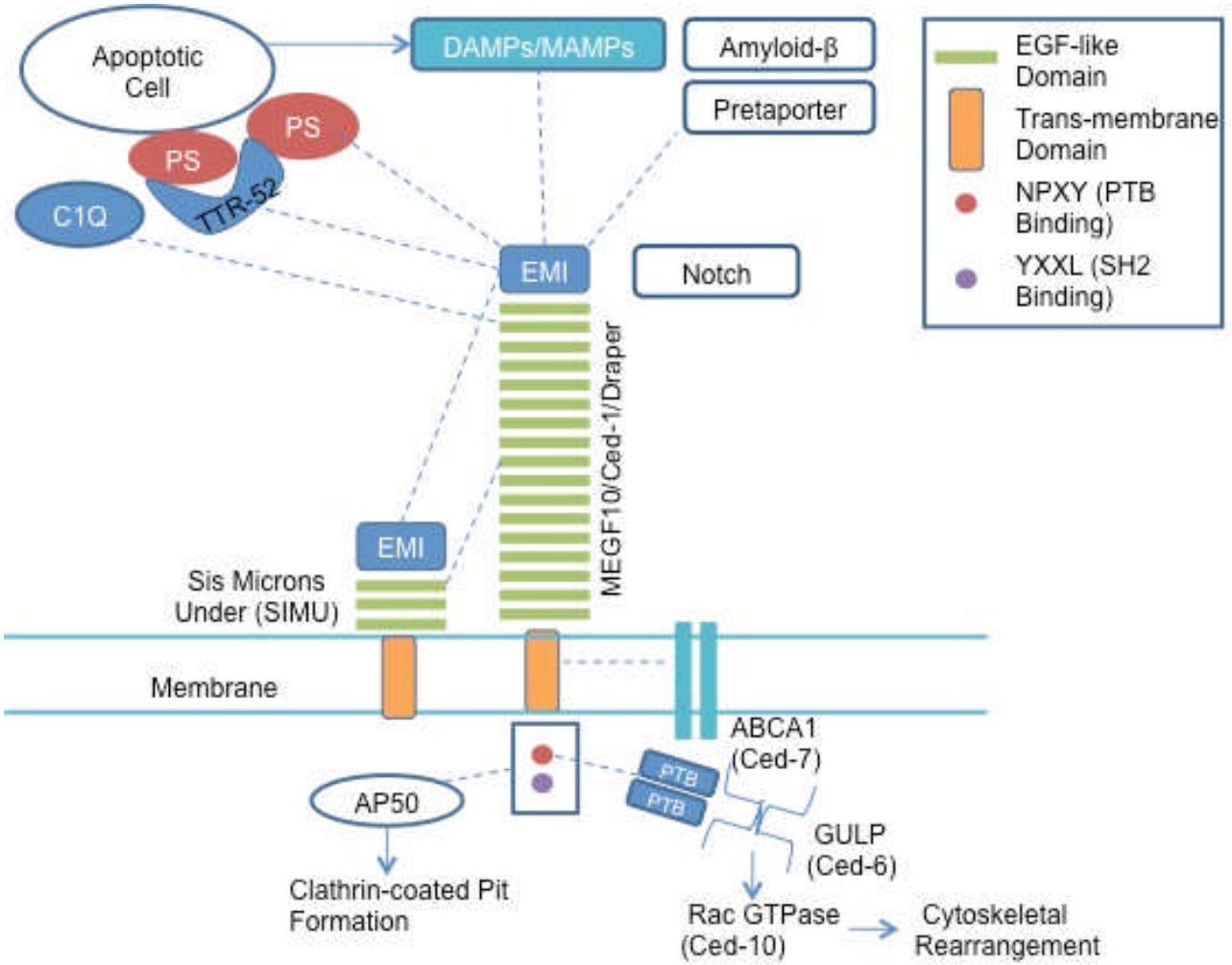

Figure 8. Summary of protein interactions with MEGF10 and its orthologues Draper and Ced-1.

MEGF10 and the corresponding proteins in *Drosophila* and *Caenorhabditis* have a number of functions as described above. A dashed line marks some of the potential interactions described in the literature. These interactions suggest that MEGF10 and its orthologues may play a number of key roles in mediating cellular homeostasis and acting as part of larger signalling pathways.

1.3.5 **The Function of MEGF10**

An analysis of the relative expression levels of MEGF10 in mouse tissues by quantitative PCR showed high levels of expression in the brain and in muscle that is regenerating, 3 days after injection of the cobra cardiotoxin (ctx), while levels of MEGF10 in normal muscle are low (Holterman et al., 2007). Ctx is a type of phospholipase A2, which binds to the muscle plasma membrane and disrupts its integrity (Gutierrez and Ownby, 2003). This promotes muscle fibre degeneration while leaving the nerve and blood supply intact (Cooper et al., 1999). Additional papers investigating the function of MEGF10 have focused on either the protein's neuronal or skeletal muscle roles, giving a complex picture of MEGF10 playing different and seemingly unconnected roles in both skeletal muscle and the brain. While the function of MEGF10 in engulfment, and how this is important in the brain or neuronal development, is becoming clearer, it is much less clear how MEGF10 functions in skeletal muscle.

1.3.6 **The function of MEGF10 in engulfment and apoptosis**

Engulfment and apoptosis are important processes in development and neuronal remodeling of the brain in response to injury and MEGF10 has been shown to play a role in mediating these processes. The role of the *C.elegans* orthologue of MEGF10, Ced-1, has been identified as one of a number of proteins that plays a role in development and apoptosis through engulfment, interactions and signaling by a number of Ced proteins (Hengartner, 2001; Lettre and Hengartner, 2006; Mangahas and Zhou, 2005). Ced-1 has also been shown to play a role in enabling the unfolded protein response and its reaction to an innate immune response (Haskins et al., 2008; Lamitina and Cherry, 2008).

In mammals, apoptotic cells express specific signals marking them for degradation. These include PS, which translocates from the inner leaflet to the outer leaflet of the cytoplasmic membrane in apoptotic cells. The MEGF10 orthologue Ced-1 has previously been shown to bind to phosphatidylserine (PS) and may even be a novel apoptotic signal mediating phagocytosis of apoptotic cells (Scheib et al., 2012; Wu et al., 2009). The conserved NPXY and YXXL motifs in the intracellular domain of Ced-1 have been shown to be critical for mediating phagocytosis through cytoskeletal rearrangement (Park et al., 2014; Zhou et al., 2001). Transthyretin-like protein 52

(TTR-52) is a soluble protein which has been shown to mediate interaction between Ced-1 in phagocytic astrocytes and astrocytes undergoing apoptosis that express PS via the ECD of Ced-1 (Tung et al., 2013). Conversely, the MEGF10 orthologue in *Drosophila*, Draper, has been shown to interact with PS directly via the EMI domain to recognize apoptotic cells and induce apoptotic cell clearance (Tung et al., 2013) (Interactions are outlined in Figure 8.).

The role of MEGF10 as an engulfment receptor that mediates apoptosis has also been shown in mammals through the cooperative working of MEGF10 and ABCA1 (Hamon et al., 2006). In glial cell engulfment, whilst Draper has been shown to interact with PS, in mammals MEGF10 has recently been shown not to interact directly with PS but instead binds to the P-binding protein C1q through the EMI domain (Doliana et al., 2000; Iram et al., 2016). C1q is a component of the C1 complex, which forms part of the classical complement pathway and the interaction between C1q and MEGF10 has been suggested to enable astrocyte mediated clearance of apoptotic mammalian cells (Iram et al., 2016). Mutations in MEGF10, which cause myopathy, were also investigated in this study, however the mutations were explored in a neuronal context and not a muscle environment. This makes extrapolation of the results to the muscle phenotype seen in EMARDD patients difficult, particularly as these patients do not appear to present with any neurological symptoms (Iram et al., 2016).

Overexpression of MEGF10 in mammalian cells results in an irregular mosaic-like pattern of MEGF10 in the cytoplasmic membrane and accumulation of protein at the points of contact between apoptotic Flp-In T-REx 293 cells expressing cytoplasmic DsRedMonomer and stably expressing MEGF10_eGFP in co-culture experiments (Suzuki and Nakayama, 2007a). This group also showed that exogenously expressed MEGF10 in mammalian cells directly interacts with the clathrin assembly protein complex 2 (AP2) medium chain (AP50), a cytosolic adaptor protein localised at clathrin coated pits (Kay et al., 2012; Singh et al., 2010; Smith et al., 2006; Suzuki and Nakayama, 2007a). AP50 has also been shown to be required for the activity of the specific vacuolar ATPase that promotes the acidification of endosomes and lysosomes (Suzuki and Nakayama, 2007b). GFP-tagged MEGF10 was also found to bind strongly to the culture dish, outside of the cells, and could be isolated after lysing the cells and washing them away from the dish. Several co-purifying components were identified by Liquid chromatography–mass spectrometry (LC-MS/MS), including beta-actin (Suzuki

and Nakayama, 2007b). However, this interaction may be indirect and potentially mediated by binding to Ced-6, whose mammalian orthologue is engulfment adaptor protein GULP which, may help to reorganise the actin cytoskeleton at sites of interaction with cells undergoing apoptosis (Suzuki and Nakayama, 2007b). These interactions further highlight the role of MEGF10 in engulfment and mediating interactions between cells (Hengartner, 2001; Lettre and Hengartner, 2006; Mangahas and Zhou, 2005).

MEGF10 has further been associated with apoptotic engulfment through its interaction with ABCA1, which transports a number of molecules across membranes both within the cell and at the plasma membrane, such as cholesterol. Co-expression of MEGF10 and ABCA1 has been shown to increase the capacity of cells to mediate engulfment of apoptotic cells (Hamon et al., 2006). It has been proposed that activation of ABCA1 in apoptosis may lead to the membrane being remodelled and PS being translocated to the outer leaflet, potentially increasing the efficacy of MEGF10 in mediating engulfment (Hamon et al., 2006) (Interactions are summarized in Figure 8.).

1.3.7 **The neuronal function of MEGF10.**

High expression of MEGF10 in the brain suggests a neurological function (Holterman et al., 2007). MEGF10 acts as a receptor enabling the uptake of amyloid-β through li pid raft mediated endocytosis via the NPXY and YXXL consensus sequences in the intracellular domain. This role of MEGF10 in the brain may therefore provide a novel target for the treatment of Alzheimer's disease (Singh et al., 2010).

MEGF10 and its family protein MEGF11 have been shown to be necessary for the mosaic spacing of retinal starburst amacrine cells and horizontal cells through cell – cell adhesion contacts. Mutations in MEGF10 and MEGF11 cause the retinal neurons to become disarranged (Kay et al., 2012). The role of MEGF10 in astrocyte mediated clearance of dead cells following brain injury was shown by the addition of dead cells to an astrocyte cell population which, caused an increase in the level of MEGF10 protein expression (Loov et al., 2012).

Whilst in *Drosophila* Draper was identified as a playing a role in engulfment via activation by the tyrosine kinase Shark (Ziegenfuss et al., 2008) mammalian homologue tyrosine kinase Syk has been identified as a signal transducer for both MEGF12 and

MEGF10 through interactions with the intracellular domains. Expression of MEGF10 in HeLa cells was shown to promote engulfment and mutations to the tyrosine residue within the intracellular domain prevented engulfment (Scheib et al., 2012). MEGF10 has also been shown to be critical in synapse remodeling mediated by astrocytes through the MEGF10 and c-Mer receptor tyrosine kinase (MERTK) phagocytic pathways (Chung et al., 2013). The remodeling of synapses is important in the development of the mammalian nervous system and MEGF10 in conjunction with proteins including Jedi-1 (MEGF12) and Six-microns-under (SIMU) plays a crucial role in facilitating downstream signaling in this process as summarized in Figure 7 (Eroglu and Barres, 2010; Wu et al., 2009).

1.4 The role of MEGF10 in skeletal muscle

Whilst the role of MEGF10 and its related signaling pathways in neuronal cell engulfment is relatively well described, the role of MEGF10 in skeletal muscle is less clear. A number of papers linking MEGF10 to skeletal muscle disease have been published. However, the results so far do not give a clear picture of the mechanisms by which disease mutations in MEGF10 produced the reported skeletal muscle phenotypes. The leading hypothesis is that MEGF10 is expressed in satellite cells and plays a key role in regulating the progression of myogenesis (Holterman et al., 2007). Skeletal muscle is a highly ordered tissue, composed of myofibres arranged within a sheath of extracellular matrix and connective tissue (Figure 9 and Figure 10). Skeletal muscle is formed by early embryonic myogenic precursors, marked by paired-box 3 (Pax3) expression. Pax3/Pax7 cells migrate away from the paraxial mesoderm / dermomyotome into the limbs to form skeletal muscle, and Pax3 is essential for this migration (Bober et al., 1994; Borycki et al., 1999)

In addition, Pax3 is important for embryonic myoblasts, and Pax7 for foetal myoblasts. Three groups of founder stem cells (FSCs) migrate from the dermomyotome and play different roles in forming the myotome in somites, which subsequently become skeletal muscle in the limb bud. This occurs in two stages; myogenesis begins with the formation of the myotome. Embryonic myoblasts then fuse to the myotomal cells to form primary muscle fibres. A second set of foetal myoblasts, expressing Pax7, continue to proliferate, differentiating later in development and fusing to form secondary fibres which, surround the primary fibres and establish the satellite cell pool (Maqbool and Jagla, 2007). A number of transcriptional regulators control embryonic muscle development from the somitic skeletal muscle lineage specification to myoblasts forming premuscle masses and subsequently primary and secondary myofibres (Shi and Garry, 2006) including Myf5 and MyoD (Berkes and Tapscott, 2005). Once fibres have begun to form, the basal lamina is laid down giving satellite cells their defining localization. During pre- and post-natal development satellite cells proliferate and some of these cells fuse with neighbouring fibres to increase

fibre size. In juvenile and adult muscle satellite cells enter quiescence becoming activated in response to signals of damage or injury from the muscle fibres (Buckingham, 2001; Cossu and Sampaolesi, 2007; Shi and Garry, 2006). The processes of myofibre formation and maintenance in embryonic development and adult skeletal muscle fibres rely on different mechanisms as reviewed by (Tajbakhsh, 2009) (Figure 10 A.).

Adult skeletal muscle is composed of bundles of multinucleated myofibres with myonuclei spaced at regular intervals along the fibre. In mature muscle fibres the turnover of cells is typically low, although muscle regeneration can occur under conditions of injury, disease or exercise (Hawke and Garry, 2001; Shi and Garry, 2006). A wide range of input signals and down-stream signalling events enables skeletal muscle plasticity in response to differing conditions (Hoppeler, 2016). The development and maintenance of matured muscle fibres are a tightly controlled process regulated by a diverse series of genetic factors and therefore study in simpler systems such as *Drosophila* have proven useful in better understanding the genetic regulation of this process (Maqbool and Jagla, 2007).

In the adult muscle, the processes of growth, regeneration and maintenance of skeletal muscle are primarily performed by a small and highly dispersed population of stem cells, called satellite cells (Mauro, 1961). Located between the basal lamina and the myofibre plasma membrane, it has been shown that these cells act as progenitor cells capable of repairing skeletal muscle fibres after damage (Dhawan and Rando, 2005; Kuang and Rudnicki, 2008; Mauro, 1961). However, aside from these classical satellite cells, other cells expressing myogenic marker proteins which may have myogenic potential can be isolated from other sources including the bone marrow (Ferrari et al., 1998), vasculature (De Angelis et al., 1999), and endothelial cells (interstitial cells) (Liadaki et al., 2012). Indeed, stem cells from blood vessels (such as mesangioblasts and pericytes) express similar genes to those of adult satellite cells (Seale et al., 2004; Dellavalle et al., 2007), however it has also been suggested that only native satellite cells fully contribute to myogenic regeneration (Figure 9.) (Sherwood et al., 2004). The microenvironment, including the myofibres, motor neurons, inflammatory cells and local vascular networks, which surrounds satellite

cells, is described as the satellite stem cell niche (Kuang and Rudnicki, 2008; Shi and Garry, 2006). This protects the satellite cells from most extracellular stimuli, thereby only activating the cells under specific conditions such as muscle fibre damage due to injury or disease (Siegel et al., 2009).

Satellite cells become activated in response to a number of physiological and damage response signals including hepatocyte growth factor (Holterman et al., 2007; Jennische et al., 1993; Tatsumi et al., 1998) and nitric oxide (Anderson, 2000; Wozniak and Anderson, 2007). In response to muscle damage satellite cells become activated and undergo multiple rounds of cell division before they leave the stem cell niche on the myofibre and migrate to the site of damage. These activated satellite cells terminally differentiate to repair pre-existing muscle fibers or to form multinucleate myofibres de novo (Seale et al., 2000).

Activated satellite cells down regulate Pax7 expression before differentiation into myotubes, whilst various muscle TFs (TFs) including myogenic factor 5 (Myf5), myoblast determination protein (MyoD), muscle specific regulatory factor 4 (MRF4/MRF6) and myogenin are upregulated during the process of activation and differentiation (Summarised in Figure 10). MyoD and Myf5 are both important for determination of myoblasts. Knockdown of MyoD has only minor effects on muscle formation, but results in upregulation of Myf5 (Holterman et al., 2007), and when both Myf5 and MyoD are knocked out, no muscle fibres or myoblasts form (Bentzinger et al., 2012; Rudnicki et al., 1993). (Rudnicki et al., 1993) Therefore Myf5 and MyoD have been suggested to play a role in specifying myoblasts for terminal differentiation. Myogenin is a downstream target of MyoD, and is important in regulating differentiation into myotubes by triggering the expression of genes expressed by differentiated myofibres (Bentzinger et al., 2013). Interestingly, Pax7 may not be essential for embryonic muscle development (Bentzinger et al., 2013; Seale et al., 2000) as well as in adult satellite cells as shown by the conditional inactivation of the Pax7 gene at specific points in skeletal muscle development (Lepper et al., 2009; Tajbakhsh, 2009). These TFs do not act in a linear manner but as a series of interacting feedback and feed-forward networks. Beyond these TFs it has been suggested that there are

other mechanisms by which myogenesis is regulated including microRNAs such as miR206 (Bentzinger et al., 2012). Satellite cell activation, proliferation and differentiation are summarised in Figure 10. B. and Table 1.

A.

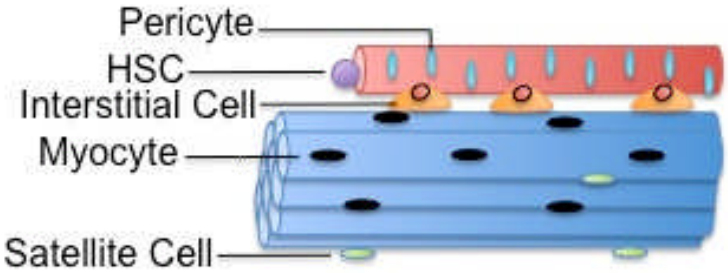

Cell Type	Markers	Directly myogenic	Indirectly myogenic	Fibroblastic & non-myogenic	Differentiate into MHC$^+$ MCs	Differentiate into MHC$^+$ MCs in co-culture	Form MFs *in vivo*
Satellite Cell	CD45$^-$/Sca1$^-$/CXCR4$^+$/β1$^-$ integrin$^+$/CD34$^+$	+	-	-	+	+	+
BM	CD45$^-$/Sca1$^+$/CD34$^+$	-	-	+	-	-	-
	CD45$^-$/Sca1$^+$/CD34$^-$	-	-	+	-	+	nd
CD133$^+$ cells	CD133$^+$	+	-	-	+	nd	+
Endothelial cells		-	+	-	-	-	-
FAP		-	+	-	-	-	-
HSC	CD45$^+$	-	-	-	-	-	+
Pericytes	Nestin$^-$/NG2$^+$	-	+	-	-	-	-
	Nestin$^+$/NG2$^+$	+	-	-	nd	nd	+
PICs	(PW1$^+$/Pax7$^-$)	+	-	-	-	+	+

Figure 9. The contribution of non-satellite cells to myogenesis.

A. Skeletal myofibres are part of a complex environment composed of a number of different cell types with differing roles in myogenesis. **B.** A table marking the expression profiles and functional plasticity of native satellite cells, bone marrow (BM) derived cells in the circulation and haematopoietic stem cells (HSC). (No data = nd, myocytes = MCs, myofibres = MFs. Diagram adapted from (Sherwood et al., 2004).

Whilst all adult quiescent satellite cells express Pax7, the satellite population is heterogeneous with more than one type of satellite cell, falling into various subpopulations, that express a mixture of different markers (Sherwood et al., 2004). Quiescent adult satellite cells are marked by the expression of not only TFs such as Pax7 but also a number of cell surface markers including cluster of differentiation 34 (CD34) (Beauchamp et al., 2000), syndecan-4 (Cornelison et al., 2001), CXCR4 (Ratajczak et al., 2003), vascular cell adhesion molecule-1 (VCAM-1) (Jesse et al., 1998) Another marker found in both quiescent and activated satellite cells is M-cadherin (Mcad), a calcium-dependent homophilic cell-to-cell adhesion molecule (Donalies et al., 1991; Irintchev et al., 1994). and integrin alpha 7 (Blanco-Bose et al., 2001). Integrin alpha 7 is a muscle specific cell surface antigen, which has been used for the isolation of primary mouse myoblasts from a mixed cell population (Blanco-Bose et al., 2001; Holterman et al., 2007). This integrin is the main laminin receptor in muscle and typically expressed in cells which also express c-Met, a tyrosine kinase necessary for muscle regeneration in response to injury (Pawlikowski et al., 2009; Webster and Fan, 2014).

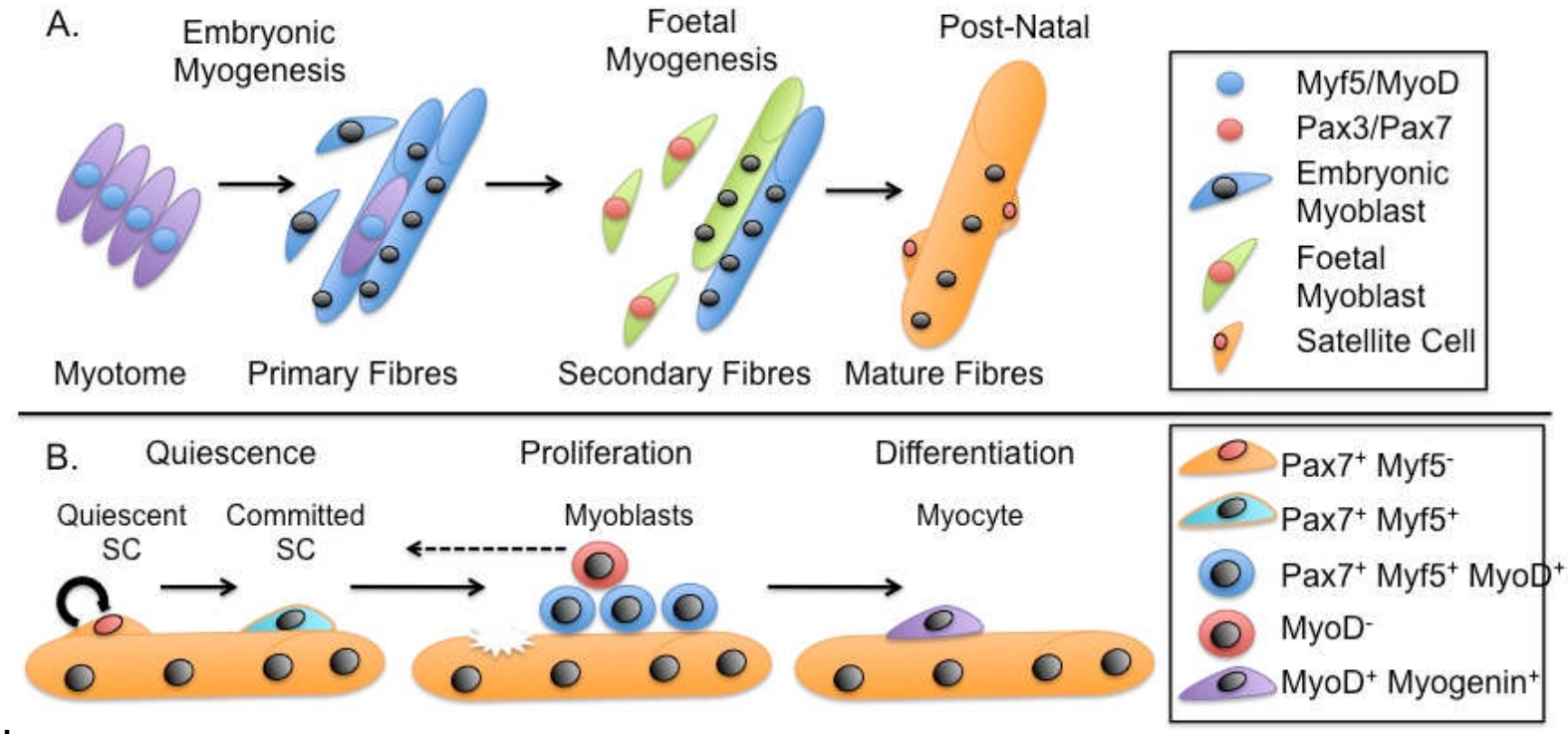

Figure 10. Satellite Cell Myogenic Progression & Marker Expression.

A. The process of muscle formation during embryogenesis. The myotome forms a scaffold for primary fibres to form before a second set of founder stem cells fuse to form secondary fibres. The formation of the basal lamina gives satellite cells their characteristic location in perinatal mature fibres. **B.** The process of satellite cell activation, proliferation and differentiation in response to muscle fibre damage. Quiescent satellite cells are capable of self-renewal (circular arrow) through symmetric expansion, whilst asymmetric division produces both a $Pax7^{+}Myf5^{-}$ quiescent satellite cell and a committed $Pax7^{+}Myf5^{+}$ satellite cell. Once satellite cells are activated MyoD expression rapidly increases, whilst myogenin expression marks the later stages of myoblast commitment and differentiation. Image adapted from (Zammit et al., 2006).

Table 1. Satellite Cell Markers.

A table of some of the identified factors, which play roles in satellite cell quiescence, activation, migration, differentiation and fusion for the maintenance of skeletal muscle fibres.

	Marker	**Type**	**Function**	**Reference**
Quiescence	Cluster of Differentiation CD-34	Cell surface glycoprotein	Cell-cell adhesion	Kuang and Rudnicki (2008)
	Muscle cadherin (M-cadherin)	Calcium-dependent cell adhesion molecule	Anchoring	(Kuang and Rudnicki, 2008; Fukada et al., 2007)
	Myostatin	Transforming growth factor-β superfamily member	Inhibition of satellite cell activation and myogenesis	(McCroskery et al., 2003)
	Paired Box 7 (Pax7)	Paired Box TF	Satellite cell specification, proliferation, and self-renewal	(Kuang and Rudnicki, 2008)
	Calcitonin Receptor (CTR)	G-protein coupled receptor	Regulation of quiescence through binding peptide hormone calcitonin	(Fukada et al., 2007)
	Multiple epidermal growth factor-like domains 10 (MEGF10)	Type 1 TM protein	Regulation of quiescence	(Holterman et al., 2007)

Activation	MyoD	Myogenic regulatory factor (MRF)	Satellite cell activation and myogenic differentiation	(Charge and Rudnicki, 2004; Johnston et al., 2010)
	Myf5	MRF (TF)	Myogenic commitment and transient amplification	(Kuang and Rudnicki, 2008)
	Jagged-1	Notch ligand	Induced during satellite cell activation	(Gnocchi et al., 2009)
Migration	CXC chemokine receptor (CXCR)-4	Cell surface chemokine receptor	Migration mediated by stromal derived factor-1 (sdf1)	(Brzoska et al., 2012)
	Angiotensin type 1a (AT1a) receptor	Receptor to the hormone angiotensin II	Mediate migration by chemotaxis in an angiotensin II gradient	(Johnston et al., 2010)
	Ephrin (Eph) receptors and ephrin ligands	Receptor Tyrosine Kinase that binds ephrin.	Mediate migration through Eph/ephrin signalling	(Stark et al., 2011)
Differentiation	Myogenin	MRF (TF)	Marks onset of myogenic differentiation	(Zammit et al., 2006)
	Necdin	Melanoma antigen-encoding gene family	Promotes differentiation by increasing myogenin expression	(Deponti et al., 2007)
Fusion	Vascular cell adhesion molecule-1 (VCAM-1) / very late antigen-4 (VLA-4)	VLA is an integrin which binds to its receptor VCAM-1	Myoblast fusion	(Rosen et al., 1992)

1.4.1 **Renewal of the satellite stem cell pool**

Satellite cells also replenish the quiescent stem cell pool, enabling skeletal muscle to undergo repeated rounds of regeneration and repair after subsequent injuries (Collins et al., 2005; Dhawan and Rando, 2005). As activated cells return to quiescence, MyoD and M-cadherin expression levels fall and CD34 levels rise (Dhawan and Rando, 2005). The homeobox gene Lbx1 was first described as being expressed during embryogenesis and possibly playing a role in muscle and CNS development (Jagla et al., 1995) and increased expression is seen in satellite cells on cut damaged skeletal muscle fibres (Watanabe et al., 2007a). Expression of the TF Ladybird-type homeobox 1 (Lbx1) in activated satellite cells maintains proliferation of the cells through the regulation of Pax7 whilst preventing differentiation before commitment of the cells to terminal differentiation and thereby helping to increase the stem cell pool. It may also have the capacity to force activated satellite cells back into quiescence (Kuang and Rudnicki, 2008; Watanabe et al., 2007b).

The majority of satellite cells express the TFs *Myf5* and *Pax7.* However, a small subpopulation have been identified as *Myf5* negative, and this may represent embryonic progenitors which have not become committed to the myogenic lineage (Kuang et al., 2007). These *Myf5*$^{-}$ cells are predicted to produce daughter cells for self-renewal by either symmetrical or asymmetrical division. The renewal of the satellite cell population is mediated by symmetric and asymmetric cell division, where symmetric division replenishes the stem cell pool and asymmetric division produces an activated daughter cell capable of mediating muscle regeneration (Dumont et al., 2015).

The expression of dystrophin in satellite cells regulates cellular polarity and asymmetric division and therefore helps to maintain the satellite cell pool. Muscle wasting in DMD may be due in part to dysfunction in satellite cells (Almada and Wagers, 2016; Wang and Rudnicki, 2012). This highlights the heterogeneity within the satellite cell population, and therefore the need to further investigate the role of specific satellite cell markers in both the repair

of damaged muscle but also in the replenishment of the stem cell pool (Kuang et al., 2007).

1.5 Satellite cell populations

The satellite cell population is heterogeneous, with sub-populations of cells possessing different properties. Satellite cell populations change as an individual ages and populations vary in different muscle groups enabling an alternative response during skeletal muscle regeneration in disparate muscle fibre types (Kuang and Rudnicki, 2008).

Satellite cells have primarily been identified through their expression of the sialomucin surface receptor CD34 and Myf5 (Beauchamp et al., 2000; Schultz, 1996), but more recent studies have identified a smaller sub-population of cells that do not express CD34. The relationship between these two populations of cells was assessed by fluorescence-activated cell sorting (FACS), showing that whilst CD34 negative cells are quiescent in uninjured muscle, this population increased in response to muscle injury. This CD34 negative pool of stem cells is also capable of reverting from a state of activation to repopulate the pool of CD34 positive stem cells. The number of CD34 positive satellite cells does not change in response to acute injury, suggesting that these populations of cells are tightly regulated to respond to muscle injury whilst also maintaining the CD34 positive pool of cells (Ieronimakis et al., 2010). Experiments using $CD34^{-/-}$ mice show no obvious developmental phenotype, but present with defective muscle regeneration in response to acute and chronic muscle injury. Satellite cells in this mouse model have reduced motility on the fibre and delayed myogenic progression. These results may suggest that CD34 plays a role in the early stages of satellite cell activation (Alfaro et al., 2011), which is further supported by the complete transcriptional down regulation of CD34 at the early stages of activation (Beauchamp et al., 2000).

1.6 MEGF10 and myogenic cells

Given the heterogeneity described in cells associated with myogenesis, it has been difficult to identify specific markers that are unique to the satellite

cell lineage. MyoD plays an important role in muscle differentiation, and yet its loss does not prevent muscle formation, therefore a recent screen was performed to try to identify novel specific markers for MyoD dependent muscle differentiation. Myoblasts isolated from wildtype and from MyoD$^{-/-}$ mice were used in the screen, and differences in RNA expression were analysed. The discovery of 51 differentially expressed genes were discovered, and 40 of these were analysed by western blotting in myoblasts and differentiated cells, for both the wildtype and MyoD knockout. This screen identified MD p67, the mouse homolog of human MEGF10 (XM_140362), as expressed in proliferating wildtype and MyoD$^{-/-}$ myoblasts, but not in differentiated cells, and that MyoD knockout myoblasts expressed slightly higher levels of Megf10 than wildtype cells, although it was not selected as an example of a gene with significantly higher expression in knockout cells (Seale et al., 2004).

This work was then followed up by a focused study on MEGF10 in satellite cells, confirming by qPCR that Megf10 was down regulated at the mRNA level by ~6.4 fold when primary myoblasts, isolated from wild-type mice (as described previously (Megeney et al., 1996; Sabourin et al., 1999)) terminally differentiated, and that MEGF10 expression was ~1.4 fold higher in MyoD$^{-/-}$ myoblasts, isolated from *MyoD*$^{-/-}$ mice (Ishibashi et al., 2005) , compared to wildtype myoblasts, and was down regulated by ~8 fold after differentiation (Holterman et al., 2007). FACS isolation of α7integrin^{+}, CD31^{-}/Sca1^{-}/CD45^{-} satellite cells, 94% positive for Pax7, showed ~100 fold upregulation of MEGF10 in satellite cells isolated from 8 week old mice that were activated by in vitro culture for three days compared to freshly isolated satellite cells. In situ hybridisation with an RNA probe also showed Megf10 expression in cells along the edges of muscle fibres in tibialis anterior (TA) muscle fibres, a similar localization to satellite cells. Finally, using an antibody raised to the cytoplasmic domain of MEGF10, this study also showed that MEGF10 was only expressed in Pax7 positive satellite cells (Holterman et al., 2007).

The authors then went on to express an HA-tagged full length MEGF10 protein construct in C2C12 cells, which was shown by western blotting to have a molecular weight of ~120 kDa, in which they probed with the anti-HA

antibody but not directly with an anti-MEGF10 antibody. Based on its sequence MEGF10 is predicted to have a molecular weight of 122 kDa, similar to that seen by western blot. However, this would not include any increase in size due to PTMs, which might be expected given that the majority of the protein is extracellular and primarily composed of EGF-like domains, which are typically heavily glycosylated (1.3.3). Moreover, the antibody raised against the C-terminal 290 aa of MEGF10 was only used in immunostaining without any independent characterisation of the antibody to show that it recognised the expressed HA-tagged protein either by western blotting or by immunofluorescence. Overexpression of HA-tagged MEGF10 in C2C12 cells (but not fibroblasts) slightly increased growth rates, and markedly decreased the ability of the myoblasts to fuse and differentiate into myotubes, as well as down regulating MyoD expression potentially returning the cells to a quiescent state. Using siRNA to knockdown MEGF10 expression in satellite cells on cultured muscle fibres promoted precocious activation of satellite cells, as evidenced by an increase in myogenin expression and increased differentiation in cultures of primary satellite cells. Lastly, knocking down MEGF10 by 0.56 fold in cultured $MyoD^{-/-}$ cells reduced expression of Notch 1, Notch 2 and Notch 3, and it was suggested that MEGF10 might be able to activate Notch signalling. Notch, like MEGF10, is a TM protein that contains several EGF-like repeats in its ECD and is activated by interaction with the DSL ligands of proteins such as Jagged. However, MEGF10 does not contain any DSL repeats, and therefore would have to interact with Notch via a different mechanism (Holterman et al., 2007).

These experiments led to the hypothesis that MEGF10 has a role in regulating proliferation in myogenic cells through the Notch signaling pathway. Notch has been shown to be critical in facilitating the progression of satellite cells towards myogenesis (Conboy and Rando, 2006), and is therefore important in development. Blocking of Notch signalling causes premature differentiation of myogenic progenitors, and formation of very small muscle groups, a similar phenotype to that found in EMARDD patients (Schuster-Gossler et al., 2007; Vasyutina et al., 2007). During the perinatal period in mice, satellite cells continue to proliferate until postnatal day 21,

when they adopt quiescent characteristics (White et al., 2010). This is dependent on Notch signalling, as well as target genes, Hey1, HeyI and Sprouty1, which negatively regulate tyrosine kinase signalling (Bjornson et al., 2012). Like MEGF10, activated Notch signalling suppresses differentiation of cultured C2C12 cells, suggesting a critical role for MEGF10 in maintaining the satellite cell compartment through self-renewal, possibly in a similar manner to Notch. Mutation of the Notch ligand, DLL1, or knockdown of Rbpj, the DNA binding protein, which regulates Notch expression, results in early depletion of the myogenic progenitor pool, and also results in the formation of small muscle groups that do not contain any satellite cells (Vasyutina et al., 2007; Bjornson et al., 2012). During foetal development the knockdown of Rbpj is accompanied by rapid MyoD upregulation, but ablation of MyoD does not properly rescue satellite cell depletion. Instead these cells do not migrate normally, and $Pax3^{+}$ cells are found instead in the interstitial space, and not the basal lamina, suggesting that Notch is important for regulating the formation of basal lamina around satellite cells. Therefore, activated, emerging satellite cells show disruption in expression of basal lamina components and adhesion molecules including MEGF10 through its interaction with Notch (Brohl et al., 2012).

This study also assessed the changes to MEGF10 expression in coRbpj: $MyoD^{-/-}$ (RM) and $MyoD^{-/-}$ mice compared to control mice. In contrast to the earlier report that expression of MEGF10 is increased in $MyoD^{-/-}$ mice, (Seale 2004), here it was reported that MEGF10 shows a 1.8 fold decrease in $MyoD^{-/-}$ mice, which though not significant, rose to a significant 3.1 fold decrease in the RM mice. Furthermore, induction of MEGF10 expression was shown to be dependent on DLL1, shown by a significant increase in the levels of MEGF10 in the presence of DLL1. Finally, it was reported that low levels of MEGF10 were observed in the plasma membrane of $Pax3^{+}$ cells in the RM mice, at embryonic days 15.5 and 17.5, using a commercial antibody (Santa Cruz), raised to the cytoplasmic domain of MEGF10 (Brohl et al., 2012).

Although these studies identified a possible function of MEGF10 in myogenic proliferation evidenced by a link between MyoD and MEGF10, myogenin has

also been identified as a positive regulator of MEGF10 transcription in skeletal muscle. By analysing the 5’ end of the Megf10 gene, a myogenin binding motif was identified that was shown to bind to myogenin (Park et al., 2014). Moreover, levels of MEGF10 and myogenin expression rose in ctx damaged muscle as measured by qPCR. A luciferase reporter assay that showed the activity of the MEGF10 promoter, showed an 11 fold increase in expression resulting from its interaction with myogenin, whilst Myf5 had a smaller effect increasing MEGF10 promoter activity by only 2.8 fold. Myogenin was shown to bind directly to this region of DNA and its effect on MEGF10 promoter activity is dose dependent (Park et al., 2014). However it is unclear how MEGF10 can promote proliferation, but inhibit differentiation as reported (Holterman et al., 2007), if it interacts with myogenin, which is not expressed until the cells begin to terminally differentiated, and would not be expected to affect proliferation.

Overall, these studies suggest that MEGF10 has a clear role in neuronal cells, where it is in involved in the clearance of apoptotic cells (Iram et al., 2016) as well in synapse elimination (Chung et al., 2013) by astrocytes. Both observations are consistent with the role of MEGF10 in patterning retinal neurons (Kay et al., 2012), and the observed effects of knocking out the ortholog of MEGF10 on the brain and retina in *Drosophila* (Draper et al., 2014).

However, EMARDD patients do not have a neurological phenotype, but do have a muscle deficiency, and it therefore seems likely that MEGF10 is also important in satellite cells. It has been suggested to be important for renewing the satellite cell pool, by maintaining proliferation in cells and inhibiting the progression of the myogenic program in combination with MyoD and Notch (Holterman et al., 2007; Logan et al., 2011). It has also been suggested to promote satellite cell differentiation shown by the relationship between increasing expression levels of MEGF10 and myogenin (Park et al., 2014), although overexpression of MEGF10 inhibits differentiation in vitro (Holterman et al., 2007). MEGF10 has also been suggested to influence the ability of satellite cells to populate the satellite cell niche through interactions with Notch and by promoting the adhesion of satellite cells to the basal lamina or muscle fibre (Brohl et al., 2012). It is difficult to reconcile these disparate ideas and to explain how a mutation in the *MEGF10* gene leads to a disruption of the stem cell pool, reduces the ability of skeletal muscle to regenerate leading to the reduced myofibre size seen in EMARDD patients.

1.7 Hypothesis and Aims

MEGF10 has a role in both neuronal and skeletal muscle development. This research intends to focus on the role of MEGF10 in the skeletal muscle environment. It was hypothesised that MEGF10 expression in satellite cells may act in a similar manner to Notch, which has a similar domain structure, enabling both inter- and intra-cellular signaling to effect transcriptional changes which affect muscle regeneration. It was further hypothesized that the ECD of MEGF10 may enable interaction with exposed phospholipids to enable fusion of myoblasts to form multi-nucleated myotubes.

The aim of this research was to gain a better understanding of the role of MEGF10 in skeletal muscle cell biology. In the first instance this needed the careful selection and validation of appropriate antibodies recognizing MEGF10 for use in both the immunofluorescence and western blotting experiments, which were not always performed in earlier studies (Brohl et al., 2012; Holterman et al., 2007). It then required a careful re-examination of the expression and staining patterns for MEGF10 to determine exactly when and where this protein is expressed in both cultured and primary myocyte cultures. Given the conflicting relationship between MEGF10 and MyoD or myogenin expression previously described, the re-examination of the co-expression of MyoD and myogenin was also needed to determine if there was any correlation between their expression and that of MEGF10. RNAseq was used as an alternative technique to investigate any changes in MEGF10 expression, alongside MyoD, myogenin, and other skeletal muscle markers during different stages of myoblast differentiation.

To further investigate the effects of increasing levels of MEGF10 on muscle differentiation, I also wanted to test if culturing myoblast cells in the presence of the expressed and purified ECD of MEGF10 was as effective at affecting fusion and differentiation as overexpressing MEGF10 as previously described (Holterman et al., 2007). A similar effect might be expected if the ECD of MEGF10 is a ligand for Notch 1, and thus able to induce downstream Notch signalling as effectively as overexpression of the full-length protein. Concomitant with this, expression of the ECD additionally

allowed an exploration into the nature of the PTMs present on MEGF10, which is of interest as these may be important in regulating the activity of these proteins. Finally, these experiments also allow me to investigate the effects of mutations in MEGF10, which cause EMARDD, on myoblast migration and fusion.

2 Materials and Methods.

2.1 Chemicals and Enzymes

All chemicals, enzymes and reagents were supplied by Sigma, and restriction enzymes supplied by Promega or New England Biolabs (NEB), unless otherwise stated.

2.2 Strains and Genotypes

Strain	**Genotype**	**Supplier**
NEB 5-alpha Competent *E. coli* (High Efficiency)	*fhuA2 Δ(argF-lacZ)U169 phoA glnV44 Φ80 Δ(lacZ)M15 gyrA96 recA1 relA1 endA1 thi-1 hsdR17*	NEB

2.3 Growing *Escherichia coli (E.coli)*

E.coli were cultured using Luria-Bertani (LB) broth composed of 10 g SELECT Peptone 140, 5 g SELECT Yeast Extract, and 5 g NaCl per Litre (Invitrogen) at 37°C with shaking at 220 rpm. Antibiotic selection for bacteria containing plasmids with the relevant resistance genes was performed using ampicillin and kanamycin at final concentrations of 100 µg/ml and 50 µg/ml respectively. The plasmids used in this study are listed in Table 2.

To select single colonies on agar plates, LB agar was prepared by dissolving 1 tablet in 50 ml dH_2O. LB agar was autoclaved and allowed to cool to 50°C before adding the required antibiotic stock solution to the final concentrations described above. Plates were poured and allowed to set for 30 min. All sterile work was done at the bench by a lit Bunsen flame.

2.4 Plasmids

The plasmids and sequencing primers used in subsequent cloning steps are shown in Table 2. and 3. respectively.

Table 2. Plasmids used to clone and express MEGF10 constructs.

Plasmid Name	Source	Resistance	Genes present in vector	Use
pDC315	Microbix Biosystems.	Ampicillin		Adenoviral Construct
pBHGloxΔ E1,3Cre	Microbix Biosystems.	Ampicillin		Virus rescue plasmid
pEGFP-N1	AddGene	Kanamycin	EGFP	PCR amplification of eGFP
pBluescriptIISK+	Gift from C.Johnson	Ampicillin	Contains MEGF10 cDNA	Amplification of MEGF10
pSecTag2A	Invitrogen	Ampicillin	Signal peptide for secreted expression and 6His and c-myc tags for purification	Secreted expression of protein in cultured ma mammalian cells.

Table 3. Full length MEGF10 sequencing primers.

The sequencing primer notation shows the sequence being read, the starting base pair number within the construct and forward primers marked F and reverse primers marked R.

Sequencing Primer Name	Sequence	Tm (°C)
MEGF10_553F	gagcagggcacctatggtaa	60.1
MEGF10_1147F	atgtctggagagtgtgcctg	58.8
MEGF10_1751F	ccctgccctgctactgtaaa	60.3
MEGF10_2352F	acggcactgtgagcagaagt	61.1
MEGF10_2958F	gaaacatggcggctacctc	60.6
MEGF10_655R	tgtatcctggtgggcagc	60.7
pDC315927F	ataagaggcgcgaccagc	61.5
eGFP_F1	aacatcgaggacggcagc	62.4
eGFP_F2	catcacaaatttcacaaataaagca	60.3

2.5 General Procedures

All media, plastic and glassware for bacteriological work were sterilised by autoclaving at 121°C for 15 min.

2.6 Working with DNA

All DNA was stored in aliquots at -20°C and thawed on wet ice prior to use.

2.6.1 **Spectrophotometric quantification of nucleic acids**

DNA concentrations were measured using a Nanodrop spectrophotometer and ND100-v3.7.1 software. The spectrophotometer sensor was washed three times with 10 µl dH_2O prior to initialising the instrument with 2 µl dH_2O. A blank measurement was taken using 2 µl of buffer and 2 µl of sample loaded for measurement. The purity of the sample was determined by the A260/280 ratio, where a pure sample has a value of 1.8.

2.6.2 **Precipitation and concentration of nucleic acid**

Low concentrations of DNA were concentrated by isopropanol precipitation. To a volume of DNA, half the volume of 7.5 M ammonium acetate (NH_4OAc) and 2 volumes of isopropanol were added and incubated at room temperature for 10 min. The solution was centrifuged at 16,200 *xg* for 10 min. The pellet was washed with 70% ethanol and the sample vortexed for 1 min to break up the pellet. DNA was pelleted by centrifugation at 16,200 *xg* for 10 min. Ethanol was removed and the pellet allowed to air dry for 10 min. The pellet was resuspended in a small volume of RNase- and DNase-free MilliQ pure water.

2.6.3 **'Miniprep' DNA preparations**

Small-scale plasmid DNA was purified from *E. coli* using the QIAprep® Spin Miniprep Kit (Qiagen) following the manufacturer's instructions. Briefly, 4ml of a 5ml overnight transformed NEB 5-alpha culture was transferred to sterile Eppendorf tubes. The cell suspension was centrifuged at 16,200 *xg*

for 3 min at room temperature. (All speeds are 16,200 *xg*, unless otherwise stated). The supernatant was discarded and the pellet thoroughly resuspended in 250 µl buffer P1 (resuspension buffer), containing RNaseA to remove RNA contamination and lyse blue which indicates alkaline cell lysis in cells by turning a blue colour and turns white upon neutralisation. 250 µl of buffer P2 (lysis buffer) was added and solution mixed by inversion 4-6 times. 350 µl buffer N3 (neutralisation buffer) was added and mixed as before. Lysed cells were centrifuged for 10 min to pellet the cell debris. The supernatant was applied to the Qiagen spin column and centrifuged for 60sec. The flow through was discarded and the column washed with 500 µl buffer PB. The flow through was again discarded and the column washed with 750 µl of buffer PE. The column was centrifuged for 60 sec and the flow-through discarded. Residual wash buffer was removed by centrifugation for 60 sec. The column was transferred to a sterile 1.5 ml Eppendorf and the DNA eluted in 30 µl of buffer EB.

2.6.4 **'Maxiprep' DNA preparations**

In order to have sufficient DNA for subsequent cloning steps or mammalian cell transfections, larger DNA plasmid preparations were performed using the Qiagen Hi-speed Maxiprep kit, according to the manufacturer's instructions. Briefly, a 400 ml overnight bacterial culture was removed from the shaking incubator, centrifuged at 3000 x*g* for 15 min at 5°C and the pellet resuspended in 10 ml buffer P1. 10 ml buffer P2 (lysis buffer) was added and the tube was mixed by inversion six times and incubated at room temperature for 5 min. 10 ml buffer P3 (neutralisation buffer) was added and the solution mixed by inversion 6 times. The lysate was applied to a QIAfilter Maxi Cartridge, with the cap attached, and solution allowed to settle at room temperature for 10 min. A Hi Speed Maxi Tip was equilibrated with 10 ml buffer QBT before the cleared cell lysate was applied. The lysate was allowed to enter the resin by gravity flow, enabling the DNA to bind. The QIAGEN Tip was washed with 60 ml buffer QC before the DNA was eluted with 15 ml buffer QF into a 50 ml falcon tube. The DNA was precipitated by adding 10.5 ml of room temperature isopropanol, gently mixing and

incubating at room temperature for 5 min. The DNA/isopropanol mixture was passed through a QIAprecipitator Maxi module to bind the DNA. The DNA was washed with 2 ml 70% ethanol and the precipitator membrane dried by passing air forcefully over the membrane using a syringe. The DNA was eluted into a 1.5 ml centrifuge tube with 1 ml of TE buffer and the eluate was passed through the precipitator a second time to ensure full elution of the DNA.

2.6.5 **Restriction endonuclease digestions of plasmid DNA**

Restriction endonucleases were used to cut DNA constructs for cloning and to test the presence of inserts within a vector, according to the manufacturer's instructions. For general diagnostic digests, a final volume 20 µl digest was prepared with ~20 ng DNA, 2 µl manufacturer's buffer and less than 1/10th v/v restriction enzyme (~10 U/µl). Digestions were incubated at 37°C for between 1 hr and overnight. The volume of the digestion, amount of enzyme used and time incubated was scaled up proportionally when larger amounts of DNA needed to be digested. For digestions using multiple restriction enzymes, a buffer was chosen in which both enzymes had a greater than 75% activity, as indicated by the manufacturers. When this was not possible, DNA was digested with the first enzyme before a buffer exchange was performed and the second digestion performed in the new buffer.

2.6.6 **Separation of DNA fragments by agarose gel electrophoresis**

Agarose gel electrophoresis was used to resolve and separate DNA on the basis of size. Agarose (Melford) was melted in 1x TAE buffer (0.04 M Tris-acetate, 1 mM EDTA pH8.0). DNA constructs of different size were separated using a range of agarose concentrations (Table 4.). Agarose solution was cooled prior to adding ethidium bromide (EtBr) (Thermo Fisher), at a final concentration of 0.5 µg/ml. The gel was poured into the required size of gel casing and combs, and allowed to set for 30 min. DNA samples were prepared with 6x Blue/Orange Loading Dye (Promega) (0.4% orange

G, 0.03% bromophenol blue, 0.03% xylene cyanol FF, 15% Ficoll® 400, 10 mM Tris-HCl (pH 7.5) and 50 mM EDTA (pH 8.0).) to produce a final 1x concentration. The gel was transferred to a gel tank filled with 1xTAE buffer and the samples were loaded along with 6 µl 1 kb DNA ladder or Low Mw ladder (NEB or Promega). Gels were run at 90V for ~1 hr before being imaged on the Molecular Imager® Gel Doc™ XR+ System (BioRad) and images processed using the Image Lab™ Software (BioRad).

Table 4. Agarose Gel Concentrations for DNA separation.

The percentage concentration of agarose required to effectively separate different sizes of DNA product. (Adapted from Molecular Cloning, a Laboratory Manual.)

Gel Concentration (%)	DNA Size (Kb)
0.60	1 – 20
0.70	0.8 – 10
0.90	0.5 – 7
1.20	0.4 – 6
1.50	0.2 – 3

2.6.7 **Extraction of DNA from an agarose gel**

Restriction digested DNA fragments separated by agarose gel electrophoresis were extracted and purified from the agarose using the QIAquick® gel extraction kit (Qiagen) following the manufacturer's protocol. Briefly, the gel was viewed using a Gel Doc Imager (BioRad, Molecular Imager Gel Doc XR+) and bands carefully cut out on a transilluminator using a clean scalpel. The band was transferred to a pre-weighed 2 ml Eppendorf tube and the mass of the gel band measured. Three gel volumes of buffer QG was added to the tube, where 100 mg of gel is equal to 100 µl of buffer. The bands were incubated in buffer QG for 10 min at 50°C, mixing the tube by vortexing at 2 - 3 min intervals. One gel volume of isopropanol was added to the Eppendorf tube and mixed to precipitate the DNA. The DNA was applied to a QIAquick spin column and centrifuged at 16,200 x*g* for 60 sec.

All subsequent centrifugation steps were also performed at this speed. 500 µl buffer QG was added to the column, centrifuged for 60 sec and the flow-through discarded. 750 µl of buffer PE was added to the column, centrifuged for 60 sec and the flow through discarded. The column was centrifuged for 60 sec to remove any residual wash buffer. The QIAquick column was transferred to a sterile 1.5 ml Eppendorf tube and the DNA eluted using 30 µl buffer EB after 1 min incubation.

2.6.8 **Transformation of competent cells with plasmid DNA**

Transformation of plasmid DNA into NEB 5-alpha competent *E. coli* cells (NEB) for DNA amplification was performed using either a 5 min (low efficiency) or 30 min (high efficiency) protocol. An aliquot of competent cells was thawed on ice for 5 min and 50 µl of cells transferred to a fresh 1.5 ml tube on ice. 1 pg - 100 ng of plasmid DNA was added to the cells, gently mixed, and the cells incubated on ice for a further 5 min or 30 min for low or high efficiency transformation respectively. Cells were heat shocked at 42°C for 30 seconds before returning to ice for 2 min. In the low efficiency protocol cells were spread onto selection plates and incubated at 37°C. For a higher efficiency of transformation 950 µl of room temperature Super Optimal broth with Catabolite repression (SOC) medium (NEB) was added to the cells and the cells were incubated at 37°C with 220 rpm shaking for 1 hr. The cells were then spread onto a warmed selection plate and incubated at 37°C overnight. Positively selected colonies were picked for plasmid preparations.

2.6.9 **Amplification of DNA by the polymerase chain reaction**

All primers were designed where possible to start or end with a C or G and to have a %GC content of approximately 50%. Primers were synthesised by IDT. Lyophilised DNA primers were prepared as 100 µM stocks in TE buffer and stored at -20°C. PCR reactions were performed using a T100 Thermocycler (BioRad). The PCR reaction parameters were adapted for different PCR primers and products, based on the length of the required product and the primer annealing temperature.

2.6.9.1 **Cloning primers**

Primers were designed for InFusion cloning following the manufacturer's protocol and using the InFusion primer design tool. Briefly, forward and reverse primers were designed with 15 bp homologous to the vector backbone and the remaining 18 - 20 bp covering the sequence to be amplified. Primers were therefore typically 30 - 50 bp long. The Tm was calculated without including the 15 bp overhang and was approximately 60°C.

2.6.9.2 **Sequencing primers**

To sequence large PCR products and vectors sequencing primers were designed at 600 bp intervals through the sequence so that the resulting approximately 800 bp reads from sequencing would overlap and produce a complete sequence for the DNA product. Primers were typically 18 - 20 bp long and had a Tm of approximately 60°C. MEGF10 sequencing primers are listed in Table 3.

2.6.9.3 **Colony PCR**

Standard PCR reactions for confirming positive colonies (colony PCR) were performed using Taq DNA Polymerase with ThermoPol® Buffer (NEB), following the manufacturer's recommendations. Colony PCR reactions were prepared on ice in thin-walled PCR tubes, by mixing together components for the following final concentrations 1x ThermoPol® Buffer, 200 µM dNTP, 0.5 µM forward primer, 0.5 µM reverse primer, small piece of selected colony and 0.625 U of Taq DNA polymerase made up to a total volume of 25 µl with nuclease-free MilliQ water. For colony PCR, the bacterial cells were lysed and DNA denatured by heating the PCR reaction mix at 95°C for 15 min prior to adding the Taq polymerase. The initial denaturation of DNA was at 95°C for 30 sec to enable primer annealing at 3 - 5°C below the calculated Tm for 15 – 60 sec. The DNA polymerisation to extend the annealed primers was performed at 68°C for 1 min/kb. The reaction was repeated for

30 cycles prior to a final 5 min extension at 68°C. PCR products were resolved by agarose gel electrophoresis.

2.6.9.4 **Phusion® High-Fidelity PCR**

For InFusion cloning Phusion® High-Fidelity DNA Polymerase (NEB) was used to reduce the error rate in PCR products. Phusion PCR reactions were prepared on ice in thin-walled PCR tubes, by mixing together components for the following final concentrations 1x Phusion HF Buffer, 200 µM dNTP, 0.5 µM forward primer, 0.5 µM reverse primer, < 250 ng template DNA and 1 U of Taq DNA polymerase made up to a total volume of 50 µl with nuclease-free MilliQ® water. The initial denaturation of DNA was at 98°C for 30 sec, before denaturation at 98°C for 5 - 10 sec to enable primer annealing at 3°C above the Tm of the lower Tm primer for 10 - 30 sec. The DNA polymerisation to extend the annealed primers was performed at 72°C for 15 – 30 sec per kb. The reaction was repeated for 35 cycles prior to a final 5 - 10 min extension at 72°C. PCR products were resolved by agarose gel electrophoresis.

2.6.10 **InFusion Cloning**

The cloning of MEGF10 constructs into a range of vectors was performed using the In-Fusion® HD EcoDry™ Cloning Kit (Clontech), in which PCR primers are designed specific for the gene of interest but with an additional 15 bp homologous to the vector ends. The amplified insert can then be cloned into a digested vector by homologous recombination between the vector and overlapping portions added to the insert by high fidelity PCR amplification. The InFusion Molar Ratio Calculator was used to calculate the required volumes of purified PCR fragment and linearised vector to enable an efficient InFusion cloning reaction. The calculated volumes of PCR insert and vector were added to lyophilised InFusion HD EcoDry pellet and the volume made up to 10 µl with distilled water. The InFusion cloning reaction was performed in the T100 thermocycler (BioRad), incubating the reaction to 37°C for 15 min then 50°C for 15 min. The 10 µl reaction was diluted with

40 µl Tris EDTA (TE) (pH8) before performing a high efficiency transformation into *E.coli*.

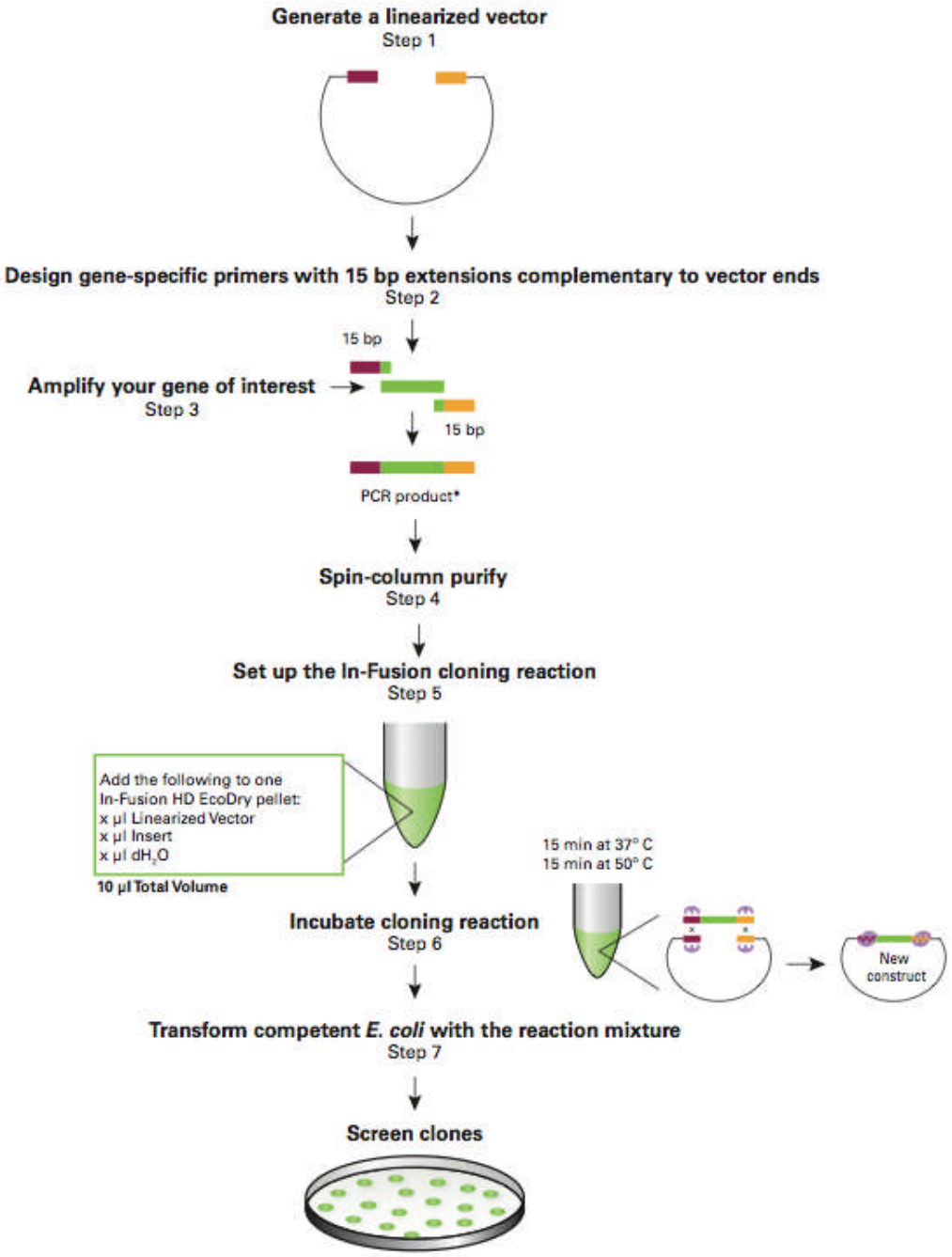

Figure 11. An overview of the steps for InFusion cloning.

A diagram depicting the steps involved in InFusion cloning. A linearised plasmid and PCR amplified gene of interest are mixed in the InFusion cloning reaction for 15 min at 37°C and then 15 min at 50°C. Reaction mixtures were transformed into NEB-5 alpha competent *E.coli* and positive clones selected. Adapted from InFusion HD Cloning Kit User Manual (Clontech).

2.6.11 **DNA sequencing**

Cloned constructs were sequenced by Source Bioscience or GATC Biotech Ltd. Available universal primers were used for common sites but custom sequencing primers were designed for DNA constructs larger than 700 bp (Sequencing primers listed Table 3.). Sequences were aligned and checked using Serial cloner 2-6.

2.6.12 **Site directed mutagenesis**

Single point mutations identified in EMARDD patients were made in MEGF10 constructs creating disease relevant mutant proteins. Mutagenesis of MEGF10 in pDC315 and pSecTag2a vectors was performed using QuikChange XL Mutagenesis Kit (Agilent Technologies) following the manufacturer's instructions. Briefly, a pair of 30 - 31 bp mutagenic primers were designed, each containing the desired mutation in the centre and capable of annealing to the same sequence on opposite strands of the plasmid. Primers had a melting temperature (T_m) greater than 75°C, a GC content of 40 - 50% and terminated in one or more C or G bases. Primers were synthesised by IDT.

The T_m was calculated by: $Tm = 81.5 + 0.41(\%GC) - (675/N) - \%mismatch$

Where *N* denotes the primer length in base pairs and the values for %GC and %mismatch are whole numbers.

The mutagenesis reaction was prepared for thermal cycling using the reaction mixtures described below and the components added in the order listed in Table 5. The thermal cycling conditions used are listed in Table 6.

The reaction was placed on ice for 2 min and a *Dpn* I digest performed to digest the parental (non-mutated) ds-DNA. For digestion 1 µl 10 U of *Dpn* I was added to each reaction and incubated at 37°C for 1 hr.

Table 5. Site directed mutagenesis reaction mixture.

Reaction Component	Amount
10x Reaction buffer	5 µl
dH_20	To a final volume of 50 µl
Template DNA	10 ng
Forward primer (10 µM)	1 µl
Reverse primer (10 µM)	1 µl
dNTP mix	1 µl
Quick Solution	3 µl
PFU Turbo DNA polymerase (2.5 U/ µl)	1 µl

Table 6. Site directed mutagenesis PCR cycling parameters.

Cycles	Step	Temperature (°C)	Time
1	Initial Denaturation	95	1 min
30	Denaturation	95	50 sec
	Annealing	60	50 sec
	Extension	68	1 min per kb of plasmid
1	Final Extension	68	7 min

2.7 Mammalian Cell Culture

All cell culture media and reagents were obtained from Gibco (Thermo Fisher Scientific). All reagents and materials used were sterile and all work was performed in a class II biological safety cabinet. All media was heated to 37°C prior to use. The media and growth conditions used for each cell line are listed in Table 7.

Table 7. Cell Lines and Media.

Cell Line	Media	Growth Conditions	Differentiation Conditions
C2C12	DMEM + 20% FBS + 1% P/S + 2% CEE	37°C, 5% CO_2	DMEM + 4% H/S, 1% P/S 37°C, 5% CO_2
C1F		33°C, 10% CO_2	
HEK-293	DMEM + 10% FBS + 1% P/S	37°C, 5% CO_2	n.a.
Ad293			n.a.

2.7.1 **C1F myoblasts**

The C1F cell line was derived from skeletal muscle tissue from the Immortomouse *H-2K*^{b}-tsA58 heterozygotes. To drive C1F cells muscle was dissected from the hindlimbs of one day old neonatal mice and digested with 0.1% collagenase and 0.6% trypsin. Cells were plated onto 0.01% gelatin coated 6 well plate wells in DMEM supplemented with 20% FBS, 2% CEE and gamma-interferon (γ-IFN). Cells were incubated at 33°C, 10% CO_2 clones of cells with the small, round morphology of myogenic cells were isolated and grown under permissive conditions. Cells were determined as myogenic based upon their ability to form multinucleated myotubes, when cultured at 39°C and were further characterized by staining for key markers of myogenic cells (Morgan et al., 1994; Peltzer et al., 2008). These cells possess a mutant T-antigen gene (tsA58), derived from SV40 virus, which is temperature sensitive and maintains the cells in a proliferative state. This gene is under the regulation of the γ-IFN inducible *H-2K*^{b} promoter. The cells proliferate in the presence of γ-IFN (20 U/ml) at 33°C and differentiate into multinucleated myotubes once γ-IFN is withdrawn and the incubation temperature increased to 37°C. Cells were seeded onto 13mm diameter

glass coverslips coated with 0.1% gelatin at a density of $1x10^4$ cells and incubated overnight in culture media (Table 7.).

2.7.2 **Differentiation of C1F myoblasts**

To induce differentiation in C1F cells the serum content of the media was reduced, the γ-IFN was withdrawn and the incubation temperature raised to 37°C with 5% CO_2. Differentiation media was composed of DMEM + GlutaMAX (Gibco) supplemented with 4% H/S, 1% chick embryo extract (E.G.G. Technologies) and 1% (v/v) Penicillin/Streptomycin (Gibco). Cells were incubated in differentiation media for between 3 and 7 days until the myoblasts had fused to form multinucleated myotubes (Morgan et al., 1994; Peltzer et al., 2008).

2.7.3 **Growth of Ad293 and HEK-293 Cells**

HEK-293 cells were first described by Graham et al. in 1977, and are derived from human embryonic kidney cells transformed with fragments of human adenovirus type 5 DNA to maintain growth in culture (Graham et al., 1977).

Ad293 cells are derived from the HEK-293 cell line but display increased cell adhesion compared to HEK-293 cells, which makes these cells less susceptible to disruption when grown as a monolayer in plaque assays. Ad293 cells express the adenovirus E1 gene in *trans*, which enables the production of infectious adenovirus particles when cells are transfected with E1-deleted adenovirus vectors, such as the pBHGlox vector (Ausubel, 1987; Graham et al., 1977).

These non-myoblast cells were cultured in DMEM supplemented with 10% FBS and 1% Pen/Strep at 37°C, 5% CO_2. Cells were typically passaged 2 - 3 times per week, once cells were ~70% confluent and media changed as required. To seed cells onto coverslips cells were prepared at $1x10^5$ cells/ml and seeded at 10^4 cells/coverslip.

2.7.4 **Recovery of cells from liquid nitrogen storage**

Vials of cells were recovered from liquid nitrogen storage by rapidly thawing the vial of cells at 37°C. The 1 ml of thawed cells was diluted into 10 ml of warmed media in a tissue culture flask. The flask was incubated in a humidified incubator with 4% CO_2.

2.7.5 **Passaging cells**

Once cells had reached a confluence of ~70% they are ready to be harvested and seeded at a lower density on a fresh tissue culture flask. Media was removed from the flask and the cells were gently washed with 5ml Dulbecco's phosphate buffered saline (DPBS) before being detached from the flask with 2 ml trypsin replacement TrypLE per 75 cm^3 flask. Cells were incubated with TrypLE for no longer than 5 min before recovering the cells with 8 ml media to give a final volume of 10 ml. Cells were centrifuged at 1000 *x g* for 5 min to pellet before resuspending in 10 ml fresh growth media. Cells were counted using a haemocytometer (Hawksley BS.748) and the cells seeded onto flasks at the required density in growth media.

2.7.6 **Storage of cells**

Stocks of cells at a low passage number were stored in liquid nitrogen for future use. Cells were harvested with TrypLE, pelleted and resuspended at ~$1x10^6$ cells/ml in growth media supplemented with 10% DMSO, to act as a cryo-protectant. 1 ml of cell suspension was transferred to cryovials (Nunc) and frozen in a polystyrene box at -80°C overnight. For long-term storage cryovials were transferred to a liquid nitrogen tank.

2.7.7 **Preparation of coverslips**

To visualise cells by microscopy cells were seeded onto 13 mm diameter coverslips at a density of $1x10^4$ cells in 0.5 ml culture media. Coverslips were prepared by performing an acid wash, in which coverslips were thoroughly washed with a 37% hydrochloric acid solution in water (Acros

Organics), washed five times with MilliQ pure water, and stored in 70% ethanol in the tissue culture hood.

2.7.8 **Seeding cells onto coverslips**

Prior to seeding with cells, individual coverslips were separated, excess ethanol allowed to evaporate before the coverslips were transferred to 4 or 24 well plates. Coverslips were coated with 0.1% gelatin for 20 min. Gelatin was aspirated and the harvested cell suspension was prepared at $1x10^5$ cells/ml and 100 µl cells added per coverslip. Cells were incubated at required growth temperature for 30 min to enable cells to attach before adding sufficient growth media to the wells.

2.7.9 **Transfection of mammalian cells**

To introduce DNA constructs to cell lines different techniques were used to efficiently transiently transfect or produce stable cell lines.

2.7.10 **Calcium chloride transfection**

For the production of stable cell lines HEK-293 cells were transiently transfected using calcium chloride. A 75 cm^3 flask was seeded with $4x10^5$ HEK-293 cells to give 10 - 20% confluence. Cells were incubated for 1 - 2 hr at 37°C to allow cells to attach. During the incubation 2 x HBS was warmed to room temperature and 20 min before transfection the transfection solution was prepared in a 15 ml tube. 25 µg DNA was prepared with sterile water to a volume of 439 µl and 61 µl of sterile-filtered 2 M calcium chloride added and mixed. 500 µl of freshly thawed 2x HBS (274 mM sodium chloride, 0.4 mM $Na_2HPO_4.7H_2O$, 55 mM HEPES, pH7.0) was added dropwise with constant mixing to generate a fine calcium phosphate-DNA precipitate. The transfection solution was added dropwise over the HEK-293 cells and cells returned to the incubator.

2.7.11 **Lipid-based transfection (FuGene®)**

For transient transfections coverslips were seeded with $1x10^4$ cells and incubated overnight. FuGene6 Transfection Reagent (Promega) was warmed to room temperature and 6 µl was mixed with 200 µl 4°C serum-free DMEM media in a 1.5 ml Eppendorf tube and incubated for 5 min. 2 µg of DNA was added to the FuGene, mixed gently by flicking and incubated at room temperature for 15 min. The growth media was removed from the coverslips and 450 µl of fresh media was added. 50 µl of the transfection mixture was added dropwise to the centre of each well and incubated at required growth conditions for 24 – 48 hrs.

2.8 Immunocytochemistry

Immunocytochemistry was performed to visualise expression of specific proteins within cultured cells. Cells were seeded onto coverslips as previously described (2.7.8).

2.8.1 **Fixation of cells**

Cells were grown, transfected or manipulated as required and then fixed by adding a final concentration of warmed 2% paraformaldehyde (PFA) diluted in media and incubated at room temperature for 20 min. Cells were washed three times with DPBS and stored at 4°C.

2.8.2 **Antibodies**

Table 8. Primary antibodies.

Primary antibodies used in immunofluorescence and western blotting. Listed in alphabetical order.

Antibody	Company	Species	Dilution (IF)	Dilution (WB)
A4.1025	Hybridoma	Mouse	1:10	
CD34 (RAM34)	BD Pharminogen	Mouse	1:50	
C-myc (9E10)	Sigma	Mouse		1:5000
GAPDH	Sigma	Rabbit		1:5000
GFP (AB10145)	Millipore	Rabbit		1:1000
GFP	CUSABIO	Mouse		1:1000
MEGF10 (ABC10)	Millipore	Rabbit	1:200	1:1000
MEGF10 (S-18) sc-54244	Santa Cruz	Goat	1:50	1:250
MEGF10 (HPA026876)	Sigma Prestige	Rabbit	1:200	1:1000
MyoD (MA1-41017)	Thermo Scientific	Mouse	1:100	1:500
Myogenin (F5D)	DSHB	Mouse	1:50	1:1000
Pax7 sup.	DSHB	Mouse	1:20	1:50

Table 9. Secondary antibodies.

Secondary antibodies used in immunofluorescence and western blotting.

Antibody		Species	Dilution (IF)	Dilution (WB)
Alexa 488 anti-mouse	Invitrogen	Goat	1:400	-
Alexa 546 anti-mouse		Goat	1:400	-
Alexa 488 anti-rabbit		Goat	1:400	-
Alexa 546 anti-rabbit		Goat	1:400	-
Alexa 488 anti-rat		Donkey	1:400	-
Alexa Fluor 647 anti-rabbit		Goat	1:400	-
FITC Phalloidin	Sigma		1:100	-
TRITC Phalloidin	Sigma		1:100	-
DAPI	Sigma		1:500	-
Anti-mouse IgG poly-HRP	Sigma	Goat	-	1:5000
Anti-rabbit IgG poly-HRP	Pierce	Goat	-	1:5000

2.8.3 **Permeabilisation, immunocytochemistry and mounting coverslips**

Coverslips were transferred to the staining board to reduce the volume of antibodies needed to stain cells. To enable antibodies to recognize proteins within the cell, the membrane was permeabilised by adding 50 µl 0.1% Triton X-100 diluted in PBS with 1% (w/v) bovine serum albumin (BSA) to each coverslip for 5 min prior to staining. Primary antibodies were diluted in wash buffer (PBS with 1% (w/v) BSA) using dilutions described in Table 8. The primary antibody was added to each coverslip, diluted in 50 µl PBS, and incubated at room temperature for 1 hr in a moist, dark chamber. Coverslips were washed five times in wash buffer before adding the secondary antibody solution diluted in wash buffer at dilutions listed in Table 9. Secondary antibody was added to each coverslip, diluted in 50 µl PBS, and incubated for 1 hr as before. Coverslips were washed five times in wash buffer, and once in PBS prior to mounting on microscope slides using ProLong® Gold anti-fade mountant (Invitrogen), a curing mountant that forms a optical path with a refractive index (RI) of 1.47 suitable for imaging and allows longer-term storage of slides. Slides were allowed to dry overnight at room temperature in the dark and stored at 4°C prior to visualisation.

2.8.4 **Visualisation**

Cells were imaged by deconvolution microscopy using the Delta Vision Widefield Deconvolution microscope, (Delta Vision, USA). The system uses an Olympus IX-70 epifluorescence microscope equipped with excitation/emission filters for DAPI (ex 360/40 nm, em 457/50 nm), FITC / GFP (ex 490/20 nm, em 528/38 nm), TRITC / Rhodamine (ex 555/28 nm, em 617/73 nm) and Cy5 / AlexaFluor647 (ex 640/20 nm, em 685/40 nm). The camera, shutters and software are controlled by SoftWoRX software (Applied Precision Inc.).

2.9 Isolation of single fibres from murine skeletal muscle

Thanks to Sara Cruz Migoni from the Borycki lab (Sheffield) for teaching me the single fibre isolation technique.

Six week old C57BL/6J wildtype mice were euthanized by cervical dislocation before being handed out from the animal facility to be dissected. The extensor digitorum longus (EDL) was dissected from the leg, although the gastrocnemius was also dissected to enable sufficient fibres to be isolated for staining. The whole leg was cleaned with 70% ethanol and the hindlimb shaved using a scalpel. Loose hairs were removed and skin cleaned with 70% ethanol.

2.9.1 **Dissection of muscle**

2.9.1.1 **Dissection of extensor digitorum longus (EDL)**

To isolate the EDL, a small incision was made through the skin from the knee down to the paw. The skin was pulled back from the underlying muscle on both sides of the incision. The mouse was pinned onto a dissecting board and the connective tissue that covers the muscles was carefully removed using Cohan-Vannas spring scissors and tweezers. The four tendons of the EDL were exposed in the foot and tweezers were used to help cut the four tendons at once. The large TA tendon, located near the ankle on the interior side of the leg, was cut with the Cohan-Vannas scissors. To release the EDL muscle both the EDL and TA muscle tendons were exposed and cut. The four long EDL tendons were teased out at the ankle with fine tweezers. The TA muscle was lifted upwards and the EDL muscle beneath was carefully teased out by gently pulling the tendon from the knee out (Figure 12.).

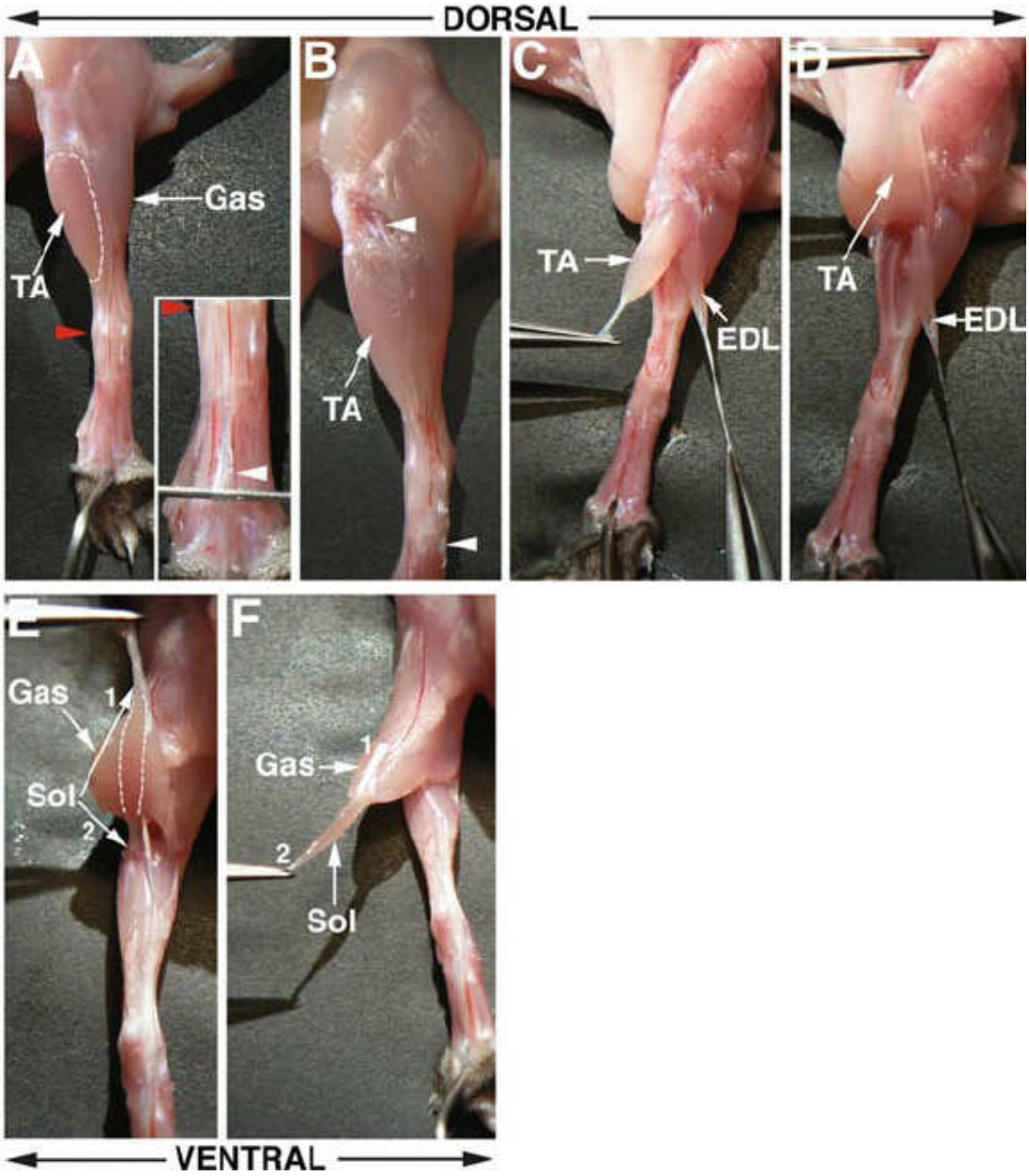

Figure 12. Dissection of murine EDL and gastrocnemius muscle.

Dorsal (A - D) and ventral (E - F) views of skeletal muscle in the leg of a C57BL/6J mouse. Arrows show EDL and gastrocnemius (Gas) muscle as well as the neighbouring soleus (Sol) and tibialis anterior (TA) muscles. (Taken from (Shinin et al., 2009).

2.9.1.2 **Dissection of gastrocnemius**

The gastrocnemius was dissected from the hindlimb by removing the fur with a scalpel. An incision was made and tweezers used to pull back the skin to expose the underlying muscle. Cohan-Vannas scissors were used to carefully cut and remove the connective tissue covering the muscles. The distal tendon of the gastrocnemius was cut and the muscle gently pulled back using tweezers. Cohan-Vannas scissors were used to gently release the muscle and cut the proximal tendons (Figure 12.).

2.9.2 **Digestion of muscle and separation of muscle fibres**

The isolated muscle was handled by the tendons to avoid damaging the muscle, and transferred to a solution of sterile-filtered 2 mg/ml collagenase Type I from *Clostridium histolyticum* (Sigma) diluted in DMEM + 1% P/S (10,000 U/ml Gibco). Muscle was digested at 37°C for 1 hr 20 min.

During the digestion 60 mm diameter tissue culture dishes (Nunc) were coated with 10% H/S diluted in PBS. Three dishes were prepared with 5ml isolation media (DMEM + 1% P/S) for each muscle digested. Sufficient dishes for subsequent culture were prepared with 5ml culture media (DMEM supplemented with GlutaMAX, Na Pyruvate [Gibco], 10% H/S, 0.5% CEE (v/v), 1% P/S).

After digestion the muscle bulk looked swollen and loose fibres were visible on the stereomicroscope. All subsequent work was performed using a stereomicroscope to clearly visualise the isolated fibres. The muscle bulk was transferred to a prepared dish of isolation media using fire-polished wide bore glass pipette coated with 10% H/S. The muscle was flushed with media using the wide bore pipette to release fibres, with care being taken not to touch the muscle bulk, until 10 - 15 fibres had been released. The muscle bulk was then transferred to a second dish of isolation media and all the fibres released as before. Single isolated fibres, defined as individual fibres that were straight, transparent and without debris, were picked and transferred to the third dish of isolation media using a fire-polished, narrow-bore glass pipette coated with 10% H/S.

2.9.3 **Culture of muscle fibres**

Isolated single fibres were transferred to 60 mm diameter tissue culture dishes (Corning) coated with 5% BSA in PBS and filled with 5 ml culture medium (DMEM + GlutaMAX + Na Pyruvate [Gibco] + 10% H/S + 0.5% CEE + 1% P/S). Fibres were cultured in suspension in culture medium (DMEM supplemented with GlutaMAX, Na Pyruvate [Gibco], 10% H/S, 0.5% CEE (v/v), 1% P/S) at 37°C, 5% CO_2 for 24 - 120 hrs.

2.9.4 **Fixation and staining of fibres**

To fix freshly isolated and cultured single fibres, the fibres were transferred to a 2 ml Eppendorf tube using a narrow-bore, fire-polished glass pipette coated with 10% H/S and allowed to settle to the bottom for 3 min. Excess medium was carefully removed with a pipette without disturbing the fibres, and the fibres were fixed with 500 µl warmed 4% PFA for 20 min. Fibres were washed three times for 3 min with 700 µl PBS. Fibres were stored in 700 µl PBS at 4°C before staining.

Fibres were stained by permeabilising membranes with 0.5% Triton X-100/PBS (PBST) for 10 min before washing three times for 3 min with PBS. Non-specific antibody binding was reduced by incubating the fibres with 500 µl blocking solution (20% H/S) for 30 min at room temperature. The primary antibody solution was prepared in PBS following dilutions described in Table 8. and fibres were incubated with 500 µl of antibody with gently rocking for 2 hrs at room temperature or at 4°C overnight. The primary antibody was removed and fibres were washed three times for 3 min with 500 µl of PBS containing 0.025% Tween. Secondary antibodies were prepared in PBS according to the dilutions described in Table 9. and fibres were incubated at room temperature for 1 hr 30 min with gentle rocking. The secondary antibody was removed and fibres washed three times for 3 min with 500 µl of PBS with 0.025% Tween and a final 500 µl PBS wash was performed. Fibres were carefully selected with a fire-polished, narrow-bore glass pipette coated with 10% horse-serum and placed on a clean microscope slide. Excess PBS was removed and fibres air dried slightly before two drops of ProLong Gold antifade mounting medium was added. A

24 x 40 mm coverslip was placed on top and excess mounting medium removed. Slides were left to cure overnight in the dark, before storage at 4°C.

The method for the isolation and staining of single muscle fibres was based upon previously published protocols (Collins, 2009; Pasut et al., 2013).

2.10 Adenoviral Production

2.10.1 **Co-transfection of Ad293 cells for viral production**

Ad293 cells were plated out onto a 25 cm^3 flask and incubated overnight. Cells were 60% confluent on the day of transfection. DNA plasmids were transfected into Ad293 cells using the FuGene protocol (2.7.11). The two DNA plasmids required for the co-transfection (pBHGlox and pDC315_MEGF10 constructs) were mixed at a ratio of 1:2. The transfection mix was added in a drop wise manner directly to the media of a T25 of Ad293 cells and incubated at 37°C, 5% CO_2 overnight. Cells were inspected visually for GFP expression using a fluorescent microscope (Nikon) using the 10x objective.

2.10.2 **Adenoviral amplification**

Transfected Ad293 cells were grown to confluence with most of the cells showing GFP expression. After 48 hrs cells were harvested using a cell scraper and used to seed two 75 cm^3 tissue culture flasks. The cells were incubated at 37°C, 5% CO_2 and inspected daily for viral production, indicated by the infected cells becoming round and detaching from the surface. After 10 days the cells showed at least 50% cytopathic effect and were harvested using a cell scraper. Cells were pelleted by centrifugation at 2000 *x g* for 10 min before the supernatant was aspirated and the pellet resuspended in 500 µl PBS and transferred to an Eppendorf tube.

Virus was released from the cells using a freeze-thaw method. Ethanol was added on top of dry ice and the cells frozen by floating the Eppendorf tube on top of the ethanol for 5 min. Cells were thawed in a beaker of room

temperature water and once defrosted the cells were mixed by vortex. The process was repeated three times. The cells were centrifuged at 5000 xg for 10 min to pellet the cell debris, leaving the adenovirus in the supernatant. A 25 cm^2 flask of Ad293 cells were incubated with 400 µl virus + 100 µl media for 2 hr. 5ml of media was then added and the cells incubated for 3 days until the viral infection caused the cells to round up and become detached from the dish. The virus was harvested as described previously.

The virus was amplified three times in Ad293 Cells to increase the adenoviral titre:

Amplification	Flasks of Ad293 Cells	Amount of Virus
1	1xT25	400 µl
2	2xT75	50 µl of amplification 1 per flask
3	5xT75	20 µl of amplification 2 per flask

After 50% of the cells had begun to show signs of infection, with the cells becoming round and detatching from the dish, in the third amplification, the cells were centrifuged and the pellet frozen at -80°C with the media from the flask before purification of the adenovirus.

2.10.3 **Adenopack adenovirus purification**

Adenovirus purification was performed using the Vivapure Adenopack 100 kit (Sartorius Stedim Biotech) following the manufacturer's instructions. Briefly, the infected cells and media were defrosted and the cells freeze-thawed, as described previously. The cells were centrifuged at 3500 *xg* for 15 min to pellet the cell debris and the viral supernatant was transferred to a 50 ml Falcon tube of thawed media. 50 µl of Benzonase® nuclease (1 µl per 1 ml of culture) was added to the viral supernatant, mixed and incubated at 37°C for 30 min. For purification of the virus, a retort stand and clamp was prepared in a tissue culture hood and all subsequent steps were performed under sterile conditions. The provided tube set and 50 ml syringe were set

up in the clamp with the feed tube in the viral supernatant. The supernatant was drawn up into the syringe and the one-way valve used to ensure all air was expelled from the syringe and tubing. A Minisart plus was attached to the syringe assembly and the supernatant filtered into a fresh container, leaving a small volume of supernatant to prevent air entering the Minisart. Loading buffer at 1/9 volume of the total filtered supernatant was added and the Minisart discarded. The Adenopack was prepared taking care to remove all air to ensure efficient viral binding. A 10 ml syringe was filled with PBS, connected to the Adenopack and 5 – 6 ml of PBS gently passed through. The syringe plunger was pumped up and down a few times to remove air from the Adenopack before the remaining PBS was passed, through leaving 1ml in the syringe to prevent air entering.

The feed tube from the 50 ml syringe and tube set was placed into the prepared sample solution. The air was removed from the syringe and valve and a wet-to-wet connection was made between the wetted Adenopack unit and the tube outlet. The prepared sample was slowly passed through the Adenopack unit at a rate of approximately 10 ml/min, determined by being able to count single drops. To prevent air entering the system 1 - 2 ml of sample was left in the syringe. The Adenopack was washed by slowly passing through 100 ml of washing buffer using a higher flow-rate, leaving 1-2 ml in the syringe to prevent air entering the system. To elute the virus, the Adenopack was removed from the tube set and attached to a 10 ml syringe filled with 5 ml elution buffer. The syringe was held over a sterile 15 ml tube and 1 ml of elution buffer was very slowly passed through the Adenopack over 1 - 2 min. The Adenopack was then incubated for 10 min at room temperature before slowly passing the remaining elution buffer through at approximately 1 ml/min.

2.10.4 **Storage of adenovirus**

The virus was concentrated and the buffer exchanged to storage buffer (20 mM Tris/HCl, 25 mM NaCl, 2.5% glycerol (w/v), pH8). 1 ml of the purified virus in storage buffer was dispensed into 10 x 50 µl and 1 x 500 µl aliquots.

2.10.5 **Viral Titre Assay**

The viral titre was calculated using the tissue culture infectious dose 50 ($TCID_{50}$) method (AdEasyVector System, Qbiogen, Inc.). A 96 well plate was prepared with $1x10^4$ Ad293 cells per well incubated at 37°C, 5% CO_2 overnight. The purified virus was serially diluted in media to give dilutions of 10^{-1} to 10^{-10} and one concentration was added to 10 wells per row of the 96 well plate, with the remaining two wells being left as a control without virus.

Cells were incubated for 10 days and the numbers of wells showing signs of viral infection (cytopathic effect, CPE.) were counted. The ratio of the number of wells showing cytopathic effect out of the 10 wells set up was calculated for each viral dilution. The sum of the ratios was calculated and denoted as 's'. The log^{10} of each viral dilution is denoted as 'd'.

To calculate the viral titre:

$T = 10^{1+d(s-0.5)}$

$T = 10^{1+1(7.7-0.5)} = 10^{8.2}$ for 100 µl dilution. Therefore $TCID_{50}$ is $10^{9.2}$/ml

To calculate the PFU/ml: $T = 1x10^{9.2-0.7} = 1x10^{8.5}$ PFU/ml = $3x10^{8}$ PFU/ml

2.11 Protein expression, purification and quantification

2.11.1 **Production of stable cell lines expressing secreted protein constructs**

Stable cell lines expressing secreted constructs of MEGF10 were produced for mammalian protein expression. pSecTag plasmid constructs were transfected into HEK-293 cells by calcium chloride transfection (2.7.10). Cells were harvested from 75 cm^3 flasks 48 hrs post-transfection, counted by haemocytometer and prepared at $1x10^5$cells/ml. Two 100 mM diameter tissue culture dishes (Corning) were seeded with $2x10^4$ cells in 10 ml selection media (DMEM supplemented with 10% FBS, 1% P/S and 200 µg/ml Zeocin). Selection media was changed every 3 – 4 days, for

10 days, until cells not expressing the plasmid died and only single colonies of cells expressing the Zeocin resistance in pSecTag2A vector survived. After 10 days single colonies from each plate were picked using a blue plastic pipette tip and used to seed duplicate wells in two 24 well plates. Colonies were plated in non-selective media to enable to cells to recover and grow. Plates were incubated at 37°C, 5% CO_2 for 10 days changing the media every 3 - 4 days. Media samples were taken from each well to be analysed by dot blot to determine the clone with the highest expression level of secreted protein.

2.11.1.1 **Dot blot**

A dot blot was performed as a relatively rapid diagnostic test to determine the level of secreted protein expression into the media of HEK-293 cells. A nitrocellulose membrane was cut to the required size and equilibrated in PBS for 20 min prior to use. The dot blot apparatus was cleaned with 70% ethanol and a piece of 3 mm Whatman chromatography paper placed in the base of the apparatus. A piece of 3 mm Whatman chromatography paper was pre-soaked in PBS and placed on the 96 well plate layout at the centre of the dot blot apparatus (ScotLab) and the equilibrated nitrocellulose membrane placed on top. The top portion of the dot blot apparatus was placed on top and fixed in position by firmly tightening the screws. The lid was sealed in place by turning on a vacuum pump. Samples were loaded with the vacuum pump switched off to ensure even distribution onto the membrane beneath. 100 µl of each sample was loaded into the respective wells of the dot blot apparatus and the vacuum switched on to allow media to be drawn onto the membrane. The membrane was removed from the apparatus and transfer to a 50 ml falcon tube and blocked with 3% (w/v) milk for 1 hr at room temperature for 1 hr. The membrane was then treated in the same way as a western blot membrane for antibody incubations, washes and development (2.12.5). Layout of the dot blot is shown in Figure 13 A. and B.

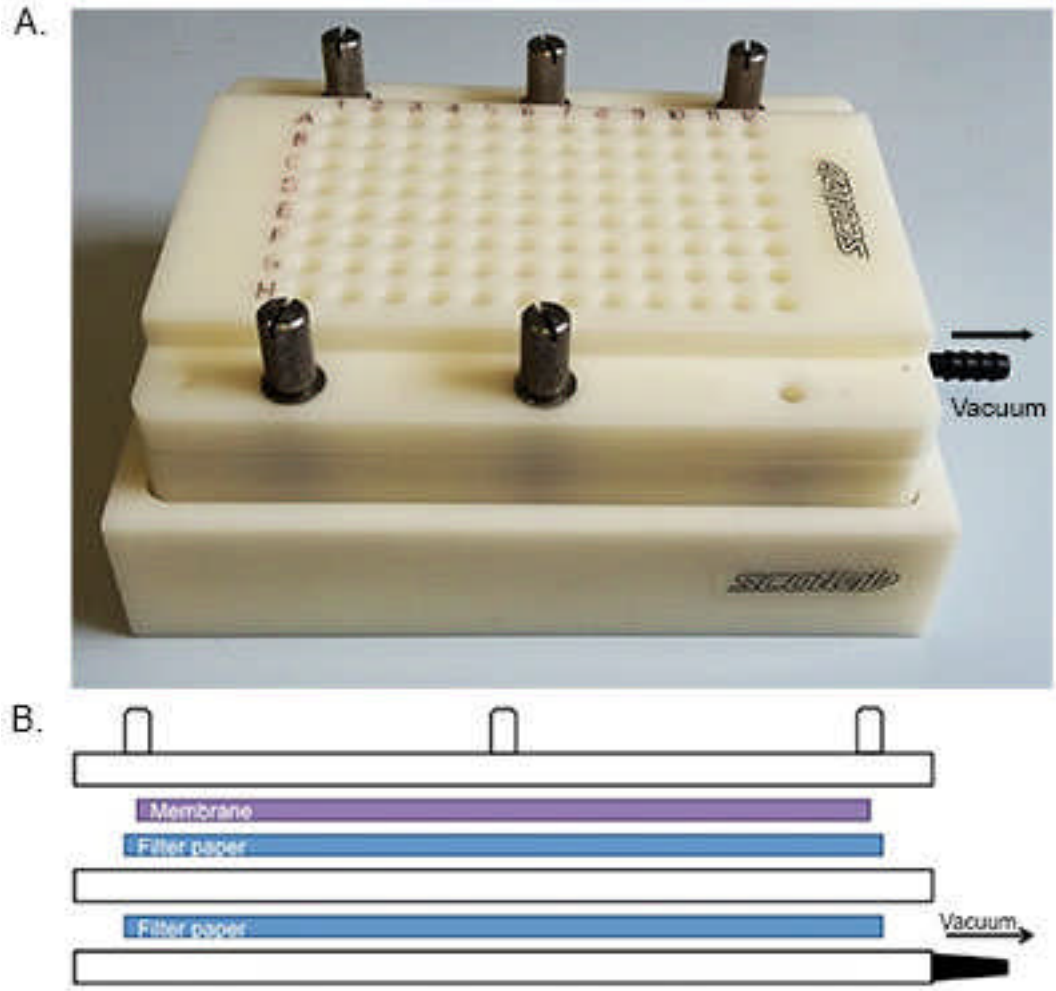

Figure 13. Dot blot apparatus.

A. Image of the dot blot apparatus (Scotlab), showing the connection to the vacuum pump and 96 well plate layout. **B.** Diagram of the layout of the three pieces of the dot blot apparatus, with 3 mm Whatman chromatography filter paper and membrane.

2.11.2 **Mammalian secreted protein expression in HEK-293 cells**

For efficient expression and purification of secreted mammalian protein constructs, HEK-293 stable cells lines were seeded onto five 75 cm^3 flasks coated with 20 µg/ml poly-L lysine. To coat flasks with poly-L lysine flasks were incubated with 7 ml of 20 µg/ml poly-L lysine diluted in dH_20 for 20 min at 37°C before it was removed and flasks allowed to dry overnight at 37°C. Cells were grown to 80% confluence in normal growth media (2.7) and then the medium was exchanged for OptiMEM low serum media (Gibco) to reduce contaminants in the later purification stages. Cells were cultured in OptiMEM for 3 days prior to harvesting the media and purifying the protein.

2.11.3 **Protein purification using nickel affinity chromatography**

The secreted protein constructs had a six histidine tag (6His) tag to enable purification by nickel affinity chromatography. OptiMEM media was harvested, centrifuged at 1000 *x g* for 5 min to pellet cells and incubated with 1 ml Complete His-Tag Purification Resin slurry (Roche) and Complete EDTA-free protease inhibitor cocktail tablet (Roche) for 30 min on a roller. Media was applied to the 5 ml column and the flow through collected. The resin was washed with five times column volume wash buffer (300 mM sodium chloride, 50 mM sodium phosphate). Protein was eluted with elution buffer (300 mM sodium chloride, 50 mM sodium phosphate and 200 mM imidazole).

2.11.4 **Protein dialysis**

Protein eluates in 300 mM sodium chloride, 50 mM sodium phosphate and 200 mM imidazole were pooled together and dialysed into 1 L PBS at 4°C overnight, using a Gebaflex Maxi Dialysis Tube (MWCO = 3.5 kDa) (Generon).

2.11.5 **Freezing purified proteins**

Purified proteins were stored in aliquots at -80°C.

2.11.6 **Measuring protein concentration by spectrophotometry**

The concentration of purified proteins was measured using a Cary® 50 Bio UV-visible spectrophotometer [Varian]. 1 ml of buffer was used as a blank before 1 ml of the sample was placed into a cuvette (Fisher) and the absorbance measured at 280 nm.

The concentration was calculated based on the extinction coefficients predicted for each construct assuming all pairs of Cys residues form cysteine bonds by Protparam (Gasteiger et al., 2003).

2.12 Protein isolation and separation

2.12.1 **Preparation of whole cell extracts**

Samples were prepared by scraping cells directly into 2x sample buffer prior to boiling at 100°C for 10 min and freezing aliquots at -80°C.

Alternatively proteins were extracted and quantitated by BCA assay prior to preparing samples for SDS-PAGE and western blot. All steps were performed on ice. Immediately before use 1 ml lysis buffer (150 mM NaCl, 50 mM Tris (pH8), 1% Triton X-100, 1 mM EDTA (pH8)) was prepared with 10µl Halt Protease Inhibitor, single-use cocktail (Thermo Scientific). The harvested cell pellet was washed in PBS and transferred to a 1.5 ml centrifuge tube and the cells pelleted by centrifugation at 300 *xg* for 5 min at 4°C. The supernatant was removed and the pellet resuspended in 50 µl lysis buffer with protease inhibitor. The cells were incubated on ice for 30 min and were mixed by vortex every 5 min. Cells were centrifuged at 17,000 *xg* for 20 min at 4°C. The supernatant was transferred to a fresh 1.5 ml centrifuge tube and the lysate stored at -20°C.

2.12.2 **Quantification of protein using the BCA assay**

Protein concentration was calculated using the Pierce ® Micro BCA Protein Assay Kit (Thermo Scientific) for microplate procedure. Briefly, a BSA standard curve was prepared in Eppendorf tubes, changing tips and mixing

thoroughly by vortex in between each dilution. (2 mg/ml BSA stock solution, Pierce)

Tube	Vol. of MilliQ (µl)	Vol. and Source of BSA	Final [BSA] (µg/ml)
A	1900	100 µl of stock solution	100
B	600	400 µl of A	40
C	667	330 µl of A	30
D	500	500 µl of B	20
E	500	500 µl of C	15
F	500	500 µl of D	10
G	500	500 µl of F	5
H	500	500 µl of G	2.5
I	500	-	0 (Blank)

Cell lysates were diluted 1:250 to bring the concentration values within the range of the standard curve. Sufficient working reagent was prepared by calculating the number of samples to be tested:

(number of standards + number of unknowns) x number of replicates x volume of WR per sample = Total WR (ml)

The working reagent is composed of three reagents: Reagent A (MA), Reagent B (MB), Reagent C (MC) at a ratio of 25 : 24 : 1.

150 µl of each sample and the standard curve was pipetted in triplicate into the wells of a flat-bottomed, clear plastic 96 well plate (Nunc). The prepared working reagent was transferred to a reservoir and 150 µl was added to each well using multichannel pipette. The plate was gently mixed for 30 sec before being incubated at 37°C for 2 hrs. The plate was removed from the incubator and cooled to room temperature before reading. The absorbance at 544 nm was measured using a Polstar Optima plate reader. The concentration of the sample proteins was calculated based on the standard

curve of the average, blank corrected measurements for each BSA standard.

2.12.3 **SDS-PAGE**

Sodium dodecyl sulphate polyacrylamide gel electrophoresis (SDS-PAGE) was performed in order to separate protein samples according to their size. Glass gel plates at the required spacer thickness (Table 10. B.) (BioRad) were washed with detergent, cleaned with ethanol and dried prior to assembling gel casings. Gel casings were placed in a casting stand and checked for leaks with water. A separating gel was prepared and the percentage acrylamide used was determined according to the size of proteins to be resolved. Reagents were added in the order listed in Table 10., with the APS and TEMED being added simultaneously at the end immediately before the gel was poured. A layer of 70% ethanol was added on top to give the separating gel a level top and the gel was polymerized for 20 min at room temperature until fully set. Once the gel has set a 4% stacking gel was prepared and poured on top of the separating gel (Table 11.). The comb (10 or 15 well) was inserted and the gel allowed to set for 20 min.

Table 10. SDS-PAGE Separating Gel Composition.

The volume of reagents required to make 10 ml of 7.5 – 15% SDS-PAGE gels.

	15%	12%	10%	7.5%
Distilled Water (ml)	2.35	3.35	4.02	4.85
1.5 M Tris-HCl pH8.8 (ml)	2.50	2.50	2.50	2.50
10% (w/v) SDS stock (µl)	100.00	100.00	100.00	100.00
Acrylamide/Bis* (30% stock) (ml)	5.00	4.00	3.33	2.50
10% APS (µl)	50.00	50.00	50.00	50.00
TEMED (µl)	5.00	5.00	5.00	5.00
Total (ml)	10.00	10.00	10.00	10.00

(10% APS = 100 mg APS in 1 ml dH_2O)

Calculated volumes (in ml) required per gel slab: Mini Protein II system.

Spacer Thickness (mm)	Volume (ml)
0.50	2.80
0.75	4.20
1.00	5.60
1.50	8.40

Table 11. 4% Stacking Gel Composition

The volumes of each reagent needed to produce a 4%, 0.125M Tris, pH6.8 SDS-PAGE stacking gel.

	4%
Distilled Water (ml)	6.10
0.5M Tris-HCl, pH6.8 (ml)	2.50
10% (w/v) SDS (µl)	100.00
Acrylamide/Bis* (30% stock) (ml)	1.30
10% APS (µl)	50 (0.05%)
TEMED (µl)	10 (0.1%)
Total Volume (ml)	10.00

2.12.4 **Running SDS-PAGE gel**

Gels were transferred to the gel tank (BioRad); 1X running buffer was prepared from 10x stock (30 g/l TRIS base, 144 g/l Glycine, 10% SDS) by diluting 100 ml into 1 L of dH_2O and added to the centre of the apparatus. To determine the size of proteins separated by SDS-PAGE, 5 µl of PageRuler plus pre-stained protein ladder (Thermo Scientific) was loaded into the first well. Protein samples were loaded in subsequent wells. Typically a gel was run at a constant voltage of 100 V for 1 hr.

2.12.5 **Western Blot**

In order to detect a protein of interest in a complex cell lysate separated on an SDS-PAGE gel, proteins were transferred to a Hybond-ECL nitrocellulose membrane (Amersham). 1 L of 1x transfer buffer was prepared (10x Pierce Western Blot Transfer Buffer). The gel was removed from the running apparatus and the stacking gel cut off. The transfer stack was prepared in transfer buffer as depicted in Figure 14.

All the components were fully soaked in transfer buffer and the stack was carefully smoothed to ensure that air bubbles were removed. A corner of the nitrocellulose membrane and the corresponding corner of the gel were cut in order to allow orientation of the membrane. The cassette was transferred to the Bio-Rad transfer apparatus, the tank was filled with running buffer and the transfer was run at 400 mA for 1 hr.

Once the transfer was complete, the stack was removed from the apparatus and the membrane was checked to see if the coloured protein bands from the re-stained ladder had properly transferred. The membrane was blocked in 5% non-fat milk in PBS (AppliChem) for 1 hr at room temperature on a roller. Primary antibody was prepared in 5 ml antibody buffer (2% milk in PBS) and membrane was incubated with antibody overnight at 4°C. After incubation overnight at 4°C, the membrane was washed 5 times over the course of 1 hr with PBS + 0.05% Tween, with each wash being incubated at room temperature. The secondary HRP conjugated antibody, was diluted 1:5000 in 5 ml antibody buffer (2% w/v milk protein dissolved in PBS).

The membrane was incubated with the secondary antibody at room temperature, on the roller for 1 hr. The membrane was then washed five times with PBS + 0.05% Tween as before with a final 5 min wash with PBS alone. The membrane was then gently blotted on filter paper and transferred to a sheet of acetate. 2 ml of Super Signal West Pico Chemiluminescent Substrate (ThermoFisher) was applied to the membrane and incubated at room temperature for 10 min. The membrane was blotted dry on filter paper and returned to the acetate and covered with a second sheet of acetate and the casing sealed. The membrane was transferred to a dark room and exposed to Lumi-Film Chemiluminescent Detection Film (Roche) for between 1 sec and 25 min to obtain the correct exposure. The film was then developed using an X-Ograph imaging system compact x4.

Membranes were stored at 4°C in PBS. To reprobe a membrane for a different protein the membranes were stripped for 10 min in 5 ml Restore West stripping buffer before washing three times with 10 ml PBS. Membranes were then blocked with 5% (w/v) milk in PBS for 1 hr and probed as described above.

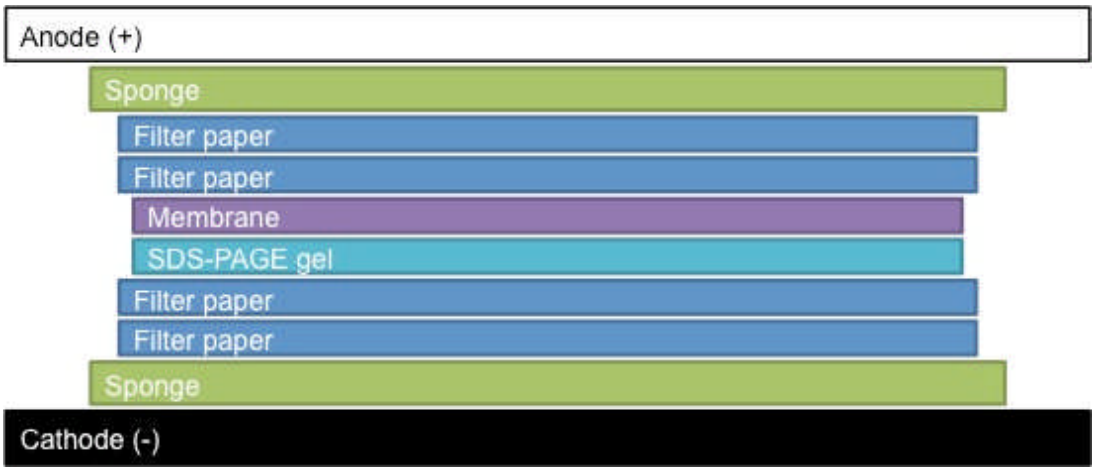

Figure 14. The layout of a western blot sandwich.

The black band represents the side of the sandwich, which is present closest to the anode. Green indicates the sponges and blue the filter papers at either side of the sandwich.

2.12.6 **Data anaylsis**

Notation in figure legends presents the number of biological repeats (n=) graphs show the mean average results and, where appropriate, error bars depict either the standard error of the mean (S.E.M.) or standard deviation (S.D.). To analyse statistical significance between conditions unpaired t-tests were performed, using GraphPad Prism version 6 for Mac, GraphPad Software, La Jolla California USA, www.graphpad.com. In figures the condition marked # was used as the reference against which the other conditions were compared. The level of statistical significance is indicated by the number of asterisks displayed.

3 Expression and localisation of endogenous MEGF10 in muscle tissue.

3.1 Introduction

MEGF10 has been shown to be important for the normal function of satellite cells within the skeletal muscle environment (Bröhl et al., 2012; Holterman et al., 2007). Levels of MEGF10 are ~ 8 fold higher in C2C12 myoblasts than in differentiated cells, as shown by qPCR, and ~100 fold in activated satellite cells isolated from 8 week old mice (Holterman et al., 2007). Overexpression of MEGF10 inhibited fusion (Holterman et al., 2007), this effect is similar to that found for high levels of Notch signalling (Bröhl et al., 2012), and MEGF10 has also been linked to Notch signalling (Holterman et al., 2007). Conversely, a double knockout of both the downstream effector of Notch signalling (Rbpj) and MyoD in mice increased levels of MEGF10 expression. In these double knockout animals, the satellite cells remain in the interstitial space and do not migrate to their characteristic location beneath the basal lamina of skeletal muscle fibres. This led to the suggestion that Notch signalling is important for the formation of the basal lamina around satellite cells, with MEGF10 playing a role in the adhesion of the satellite cells to muscle fibres under the basal lamina (Bröhl et al., 2012).

In contrast, other research has linked increases in MEGF10 to increases in myogenin, with changes in expression occurring in parallel, rather than linked to changes in MyoD expression (Holterman et al., 2007). Furthermore, this study showed that myogenin binds to the promoter region of MEGF10 to induce its expression suggesting that the mechanisms by which MEGF10 expression is regulated may be more complex than previously described (Park et al., 2014). Outside of these mouse models of MEGF10 function, a lack of MEGF10 was shown to result in the skeletal myopathy EMARDD in humans, in which muscle fibres have a reduced fibre diameter, and fewer nuclei per fibre, consistent with the expected effects on satellite cell function (Logan et al., 2011).

Given the rare nature of EMARDD and the invasive nature of the muscle biopsy procedure (Logan et al., 2011), animal or *in vitro* studies are required to study EMARDD. Previous papers studying MEGF10 and its orthologues have used a number of different model systems including: *Caenorhabitis elegans* (Lettre and Hengartner, 2006), *Danio rerio* (Boyden et al., 2012a), *Drosophila melanogaster* (Draper et al., 2014; Tung et al., 2013) and *Mus musculus* (Holterman et al., 2007). However, whilst these model systems have their advantages in being simple to work with and to follow the myogenic process they also have some drawbacks. For example, Draper is the single orthologue of MEGF10, MEGF11 and MEGF12 in *Drosophila*, making it difficult to tease out the specific functions of MEGF10. A mouse knockout model for MEGF10 has been described (Kay et al., 2012), but this only reported on effects in the retina with no description of any muscle phenotype. MEGF10 knockdown was demonstrated in starburst amacrine cells but not in other mouse tissues.

A number of different cultured mammalian cell lines have also been used to study MEGF10, including HEK-293 cells stably expressing MEGF10_eGFP (Suzuki and Nakayama, 2007a), HeLa cells (Hamon et al., 2006; Singh et al., 2010) and C2C12 cells (Holterman et al., 2007; Mitsuhashi et al., 2013). However, HeLa and HEK-293 cells are not derived from muscle, and the cultured C2C12 myoblasts do not recreate the specific satellite cell niche *in vitro*. C2C12 cells were derived as a diploid subclone from C2 myoblasts (Blau et al., 1985). C2 myoblasts were derived from the C3H mouse 70 hr after a leg muscle crush injury and were allowed to undergo a spontaneous transformation while in culture, which led to their immortalization (Morgan et al., 1992). These murine myoblasts can be induced to form myotubes that express proteins typically present in *in vivo* muscle (Blau et al., 1985; Yaffe and Saxel, 1977). C2C12 cells have been well studied, including a thorough examination of protein expression, using LC-MS-based shotgun profiling (mass spectrometry), over the course of differentiation (Kislinger et al., 2005), in which ~1800 different proteins were investigated, and the results broadly agreed with an earlier study that used gene profiling (Tomczak et al., 2003). However, neither of these reports showed data on the expression of MEGF10.

However, C2C12 cells have the disadvantage that control over the switch from proliferation to differentiation is not complete in this cell line, due to the transformed nature of the cells. Commonly, differentiation is induced by serum deprivation however, while this promotes differentiation, it does not prevent undifferentiated cells in the culture from continuing to grow. These cells can form new muscle when implanted into nude mice but do not form mature pattern of differentiation in fibres, which may suggest their limited myogenic potential (Morgan et al., 1992). Moreover, when these cells are injected into mouse muscle in vivo, they form non-muscular tumours after a couple of weeks (Morgan et al., 2002; Morgan et al., 1993; Wernig et al., 1991).

The lack of control of differentiation and proliferation in C2C12 cells led to the derivation of alternative myoblast cell culture systems. Our laboratory commonly uses myoblast cultures derived from isolated skeletal muscle tissue from the Immortomouse *H-2K*^{b}-tsA58, which have several advantages over C2 cells (Jat et al., 1991; Morgan et al., 1994). These cells possess a temperature sensitive mutant T-antigen gene (tsA58), derived from the SV40 virus, that maintains the cells in a proliferative state. This gene is under the regulation of the γ-interferon sensitive *H-2K*^{b} promoter. Cells grown in the presence of γ-interferon at 33°C switch on tsA58 gene expression which promotes cell proliferation, with the T-antigen remaining stable at 33°C. Withdrawal of γ-interferon prevents further tsA58 gene transcription, while incubating the cells at 37 - 39°C degrades any remaining T-antigen, providing a mechanism to stop myoblast proliferation, while allowing differentiation (Morgan et al., 1994). Several clonal cell lines have been derived from this mouse model, including C1F (Morgan et al., 1994; Peltzer et al., 2008), which is a highly fusigenic clone. These cells provide a good alternative *in vitro* culture model to those of C2C12 cells, with a more controllable switch between proliferation and fusion. Furthermore, the C1F cell line is simple to culture and appears to retain some stem cell-like properties through the cells ability to differentiate after serial passage (Morgan et al., 1994). Implantation of these cells into mice leads to the formation of normal muscle but non-muscular tumours are not subsequently formed as seen in C2C12 cells (Morgan et al., 1994; Morgan et al., 2002).

C1F cells, and other clones derived from this mouse model, are capable of undergoing differentiation into fibres with a more mature phenotype than described for other myoblast lines such as C2C12 cells and primary satellite cell cultures (LaFramboise et al., 2003; Morgan et al., 2002). These characteristics of C1F cells make them a good model to investigate MEGF10 in an *in vitro* cultured myoblast system.

Whilst C2C12 and C1F myoblasts are simple to culture, this approach does not fully recreate the satellite cell niche. To investigate MEGF10 expression in activated satellite cells within the stem cells niche, a number of approaches can be used. One is to isolate single muscle fibres, and the culture of these fibres outside of the skeletal muscle environment causes satellite cells to become activated and proliferate beneath the basal lamina (Pasut et al., 2012). This approach has often been used to investigate satellite cell biology (Beauchamp et al., 2000; Cornelison and Wold, 1997; Zammit et al., 2006) and was used to investigate MEGF10 expression and localisation in quiescent and activated satellite cells (Holterman et al., 2007). Therefore, I have also used this model to perform a more in depth characterisation of the expression and localisation of MEGF10.

Finally, satellite cells can also be activated *in vivo* using a number of different strategies. A number of techniques, which provoke major muscle damage and subsequent regeneration, involve the injection of muscle with toxins such as cobra cardiotoxin (ctx); chemicals such as barium chloride and physical damage such as freeze injury. Each of these techniques have been compared and whilst each technique induces muscle regeneration the time course of the regenerative process can vary quite significantly between the different methods used (Hardy et al., 2016). Ctx treatment has already been used to show by qPCR that MEGF10 expression increases markedly 3 days after injury, as the muscle is regenerating (Holterman et al., 2007). Each of these models cause severe damage to the muscle and large reduction in stem cell number beyond what would be expected within the physiological range of muscle damage. Therefore, I have used a more physiological model of muscle damage, in which the EDL muscle is overloaded by removing the tibialis anterior (TA) muscle. This treatment both increases the sarcomere length of the EDL muscle and causes a mild

hypertrophy (Egginton et al., 2011; Egginton et al., 1998). Studies have shown that satellite cells are important in hypertrophic muscle regeneration and therefore we would expect to be able to observe activated satellite cells *in vivo* through this approach (Liu et al., 2015b; Rosenblatt et al., 1994).

I have therefore used these three approaches: an *in vitro* muscle cell culture model, an isolated fibre culture model, and an *in vivo* model to investigate the expression pattern of MEGF10 to determine its spatial and temporal localisation over the course of myogenesis. I first characterised three commercially available antibodies used within the literature to determine their specificity for MEGF10 and suitability for western blotting and immunofluorescence. To enable me to do this, I used eGFP_MEGF10 (described in Chapter 4), and the purified ECD from MEGF10, expressed using HEK-293 cells (Chapter 5). I then used the best antibody to investigate expression of MEGF10 in relation to other satellite cell markers in all three model systems. In addition, I use RNAseq to investigate the expression of MEGF10 and other muscle specific proteins in the cultured cell model during differentiation.

3.2 Methods

3.2.1 **RNAseq**

In order to determine the relative expression levels of RNA in myoblast cells at different stages of differentiation the TruSeq stranded mRNA sample preparation, low sample (LS) protocol (Illumina) was followed (an overview of the process is depicted in Figure 14.). Thanks to Clare Logan and Gabrielle Wheway, LIMM for their help in setting up the RNA seq experiment and processing the data. Sequencing was performed at at the Next Generation Sequencing Facility, LIMM.

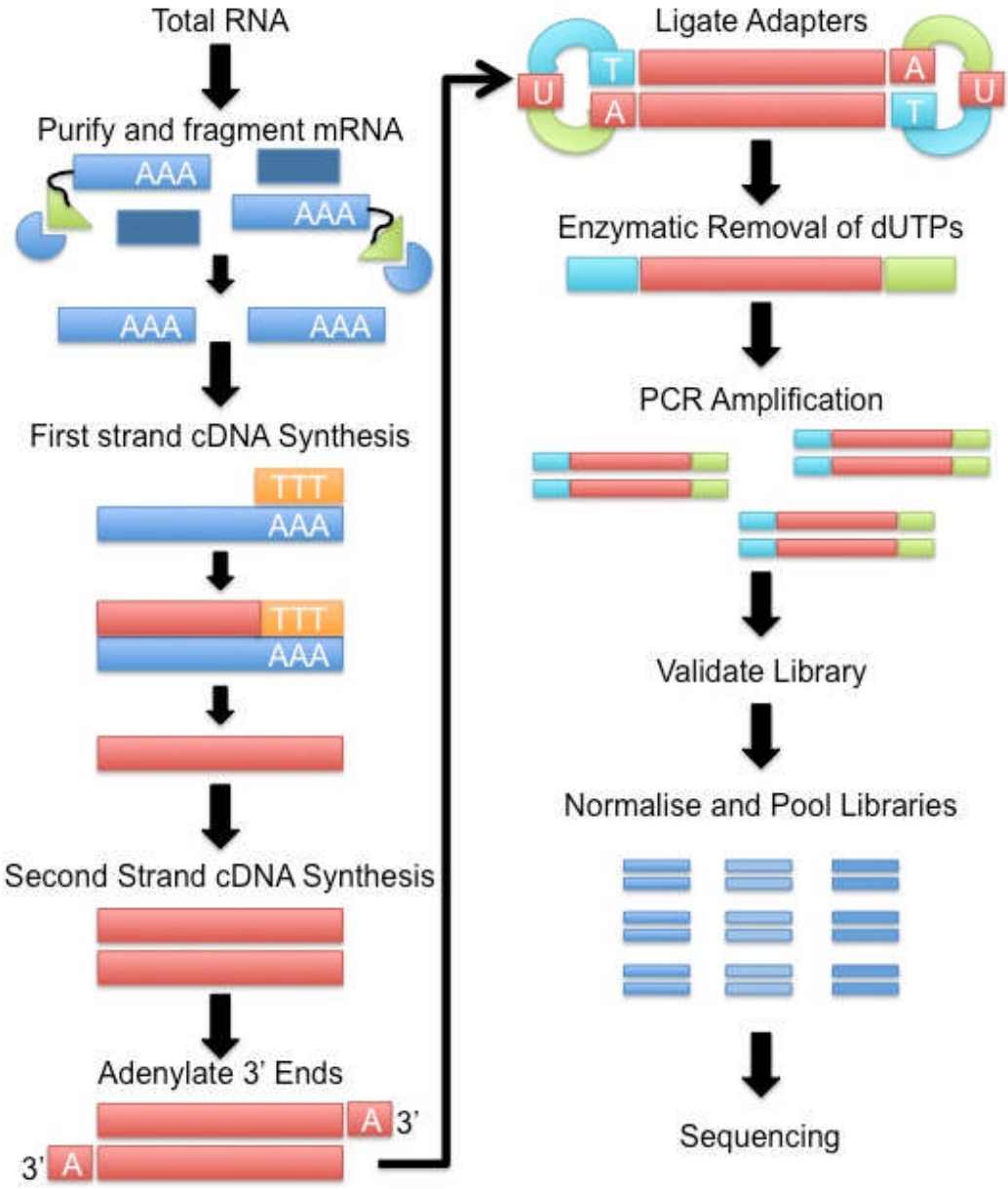

Figure 15. Overview of the TruSeq stranded mRNA protocol.

A flow diagram depicting the key stages in RNA sequencing, including the isolation and fragmentation of mRNA, the synthesis of cDNA, adaptor ligation and PCR amplification to form a validated library (Diagram adapted from the TruSeq manual).

3.2.1.1 **Handling and isolating total RNA from mammalian cells**

To determine the levels of MEGF10 expression, RNA was isolated from C1F cells at different stages of differentiation. Three 25 cm^2 flasks were seeded with $2x10^5$ C1F cells and cultured to proliferate for 24 hrs as undifferentiated myoblasts (UD) or cultured to proliferate before being switched to differentiation conditions and differentiated for one or seven days, to produce early fusing myoblasts (D1) and fully differentiated myotubes (D7) respectively. The cells were harvested from each flask by cell scraper into 5 ml fresh growth media and pelleted by centrifugation at 1000 *xg* for 5 min at 4°C, washed in 1 ml DPBS and transferred to a 1.5 ml centrifuge tube. Cells were pelleted by centrifugation at 13,000 *xg* for 5 min at 4°C and stored at -80°C.

To make RNA, C1F cells pellets were thawed and total RNA was extracted using the GenElute™ Mammalian Total RNA Miniprep Kit (Sigma) following the manufacturers' protocol. Briefly, each pellet was resuspended in 500 µl lysis solution prepared with fresh β-mercaptoethanol and mixed thoroughly by vortex. To remove cellular debris and shear any DNA the lysate was filtered using a GenElute Filtration Column at 16,200 *xg* for 2 min. 500 µl of 70% ethanol was added to the filtered lysate and thoroughly mixed by vortex.

To bind the RNA to a column the lysate was loaded onto a GenElute binding column by centrifuging at 16,200 *xg* for 15 sec. The flow-through was discarded, column washed with 500 µl wash solution 1 and centrifuged at 16,200 *xg* for 15 sec. All subsequent centrifugation steps were at 16,200 *xg*. The binding column was transferred to a fresh 2 ml collection tube and washed twice with 500 µl wash solution 2. The column was dried by centrifuging for 2 min.

The RNA was eluted from the column with 50 µl elution solution by centrifuging for 1 min. The RNA was stored on ice and the concentration measured using the Nanodrop. Absorbance was measured at 260 nm and concentration calculated using the Beer-Lambert law, which predicts a linear change in absorbance with concentration, where an A260 reading of 1.0 is equivalent to ~40 µg/ml of single-stranded RNA. The ratio of absorbance

readings at 260 nm and 280 nm was used to assess the purity of the RNA with a ratio between 1.8 and 2.1 indicating 'pure' RNA. The level of contaminants that absorb at 230 nm such as EDTA or carbohydrates were checked by measuring the 260/30 nm ratio where a ratio of 2.0 - 2.2 indicates pure RNA. RNA was stored at -80°C until ready to perform RNAseq.

3.2.1.2 **Quantification of RNA using the Agilent 2100 bioanalyser**

To check the quality and quantity of RNA samples, the RNA 6000 Nano Kit (Agilent) was used following the manufacturers' instructions. Briefly, an Agilent RNA 6000 Nano gel matrix was prepared by adding 1 µl of RNAdye concentrate to a 65 µl aliquot of sterile filtered gel. The gel was mixed by vortex and centrifuged at room temperature, at 13,000 *xg* for 10 min. An RNA nanochip (Figure 16. B.) was placed on the chip priming station and 9 µl of gel-dye mix was added to the bottom of well 'G' (Figure 16. C.1). The plunger on the chip priming station was positioned to 1ml and the chip priming station clicked shut. The chip was pressurised by pressing the plunger down until it is held by the clip (Figure 16. C.2). After exactly 30 sec the plunger was released, and after a further 30 sec was slowly pulled back to the 1 ml position. The chip priming station was opened and 9 µl of gel-dye mix was added to two wells above the well marked 'G' (Figure 16. C.3). The RNA 6000 Nano marker was loaded onto the chip by pipetting the 5 µl into the ladder well and each of the 12 sample wells (Figure 16. C. 4). The RNA ladder was thawed, heated to 70°C for 2 min to minimise secondary structure and 1 µl added to the ladder well on the chip (Figure 16. C. 5). 1 µl of each sample was added to the sample wells (Figure 16. C. 6). The chip was mixed at 2400 rpm or 1 min on an IKA vortexer. The chip was run in an Agilent 2100 Bioanalyzer, using the 2100 expert software (Figure 16. A.).

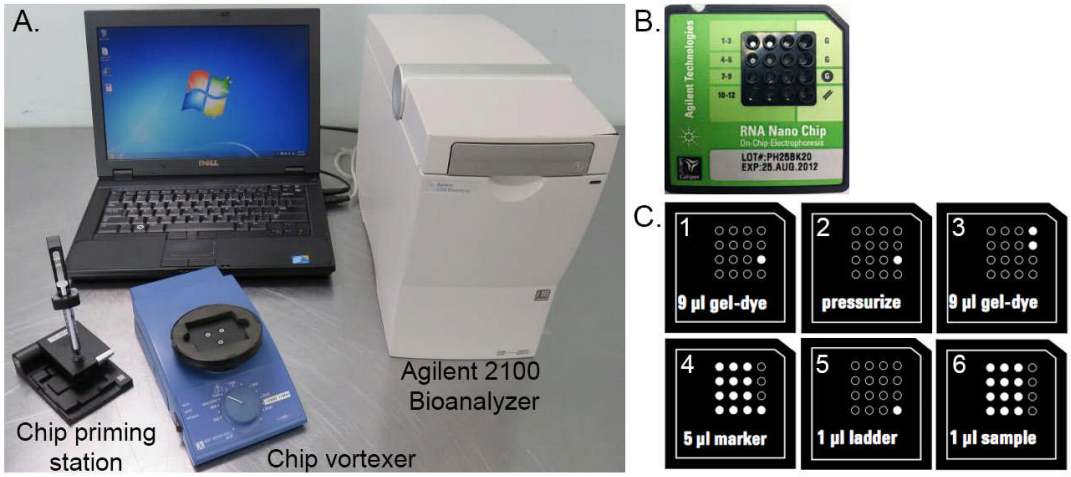

Figure 16. Agilent 2100 bioanalyzer equipment.

A. An example of the equipment used to measure RNA concentration (adapted from http://www.thelabworldgroup.com/agilent-g2938b-bioanalyzer). **B.** The RNA nano chip (Agilent), used to measure the concentration of RNA. **C.** The steps of priming, and loading the chip ready for analysis (Adapted from Agilent RNA 6000 Nano Kit protocol).

3.2.1.3 **Purification and fragmentation of mRNA**

To isolate the mRNA and fragment the RNA for sequencing, 1 µl isolated total RNA was diluted into 49 µl nuclease-free water to give a minimum concentration of 250 ng RNA in 50 µl. The RNA was transferred to a 96-well PCR plate and 50 µl of RNA purification beads were added to each well and mixed to enable binding of the polyA RNA to the oligo dT magnetic beads. The PCR plate was sealed and the RNA denatured by incubating at 65°C for 5 min, then cooled to 4°C before incubating on the bench for 5 min to enable RNA binding to the beads. The plate was placed on a magnetic stand for 5 min at room temperature to pull the beads out of solution and the supernatant discarded. The plate was removed from the magnetic stand and the beads were washed with 200 µl of bead washing buffer to remove any unbound RNA. The plate was returned to the magnetic stand for 5 min and the supernatant, containing ribosomal and other non-messenger RNA, was carefully removed. The plate was removed from the magnetic stand and 50 µl of elution buffer was added to each well and mixed to resuspend the beads. The plate was sealed and incubated in a thermal cycler at 80°C

for 2 min, then cooled to 25°C to release the mRNA and any contaminating rRNA from the beads.

Working on the bench, 50 µl of bead binding buffer was added to each well and mixed to allow mRNA to rebind to the beads. The plate was incubated at room temperature for 5 min and then transferred to the magnetic stand for a further 5 min. The supernatant was removed, the plate removed from the stand and the beads washed with 200 µl bead washing buffer. The plate was returned to the magnetic stand for 5 min and the supernatant, containing rRNA and additional contaminants, was removed. The plate was removed from the magnetic stand and 19.5 µl fragment, prime, finish mix, which contains random hexamers for reverse transcription priming, was added to each well and beads resuspended by mixing. The plate was sealed and incubated in a thermal cycler at 94°C for 8 min, cooled to 4°C and briefly spun down to elute, fragment and prime the RNA.

3.2.1.4 **First strand cDNA synthesis**

The plate seal was removed and plate transferred to the magnetic plate stand for 5 min. 17 µl of the supernatant was transferred to a fresh PCR plate and SuperScript II was diluted into first strand synthesis act D mix tube at a ratio of 1:9 and 8 µl added to each well and mixed. The PCR plate was sealed and incubated in a thermo cycler at 25°C for 10 min, 42°C for 15 min, 70°C for 15 min before cooling to 4°C.

3.2.1.5 **Second strand cDNA synthesis**

The plate seal was removed and 5 µl resuspension buffer and 20 µl second strand marking master mix was added to each well and mixed. The plate was sealed and incubated in a thermal cycler at 16°C for 1 hr. After bringing the plate to room temperature, 90 µl of well-mixed AMPure XP beads was added to each well and mixed. The plate was incubated at room temperature for 15 min, transferred to a magnetic stand and incubated for 5 min to separate the beads from the supernatant. 135 µl of the supernatant was removed and discarded from each well and 200 µl freshly prepared 80%

ethanol was added without disturbing the beads. The plate was incubated for 30 sec before removing the supernatant from each well. The 80% ethanol wash was repeated twice. The plate was dried at room temperature for 15 min before removing from the magnetic stand. 17.5 µl of resuspension buffer was added to each well and beads thoroughly resuspended by mixing. The plate was incubated at room temperature for 2 min before transferring to the magnetic stand for 5 min. 15 µl of the supernatant was transferred to the wells of a fresh 96 well PCR plate.

3.2.1.6 **Adenylation of 3' ends**

In order to prevent blunt fragments ligating to one another during the adaptor ligation reaction, a single 'A' nucleotide was added to the 3' end, which is recognised by a 'T' nucleotide at the ' end of the adaptor and allows ligation. To each well 2.5 µl of resuspension buffer and 12.5 µl of A-Tailing mix was added and mixed thoroughly. The plate was sealed and incubated in a thermal cycler at 37°C for 30 min, 70°C for 5 min and then cooled to 4°C.

3.2.1.7 **Ligation of adaptors**

Indices were selected for each sample to give a unique 6 nucleotides at the end and allow identification of sample specific sequences.

Sample	RNA Adapter Index	Sequence
Undifferentiated	19	GTGAAA(C)
Day 1 Differentiation	2	CGATGT(A)
Day 7 Differentiation	4	TGACCA(A)

The plate seal was removed and 2.5 µl resuspension buffer, 2.5 µl ligation mix and 2.5 µl RNA adapter index was added to each well and mixed. Plate was sealed, centrifuged at 280 *xg* for 1 min and incubated in a thermal cycler at 30°C for 10 min. The plate seal was removed and 5 µl stop ligation buffer was added to each well and mixed. AMPure XP beads were thoroughly resuspended by vortex and 42 µl added to each well and

incubated at room temperature for 15 min. The PCR plate was transferred to the magnetic stand for 5 min until the liquid is clear and 79.5 µl of the supernatant was removed, taking care not to disturb the beads. The beads were washed twice with 200 µl freshly prepared 80% ethanol as before.

Samples were air-dried at room temperature for 15 min before removing from the magnetic stand. Beads were resuspended in 52.5 µl resuspension buffer, thoroughly mixed and incubated at room temperature for 2 min. The plate was returned to the magnetic stand for 5 min and 50 µl of supernatant transferred to fresh tube on a 96-well PCR plate for a second clean up step. AMPure XP beads were fully resuspended and 50 µl added to each sample and mixed. The plate was incubated at room temperature for 15 min before transferring to the magnetic stand for 5 min. 95 µl of the supernatant was removed from each well and the beads washed twice with 80% ethanol as described previously. The plate was air-dried for 15 min before removing from the magnetic stand and 22.5 µl of resuspension buffer added to each well. The plate was incubated at room temperature for 2 min before being transferred to the magnetic stand for 5 min. 20 µl of the supernatant was transferred to a fresh well of a 96 well PCR plate.

3.2.1.8 **DNA fragment enrichment**

DNA fragments with adapter molecules at both ends were selectively enriched by PCR to amplify the amount of DNA in the library. To set up the PCR reaction 5 µl of PCR primer cocktail and 25 µl PCR master mix were added to the 20 µl of sample in each tube and mixed. The plate was sealed, transferred to a thermal cycler and the PCR programme run as 15 cycles of 98°C for 10 sec, 60°C for 30 sec, 72°C for 30 sec and 72°C for 5 min. The seal was removed from the plate and 50 µl resuspended AMPure XP beads were added to clean up the PCR product. The plate was incubated at room temperature for 15 min before being transferred to the magnetic stand for 5 min. 95 µl of the supernatant were removed and beads washed twice as before with 80% ethanol. Beads were resuspended in 32.5 µl resuspension buffer and incubated at room temperature for 2 min. Plate was transferred

to the magnetic stand for 5 min before transferring 30 µl of supernatant to a fresh well on a 96 well PCR plate.

3.2.1.9 **Library validation**

The quality and quantity of the cDNA libraries were validated using the high sensitivity D100 screen tape assay. An 8 x strip of optical tubes (Agilent) was prepared by adding 2 µl high sensitivity D1000 sample buffer to each tube. To the first tube 2 µl of ladder was added and 2 µl of each sample added to the remaining tubes. Tubes were mixed by vortex at 2000 rpm for 1 min using the IKA vortexer. Samples were briefly spun to move liquid to the bottom of the tube and transferred to the TapeStation. The Agilent 2200 TapeStation software was loaded, sample details entered and programme run to determine the concentration and purity of the cDNA.

3.2.1.10 **RNAseq pooling**

The peak molarity measured on the TapeStation was used to pool the RNA samples for sequencing. The samples were pooled together each at a final concentration of 10 nM in 25 µl and sent for sequencing at the Next Generation Sequencing Facility, LIMM using the Illumina Hiseq 2500 sequencer.

3.2.1.11 **Analysis of RNAseq data**

The fastq.gz files generated from the RNA sequencing were analysed using UNIX commands in Terminal (Mac). The analysis protocol used was based upon the Nature Protocols method (Trapnell 2012). Briefly, TopHat2 was used to analyse the data by mapping the reads to the *Mus musculus* genome. The Bowtie command was used to align the short sequencing reads against the genome. The identified, aligned RNAseq transcripts were assembled and abundance estimated using the Cufflinks command. The programme Cuffcompare was used to compare transcripts from each C1F sample to known transcripts in a reference transcriptome. The Cuffmerge command was used to merge the transcripts from each sample to enable

further analysis into differential expression. The Cuffdiff command was then used to find significant changes in transcript expression, splicing, and promoter usage between the C1F samples. Results were copied and opened using Microsoft Excel.

3.2.2 **Colocalisation calculation**

To determine the efficacy of each of the commercially available antibodies tested (Table 12.) to recognise exogenously expressed MEGF10, in a quantitative manner, the colocalisation between expressed MEGF10_GFP protein and anti-MEGF10 antibodies in cultured myoblasts was determined. C1F cells were infected with 100 MOI MEGF10_GFP adenovirus, incubated for 24 hrs prior to fixing and staining the cells for MEGF10 (Millipore, Santa Cruz or Sigma Prestige). Colocalisation was calculated, following the protocol described in http://imagej.net/Coloc_2, using the Coloc2 plugin in Fiji, using 100 iterations of the Costes statistical significance test. The colocalisation is quantified using Pearson's R-value where a value of 0 indicates no colocalisation and a value of 1.0 shows perfect colocalisation (Dunn et al., 2011).

3.2.3 **Muscle hyperplasia model**

Thanks to Professor Stuart Egginton and Roger Kissane for their help in performing the mouse surgery under project licence number PPL 70/8674.

3.2.3.1 **Hyperplasia model surgery**

In order to determine if changes in MEGF10 expression occur in regenerating muscle an *in vivo* mouse muscle hyperplasia model was set up (Egginton et al., 2011; Egginton et al., 1998). In this, the tibialis anterior (TA) was removed from the right leg of a C57BL/6 mouse to increase the load on the underlying extensor digitorum longus (EDL) muscle causing muscle hyperplasia. Changes in satellite cells and MEGF10 expression were examined in the hyperplasia and the contralateral EDL.

Twelve 6 week old male C57BL/6 mice were divided into six cages with two mice per cage. Two mice were retained as controls and did not undergo surgery. Mice were anaesthetised with 5% isoflurane in 2 L/min oxygen prior to shaving the right leg and injecting the mice in the scruff of the neck with analgesic and anti-infective Enrofloxacin (Baytril® 2.5%). The subsequent steps of the operation were performed with the mouse anaesthetised with 2.5% isoflurane in 2 L/min oxygen. The skin on the shaved right leg was cleaned by wiping with chlorhexadine to remove any surface bacteria. All work was performed using sterile instruments under a dissection microscope. A single incision was made to expose the TA muscle. Tweezers were used to identify and lift up the superficial distal TA tendon. The TA tendon was cut and TA muscle dissected out with a scalpel leaving the EDL muscle below. The TA muscle was briefly returned to the wound to release cytokines that aid clotting and reduce bleeding but was removed fully before closing the wound. The wound was sealed by suturing with Mersilk 4 - 0 silk braided sutures and sterile saline used to remove any blood to reduce irritation. The mouse were allowed to recover in a chamber heated to 35°C, because of their small size, before returning to their cage. Mice were kept in a clean air filtered room with regular food and water *ad*

libitum over the course of 14 days (Egginton et al., 2011; Egginton et al., 1998).

3.2.3.2 **Sample isolation and storage**

Changes in muscle were measured in control mice, 1, 3, 6, 10 and 14 days post-surgery. At each time point two mice were euthanized by cervical dislocation and weighed prior to dissecting the damaged and contralateral EDL muscles. The dissected muscle was weighed prior to sample preparation. The damaged muscle and contralateral muscle from one mouse were snap frozen in liquid nitrogen for protein extraction and stored at -80°C. The muscles from the second mouse were isolated and transferred to medium 199 (Gibco) prior to digestion in 2 mg/ml collagenase for single fibre isolation (2.9).

3.2.3.3 **Protein sample isolation**

RIPA buffer (150mM NaCl, 1% IGEPAL® CA-630, 0.5% sodium deoxycholate, 0.1% SDS, 50mM Tris pH8) was prepared and cooled on wet ice. Muscle was ground to a fine powder by pestle and mortar under liquid nitrogen and transferred to a 1.5ml Eppendorf tube. The muscle was resuspended in 200 µl lysis buffer (RIPA buffer supplemented with 1% Triton X-100, 1% glycerol and Halt Protease Inhibitor Cocktail (Roche)). Samples were incubated on ice for 30 min, mixing by vortex every 5 min. Samples were centrifuged at max. speed (13,600 *x g*) for 30 min at 4°C. The supernatant was transferred to a fresh 1.5 ml Eppendorf tube and 4 µl used for BCA Assay (2.12.2).

3.3 Results

3.3.1 **Antibody selection for fluorescence microscopy and western blotting applications**

To test three different commercially available antibodies against MEGF10 (Table 12.) for their ability to recognise MEGF10 by immunostaining, C1F myoblasts expressing a MEGF10_eGFP adenoviral construct were stained with each antibody. MEGF10_eGFP was localised to the Golgi, intracellular vesicles, and to the plasma membrane (Figure 17. A. and inserts). The colocalisation between expressed MEGF10_GFP and anti-MEGF10 antibodies was quantitated using ImageJ (Figure 17. B). Co-staining with both the Millipore and Sigma Prestige antibodies showed good co-localisation with a mean Pearson's R value 0.91 and 0.93 respectively, in which the majority of the staining observed for the antibody matched that see for MEGF10_eGFP. In contrast, the antibody from Santa Cruz showed significantly lower co-localisation (Pearson's R value 0.83) compared to the Millipore ($p=0.0026$) and Sigma Prestige ($p=<0.0001$) antibodies, suggesting that this antibody does not specifically recognise MEGF10. There is no significant difference between the colocalisation of the Millipore and Sigma Prestige antibodies with the expressed MEGF10_eGFP ($p= 0.1884$) (Figure 17. B.).

Table 12. Commercially available anti-MEGF10 antibodies tested.

Details of the three commercially available antibodies tested for their efficacy at recognising MEGF10 by immunocytochemistry and western blot. The source and species of each antibody, the region of MEGF10 that the antibody was raised against, and an example of a publication that has previously used each antibody is provided.

Company	Recognition site	Species	Reference
Millipore	Cytoplasmic domain of mouse MEGF10	Rabbit	(Kay et al., 2012)
Santa Cruz	Cytoplasmic domain of human MEGF10	Goat	(Bröhl et al., 2012)
Sigma Prestige	EGF domains 5 - 8 of human MEGF10	Rabbit	(Chung et al., 2013)

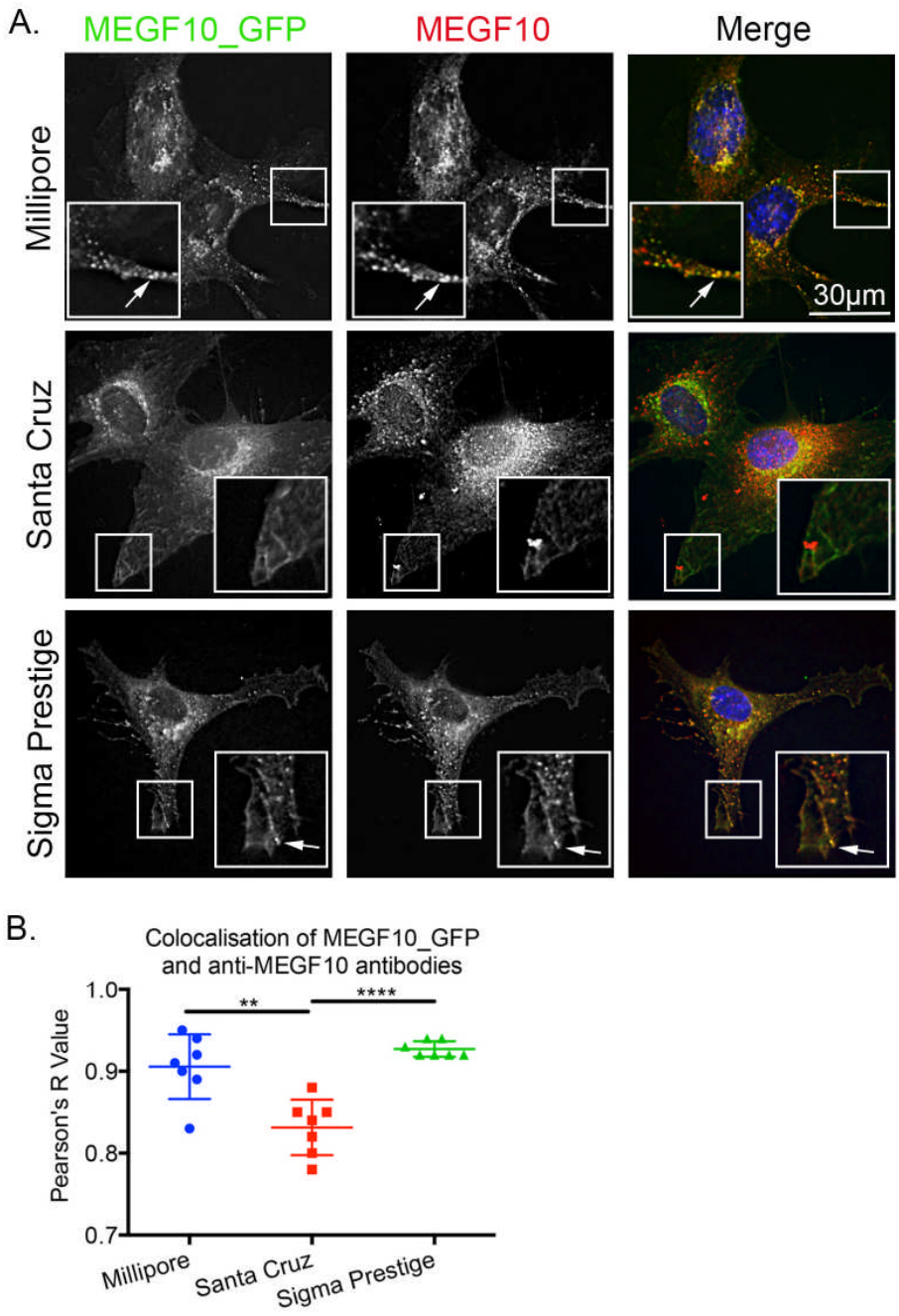

Figure 17. Localisation of MEGF10_GFP and anti-MEGF10 antibodies in myoblasts.

A. Immunocytochemistry showing antibody staining against MEGF10 in red, MEGF10_GFP in green and the nuclei, stained with DAPI, in blue. Arrows in inset show colocalisation. **B.** MEGF10_GFP and anti-MEGF10 antibody colocalisation quantitated by the Pearson's R value. Colocalisation is significantly lower when staining with the Santa Cruz antibody, ** p = 0.0026 and **** p = <0.0001. There is no significant difference between the Millipore and Sigma Prestige antibodies (p = 0.1884). (Mean values +/- S.D.).

To test the abilities of each antibody to recognise MEGF10 by western blotting, cell extracts from C1F cells, transfected with the adenoviral construct expressing full length MEGF10_eGFP (Chapter 4.), together with the expressed and purified ECD of MEGF10 (Chapter 5.), were used. Only the Sigma Prestige antibody (raised to the ECD of MEGF10) recognised MEGF10 on western blots. This antibody was expected to recognise both MEGF10_eGFP and the purified ECD. However, while it recognised the purified ECD of MEGF10 (Figure 18.), it did not recognise MEGF10_eGFP expressed in C1F cells, possibly because the protein levels were too low for detection. A further blot, using Ad293 cells expressing MEGF10_eGFP, did show a band of the correct size using the Sigma Prestige antibody (Figure 18. A.). The size of the detected band for the purified ECD is higher than expected (120 kDa), but this is due to extensive post-translational modification of this protein.

Neither the Millipore antibody nor the Santa Cruz antibody recognised the purified ECD of MEGF10, which was expected since both antibodies were raised against the cytoplasmic domain of MEGF10, which is absent from the purified peptide. However, neither antibodies showed a band of the expected size for MEGF10_eGFP in cell extracts, and the Millipore antibody additionally showed a band of an incorrect size (~60 kDa) (Figure 18. A.). MEGF10_GFP in the cell extracts was recognised by an anti-GFP antibody. A dilution series of the purified ECD of MEGF10 showed the Sigma Prestige antibody could be used to detect concentrations as low as ~ 25 ng of protein (Figure 18. B.), and thus expression levels of the MEGF10_eGFP in cell extracts must be below this detection limit for the anti-MEGF10 antibodies.

I chose to use only the Sigma Prestige antibody in future experiments, since it was the only antibody tested that recognised MEGF10 in both immunostaining and western blot applications, even though it was unable to recognise low concentrations of MEGF10_GFP.

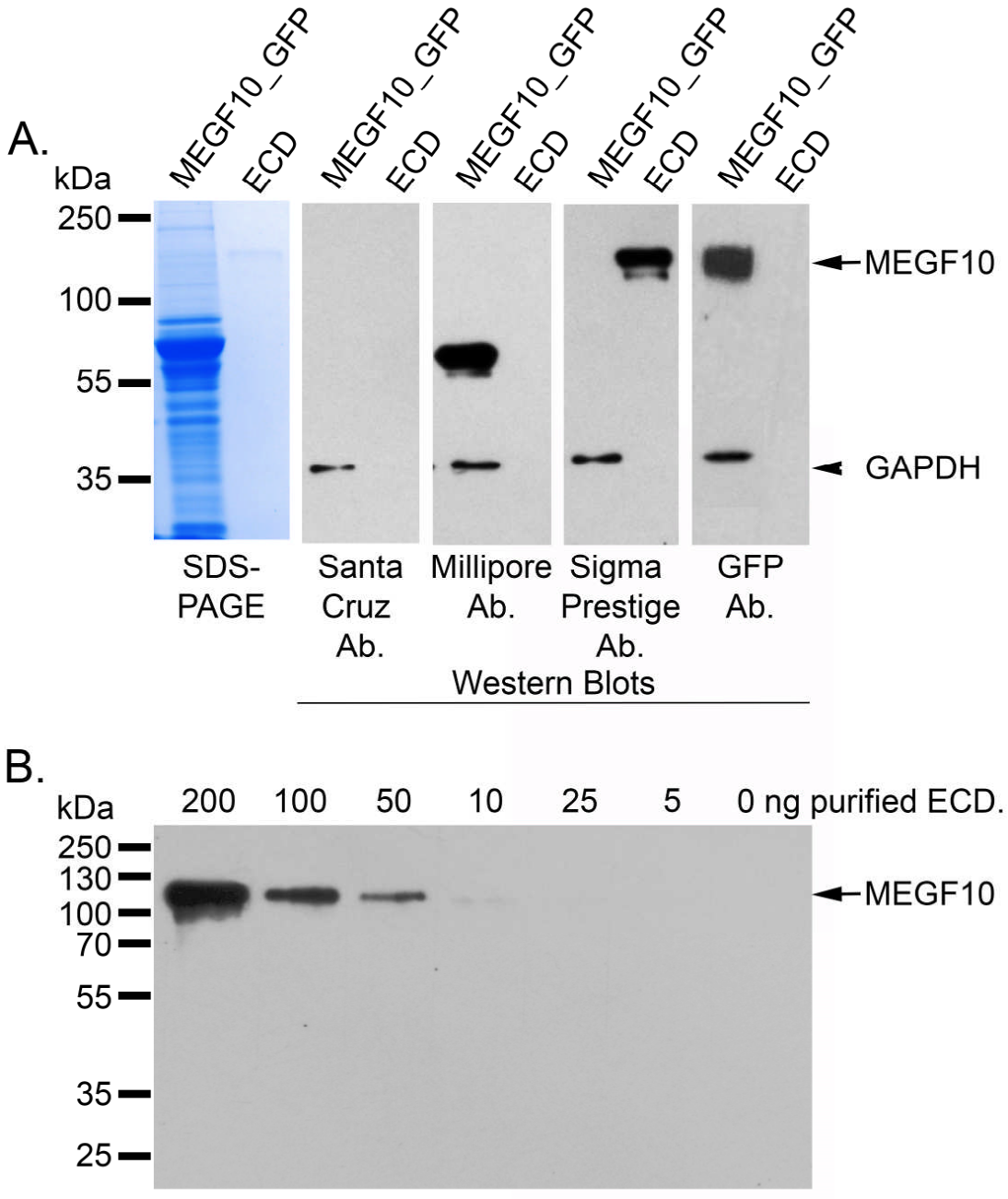

Figure 18. Anti-MEGF10 recognition of MEGF10 by western blot.

A. SDS-PAGE gel showing the cell extract for C1F cells expressing MEGF10_GFP (Expected size ~145 kDa) and the purified ECD protein (expected size 120kDa). Western blots probed with anti-MEGF10 antibodies from Santa Cruz, Millipore and Sigma Prestige (indicated by arrow). All blots include GAPDH as a positive control (indicated by arrow head). **B.** A western blot testing the sensitivity of the anti-MEGF10 antibody (Sigma Prestige) in recognising purified ECD protein (5 min exposure).

3.3.2 **Endogenous expression of MEGF10 in C1F cells is below the detection limit by immunofluorescence and western blot**

Immunostaining of C1F cells using the Sigma Prestige antibody did not convincingly show that C1F cells expressed significant levels of endogenous MEGF10 (Figure 19. A.) either in myoblasts or in differentiated cells. Staining patterns were not significantly different from those seen for negative controls, which used secondary antibody only (Figure 19. B.). Actin staining shows that the cells start to differentiate into myotubes by day 3, with multiple myotubes observed at days 5 and 7 (Figure 19.). The majority of fusion into myotubes occurs between days 1 and 3. If MEGF10 expression levels decrease upon differentiation (by ~6 fold) as reported (Holterman et al., 2007), this should have been evident in the staining shown.

Western blotting of C1F cells at different stages of differentiation also did not show a band for MEGF10 (Figure 20.), although bands were detected in the positive control. Therefore, if the C1F cells do express MEGF10 it is at such low levels that it is below our detection limit for both western blotting and immunostaining.

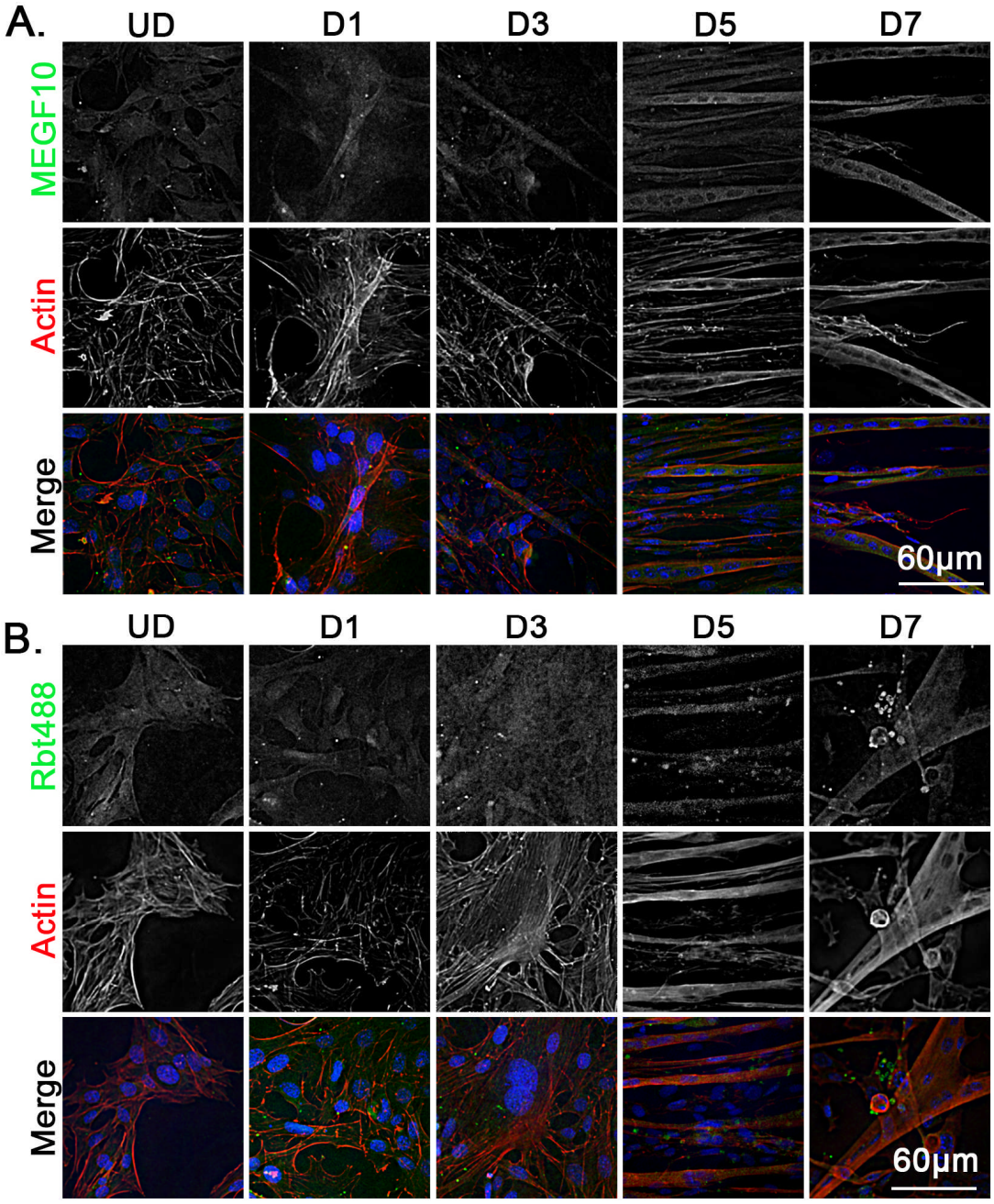

Figure 19. Endogenous expression of MEGF10 in C1F cells and non-specific secondary antibody staining.

Immunostaining of undifferentiated (UD) to day seven differentiated (D7) C1F cells (Actin is stained with fluorescent phalloidin in red and the nuclei, stained with DAPI, are shown in blue in the merged image. **A.** Anti-MEGF10 (Sigma Prestige) staining is shown in green. **B.** Secondary anti-rabbit (Rbt488) only staining is shown in green.

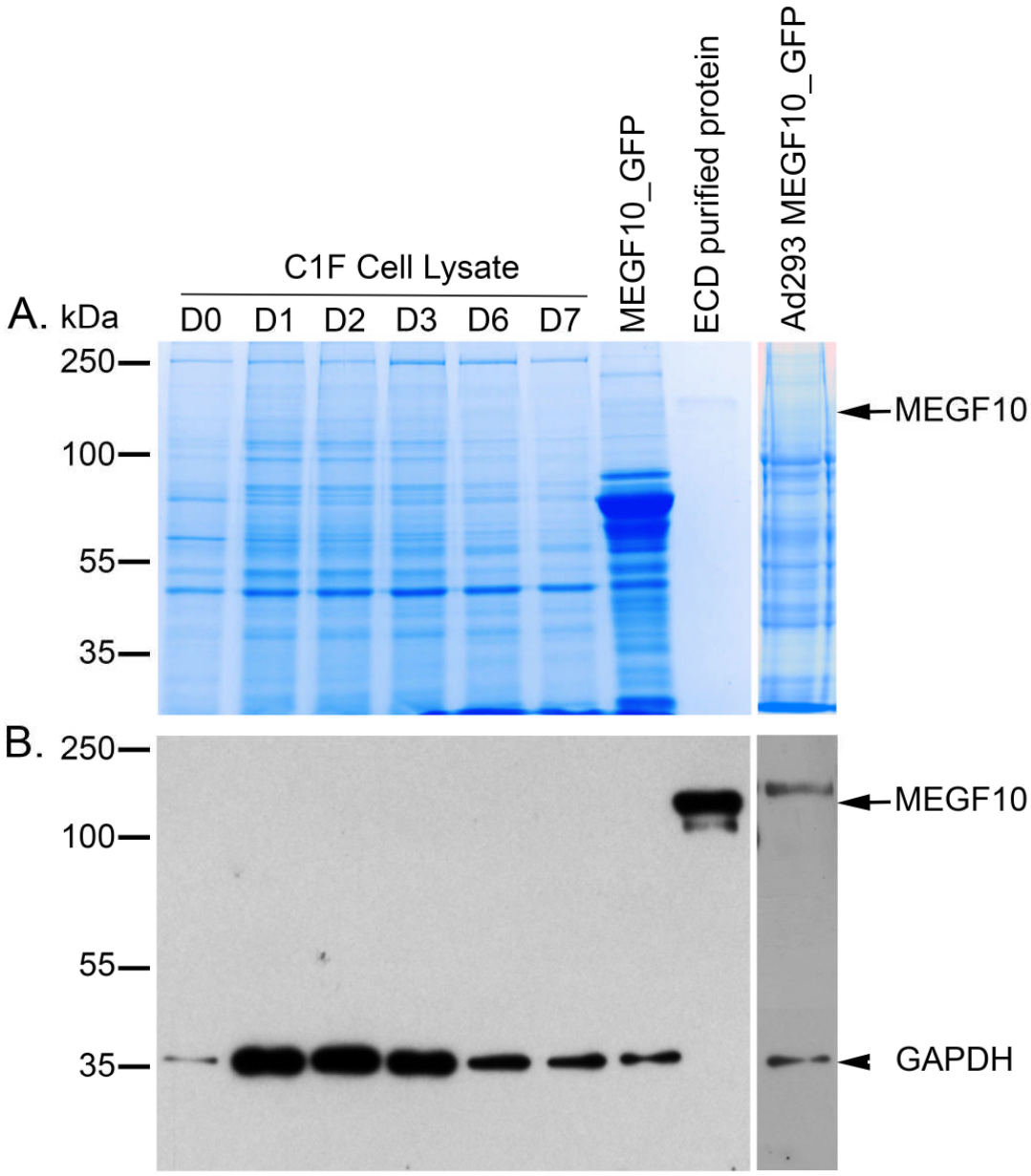

Figure 20. Endogenous expression of MEGF10 in C1F cells and anti-MEGF10 antibody test.

A. SDS-PAGE gel showing the lysates of mouse myoblasts (C1F) differentiated over 7 days. MEGF10_GFP overexpressed in C1F cells (Expected size 145 kDa) and eMEGF10 purified protein (Expected size 120 kDa) were used as positive controls. **B.** Western blot probed with anti-MEGF10 (Sigma Prestige) and GAPDH (Expected size 37 kDa) as a loading control.

3.3.3 Low level expression of MEGF10 in C1F cells is confirmed by RNAseq

As I was unable to detect expression of MEGF10 by immunostaining or western blotting, I next used RNAseq to characterise the expression of MEGF10. Whilst qPCR could have been used to study changes in MEGF10 and related protein expression, this had already been performed by Holterman *et al*, and it was hoped that by performing the more laborious RNAseq method information on the expression of MEGF10 and a wide range of potentially related proteins could be explored in differentiating myoblasts as well as giving information on the distribution of MEGF10 isotypes. These experiments confirmed that endogenous MEGF10 expression levels were low and that they did not change significantly during C1F myoblast differentiation. A small reduction in MEGF10 expression was observed during differentiation, but this change was not significant. In contrast, levels of ACTA1 (skeletal muscle specific actin) increased after seven days of differentiation as expected. Pax7, a TF found in quiescent satellite cells, was present at low levels in undifferentiated and differentiated cells as expected. Levels of MyoD, a myoblast determination protein that is upregulated during differentiation, was markedly increased at day 7 of differentiation was not expected, however this may reflect previously high levels of MyoD, which are still decreasing at day 7 and would have dropped further over subsequent days. Unfortunately, these timepoints do not cover each stage of myogenesis. Similarly, levels of myogenin, a second muscle specific TF upregulated during differentiation, had also markedly increased by day seven (Figure 21. A. and B.). Thus, the C1F cells do show the expected changes in muscle-specific markers. Taken together, these data suggest that MEGF10 levels are extremely low in cultured myoblasts, limiting their usefulness in studying endogenous MEGF10.

MEGF10 is predicted to be present in two isoforms, the predominant full length construct and a second truncated isoform (UniProtKB). RNAseq analysis identified the presence of the two isoforms of MEGF10, however the second isoform was at a very low level. There is no change in the relative proportions of the two isoforms over the course of myoblast differentiation. Further repeats of the RNAseq along with alternative analysis

techniques may give a better insight into the possible changes in isoform expression.

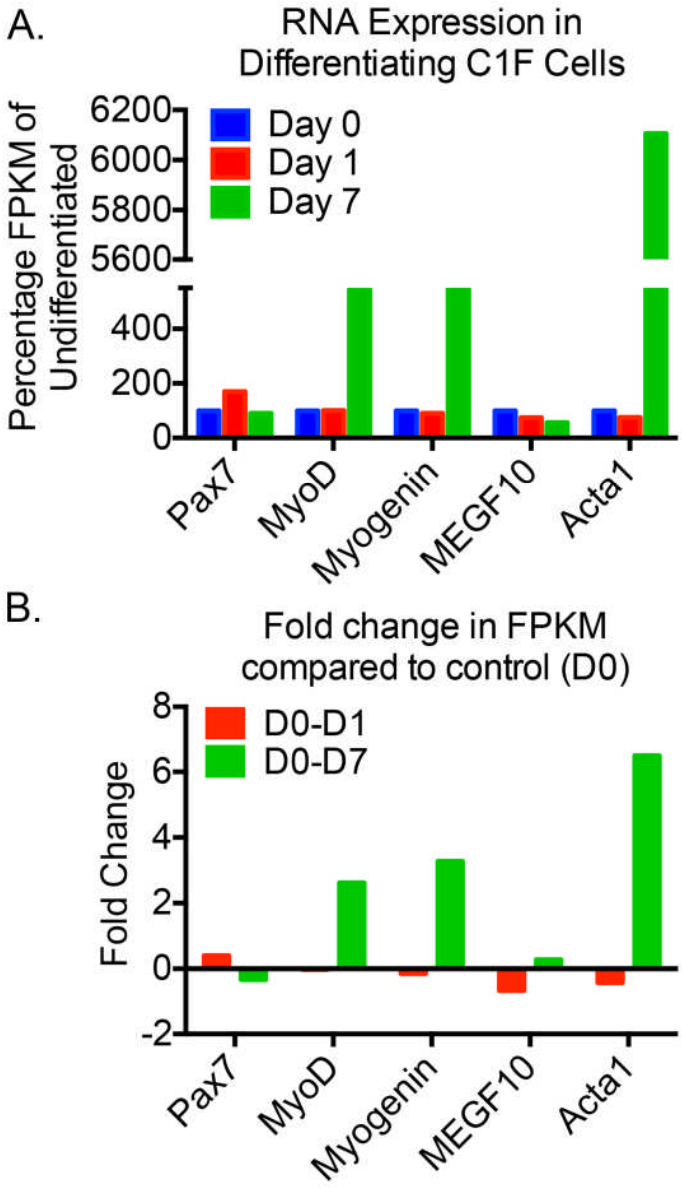

Figure 21. Changes in RNA expression levels in differentiating C1F cells.

A. Undifferentiated, day 0, early differentiating, day 1, and fully differentiated, day 7, C1F cells were analysed for mRNA expression levels by RNAseq. Pax7, MyoD and myogenin are expressed in quiescent, activated and differentiated cells respectively. Acta1, the gene encoding skeletal muscle actin was included as an additional positive control for differentiated myotubes. The graph shows the fragments per kilobase million (FPKM), estimating transcript abundance, as a percentage of the value for undifferentiated C1F cells. **B.** The fold change in FPKM between undifferentiated and day 1 (red) and day 7 (green) cells. (FPKM values, n=1).

3.3.4 **Endogenous expression of MEGF10 in isolated single fibres**

Since the expression of endogenous MEGF10 in cultured myoblasts is very low, I next looked at MEGF10 expression in satellite cells *in situ* on isolated muscle fibres, cultured for up to 5 days *in vitro*. Under these conditions, the quiescent satellite cells should become activated, allowing the determination of changes in MEGF10 expression during activation of these primary cells in their niche environment beneath the basal lamina. To enable identification of satellite cells, co-staining was performed for CD34, a positive marker expressed in the membrane of the majority of satellite cells (Beauchamp et al., 2000). Low magnification images show the low numbers of satellite cells per fibre, with a mean average of 2.65 satellite cells per fibre in day 0 fibres with the most satellite cells seen in fibres 4 days post-isolation which had a mean average of 9.4 satellite cells per fibre (Figure 22.). Furthermore, the difficulty in identifying which satellite cells were positive for CD34 and the TF being tested, that were also stained positively for MEGF10 gave inconclusive results (Figure 22.). Thus, further analysis of co-staining was performed using higher magnification images (Figures 23. and 24.).

A comparison of the MEGF10 staining pattern for satellite cells on cultured fibres at high magnification (Figures 23. and 24.) shows that quiescent satellite cells (day 0) did not express MEGF10. However, MEGF10 staining was observed at day 1, in some $Pax7^+/CD34^+$ satellite cells (Figure 23.), and in day 2, for some $MyoD^+/CD34^+$ satellite cells. In day 1 and 2 cells, MEGF10 was co-localised with CD34 at the plasma membrane (Figures 23. and 24.). At day 3 or 4, staining was more variable. Some $MyoD^+/CD34^+$ satellite cells did not show positive staining (Figure 23.) but others did (Figure 24.). At day 4, some $myogenin^+/CD34^+$ cells could also be found that show positive staining for MEGF10. Note that at days 3 and 4, satellite cells have already undergone cell division, and the examples show two adjacent satellite cells. By day 5, $myogenin^+/CD34^+$ cells may show some MEGF10 staining as shown in this example of a cluster of satellite cells, however it is more likely that the limited staining remaining is simply autofluorescence. Therefore there appears to be a peak of MEGF10 expression 2 - 3 days post-isolation as the satellite cells become activated,

and increased MEGF10 expression was associated with both $Pax7^+$ and $MyoD^+$ cells, but less so with $myogenin^+$ cells.

Quantification of these data (Figure 25.) showed that while $CD34^+$ cells could be found at each time point, not all of these cells were additionally MEGF10 positive. Three days post-isolation, when satellite cells were most abundant, only ~50% of the $CD34^+$ cells were also positive for MEGF10. Overall, it is not clear that the single fibre culture model provides a clear picture of how MEGF10 expression is upregulated. Levels of CD34 decrease after 4 days.

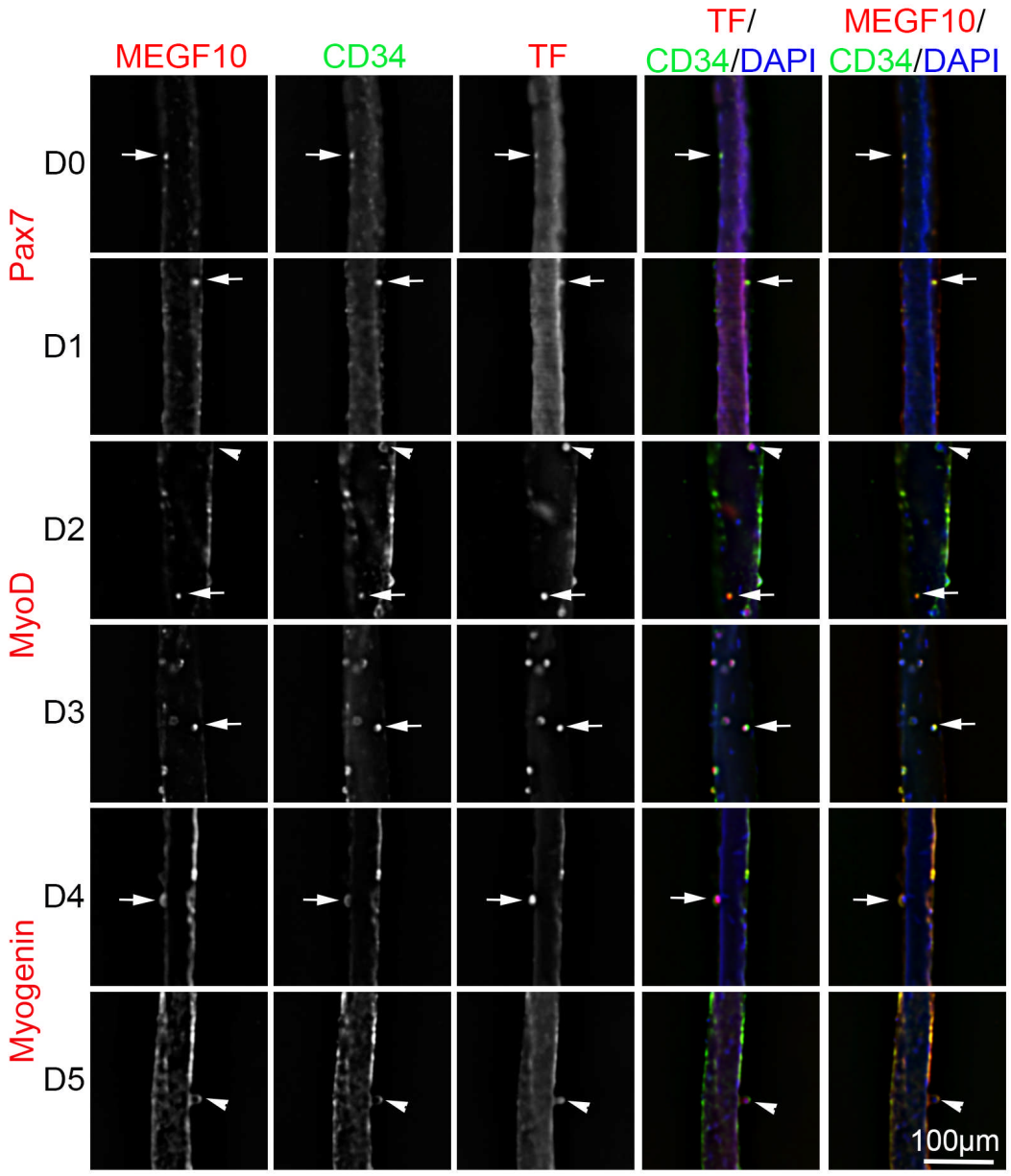

Figure 22. Immunostaining of fibres isolated from murine gastrocnemius muscle.

Gastrocnemius fibres cultured over 5 days (D0 – D5) and stained for MEGF10 in far-red, CD34 in green, each TF, Pax7, MyoD, Myogenin in red and the nuclei stained with DAPI in blue. Examples of possible MEGF10/CD34/TF^{+} cells are shown with an arrow and TF/CD34^{+} cells by an arrow head.

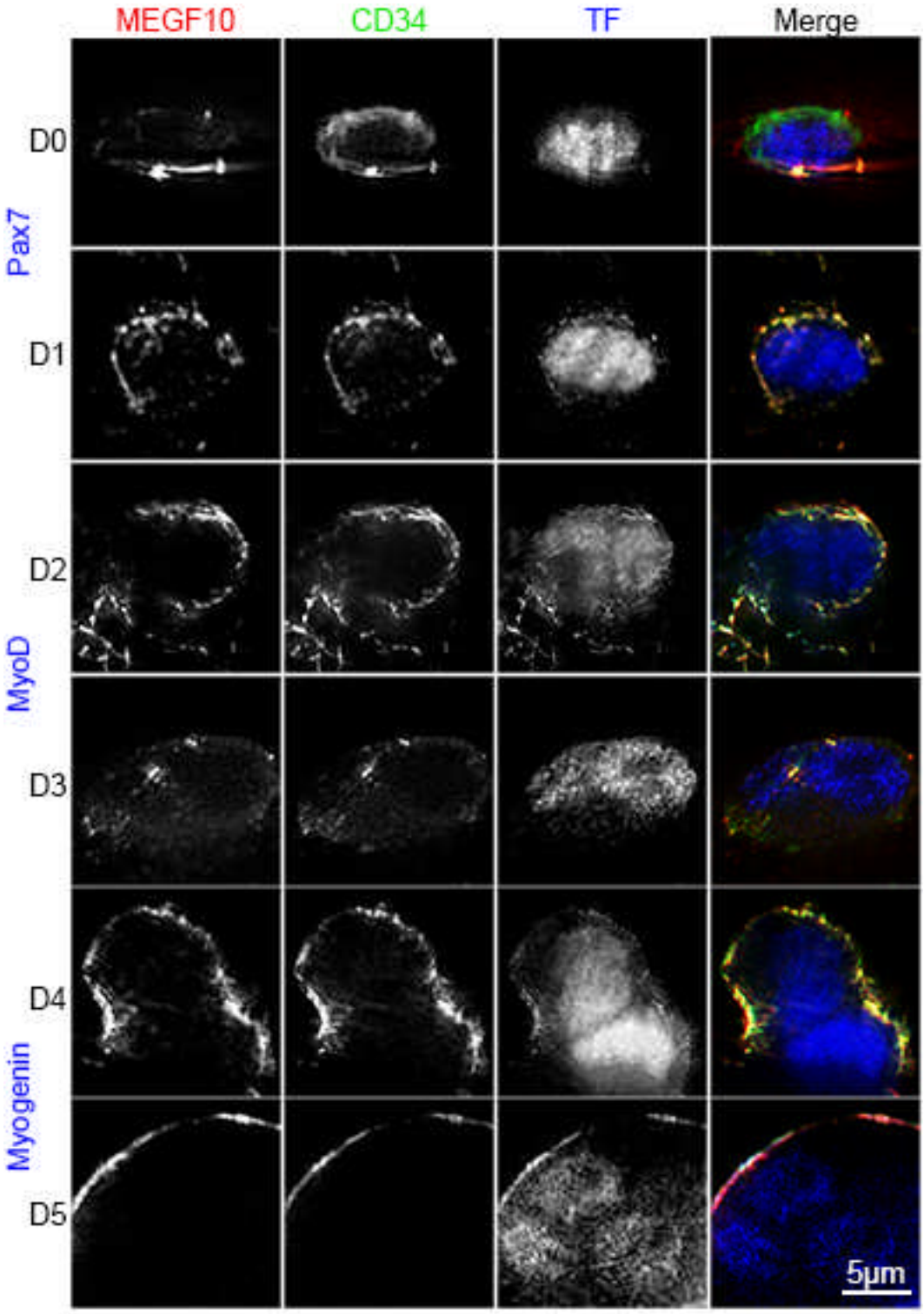

Figure 23. Time course of MEGF10 expression in isolated single fibres. Gastrocnemius fibres cultured were cultured over 5 days (D0 – D5) and stained for MEGF10 (red), CD34 (green) and each TF either Pax7 (for day 0, 1), MyoD (for day 2, 3) or Myogenin (for day 4, 5) as satellite cell markers (blue).

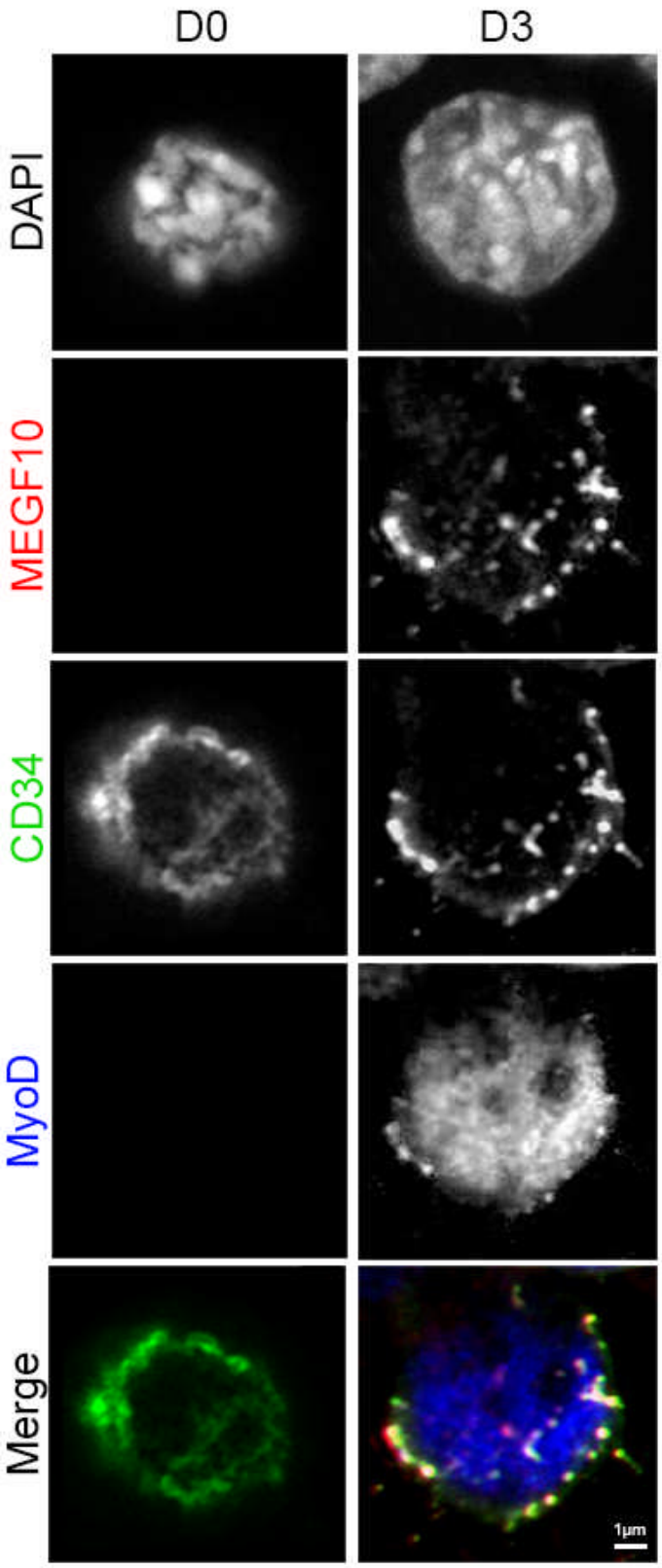

Figure 24. Satellite cells co-stained for MyoD, CD34 and MEGF10.

Isolated single myofibres fixed immediately (D0) and 3 days (D3) post-isolation were stained for nuclear TF MyoD shown in blue, CD34 shown in green and MEGF10 shown in red. Cells were imaged on the LSM880 confocal.

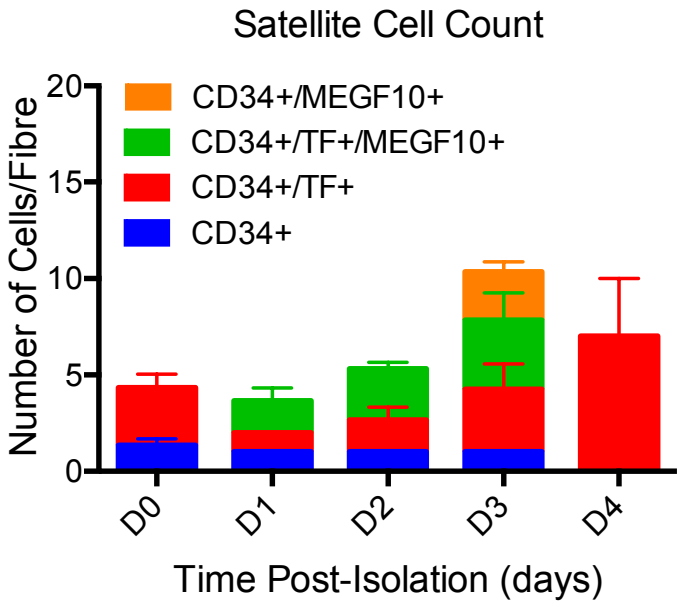

Figure 25. Satellite cell populations counted on single fibres isolated from murine gastrocnemius muscle.

Single fibres isolated from the gastrocnemius stained for MEGF10, CD34 and TFs (TF) Pax7, MyoD, myogenin that, act as markers of satellite activation. Satellite cells were counted on five fibres and expression of each marker used to classify satellite cells into distinct populations. (Mean values +/- S.E.M. with a minimum of five fibres analysed for each repeat; n=3).

3.3.5 **Muscle hyperplasia model**

To try to develop a better model for investigating MEGF10 expression in response to satellite cell activation, I used a hyperplasia model, in which a load applied to the EDL muscle is expected to stimulate satellite cells *in vivo*. Loading the EDL muscle increased its mass by ~ 20%, six days post-surgery, compared to the control muscles (Figure 26.), a value similar to the ~15% change described earlier for this type of model (Egginton et al., 2011). This increase in muscle mass was maintained over the remaining ten days (Figure 26.). The initial increase in EDL muscle mass observed one day post-surgery is due to oedema rather than an increase in muscle mass (Egginton et al., 2011). However, the statistical significance of the increase seen between control and loaded muscle could not be determined due to the low sample size.

We expected that this level of hyperplasia might activate satellite cells. Quantifying the numbers of $CD34^+$ satellite cells present on the fibres (Figure 27. A.) did appear to show an increase in satellite cell number in the hyperplasia muscles compared to control muscles with time, however the difference between the control and hyperplasia muscle were not significant (Figure 27. B.). Positive MyoD expression was used as an indicator of $CD34^+$ satellite cell activation and the number of satellite cells counted (Figure 27. C.).

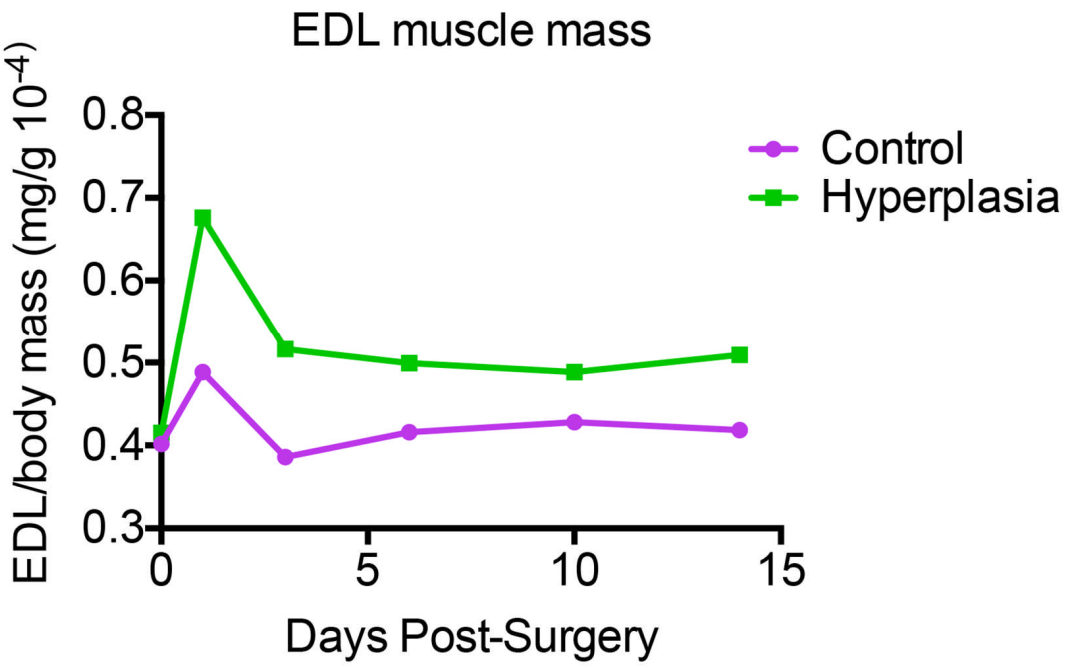

Figure 26. EDL muscle mass changes in hyperplasia model.

The EDL muscle mass is shown as a proportion of the total body mass of the mouse. Control EDL muscle was compared to hyperplasia EDL muscle post-surgery over the course of two weeks. (Mean values with 2 muscles analysed for each repeat; n=1).

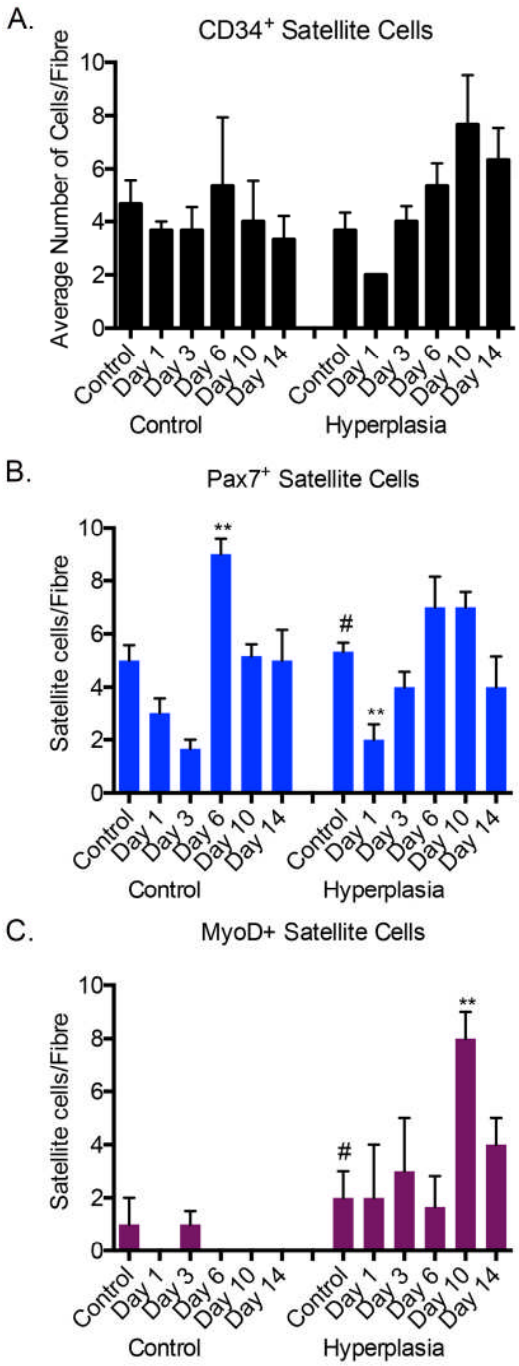

Figure 27. Satellite cell populations on isolated EDL muscle fibres.

Isolated EDL muscle fibres stained for satellite cell markers Pax7, MyoD and myogenin were imaged and counted. Satellite cells were identified by $CD34^+$ staining. **A.** The average number of CD34 positive cells counted per fibre. **B.** shows the number of $Pax7^+$ cells per fibre (** p = <0.008), and **C**. the number of $MyoD^+$ cells per fibre (** p = 0.0018). (Mean values +/- S.D. with a minimum of five fibres analysed for each repeat; n=3. # indicates the condition used as a comparison for t-test statistical analysis and asterisks indicate statistically significant changes.)

3.3.6 **Immunostaining of isolated single fibres from EDL muscle**

Analysis of satellite cells on loaded hyperplasia muscle fibres, showed an increase in activated satellite cell number shown by $CD34^+/MyoD^+$ staining in the loaded muscles compared to unloaded muscles with time (Figure 27.). Staining for MyoD and Pax7 (Figures 28 – 30.) showed that levels of $MyoD^+$ satellite cells increased with time in the loaded muscles, but not in the unloaded controls (Figure 27. C). Pax7 levels varied with time, but did not markedly differ between loaded muscles and controls (Figure 27 B.).

Co-staining fibres for Pax7, CD34 and MEGF10 showed that while that $Pax7^+/CD34^+$ satellite cells could be found throughout the fibres (from day 1 to day 14) in loaded muscles, none of these cells expressed MEGF10 (Figures. 28., 29. and 30.). Staining for MyoD, CD34 and MEGF10, additionally showed that $MyoD^+/CD34^+$ cells did not express MEGF10. I also stained for myogenin, but was unable to find any $myogenin^+/ CD34^+$ cells at any of the time points, suggesting that while satellite cells become activated, as indicated by expression of MyoD, they have not gone on to express myogenin by day 14. Staining of control fibres showed that the majority of the satellite cells were primarily Pax7 positive and therefore quiescent (Figure 28. A. and 29. A.).

However, while analysing the fibre images, I noticed that there were cells that had stained positively for MEGF10, which were $CD34^-/Pax7^-$. These cells were adjacent to $CD34^+$ cells. On re-evaluating this in the loaded sample, I found many more examples of this type of cell ($Pax7^-/CD34^-/MEGF10^+$) on hyperplasia muscle fibres (Figure 31.). It is unclear what the identity of these cells is, but unlike the more conventional $CD34^+/Pax7^+$ satellite cells, which do not express MEGF10, these cells do show very clear MEGF10 positive staining.

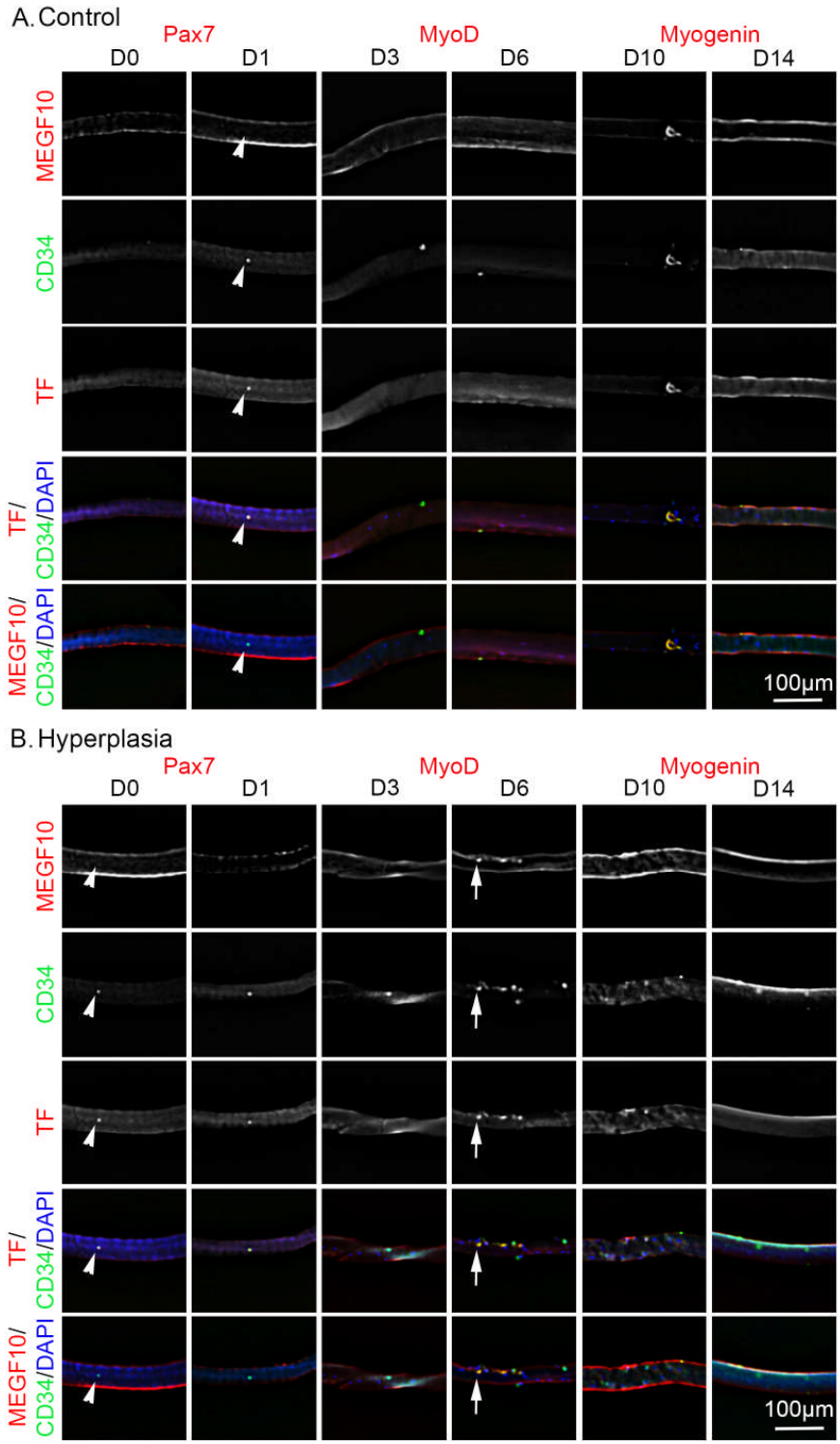

Figure 28. Low magnification images of Isolated fibres from control and hyperplasia EDL muscle.

Single fibres isolated over 14 days post-surgery (D0 – D14) from control **A.** and hyperplasia muscle **B.** Fibres were stained for TFs Pax7, MyoD or Myogenin in red, CD34 in green, MEGF10 in red and nuclei stained with DAPI in blue. Examples of possible MEGF10/CD34/TF^{+} cells are shown with an arrow and TF/CD34^{+} cells are shown by an arrow head.

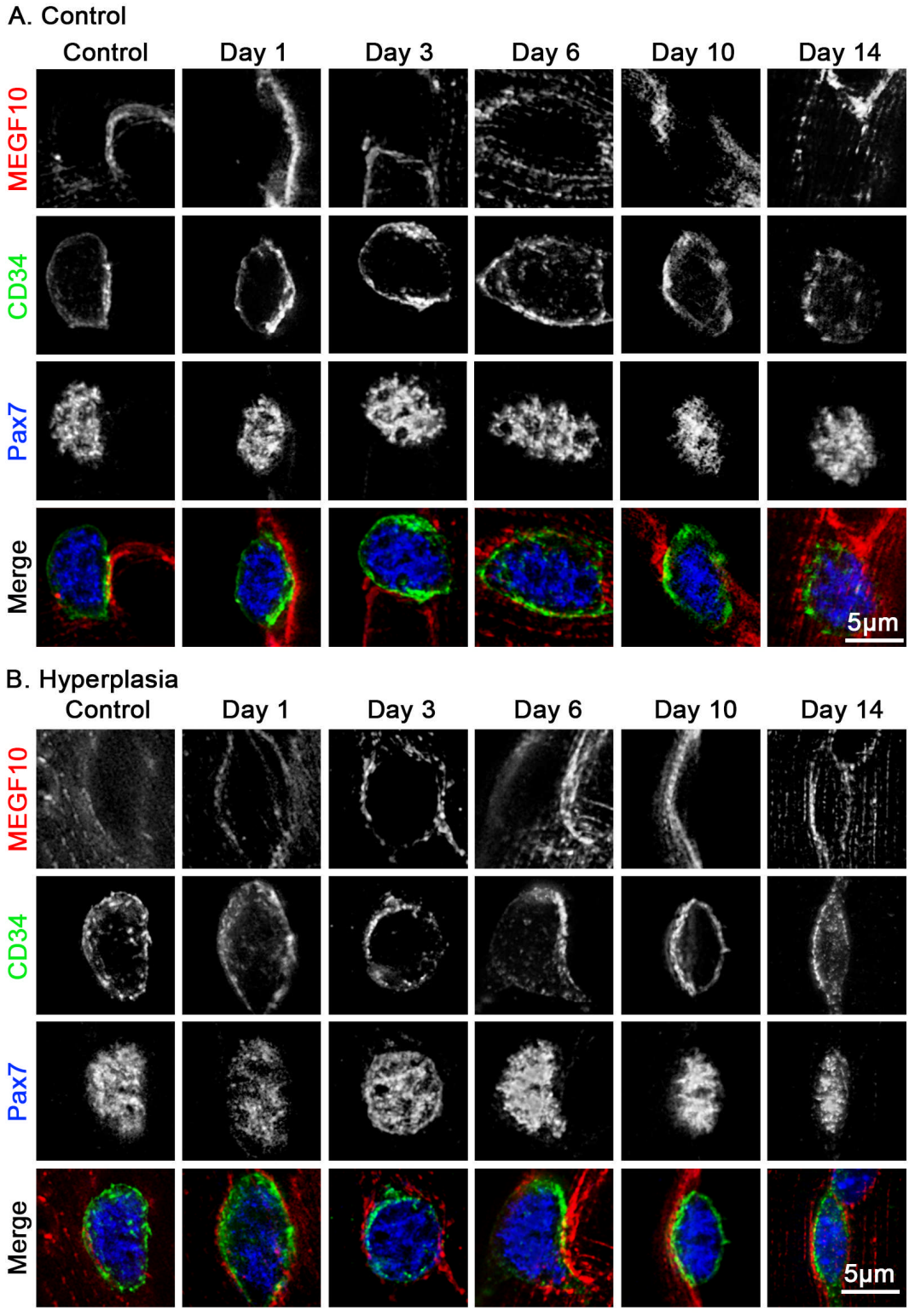

Figure 29. Satellite cells from control and hyperplasia EDL fibres.

Satellite cells on fibres from control **A.** and hyperplasia **B.** EDL muscle isolated over 14 days post-surgery and stained for MEGF10 in red, CD34 in green and Pax7 in blue.

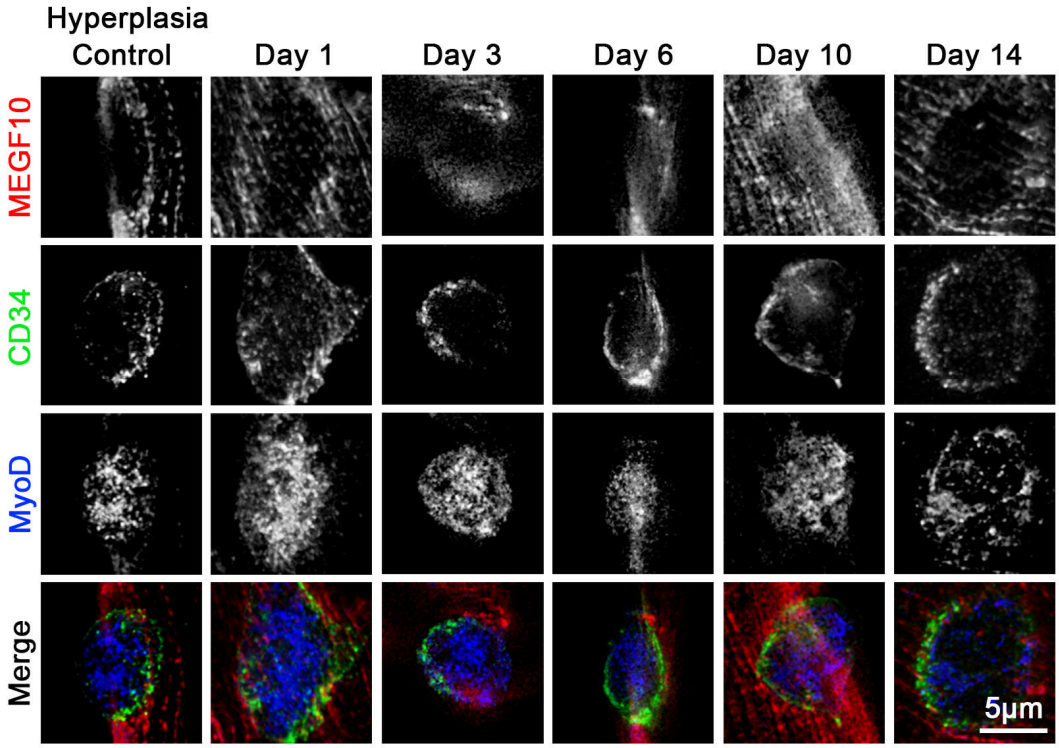

Figure 30. Staining of satellite cells on isolated fibres from hyperplasic EDL muscle.

Satellite cells imaged on isolated single fibres from hyperplasia EDL muscle over 14 days post-surgery. Cells were stained for MEGF10 in red, CD34 in green and MyoD in blue.

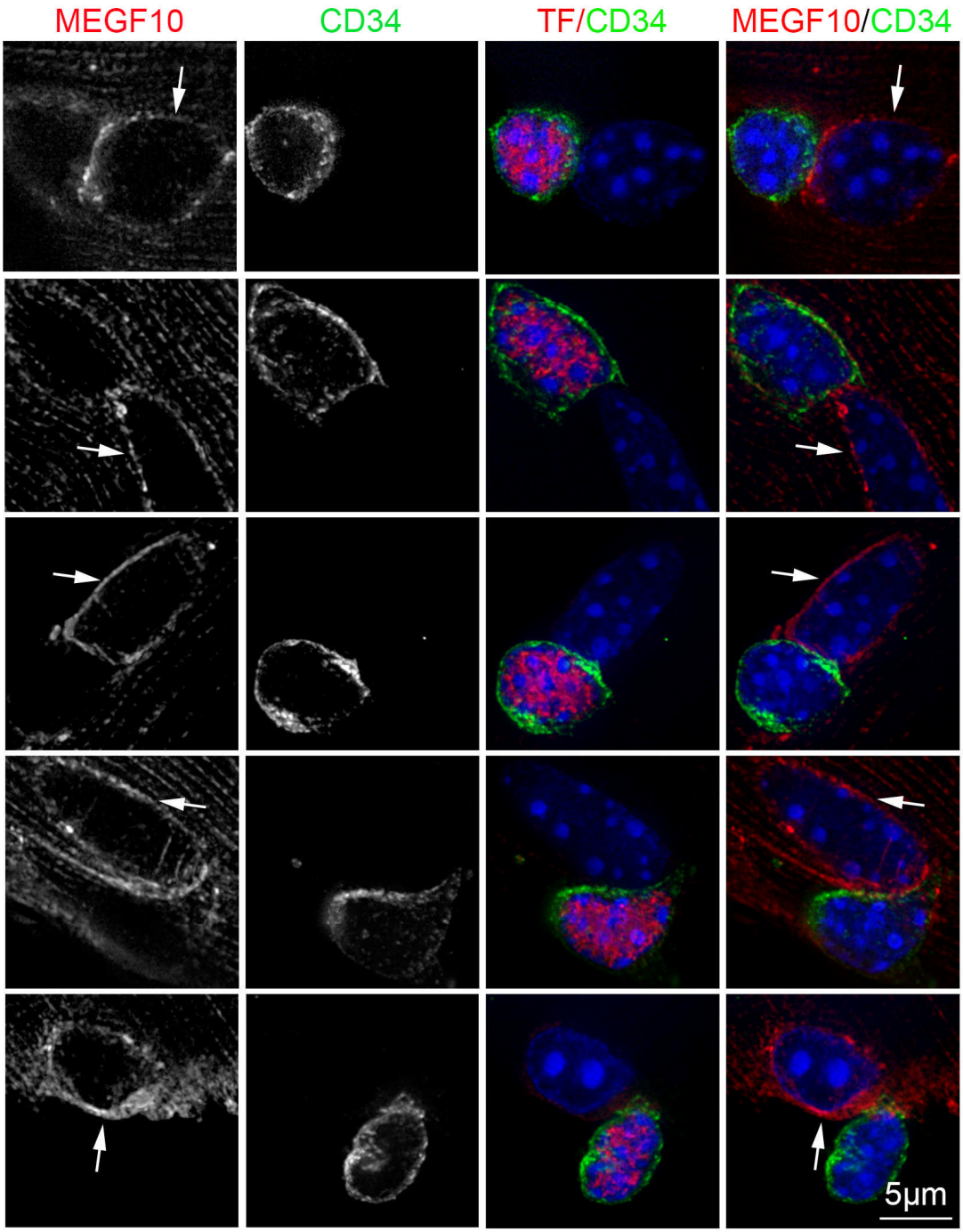

Figure 31. Localisation of MEGF10^{+}/CD34^{-} cells adjacent to CD34^{+} cells on hyperplasia EDL muscle fibres.

Satellite cells on isolated EDL fibres stained for MEGF10 in red, CD34 in green, and nuclei stained with DAPI in blue. Merged images also show TF (Pax7/MyoD) staining in red. Arrows indicate MEGF10 expression in neighbouring CD34 negative cells.

3.3.7 **Western Blot of EDL muscle samples.**

I also performed western blotting to assess any changes in expression level for MEGF10 as a result of hyperplasia. An equal amount of protein was loaded into each well of the gel as confirmed by SDS-PAGE (Figure 32. A.) and GAPDH staining (Figure 32. C.). The blots showed a band for MEGF10 at the expected size (122 kDa) but an additional high molecular weight band (>250 kDa) of unknown size and identity was also present. It is unclear what this band is, but it may result from oligomerisation of MEGF10, possibly through its multiple cysteine residues (Figure 32. B.). Overall levels of MEGF10 (122 kDa band) were very low at the start of the experiment, but increased steadily over the next 14 days. However, there was no striking difference between expression levels in the loaded muscle and unloaded controls. A similar pattern was seen for the high molecular weight band, suggesting it may indeed be derived from MEGF10. However neither band showed a clear increase in MEGF10 in hyperplasic samples compared to controls, and in fact levels of MEGF10 were perhaps even lower in the hyperplasic samples. Overall, these results do not indicate that there is a clear effect of hyperplasia on MEGF10 expression (Figure 32.).

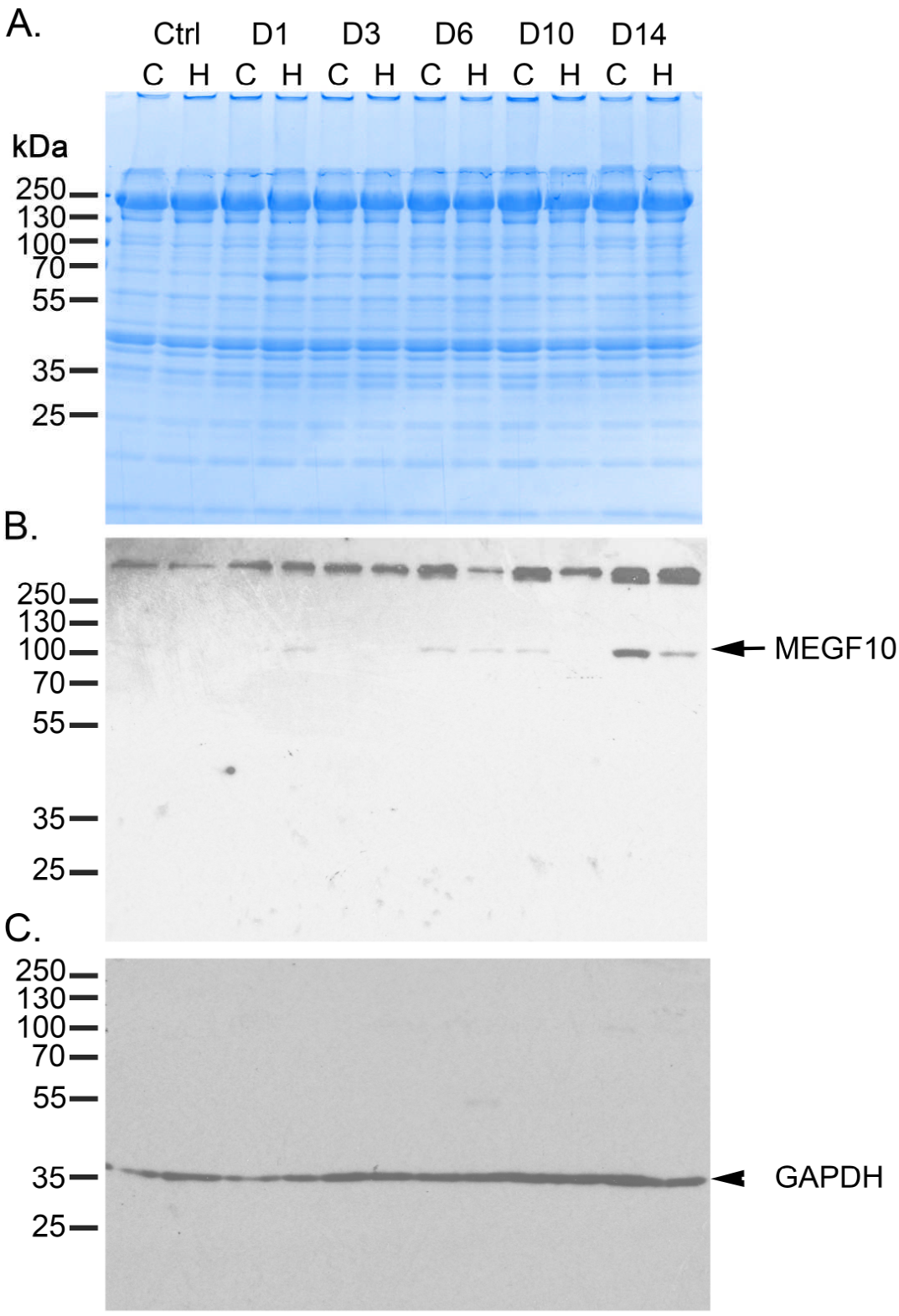

Figure 32. EDL Muscle Western Blot.

A. SDS-PAGE gel of 30 µg Control (C) and Hyperplasia (H) EDL whole muscle samples taken over 14 days (D1 – D14). **B.** Western blot probed with anti-MEGF10 (Sigma Prestige), (expected 120 kDa), 25 min exposure. **C.** Western blot probed with anti-GAPDH (expected 37 kDa), 1 min exposure.

3.4 Discussion

These data show that cultured myoblasts and quiescent satellite cells either do not express MEGF10 or express very low levels of the protein. Activated $MyoD^{+}/CD34^{+}$satellite cells imaged *in situ* on isolated muscle fibres appear to express MEGF10, which colocalises with CD34 in the membrane of satellite cells. In contrast, $MyoD^{+}/CD34^{+}$ cells in the hyperplasia model do not express MEGF10. However, $MyoD^{-}/CD34^{-}$ cells adjacent to $MyoD^{+}/CD34^{+}$ cells were found to express MEGF10. These data show that MEGF10 is not consistently associated with satellite cells as previously assumed, but that MEGF10 appears to be associated with other cells of unknown origin, that are not typical satellite cells but are associated with muscle fibres.

The finding that there is very little or no expression of MEGF10 in cultured myoblasts is in contrast to earlier findings (Holterman et al., 2007; Seale et al., 2004). In the first study (Seale et al., 2004), MEGF10 expression was analysed by northern blotting and found to be expressed at relatively high levels in proliferating cells, and then down regulated upon differentiation. In the second study (Holterman et al., 2007), MEGF10 expression was analysed by qPCR and again found to decrease during differentiation, while in $MyoD^{-/-}$ myoblasts, levels of MEGF10 did not change. Knockdown of MEGF10 expression by ~50% in the primary cultured cells also decreased levels of Pax7, MyoD and myogenin while increasing expression of skeletal muscle myosin heavy chain, which was provided as evidence of premature differentiation. In contrast, overexpression of MEGF10 inhibited fusion. However, given the very low levels of MEGF10 in cultured myoblasts that we observed, it is unclear how it plays such a key role in myoblast fusion as described.

This data failed to show a clear link between MyoD or myogenin expression and any changes in MEGF10 expression. In earlier studies, MEGF10 expression was associated with a loss of MyoD, when a high level of MEGF10 expression seen in proliferating wildtype and $MyoD^{-/-}$ primary myoblast cultures (Seale et al., 2004). Furthermore, an increase in MEGF10

mRNA levels was recently associated with an increase in myogenin expression in C2C12 cells (Park et al., 2014). However, our RNAseq data for cultured myoblasts did not show any marked change in MEGF10 expression levels when either MyoD or Myogenin levels increased. In addition, we found evidence that MEGF10 expression increased rather than decreased, when MyoD started to be expressed in the *in vitro* fibre model, while it was not associated with an increase in myogenin expression. There is also no or very little MEGF10 expressed in quiescent satellite cells, therefore it is unlikely to be required for maintaining stem cell quiescence as suggested earlier (Brohl et al., 2012). However, that study used the Santa-Cruz antibody to MEGF10 to identify MEGF10 staining in satellite cells in embryonic muscle, and our tests on this antibody failed to show that it recognised MEGF10.

Strikingly $CD34^+/MyoD^+$ or $CD34^+/Pax7^+$ cells in all the models we tested had relatively low levels of MEGF10 expression. However, in hyperplasic muscle, cells adjacent to $CD34^+/Pax7^+$ or $CD34^+/MyoD^+$ satellite cells were positive for MEGF10. It is unclear what the identity of these cells are. Approximately 20% of satellite cells are $CD34^-$ and thus it is possible that these cells fall in this population. These $CD34^-$ cells are still capable of mediating muscle regeneration (Beauchamp et al., 2000), since once isolated they have been shown to be myogenic both *in vivo* and *in vitro*. (Pisani et al., 2010). In addition, the presence of this side population of cells has been linked to skeletal muscle response to acute injury (Ieronimakis et al., 2010). However, these $MEGF10^+/CD34^-$ cells were also negative for Pax7 and MyoD, which suggests that they are not myogenic cells at all, as they would be expected to stain for muscle TFs. It is possible that they are some other cell type such as pericytes, which have been shown to play a role in myogenesis. To characterise these cells further, future experiments may look at individual cell populations such as pericytes, PICS and FAPS separated by FACS cell sorting for MEGF10 expression.

In conclusion, despite testing three different model systems for MEGF10 expression, we were unable to conclusively find satellite cells that stain for MEGF10 at a defined time point, and always associated with a specific muscle TF such as MyoD or myogenin. However, we did find MEGF10 cells

that were not positively stained for muscle TFs or other markers. The identity of those cells is unclear.

4 Effect of Overexpression of Wildtype and Mutant MEGF10 on Cellular Function.

4.1 Introduction

Previously, MEGF10 has been overexpressed in C2C12 cells by retroviral infection (Holterman et al., 2007). That study showed that over-expression of MEGF10 increased cell proliferation 24 - 72 hrs post-infection and inhibited myoblast fusion five days post-differentiation. Over-expression of MEGF10 also maintained myoblasts in a quiescent state and down regulated the expression of the key myogenic proteins MyoD and Pax7 (Holterman et al., 2007). Cells overexpressing MEGF10 also failed to increase expression levels of skeletal myosin heavy chain and myogenin, when induced to differentiate. In those experiments, the MEGF10 was tagged with an HA epitope, which allowed the localisation of the expressed MEGF10 to be visualised in fixed C2C12 cells using an anti-HA antibody. This showed that the HA-tagged MEGF10 was found mainly in the cytoplasm with some localisation to the plasma membrane. However, no high magnification images were shown to clearly see the protein localisation.

As overexpression of MEGF10 appears to have distinct effects on proliferation and differentiation on myoblasts, this could be a useful system in which to compare the effects of wildtype and mutant isoforms of MEGF10. Mutant isoforms may not be able to elicit the same response as the wildtype protein when overexpressed, and may have less effect on proliferation or differentiation. In addition, expression of a GFP-tagged MEGF10 would allow direct visualisation of MEGF10 in live cells. Therefore, I generated expression constructs for wildtype and mutant MEGF10 with a C-terminal GFP tag. An additional 6His tag was also included (A diagram of wildtype and mutant constructs is presented in Figure 33).

I used an adenoviral system to express MEGF10_eGFP in cultured C1F myoblasts (protocol described in 2.10). Infection with the adenovirus typically involves attachment of the virus to receptors such as coxsackie- and

adenovirus receptor (CAR) as well as interactions with sialic acid. After attachment to the cell the virus is internalised by interaction with receptors including integrins, which, initiate the process of viral entry in clathrin-coated vesicles and transported to endosomes. Upon acidification the virus leaves the endosome, enters the cytoplasm and is transported to the nucleus for replication (Rux and Burnett, 2004; Zhang and Bergelson, 2005). It has previously been shown that commonly used C2C12 myoblasts lack the coxsackie receptor, which reduces the efficacy of viral uptake. This means that a high MOI is required for effective adenoviral transduction and gene expression in the C2C12 cells (Nalbantoglu et al., 1999; Tanaka et al., 2011). However, the RNAseq data for undifferentiated C1F cells, (Chapter 3.) shows the presence of a low level of RNA (FPKM = 4.06) for the *CXADR* gene, which encodes CAR, and thus adenoviral infection was expected to work for the C1F cells, although a high MOI may still be needed.

Four different MEGF10_eGFP constructs were made: wildtype, and the three mutants: C774R, W520X and R71W. C774R is in the 16th EGF-like (EGF-laminin) domain. This mutation to arginine will disrupt one of the di-sulphide bonds between pairs of cysteines in this domain, and may affect the overall folding and stability of the protein. Mutation R71W that replaces an amphipathic arginine with a hydrophobic tryptophan in the EMI domain. The difference in chemical structure and size of tryptophan may have a large effect on protein stability and the ability to form interactions. Replacement of the arginine, which are typically found at protein binding sites, such as in SH2 domains, may further disrupt protein interactions with the ECD. Mutation W520X is a substitution of a tryptophan residue for the termination codon, and thus would be expected to produce a shorter non-functional protein unless there is ‘read-through’ of the termination codon. Despite being rare in mammalian genes, an increasing number of genes have been identified as having stop codon read-through (Loughran et al., 2014). Each mutant construct is depicted in Figure 33.

All 4 MEGF10_GFP constructs were expressed in C1F cells, and the effects on myoblast differentiation and cell motility was measured by immunostaining of fixed cells during differentiation, and by differential interference contrast (DIC) imaging of live C1F myoblasts respectively. It

was expected that wildtype MEGF10_eGFP would inhibit myoblast fusion as previously reported (Holterman et al., 2007), whereas mutant isoforms may have different effects. Live cell imaging of MEGF10_GFP expressed in Cos-7 cells was also performed to determine the localisation of MEGF10 within cultured cells and the addition of TRITC labelled dextran was used to explore the possibility of endocytic cycling of MEGF10 as previously predicted (Barry and Camargo, 2013; Singh et al., 2010; Suzuki and Nakayama, 2007a).

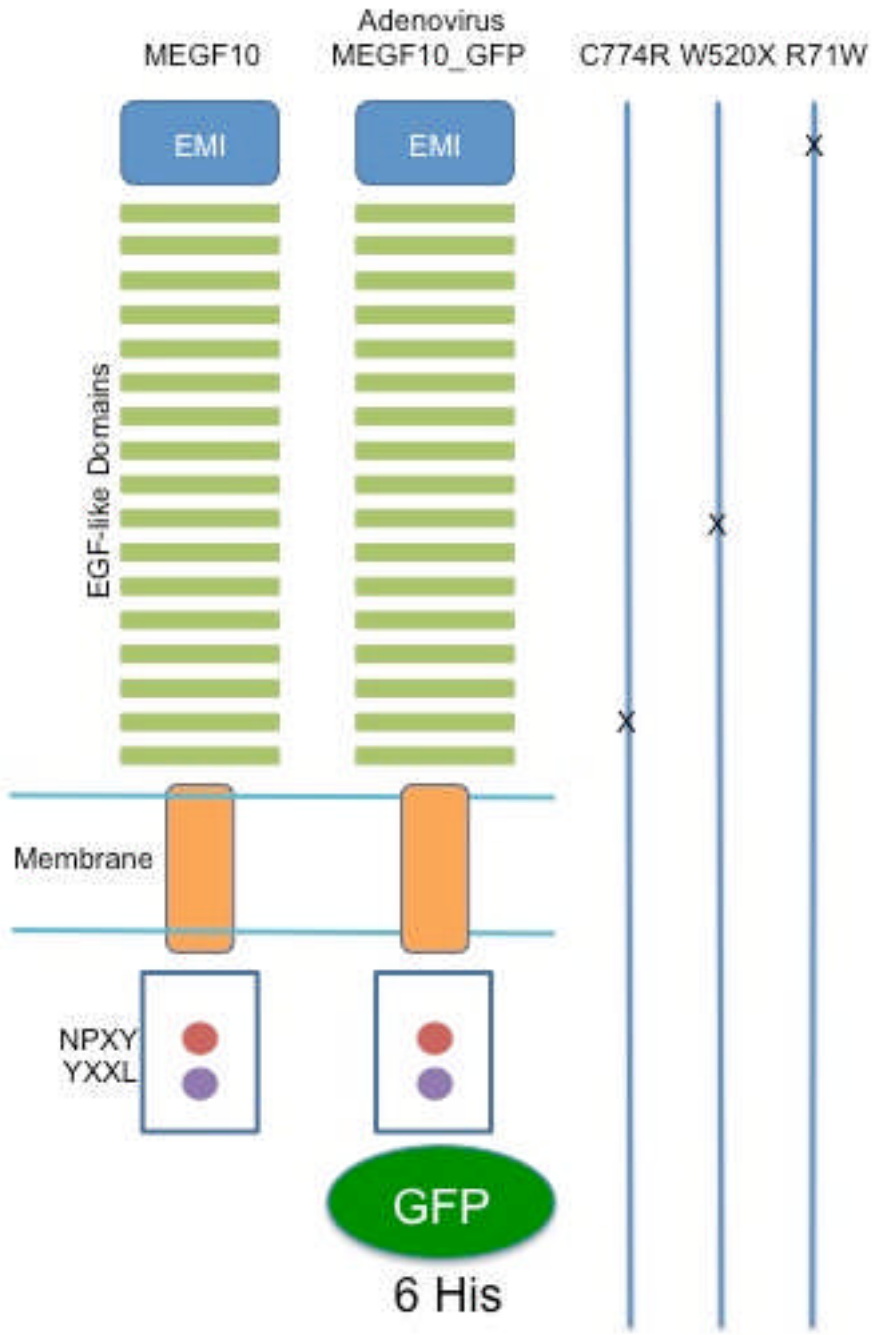

Figure 33. MEGF10 adenoviral constructs.

A diagram showing full length MEGF10 and mutant adenoviral constructs designed with C-terminal GFP and 6 His tags. Full-length wildtype MEGF10 and full length MEGF10 with pathogenic mutations (indicated by x) for exogenous expression in myoblast cells are shown. The mutations are: c.2320T>C p.C774R, c.1559G>A p.W520X and c.211C>T p.R71W.

4.2 Methods

4.2.1 **Cloning**

To express MEGF10 as an adenoviral construct, full length MEGF10 was cloned into the pDC315 vector with C-terminal 6His and enhanced green fluorescent protein (eGFP) tags in a two-step process. Firstly, full length MEGF10 cDNA was PCR amplified from the pBluescript II SK+_MEGF10 plasmid using InFusion primers which added an NheI site to the N-terminus followed by a Kozak sequence and initiation codon (pDC315_MEGF10_FWD). The reverse primer corresponded to the C-terminus of MEGF10 removing the stop codon (NS), and adding a SalI restriction site (pDC315_MEGF10_NS_REV) (Figure 34. A.). Using InFusion cloning, MEGF10_NS was cloned into the AdMax system shuttle vector pDC315 (Figure 34. B.). The second step of cloning was to add a C-terminal 6His and eGFP, separated from MEGF10 by a flexible linker composed of three glycine residues. Full length eGFP was PCR amplified from the pEGFP-N1 vector using InFusion primers; the forward primer was designed to add the last 15 bp of the MEGF10 construct and the 3 glycine linker to the N-terminus of eGFP to allow InFusion cloning into the pDC315_MEGF10 vector at the SalI site. The reverse primer was designed to incorporate a 6His-tag, stop codon, SalI site and bases of pDC315 vector to the C-terminus of eGFP to enable InFusion cloning into the SalI site (eGFP_6His_REV) (Figure 34. C.). Colonies from cloning steps were analysed by colony PCR (Figure 34. D.) and restriction digests (Figure 34. E.) (InFusion cloning primers are listed in Table 13.). Positive clones were Sanger sequenced to confirm clones were in-frame and no additional mutations had been introduced into the vectors (Sequencing primers are listed in Table 3.). The full pDC315_MEGF10_GFP_6His vector map shows the final construct (Figure 34. F).

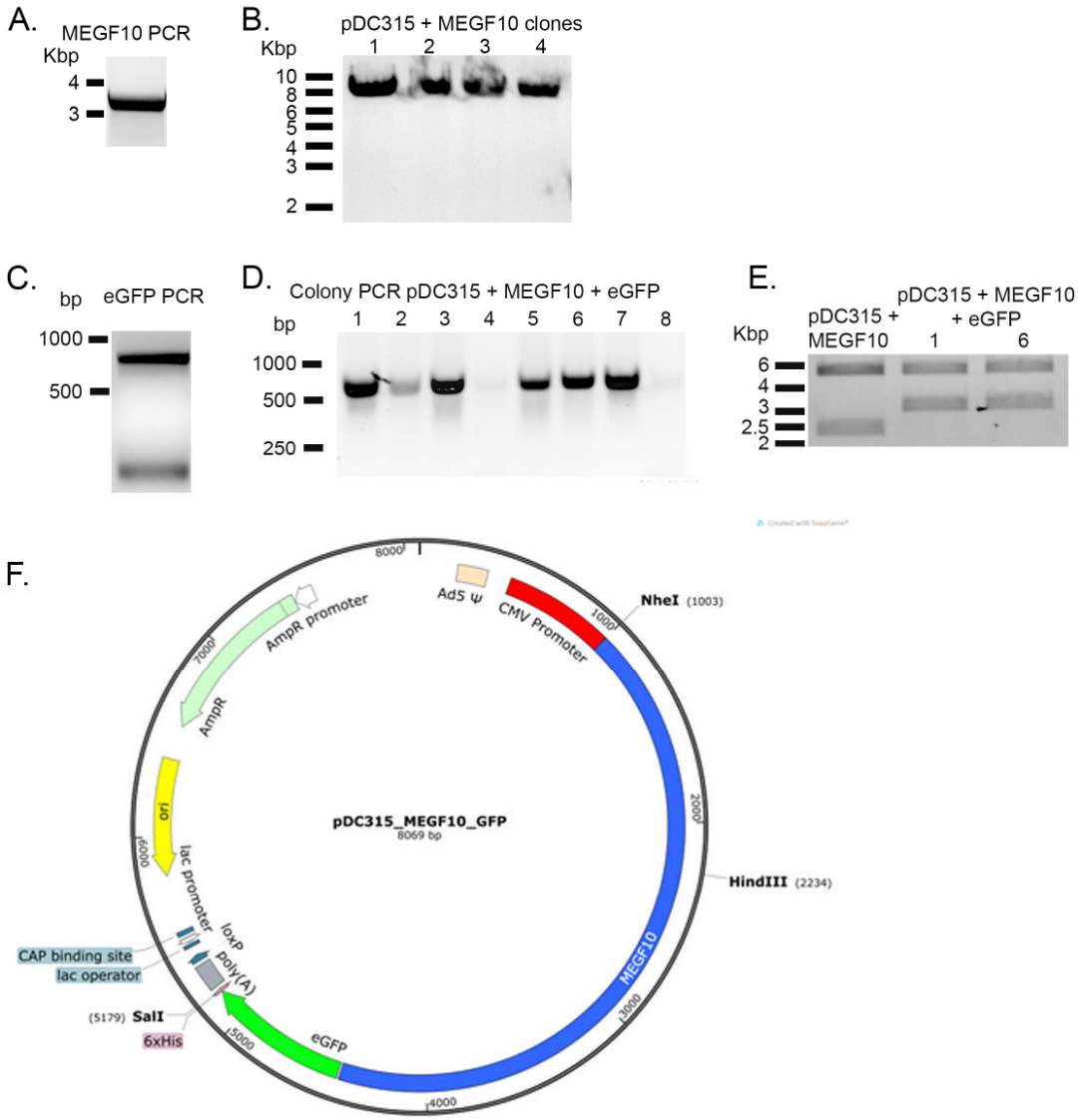

Figure 34. Cloning of MEGF10_GFP into adenoviral vector pDC315.

A. A 0.7% agarose gel of full length MEGF10 PCR product (Expected size: 3423 bp). **B.** Sal I restriction enzyme digest of pDC315_MEGF10 colonies 1 - 4 (Expected size: 8.3 Kb (vector 3.9 Kb + insert 3.4 Kb). **C.** eGFP PCR product amplified from the GFP_N1 plasmid (Expected size: 750 bp). **D.** A colony PCR of the EGF domain of pDC315_MEGF10_6His_GFP colonies 1 - 7 and lane 8 is the pDC315_MEGF10 vector without GFP/6His Tag (Expected size: 750 bp). **E.** HindIII/SalI restriction digest confirming the presence of the MEGF10_GFP insert in Control pDC315_MEGF10 and colonies 1 and 6 pDC315_MEGF10_GFP(Two bands with a size of ~ 5 Kb and 3 Kb were expected). **F.** pDC315_MEGF10_GFP vector map.

4.2.2 **MEGF10 adenovirus in vitro mutagenesis**

Mutagenesis primers were designed according to the parameters described in (Table 14.). Briefly, mutations c.2320T>C, c.1559G>A and c.211C>T (for the mutations: C774R, W520X and R71W respectively) were introduced into pDC315_MEGF10_GFP construct using the QuikChange XL Mutagenesis Kit (Agilent Technologies). Each point mutation was placed in the centre of the primers. Clones were sequenced using the sequencing primers listed in (Table 3.) to ensure that the mutagenesis had been successful and that *de novo* mutations had not been introduced.

Table 13. InFusion cloning primers

Primer Name	Primer sequence (5'to 3')	Tm (°C)
pDC315_MEGF10_FWD	aattcaagctgctagcgccaccatggttatttctttgaactcatgc	83.12
pDC315_MEGF10_NS_REV	gttgctcgaagtcgacttcactgctgctgctgttgct	85.80
GGG_eGFP_FWD	agcagcagcagtgaaggaggcggtgtgagcaagggcgaggag	90.89
eGFP_6His_REV	gttgctcgaagtcgactcagtgatggtgatggtgatgcttgtacagctcgtccatgcc	91.50

Table 14. Mutagenesis primers

Single nucleotides targeted for in vitro mutagenesis base pairs are highlighted in bold.

Primer Name	Primer sequence (5' to 3')	Length	Tm (°C)
c.2320T>C forward	cacatttctgggcag**c**gtacttgccgcactg	31	80.51
c.2320T>C reverse	cagtgcggcaagtac**g**ctgcccagaaatgtg	31	80.51
c.1559G>A forward	cgtgtgcacctggat**a**gcgcggggagaaatg	31	81.73
c.1559G>A reverse	catttctccccgcgc**t**atccaggtgcacacg	31	81.73
c.211C>T forward	tggtttaaatgcacg**t**ggcacagagtcagc	30	76.50
c.211C>T reverse	gctgactctgtgcc**a**cgtgcatttaaacca	30	76.50

4.2.3 **MEGF10 adenovirus titre**

Adenoviral constructs were prepared as described in 2.10 and the viral titre was calculated, as described in 2.10.5, to ensure that cells were infected with the same MOI of virus in subsequent experiments. Each viral construct showed good GFP expression in cultured cells, including mutant W520X which was not expected to produce the GFP protein due to the premature stop codon introduced by the mutation. This suggests that there may be read-through through the premature stop codon enabling continued expression of the protein.

Virus Construct	Viral Titre (PFU/ml)
eGFP	$6.3x10^8$
MEGF10	$3x10^8$
C774R	$6.3x10^8$
W520X	$7.9x10^8$
R71W	$1.6x10^9$

4.2.4 **Fusion Index Calculation**

To determine the effect of MEGF10 constructs on myoblast differentiation the fusion index was calculated. Briefly, C1F cells were seeded onto 13 mm diameter coverslips, coated with 0.1% gelatin and differentiated for seven days. Cells were fixed with pre-warmed 4% PFA prior to permeabilisation with 0.1% Triton X-100 in PBS. The nuclei were stained with DAPI, actin stained with fluorescently labelled phalloidin and myotubes indicated by staining for skeletal myosin using the A4.1025 antibody (Cho et al., 1994; Maggs et al., 2000).

The fusion index is the percentage of cells in skeletal myosin positive myotubes as a percentage of the total number of cells. The total cell number is determined by counting the number of DAPI stained nuclei. Only skeletal myosin positive myotubes with three or more nuclei were classed as

myotubes. For each condition, five fields of view were imaged and cells counted from three biological replicates.

4.2.5 **Cell Motility Assay**

To determine the effect of MEGF10 over-expression on cell motility, cells were imaged overnight by differential interference contrast (DIC) microscopy. Briefly, a 96 well plate with a borosilicate glass bottom (Iwaki) was seeded with 50 µl of C1F cells prepared at $1x10^5$ cells/ml. Cells were incubated with 50 µl of culture media at 33°C and 10% CO_2. 100 MOI of each adenoviral construct was added to each well in 500 µl culture media and the plate incubated overnight. The cells were filmed over 14 hrs, capturing images at 10 min intervals using a 10x lens (512 x 512 total pixel size, 2 x 2 binning). Imaging was performed on a DeltaVision deconvolution system with a motorised stage and incubator. For each condition, five fields of view were imaged and cells tracked from three biological replicates. Cell motility was analysed using ImageJ software (MTrackJ plugin), tracking 10 cells per field of view.

4.2.6 **Live cell imaging of MEGF10_GFP in cultured cells**

The fibroblast-like cell line, Cos-7, derived from African green monkey kidney was used for live cell imaging experiments. Cos-7 cells were cultured in DMEM supplemented with 10% FBS and 1% P/S, and cultured 2 - 3 times a week as described for other cell lines (2.7). For live cell imaging, Cos-7 cells were plated onto glass-bottomed dishes (Ibidi) at $1x10^5$ cells/ml. Cos-7 cells were infected with 100 MOI MEGF10_GFP adenovirus and incubated at 37°C for 24 hr prior to imaging. For live cell imaging, the culture media was supplemented with 50 mM HEPES. For the dextran endocytosis assay TRITC_dextran was prepared at 1 mg/ml in serum-free media and 250 µl was added to 2 ml media in each dish. The cells were incubated with dextran at 37°C, 5% CO_2 for 20 min. Excess dextran was washed out with PBS prior to imaging. Cells were imaged on the LSM 880 confocal microscope (Zeiss) using the 63x objective and the chamber heated to 37°C.

Cells expressing MEGF10_GFP were imaged as a time series, with 665 cycles at a time interval of 500 ms. Cells expressing MEGF10_GFP and with TRITC_dextran uptake were imaged for 200 time points taken every 500 ms.

4.3 Results

4.3.1 The optimal MOI for the MEGF10_eGFP adenoviral infection of C1F cells was 100

The MOI required to infect C1F myoblasts was determined by incubating the cells with a range of viral MOIs (50 to 500 MOI). The MOI (multiplicity of infection) is defined as the ratio of viral particles to cells, where a 50 MOI is 50 viral particles per cell). An MOI of 100 was optimal for the efficient infection of the cells without causing the aggregation of the protein. High MOIs (250 - 500 MOI) resulted in high levels of fluorescence close to the nucleus, which may have been MEGF10_eGFP that was trapped in the Golgi, rather than being transported to the membrane. The lower MOI of 50 resulted in low levels of expression that were difficult to image successfully. A 100 MOI infection produced sufficient MEGF10 expression that was distributed throughout the cell and correctly targeted to the plasma membrane (Figure 35.). An MOI of 100 was therefore used for subsequent experiments.

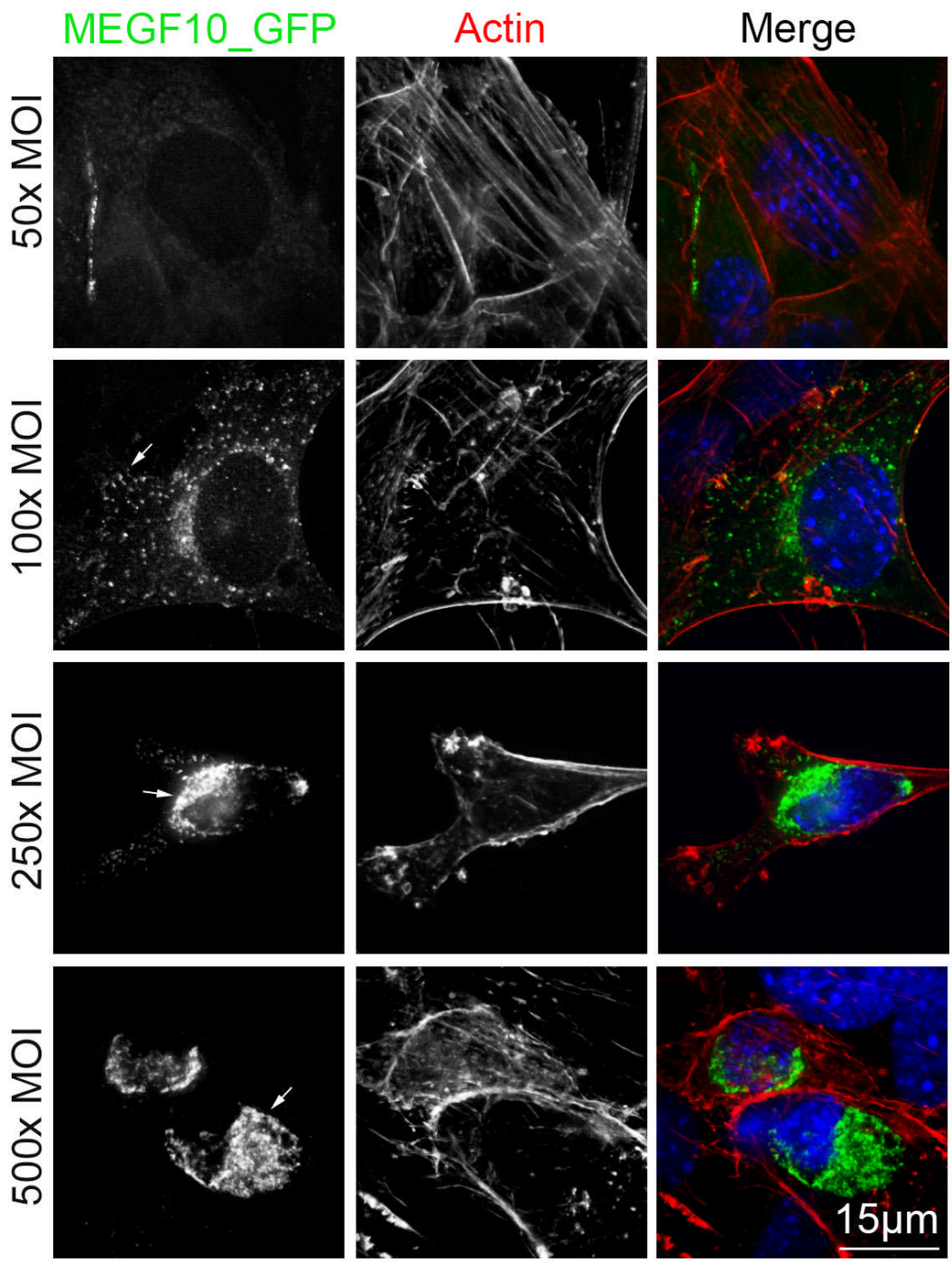

Figure 35. C1F adenoviral MOI infection.

Representative images of C1F cells infected with 50 - 500 MOI MEGF10_GFP adenovirus. Cells were fixed 24 hr post infection and stained for actin with phalloidin (red), the nuclei stained with DAPI (blue) and the MEGF10 adenovirus tagged with GFP (green). Cells were imaged using the same microscope settings.

4.3.2 **Mutant MEGF10_eGFP constructs showed a markedly different localisation compared to wildtype in C1F myoblasts**

In C1F myoblasts, MEGF10_eGFP was localised to the membrane and throughout the cytoplasm, where it was mostly found in vesicles, and to a perinuclear region that was most likely the Golgi (Figure. 36.). As MEGF10 has to be transported to the membrane, and is most likely endocytosed once at the membrane, the vesicles are likely to be either secretory vesicles or endosomes. Live cell imaging showed that many of these vesicles were highly motile (Figure. 37. A). The addition of texas-red dextran to the cells, which is taken up into endosomes via endocytosis additionally showed that many of the MEGF10_GFP positive cells also stained positively for texas-red dextran (Figure. 37. B).

In contrast to wildtype MEGF10_eGFP, all 3 mutant MEGF10_eGFP isoforms tested do not localize to the membrane but form aggregates. (Figure. 36.). In each case, the majority of these aggregates were found close to the nucleus. The mutant C774R forms an almost continuous ring around the nucleus, whilst aggregates of mutants W520X and R71W are smaller.

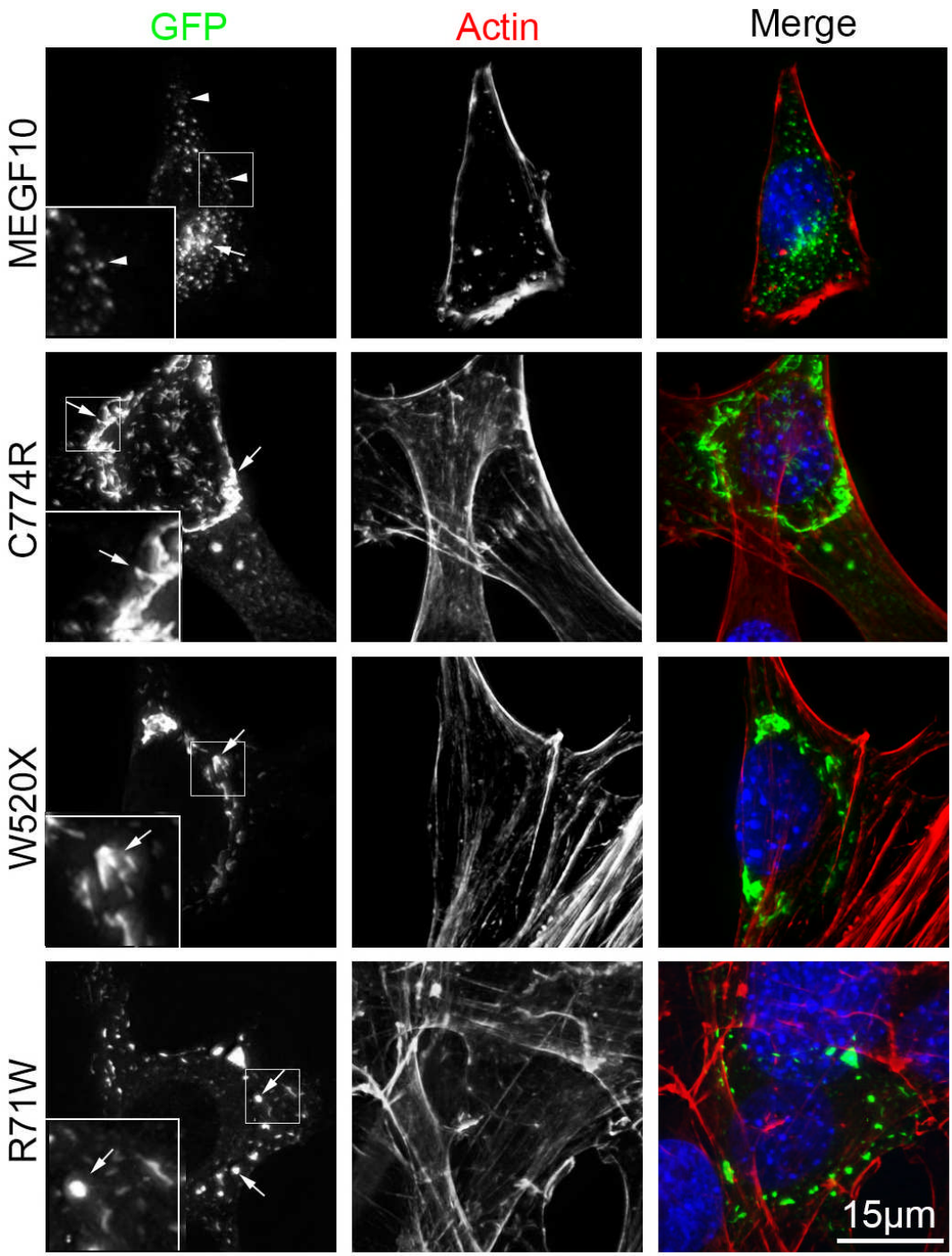

Figure 36. Localisation of MEGF10 and Mutant Adenovirus in C1F cells. Immunofluorescence staining of C1F cells infected with MEGF10 and the three mutant adenoviral constructs. Cells were stained for actin, with phalloidin, in red, the nucleus with DAPI in blue, and GFP tagged MEGF10 in green. Inset shows zoomed in region of the cell. Arrows indicate clumps of GFP; arrowheads indicate GFP in the membrane).

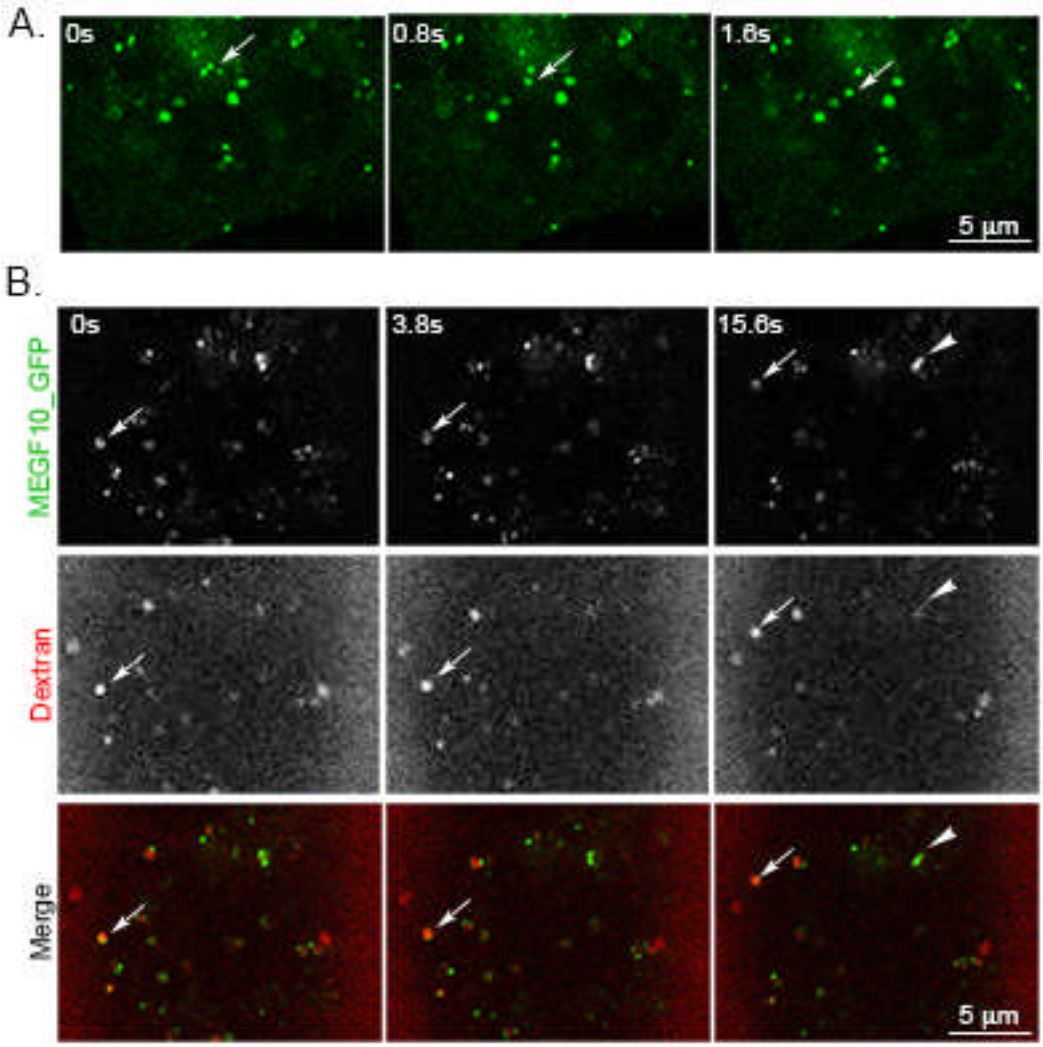

Figure 37. MEGF10_GFP is localised in vesicles and endosomes.

A. Images Cos-7 cells overexpressing MEGF10_GFP and imaged over time, showing the dynamic movement of MEGF10 within vesicles (GFP fluorescence in a predicted vesicle is tracked, as shown by arrows). **B.** Cos-7 cells infected with MEGF10_GFP partially colocalised with dextran, suggesting an endosomal localisation (indicated with arrows). Not all MEGF10_GFP is colocalised with dextran (shown with arrow heads).

4.3.3 **Expression levels of wildtype and mutant MEGF10 constructs in cultured cells were similar.**

To confirm that the differences in localisation observed for the wildtype and mutant constructs were not due to higher levels of expression of the mutant MEGF10 constructs, expression was assessed by western blot. Cells were infected with 100 MOI of each viral construct and the protein extracted and prepared for western blotting as described (2.12). An adenoviral construct that only expressed eGFP, and the purified ECD of MEGF10 (Chapter 5) were used as positive controls on the blot. An equal amount of whole cell lysate (30 µg) was loaded per well of a 10% SDS_PAGE gel and a western blot performed. The blot was probed for MEGF10 (Sigma Prestige) and GFP (CUSABIO). The results showed that an MOI of 100 produced a similar level of protein expression in cultured cells for both the wildtype and mutant constructs. It also demonstrates that there must be read-through of the termination codon in the W520X mutant, as otherwise a full-length protein that is recognised by the anti-MEGF10 antibody would not be produced (Figure 38).

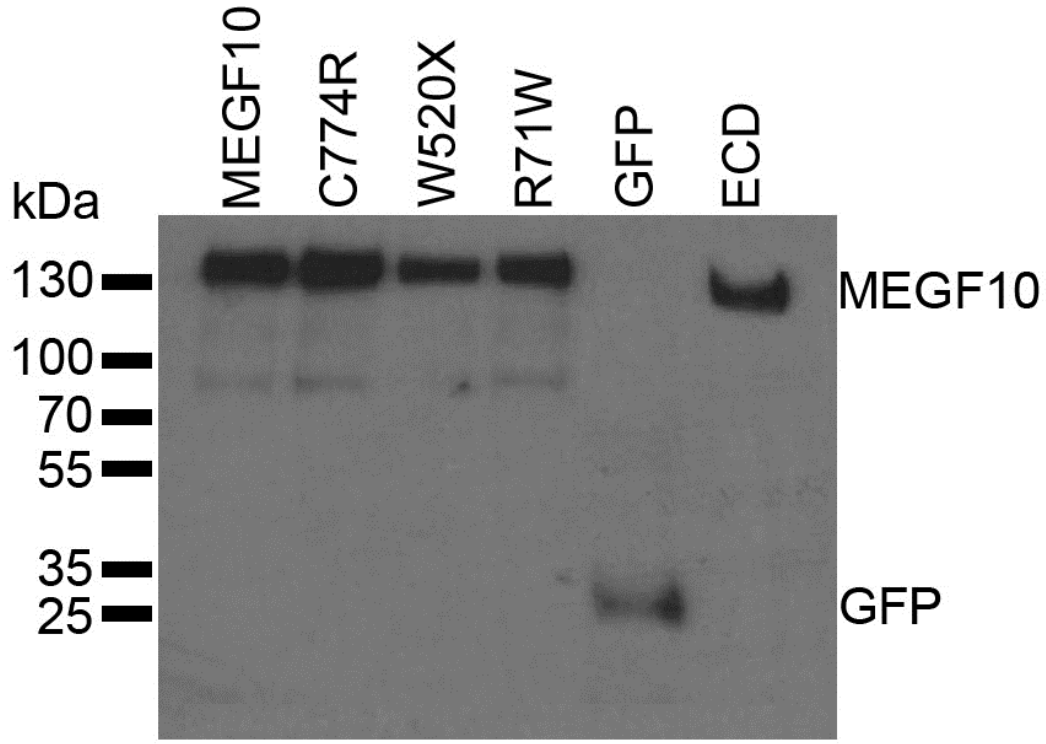

Figure 38. Expression levels of MEGF10 constructs in cultured cells.

A western blot showing the even expression of MEGF10_GFP adenoviral constructs in cultured cells. A GFP only adenoviral construct (27 kDa) and purified MEGF10 ECD (~130 kDa) were used as positive controls. The membrane was probed with anti-MEGF10 (Sigma Prestige) and anti-GFP (CUSABIO) antibodies.

4.3.4 **Expression of MEGF10 affects myoblast fusion.**

Over-expression of wildtype and each of the 3 mutant MEGF10_GFP isoforms in C1F cells inhibited myoblast fusion (Figure 39. A. and B.). Uninfected C1F cells fused into multinucleated myotubes with high efficiency (fusion index of ~80%, Figure 39. B.). Infection of C1F cells using adenovirus that only expressed GFP significantly reduced fusion to 64% ($p = 0.0039$), suggesting that viral infection alone may reduce fusion. However, the fusion index was much more markedly reduced after infection with the wildtype MEGF10_eGFP adenovirus (7.5%) and each of the mutants (C774R (9.9%), W520X (2.3%) and R71W (8.9%) ($p = < 0.0001$)) (Figure 39. B.).

To determine if the decrease in fusion was linked to a decrease in cell number caused by overexpression of MEGF10_eGFP, cell counts were performed at day 7 of differentiation. For wildtype and each of the mutant isoforms of MEGF10_eGFP, cell number was significantly reduced at day 7 of differentiation (Figure 39. C.). This effect is unlikely to be due solely to infection with the adenovirus, as expression of GFP alone using an adenoviral construct did not affect cell number (Figure 39. C.). This suggests that expression of both wildtype and mutant isoforms of MEGF10_eGFP affect either cell viability or division.

To test if the reduction in fusion arising from expression of wildtype or mutant MEGF10_eGFP isoforms was due to a reduction in C1F cell motility, live cell imaging of myoblasts was performed. Expression of GFP alone had a small effect on motility compared to control, uninfected cells (Figure 39. D. and E.). However expression of MEGF10_eGFP significantly reduced cell motility compared to the GFP control. Expression of each of the MEGF10_eGFP mutant isoforms resulted in a further significant reduction in cell motility, that was lower than that observed for cells expressing wildtype MEGF10_eGFP (Figure 39 D. and E.). This suggests that expressing MEGF10_eGFP does affect cell motility, which may contribute to a reduction in fusion.

To check if the effects on fusion were likely due to expression of MEGF10 during the early stages of myoblast fusion, expression levels of MEGF10_eGFP were measured over the course of differentiation by

analysing the number of cells positive for eGFP. This showed that levels of MEGF10_eGFP were highest at days 0 and 1 after initiation of differentiation, (1 – 2 days post-infection with adenovirus), before decreasing at day 3 of differentiation. A small subset of cells were still positive for eGFP at day 7 of differentiation (Figure 40. A. and B.). C1F cells would have undergone approximately 2 rounds of division after infection, before becoming confluent and entering the differentiation pathway suggesting that the level of MEGF10_GFP may have been diluted slightly through cell division. Therefore, levels of MEGF10_eGFP were highest during the early stages of myoblast fusion.

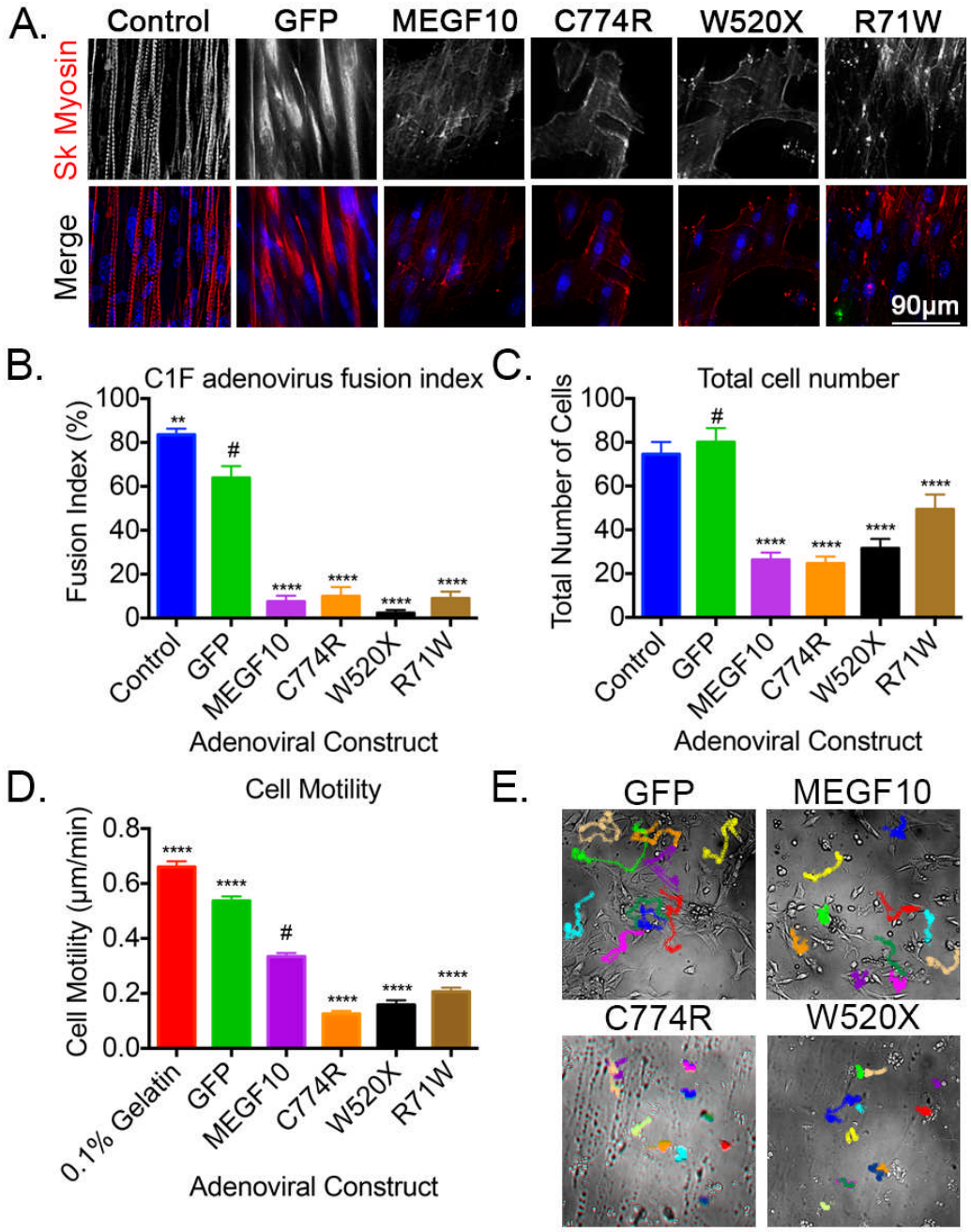

Figure 39. C1F cells seven days after differentiation.

A. Adenoviral infected C1F cells after seven days of differentiation with nuclei stained in blue and skeletal myosin in red. **B.** The fusion index of infected C1F cells after seven days of differentiation. (**** $p < 0.0001$, ** $p = 0.0039$). **C.** Total number of cells counted after seven days of differentiation. (**** $p < 0.0001$, control: $p = 0.5343$). **D.** The motility of C1F myoblasts infected with each construct measured over 14 hr. **E.** Sample fields of view showing the tracks recorded using ImageJ. (Mean values +/- S.E.M. with 10 cells tracked in a minimum of five fields of view for each repeat; n=3. # indicates the condition used as a comparison for t-test statistical analysis and asterisks indicate statistically significant changes.)

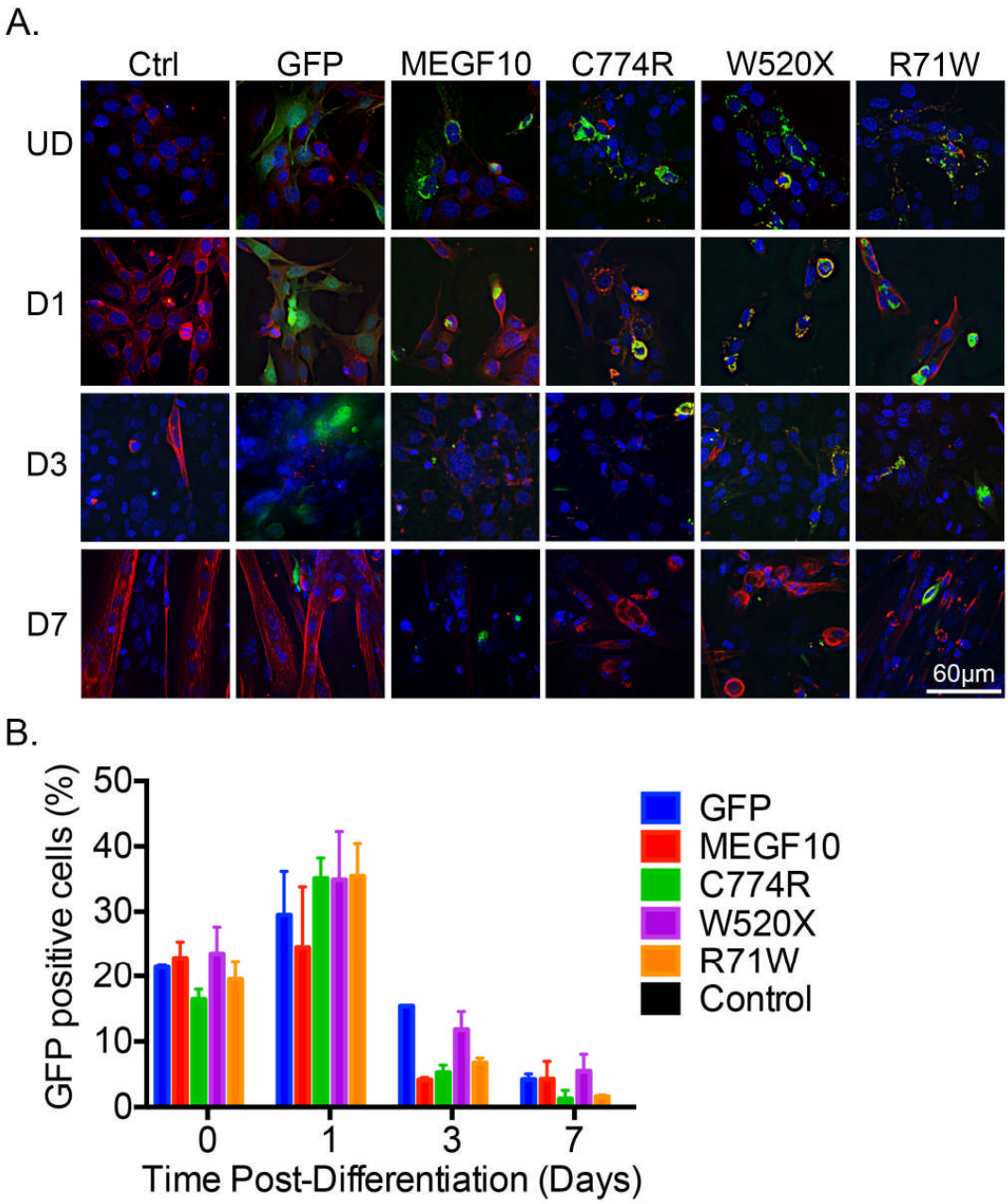

Figure 40. Viral expression in C1F cells during differentiation

A. Immunofluorescence staining of C1F cells infected with adenoviral constructs tagged with GFP in green, and stained for skeletal myosin in red and the nuclei stained with DAPI in blue. **B.** A quantification of adenoviral expression in C1F cells over seven days of differentiation. The graph depicts the percentage of the total number of cells showing positive GFP expression. (Mean values +/- S.E.M. with a minimum of five fields of view analysed for each repeat; n=3).

4.4 Discussion

These data show that wildtype MEGF10_eGFP localised to vesicular structures in the cytoplasm and to the plasma membrane, whilst each of the mutant constructs formed aggregates close to the nucleus and poorly localised to vesicles and the plasma membrane. Despite this difference in localisation, expression of both the wildtype MEGF10_eGFP and the mutant constructs significantly inhibited myoblast fusion. This was accompanied by a significant reduction in cell motility, as well as a reduced cell number by day 7 of differentiation. The mutant isoforms of MEGF10_eGFP behaved similarly to wildtype in their effects on fusion and cell number, but showed a much higher effect on cell motility compared to the wildtype.

The localisation of wild-type MEGF10_eGFP throughout the cytoplasm and at the plasma membrane is consistent with the localisation reported for the HA-tagged MEGF10 construct reported previously (Holterman et al., 2007). As MEGF10 is a membrane protein, its localisation to the plasma membrane and intracellular vesicles is consistent with what has been previously reported for proteins with similar structure (Yamamoto et al., 2010). Live cell imaging and the use of Texas-red dextran confirmed that MEGF10_eGFP was likely to be in vesicles, and that some of these were likely to be in the endocytic pathway (Barysch et al., 2010).

Localisation of MEGF10 at the plasma membrane and in intracellular vesicles could mean that MEGF10 activation can occur in both places. It is still unclear how MEGF10 is activated, as a MEGF10 binding partner has not yet been clearly demonstrated. The MEGF10 extracellular binding partner is unknown; although it has been suggested to interact with Notch (Bröhl et al., 2012; Holterman et al., 2007), it is not known if MEGF10 can be cleaved in a similar manner to Notch, or if this is important for its activation. The intracellular domain of MEGF10 interacts with and contains well known motifs for binding to other proteins (1.3) and is suggested to bind to AP50 enabling clathrin mediated endocytosis (Singh et al., 2010; Suzuki and Nakayama, 2007b).

Notch, another TM protein with multiple EGF domains, is normally activated when plasma membrane bound Notch binds to a ligand, such as Delta or

Serrate (reviewed in (Kopan and Ilagan, 2009)) on an adjacent cell. Subsequent cleavage steps of Notch result in the release of its intracellular domain, which translocates to the nucleus. Once in the nucleus it interacts with Suppressor of Hairless and Mastermind to form a transcriptional regulatory complex. However, Notch is also present in endocytic vesicles, where the cytoplasmic domain remains available on the surface of the vesicle for binding to other proteins such as Deltex, a cytoplasmic ring finger protein. Binding of Deltex promotes trafficking of Notch to the lysosome, where the intracellular domain can then be released by a similar mechanism of cleavage to that of the plasma membrane bound Notch (Baron, 2012; Hori et al., 2011; Wilkin et al., 2008). Mutations that prevent Notch from being transferred from the endosome limiting membrane into the internal endosomal compartment, result in high levels of mis-activation of Notch (reviewed in (Fortini and Bilder, 2009)). This raises the possibility that MEGF10 may also be able to be activated or participate in downstream signalling pathways both at the plasma membrane and in vesicles and it is possible that the mislocalised MEGF10 mutant isoforms, even though apparently aggregated, could interfere with this process.

The mutant MEGF10_eGFP isoforms appear to aggregate close to the nucleus, suggesting that each of the mutations causes misfolding in the otherwise rigid ECD, and that this inhibits effective transport to the cell membrane. EGF-like domains in the ECD of MEGF10 are predicted to be heavily post-translated (1.3.3) and therefore the mutations present here may also disrupt sites of post-translational modification, which may have a significant role in protein function. The impact of these pathogenic mutations on the post-translational modification of the ECD will be further explored through protein expression in the following chapter.

It is interesting that each mutation causes the resulting protein to aggregate, as one mutation is in the EMI domain (R71W), one is in an EGF-laminin domain (C774R), and the third mutation (W520X) introduces a termination codon, although a full length protein is still apparently produced. This suggests that small changes throughout the ECD of MEGF10 can have significant effects on protein localisation and function. Other recessive pathogenic conditions, such as cystic fibrosis caused by missense mutations

in the protein responsible for regulating epithelial surface fluid secretion in the GI and respiratory tracts, Cystic Fibrosis TM Conductance Regulator (CFTR) (Cutting, 2015),also result in aggregated protein causing the disease phenotype (Belcher 2010). This and other diseases caused by the misfolding and localisation of protein may give an insight into possible disease mechanisms of MEGF10 (Reviewed by Valastyan and Lindquist, 2014).

Overexpression of both wildtype and mutant MEGF10 constructs, through the expression of MEGF10_eGFP, significantly inhibited myoblast fusion, confirming previous results (Holterman et al., 2007). However, in our experiments, MEGF10 overexpression did not increase cell number as previously reported (Holterman et al., 2007), but by day 7 of differentiation, cell number was significantly reduced. This reduction in cell number may help to explain the reduction in fusion, as a lower number of cells would reduce the number of cell-cell interactions necessary for myoblast fusion and therefore inhibit myofibre formation. The reduction in fusion could also be linked to the reduction in cell motility, as cells need to migrate towards each other in order to fuse. If MEGF10 increases cell adhesion as reported (Holterman et al., 2007; Suzuki and Nakayama, 2007a), this could explain the reduction in cell motility observed. Thus, high levels of MEGF10 reduce motility and inhibit cell proliferation.

Unexpectedly, the effects of mutant MEGF10 isoforms were similar to those of the wildtype isoform in each of the experiments performed. The mutants also significantly reduced fusion, and cell number. However, they each had a larger effect on cell motility compared to wildtype MEGF10. This may suggest that the mutations in the ECD may not have a large influence on function, but that the presence of the intracellular domain of MEGF10 may be important for regulating myoblast fusion, and that the presence of intracellular MEGF10 as well as MEGF10 in the plasma membrane may be important for its function.

This study therefore has confirmed and addressed some of the previously published data on the over expression of MEGF10 and extended the work to explore the effect of pathogenic mutations on cellular function. However, it has not been able to demonstrate clearly why mutations in MEGF10 might

cause disease. If these proteins are also aggregated *in vivo*, it is possible that the resulting lack of localisation to the plasma membrane is the underlying cause of the disease. Without identifying the binding partners for MEGF10 and the downstream signalling pathways resulting from its activation, it is difficult to specifically determine the effects of the MEGF10 mutations.

5 Characterisation of the Extracellular Domain of MEGF10.

5.1 Introduction

The extracellular region of MEGF10 contains an N-terminal EMI domain and 17 EGF-like domains. The EMI domain was first described in proteins in the EMILIN family of glycoproteins and is associated with protein multimer formation (Doliana et al., 2000). Typically, EMI domains have seven cysteine residues, differing from other cysteine-rich domains, which have 6 or 8 cysteine residues. However, the EMI domain of MEGF10, whilst having the conserved consensus sequence at the C-terminus (WRCCPG(Y/F)xGxxC), only has six cysteine residues, with the second cysteine missing, as has also been described for the EMI domain in MMRN1 (multimerin) (Colombatti et al., 2012; Doliana et al., 2000). EMILIN proteins are associated with cell adhesion, migration and proliferation (Spessotto et al., 2003). MEGF10 in mammals was identified as the potential orthologue of the *C.elegans* CED-1 protein through the EMI domain and this protein has similar predicted functions to other EMILIN proteins, such as cell adhesion and cell proliferation (Callebaut et al., 2003; Holterman et al., 2007; Suzuki and Nakayama, 2007b). The EMI domain is predicted to interact with the membrane phospholipid PS which is exposed on the surface of apoptotic cells as a signal marking the cell for phagocytosis via TTR-52 (Tung et al., 2013). EGF-like domains in stabilin-2 have also been shown to directly recognise PS (Park et al., 2008). EGF-like domains are well-characterized protein domains present in a number of membrane proteins including Notch and Delta (Rao et al., 1995). There are a number of different classes of EGF domain, with differing PTMs and predicted functions (Wouters et al., 2005). MEGF10 contains two different forms of EGF-like domains: twelve EGF-like domains composed of seven conserved cysteine rich residues (Figure 41. A.), and five laminin-type EGF-domains that contain eight conserved cysteine residues capable of forming four disulphide bonds (Figure 41. B. and C.). Crystal structures of the EGF-like domains of Notch bound to Ca^{2+} show the importance of Ca^{2+} in stabilising and giving rigidity to

the rod-shape in the repeating structure of the ECD. Glycosylation of these domains has been shown to be important in regulating Notch signalling (Chillakuri et al., 2012). The structure and function of EGF-like domains has been described (Appella et al., 1988), and subsequent studies have suggested that EGF domains may have a role in mediating intercellular signalling and act in receptor-ligand interactions (Sorkin, 2001; Wouters et al., 2005).

A. EGF-like domains

```
EGF1   HCADKCVHG-----RCIAPN-TCQCEPGWGGTNCS-----------
EGF3   DCHQRCQCQNG--ATCDHVTGECRCPPGYTGAFCE-----------
EGF4   QCEQRCPCQNG--GVCHHVTGECSCPSGWMGTVCG-----------
EGF6   LCAETCQCVNG--GKCYHVSGACLCEAGFAGERCE-----------
EGF8   ACQQICSCQNG--ADCDSVTGKCTCAPGFKGIDCS-----------
EGF9   NCSSRCGCKND--AVCSPVDGSCTCKAGWHGVDCS-----------
EGF10  GCNLTCQCLNG--GACNTLDGTCTCAPGWRGEKCE-----------
EGF12  NCSLPCYCKNG--ASCSPDDGICECAPGFRGTTCQ-----------
EGF13  RCSQTCPQCVHSSGPCHHITGLCDCLPGFTGALCN-----------
EGF14  NCAGICTCTNN--GTCNPIDRSCQCYPGWIGSDCS-----------
EGF15  NCIHTCNCHNG--AFCSAYDGECKCTPGWTGLYCT-----------
EGF17  GCRQICDCLNN--STCDHITGTCYCSPGWKGARCD-----------
```

B. EGF-laminin domains

```
EGF2   -----CQCKNG--ALCNPITGACHCAAGFRGWRCEDRCEQGTYGNDC
EGF5   -----CQCHNG--GTCDAATGQCHCSPGYTGERCQDECPVGTYGVLC
EGF7   -----CPCHLENTHSCHPMSGECACKPGWSGLYCNETCSPGFYGEAC
EGF11  -----CDCSHA--DGCHPTTGHCRCLPGWSGVHCDSVCAEGRWGPNC
EGF16  -----CQCQNG--ADCDHISGQCTCRTGFMGRHCEQKCPSGTYGYGC
```

C. Cysteine-cysteine interactions

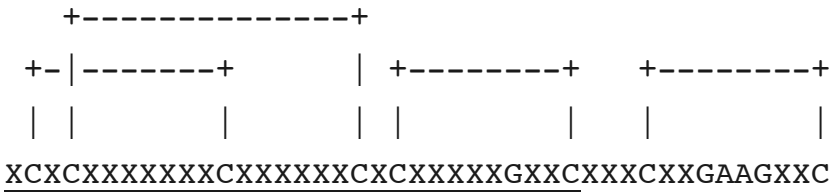

Figure 41. Alignment of EGF domains in MEGF10 and cysteine interactions.

A. The EGF-like and **B.** EGF-laminin domains in MEGF10 were aligned and the conserved cysteine residues highlighted in green. Multiple protein sequence alignment was performed using Clustal W (CLUSTAL 2.1) (Larkin et al., 2007; Thompson et al., 1994) **C.** The typical interactions between conserved cysteine residues in EGF-laminin domains are shown, the underlined portion is similar to EGF-like domains. Conserved glycine (G) and aromatic (A) residues to identify EGF-like domains are shown in the sequence (http://www.ebi.ac.uk/interpro/entry/IPR002049).

The post-translational modification of proteins with multiple EGF domains, such as Notch, have been shown to play an important role in intercellular signalling (Luther and Haltiwanger, 2009b). The sequence of MEGF10 is predicted to have multiple N-linked glycosylation sites (Figure 42.) (Gupta and Brunak, 2002). N-linked glycosylation of EGF domains has been shown to affect ligand recognition and binding in proteins (Wobus et al., 2004). EGF-like domains are further predicted to be modified by more unusual PTMs including *O*-fucosylation and interactions with sialic acid, which can affect intercellular signalling (Kao et al., 1999; Luther and Haltiwanger, 2009b).

MEGF10 has been suggested to play an important role in cell adhesion (Suzuki and Nakayama, 2007a). If this is the case, expressed and purified ECD would be expected to promote adhesion of myoblasts to a non-adhesive surface. Mutations in the ECD might exert their effects by affecting the structure of this domain, which could reduce any adhesive properties of the ECD. Removal of the EMI domain from an expressed ECD construct might also affect adhesion. Therefore, the objective of this chapter was to express and purify the ECD of MEGF10, analyse its potential to promote cell adhesion, and test the effects of mutants on this behaviour. This approach also allows further characterisation of the ECD, including an analysis of post-translational modification, and lipid binding behaviour

To express the ECD of MEGF10, I used a mammalian cell system. This approach has already proved beneficial in the expression of secreted protein products and identification of protein interactions (Dalton and Barton, 2014; Sakamoto et al., 2002). The expression vector I used allows the ECD to be secreted. This expression method should additionally generate protein that is fully post-translationally modified and correctly folded, which is likely to be important for its function. HEK-293 cells were selected as the mammalian expression cell line because they are simple to culture, amenable to transfection and stable cell lines can be readily made (Thomas and Smart, 2005). *E.coli* cannot promote PTMs, and typically lack the necessary chaperone proteins required for correct folding of many membrane proteins. Other eukaryotic expression systems such yeast and insect cells may also not enable full glycosylation of the protein (Yin et al., 2007).

Thus, the results in this chapter describe the production of various MEGF10 ECD constructs (Figure 43.) using mammalian cell expression, an analysis of their PTMs, an analysis of their lipid binding ability and tests of these constructs in their ability to promote adhesion, cell motility and differentiation for mouse myoblasts.

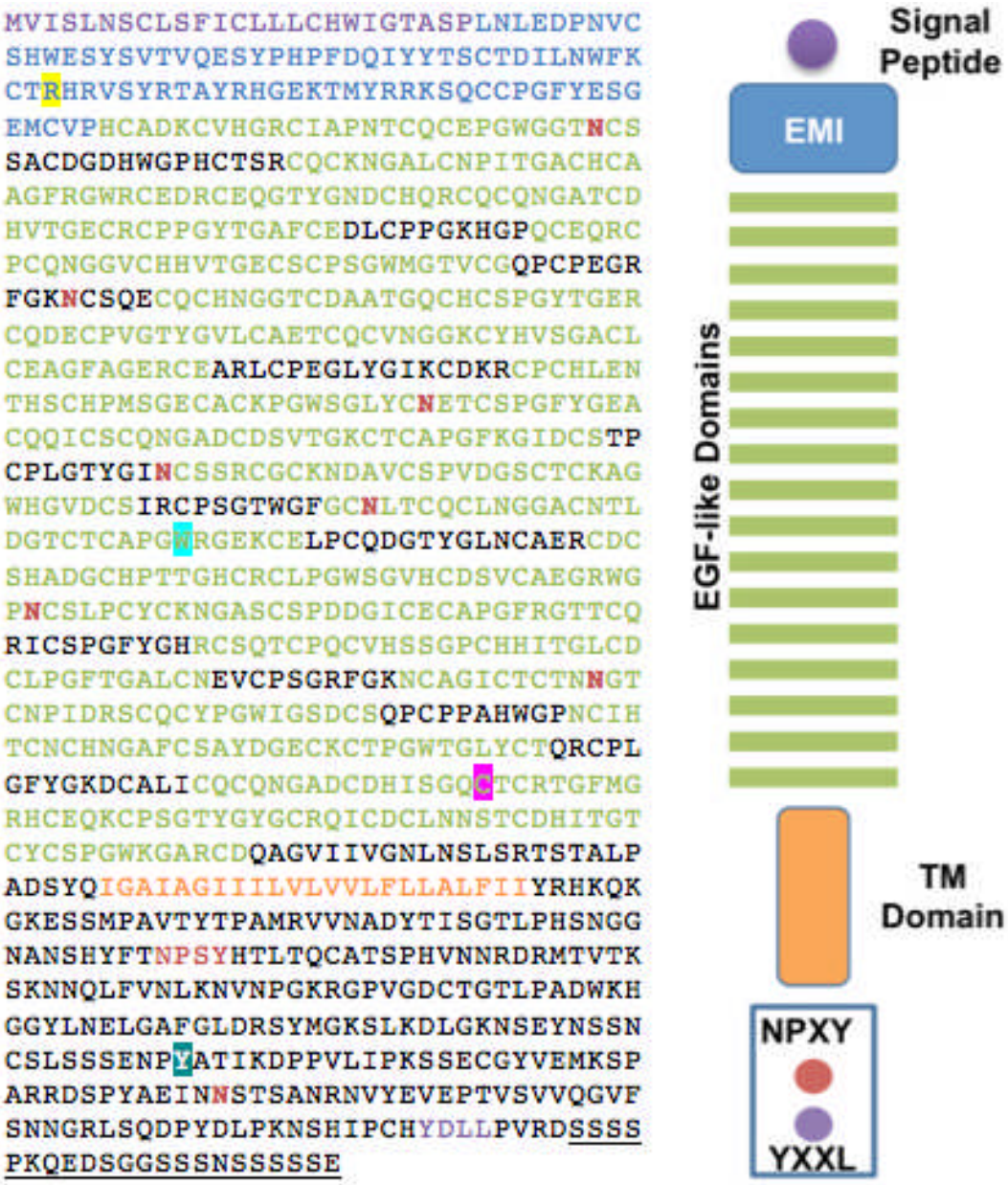

Figure 42. Predicted N-linked glycosylation of MEGF10.

The amino acid sequence of MEGF10 was analysed for predicted sites of N-glycosylation using the NetNGlyc 1.0 Server. Potential sites of N-glycosylation are highlighted in red. Mutations introduced to the ECD construct are positioned as follows R71W W520X C774R. Tyrosine Y1030 is highlighted in green Y.

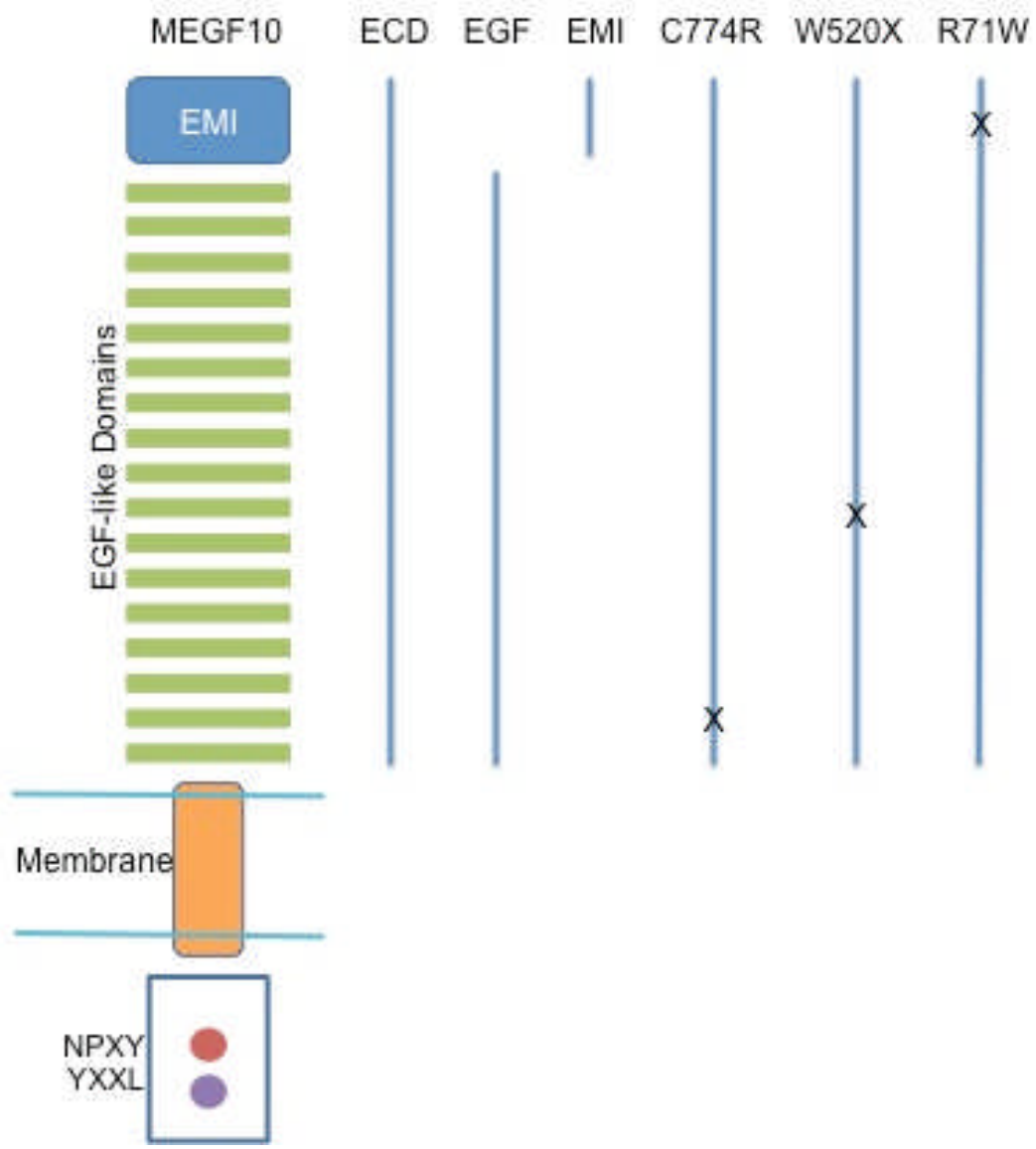

Figure 43. MEGF10 extracellular domain protein constructs.

Protein constructs for secreted mammalian expression of wild-type extracellular domain (ECD), epidermal growth factor (EGF)-like domains, and EMI domain proteins. The pathogenic mutations c.2320T>C p.C774R and c.1559G>A p.W520X. of the ECD investigated in this study are indicated by a cross (X).

5.2 Methods

5.2.1 **Cloning the extracellular domain of MEGF10 into pSecTag2A.**

The ECD of MEGF10 was cloned into the pSecTag2 vector by InFusion cloning (2.6.10). Mutagenesis was performed as described for the adenoviral constructs (2.6.12 and 4.2.2). Clones that had successfully undergone mutagenesis without introducing novel mutations were identified by Sanger sequencing.

MEGF10 ECD was cloned into the pSecTag2A vector (Invitrogen, Carlsbad, CA, U.S.A.) for the secreted expression of the protein in mammalian cells using the primers described in Table 15. A. and confirmed by Sanger sequencing using the primers listed in Table 3. The mammalian expression vector pSecTag2A has previously been used for the expression of cysteine-rich proteins similar to MEGF10 and therefore a possibly good system to use (Carlson et al., 2003). pSecTag2a contains an N-terminal secretion signal from Ig-κ for efficient protein secretion in the medium, a cytomegalovirus (CMV) promoter for high-level expression and C-terminal 6His and c-myc tags for nickel column purification and antibody detection, respectively. The vector also contains a Zeocin™ resistance gene for the selection of stable mammalian cell lines expressing each protein construct. Features are presented in each vector map designed using SnapGene software (GSL Biotech) (Figure 44.).

The pSecTag2A vector was linearised by restriction digestion with HindIII and NotI and purified by gel extraction (2.6.7). The ECD, EGF and EMI inserts were PCR amplified using the primers listed in Table 15. prior to InFusion cloning (2.6.10) (Figure 44.). Four positive colonies were selected for each construct were picked and the clone used in subsequent experiments is shown in Figure 43. Successful cloning was confirmed by restriction digest: the digestion of ECD and EGF vectors produce three bands due to an internal HindIII site in the MEGF10 ECD (Figure 44.).

Table 15. Cloning primers for ECD.

Primers used to clone the ECD, EGF and EMI domains into pSecTag2A. The base pairs in red indicate the sequence overlapping the vector for InFusion cloning.

Cloning Primer	Sequence	Tm (°C)
pSecTag2A_ECD_Fwd	GCGCCGTACGAAGCTTGCTGAATC TTGAAGACCCTAATGTG	
pSecTag2A_ECD_Rev	CCTCCTCGAGCGGCCGCCTGGTAG GAATCAGCAGGGAG	
pSec_EGF_Fwd	GCGCCGTACGAAGCTTGCACTGTG CTGATAAATGT	67
pSec_EMI_Rev	CCTCCTCGAGCGGCCGCGGGGAC ACACATTTCCCC	74

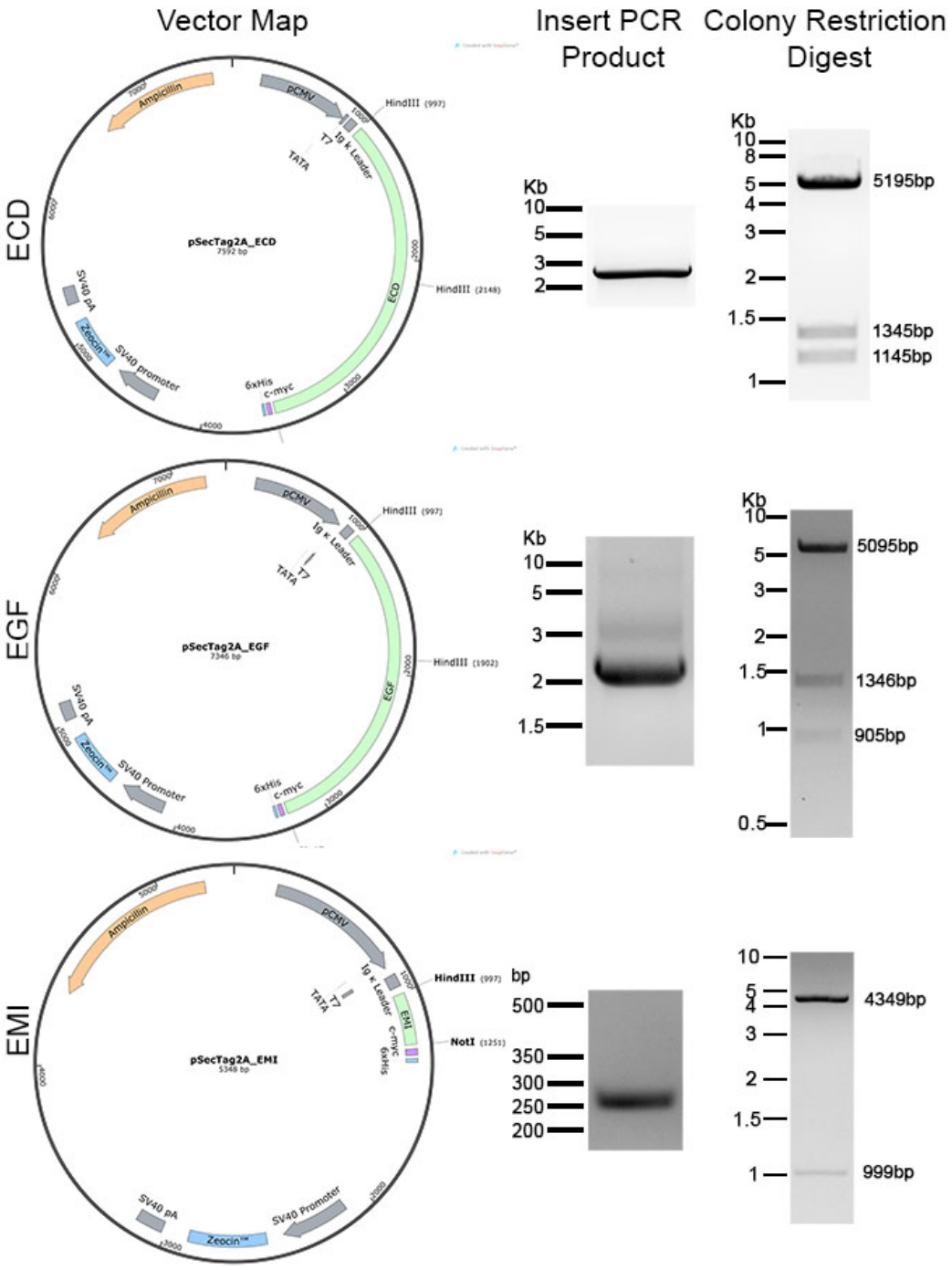

Figure 44. Cloning the ECD, EGF and EMI constructs into pSecTag2A.

ECD. ECD PCR product (Expected size: 2490 bp). HindIII/NotI digest of ECD colony 2 (Expected sizes: 5159, 1145 and 1345 bp). **EGF.** EGF PCR product (expected size: 2244 bp). HindIII/NotI digest of EGF colony 3 (Expected sizes: 5059bp, 1346 and 905 bp). **EMI.** EMI PCR product (expected size: 246 bp). SacII/SpeI digest of colony 2 (Expected sizes: 4349 and 999 bp).

5.2.2 **Production of stable cell lines expressing secreted protein constructs**

To express the ECD of MEGF10 in mammalian cells each pSecTag2A construct was transfected into HEK-293 cells and single clone colonies were selected with Zeocin™ to produce stable cell lines. High expressing clones for each construct were chosen in order to produce consistent levels of protein expression from a clonal cell pool.

The concentration of Zeocin™ required to effectively select HEK-293 cells expressing the pSecTag2A construct was determined by incubating untransfected HEK-293 cells with 0, 50, 100, 200 and 400 µg/ml Zeocin™ for five days. A concentration of 200µg/ml had the greatest cytopathic effect in the majority of cells after five days (Figure 45.). This is in line with the concentration recommended by the manufacturer (Invitrogen) and that used in other experiments (Freeze et al., 2006; Mullershausen et al., 2004).

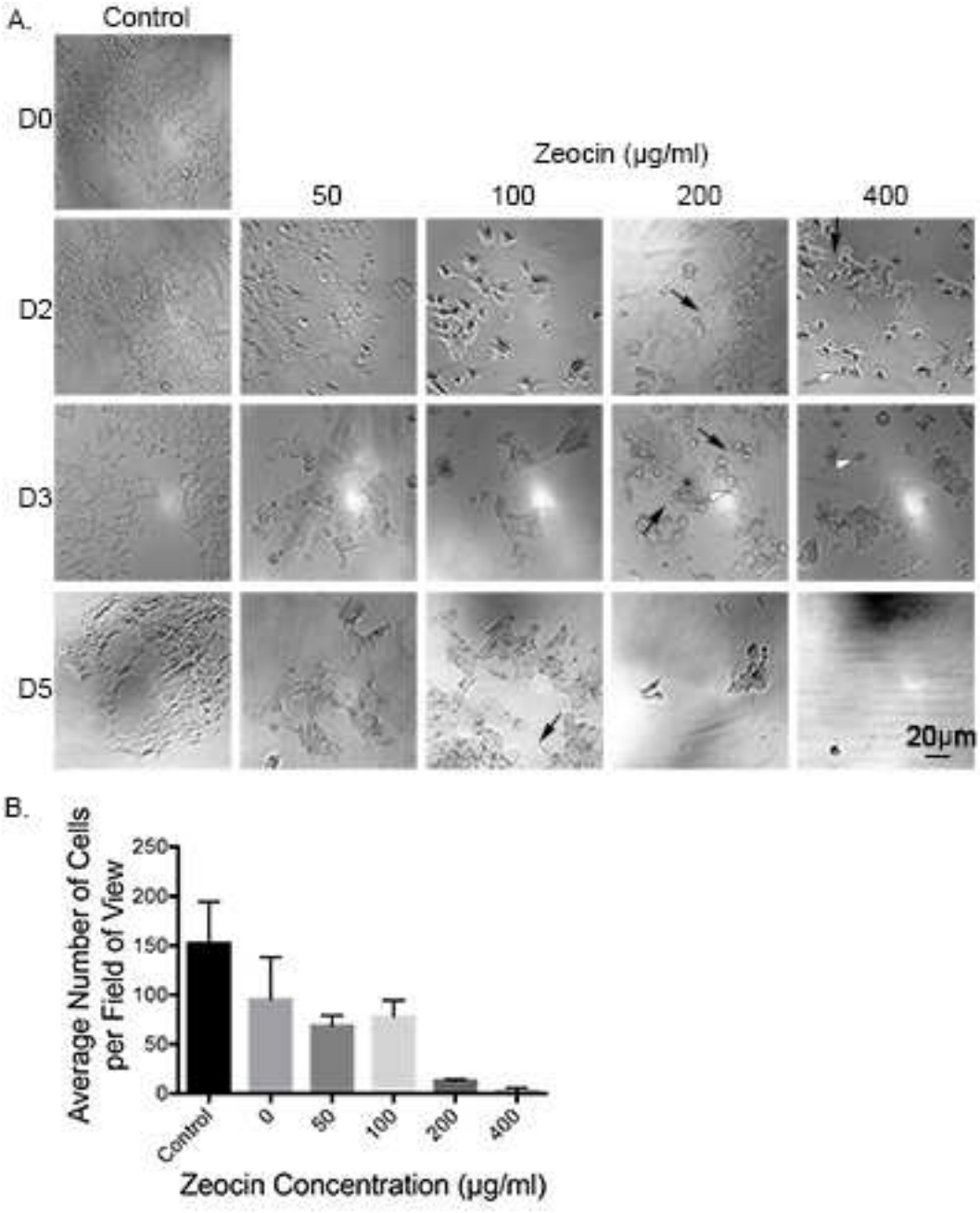

Figure 45. Zeocin™ Selection of HEK-293 cells.

A. Brightfield images of HEK-293 cells incubated with 0 – 400 µg/ml Zeocin™ and imaged for five days. Black arrows indicate Zeocin™ sensitive cells identified by the formation of long appendages formed from the breakdown of the plasma membrane. Open arrowheads show cell disintegration and cell particle release. **B.** The average number of cells counted per field of view after five days incubation with Zeocin™. Control shows the average number of cells 24 hr after plating before Zeocin™ addition. (Mean values +/- S.E.M. with a minimum of five fields of view analysed for each repeat; n=3).

5.2.2.1 **Production of stable cell lines expressing secreted protein constructs**

Stable cell lines expressing secreted constructs of MEGF10 were produced for mammalian protein expression as follows. pSecTag plasmid constructs were transfected into HEK-293 cells by calcium chloride transfection (2.7.10). Cells were harvested from 75 cm^3 flask 48 hrs post-transfection, counted using a haemocytometer and diluted to $1x10^5$ cells/ml. Two 100 mm diameter tissue culture dishes (Corning) were seeded with $2x10^4$ cells in 10 ml selection media (DMEM supplemented with 10% FBS, 1% P/S and 200 µg/ml Zeocin). Selection media was changed every 3 - 4 days, for 10 days, until cells not expressing the plasmid died and single colonies of cells expressing the Zeocin resistance in the pSecTag2A vector survived. After 10 days, single colonies from each plate were picked using a pipette tip and used to seed duplicate wells in two 24 well plates. Colonies were plated in non-selective media to enable cells to recover and grow. Plates were incubated at 37°C, 5% CO_2 for 10 days changing the media every 3 - 4 days. Media samples were taken from each well to be analysed by dot blot to determine the clone with the highest expression level of secreted protein.

5.2.2.2 **Dot blot**

A dot blot was performed as a relatively rapid diagnostic test to determine the level of secreted protein expression into the media of the selected HEK-293 cell lines. For the ECD, EGF and mutant constructs nitrocellulose membrane was cut to the required size and equilibrated in PBS for 20 min prior to use. Due to the small size of the EMI domain a 0.2 µm pore PVDF membrane was activated with methanol for 30 sec, washed in water for 5 min and equilibrated in PBS prior to blotting, to ensure the protein was efficiently captured. The dot blot apparatus was cleaned with 70% ethanol and a piece of 3 mm Whatman chromatography paper placed in the base of the apparatus. A piece of 3 mm Whatman chromatography paper was pre-soaked in PBS and placed on the 96 well plate layout at the centre of the dot blot apparatus and the equilibrated membrane placed on top. The top portion of the dot blot apparatus was placed on top and fixed in position by

firmly tightening the screws. The lid was sealed in place by turning on a vacuum pump. Samples were loaded with the vacuum pump switched off to ensure even distribution onto the membrane beneath. 100 µl of each sample was loaded into the respective wells of the dot blot apparatus and the vacuum switched on to allow media to be drawn onto the membrane. The membrane was removed from the apparatus and transferred to a 50 ml falcon tube and blocked with 3% (w/v) milk for 1 hr at room temperature for 1 hr. The membrane was then treated in the same way as a western blot membrane for antibody incubations, washes and development (2.12.4).

5.2.3 **Mammalian secreted protein expression in HEK-293 cells**

For efficient expression and purification of secreted mammalian protein constructs, HEK-293 stable expressing cells lines were seeded onto five 75 cm^2 flasks coated with 20 µg/ml poly-L lysine. To coat flasks with poly-L lysine, flasks were incubated with 7 ml 20 µg/ml poly-L lysine diluted in dH_20 for 20 min at 37°C before it was removed and flasks allowed to dry overnight at 37°C. Cells were grown to 80% confluence in growth media (Table 7.) before the media was exchanged for OptiMEM low serum media (Gibco) to reduce contaminants in the later purification stages. Cells were cultured in OptiMEM for 3 days prior to harvesting the media and purifying the protein.

5.2.4 **Protein purification using nickel affinity chromatography**

The secreted protein constructs had a 6xHis tag to enable purification by nickel affinity chromatography. OptiMEM media was harvested, centrifuged at 1000 *x g* for 5 min to pellet cells and the supernatant transferred to a fresh tube and one Complete EDTA-free protease inhibitor cocktail tablet (Roche) added per 50 ml of media. The media was incubated with 1 ml Complete His-Tag Purification Resin slurry (Roche) for 30 min on a roller. The slurry was applied to the 5 ml column and the flow through collected. The resin was washed with five times column volume wash buffer (300 mM NaCl, 50 mM NaH_2PO_4, pH 8). The protein was eluted in a total of 2 ml elution buffer (300 mM NaCl, 50 mM NaH_2PO_4 and 200 mM imidazole, pH 8). The

protein was eluted by incubating the slurry with elution buffer three times, 0.5 ml for 5 min, 0.5 ml for 10 min and 1 ml for 5 min.

5.2.5 **Protein dialysis**

Protein eluates in elution buffer were pooled together and dialysed into 1l PBS at 4°C overnight, using a Gebaflex Maxi Dialysis Tube (MWCO = 3.5 kDa) (Generon). Purified proteins were stored in 200 µl aliquots at - 80°C at a typical concentration of about 100 ng/µl.

5.2.6 **Measuring protein concentration by spectrophotometry**

The concentration of purified proteins was measured using a Cary® 50 Bio UV-visible spectrophotometer [Varian]. 1 ml of buffer was used as a blank before 1 ml of the sample was placed into a cuvette (Fisher) and the absorbance at 280 nm measured.

The concentration was calculated based on the extinction coefficients predicted for each construct assuming all pairs of Cys residues form cysteines (are not reduced) by Protparam (Gasteiger et al., 2003). Protein concentrations for each of the constructs prepared are shown in Table 16.

Table 16. Typical concentrations of expressed MEGF10 proteins.
The protein concentration of each expressed protein construct was measured by spectrophotometry.

Construct	Protein Concentration (ng/µl)
ECD	60 - 100
EGF	150 - 200
C774R	29
W520X	15

5.2.7 **Mass Spectrometry**

Purified proteins were submitted as SDS-PAGE gel bands for protein identification by mass spectrometry Briefly, 20 µl of purified protein was loaded per well and an SDS-PAGE gel run (2.12.3). Protein was stained with Instant Blue Coomassie stain (Expedeon) and the gel band cut out with a clean scalpel. The gel band was stored in 30% ethanol and submitted to James Ault at the University of Leeds Mass Spectrometry Facility for protein identification by tandem mass spectrometry.

5.2.8 **Lectin Blots**

Lectins were used to determine the nature of the glycosylation on the ECD of MEGF10. The Biotinylated Lectin Kit I (Vector Laboratories) was used and the protocol based on those described by (Freeze, 2001). 500 ng of purified MEGF10 proteins were separated by SDS-PAGE and transferred to a nitrocellulose membrane by western blot or blotted directly onto nitrocellulose by dot blot. Ovalbumin was included as a positive control.

The membrane was incubated with 2% (w/v) fish skin gelatin in Tris-Tween-Buffer-Saline (TTBS) composed of 50 mM Tris HCl pH 7.5, 150 mM NaCl, 0.1% (w/v) Tween as blocking buffer, for 30 min on a roller at room temperature. Gelatin was used instead of BSA since BSA can contain carbohydrates which may interfere with lectin binding (Freeze, 2001). The membrane was washed three times with TTBS for 15 min per wash before incubating the membrane with each biotinylated lectin (Table 17.) diluted to 1 µg/ml in TTBS for 1 hr at room temperature on a roller. The membrane was washed three times with TTBS for 10 min per wash and incubated with anti-biotin antibody conjugated with HRP (Invitrogen) diluted 1:2000 in TTBS. The membrane was washed three times with TTBS for 10 min per wash, followed by a final wash with TBS only for 10 min. The membrane was incubated with ECL reagent and exposed to film as described for western blots (2.12.4).

5.2.9 **Protein lipid overlay assay.**

Protein interactions with phosphoinositides are important for the localisation of proteins within the cell for their correct function (Hurley and Meyer, 2001; Sato et al., 2001). To determine if MEGF10 contains phosphoinositide recognition sequences and to analyse the lipid-binding specificity of the ECD of MEGF10 a protein lipid overlay assay was performed. The protein-lipid overlay assay (Dowler et al., 2000; Dowler et al., 2002) was performed using PIP strips (Molecular Probes) composed of 15 different phospholipids and a blank sample. Each PIP strip membrane was blocked for 1 hr at room temperature with blocking buffer (TTBS (10 mM Tris-HCl, pH 8.0, 150 mM NaCl, 0.1% (v/v) Tween) supplemented with 3% fatty acid–free BSA). The membrane was incubated with purified protein diluted to 0.5 µg/ml in blocking buffer overnight at 4°C. The membrane was washed with TTBS three times for 10 min. The membrane was incubated with anti-MEGF10 primary antibody diluted 1:1000 into TTBS for 1 hr at room temperature. The membrane was washed as before prior to being incubated with anti-rabbit-HRP secondary diluted 1:5000 in TTBS. The membrane was washed again with TTBS before being incubated with ECL and exposed to film as described for western blots (2.12.4).

5.2.10 **Cell attachment assay.**

To determine the ability of the ECD and the truncated and mutated proteins to mediate C1F myoblast attachment to a surface a cell attachment assay was performed. Briefly, the wells of a non-adhesive 24 well plate (Greiner), were coated with 2.5 µg protein diluted in 150 µl PBS for 20 min at 37°C. Harvested myoblast cells were prepared at $1x10^4$ cells/ml in growth media and 100 µl added to each well. Cells were incubated at 33°C, 10% CO_2 for 30 min before adding 500 µl of fresh media. After 24 hr incubation, cells were imaged on a Cytomate instrument, taking 5 different fields of view and counting the number of nuclei from each field. The experiment was repeated three times.

5.2.11 **Cell Motility Assay**

To determine the effect of an ECD surface coating on cell motility, cells were imaged overnight by DIC microscopy. Briefly, a 96 well plate with borosilicate glass bottom (Iwaki) was coated with 1.25 µg of purified MEGF10 proteins for 20 min at 37°C. The coating was aspirated and wells seeded with 50 µl C1F cells prepared at $1x10^5$ cells/ml. Cells were incubated with 50 µl of culture media at 33°C, 10% CO_2 for 24 hrs. The cells were filmed overnight and motility analysed as described in (4.2.5).

5.3 Results

5.3.1 **Expression of MEGF10 in HEK-293 cell clones**

The level of MEGF10 expression in HEK-293 cells was measured in media samples taken from 48 HEK-293 clones (2 x 24 well plates), 24 hrs after changing the media, by dot blot. This shows if the protein is expressed and secreted into the medium. All of the constructs (ECD, EGF, EMI and mutants C774R and W520X) were successfully expressed, except mutant R71W that was not expressed at all (Figure 46. A. and D.).

Four clonal cell lines expressed high levels of the ECD. One of these clones (marked with an asterisk) was selected, and used in all future experiments (Figure 46. A.). A much higher number of clones that expressed the EGF construct were obtained. One clone was selected and taken forward for future experiments (Figure 46. B.). Whilst the selected ECD clone does not appear to be the highest expressing clone on the dot blot, it grew better and gave a good level of expression in subsequent experiments. Only one clone was obtained that expressed the EMI domain, suggesting that this protein construct may not be well expressed or secreted into the media (Figure 46. C.). Only a few positive clones were obtained for the C774R and W520X mutant constructs, and one of each was selected for future experiments. No positively expressing clones were obtained for the R71W mutant, suggesting that it was either not expressed or secreted into the media in this system and therefore this mutant could not be tested in subsequent experiments (Figure 46. D.).

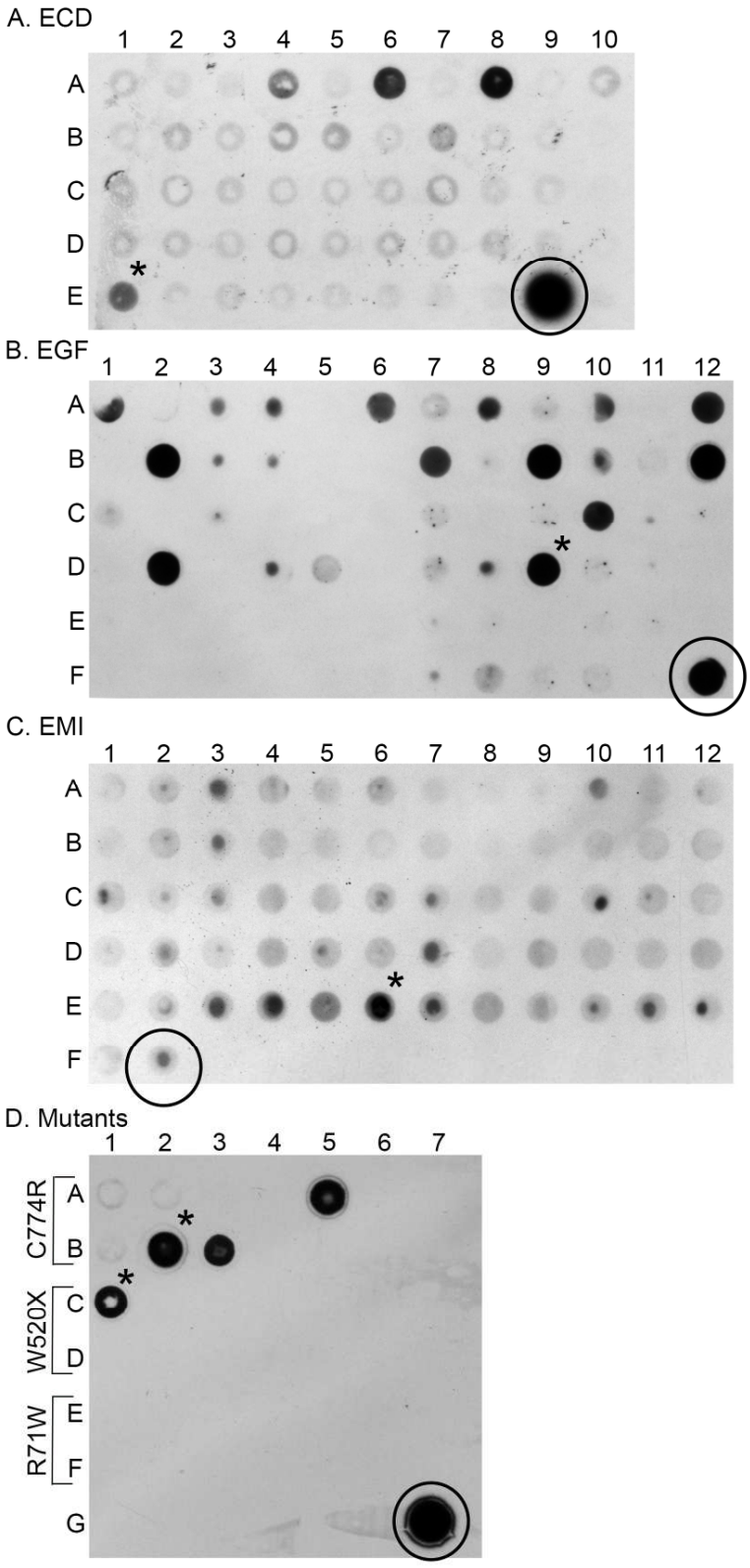

Figure 46. Dot Blots of protein expression

Dot blots probed with anti-cmyc for each protein construct; ECD (**A**), EGF (**B**), EMI (**C**), and Mutants C774R, W520X and R71W (**D**) showing positive HEK-293 clones. An asterisk marks those used in subsequent experiments. Positive controls, purified c-myc tagged protein, are ringed.

5.3.2 **Time course of MEGF10 expression.**

In order to determine the optimal time point to harvest secreted protein from the media, a time course of expression was set up using the ECD clone. A dot blot of media samples taken over the course of 8 days showed that the expression levels were highest at days 1 - 3 following a change of medium (Figure 48. A.).

To ensure that the protein was not significantly degraded over time and to be certain of the optimal time for protein expression, a western blot was then performed for samples taken from day 1 to day 3 of expression. The western blot confirmed that expression levels were highest at day three and the protein did not show any significant signs of degradation (Figure 48. B.)

The molecular weight of the expressed protein was approximately 130 kDa (Figure 48), which is about 40 kDa larger than the predicted molecular weight from Protparam (Gasteiger et al., 2003) of 91 kDa. This suggested that the secreted protein was extensively post-translationally modified as expected for secreted proteins of this kind (Chillakuri et al., 2012). To confirm this, the protein was purified from the media via its His tag and subjected to western blot and mass spectrometry.

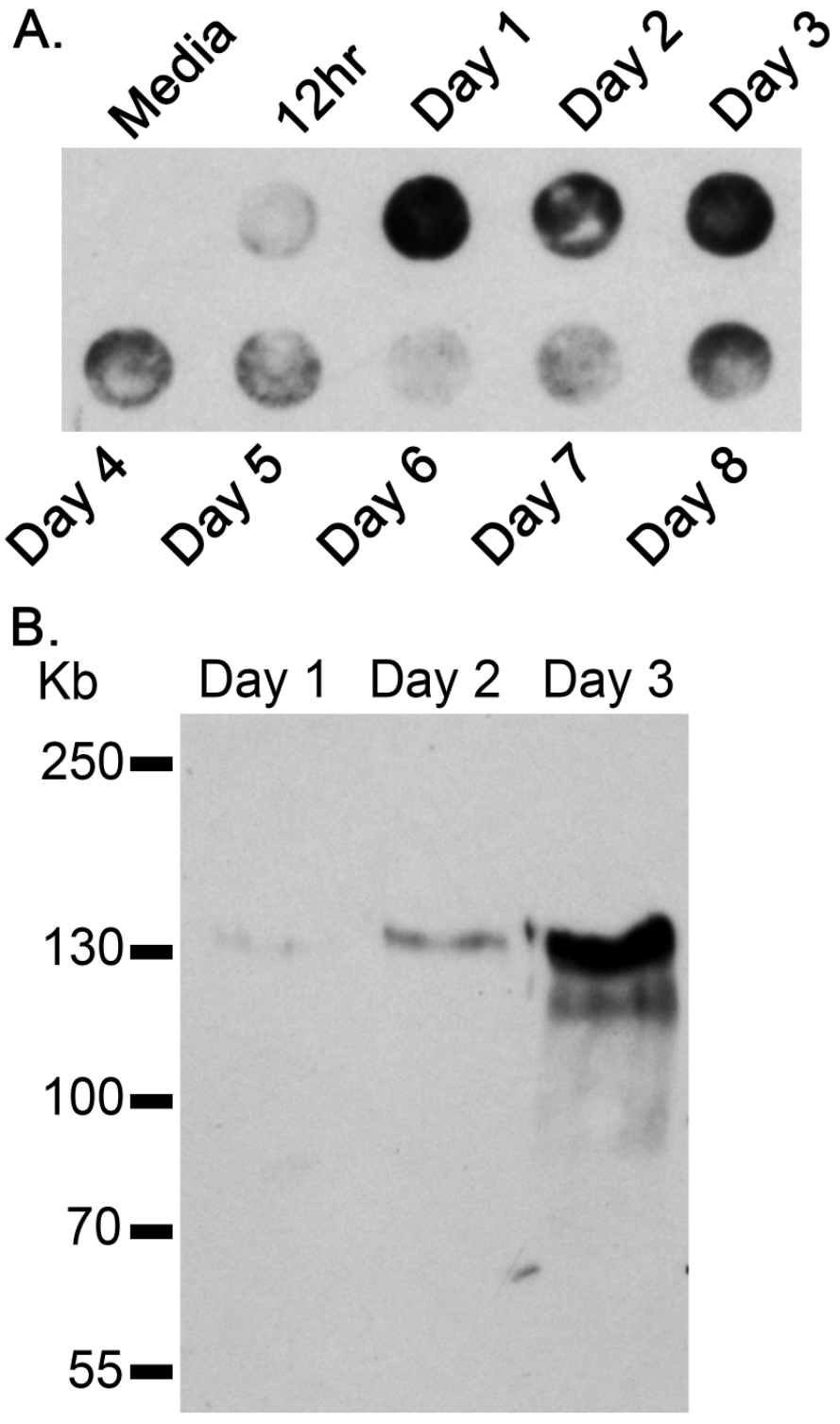

Figure 47. Time course of MEGF10 ECD expression

A. Media samples taken from the ECD clone C6-2, taken at 24 hr intervals, show that 72 hr after a media change is optimal for protein expression and secretion levels. **B.** Optimal expression after 72 hrs was confirmed by western blot against the c-myc tag.

5.3.3 **Purification of MEGF10 protein constructs**

Each protein construct was purified by nickel affinity chromatography against the His tag. Samples taken from each stage of the purification process were run on an SDS-PAGE gel and the protein identity was confirmed by western blot and mass spectrometry (Figure 48.). The eluted ECD was relatively pure with few contaminating proteins. The molecular weight of the ECD is predicted by Protparam (Gasteiger et al., 2003) to be 91 kDa, however the purified protein is running at a higher molecular weight, approximately 130 kDa, suggesting the protein may be heavily post-translationally modified.

The EGF protein was predicted to have a molecular weight of 81 kDa, however the purified protein is approximately 130 kDa, although it appears to run at a slightly lower Mw than the full ECD. The mutant construct, C774R, only has a single point mutations and therefore is predicted to have the same molecular weight as the ECD protein (91 kDa). The purified mutant protein constructs also run at a higher molecular weight suggesting that the mutations do not markedly disrupt the sites of post-translational modification. The purification of the two mutant constructs produced a low protein yield (Table 16.).

The molecular weight of the EMI domain was predicted by Protparam (Gasteiger et al., 2003) to be 12 kDa, but its apparent molecular weight on the gel appears to be ~16 kDa. The eluted sample containing purified EMI domain also contains many other bands with higher molecular weights (Figure 48.). Attempts to further purify the protein and remove the higher molecular weight contaminants were not successful. To further purify the protein, ion exchange chromatography was performed on an Äkta FPLC system and using a spin column with low molecular weight cut off (MWCO = 50k) to separate the small EMI domain from the larger molecular weight contaminants. However, neither technique was successful in purifying the EMI domain. Since the concentration of protein expressed was relatively low, the amount of protein recovered after a second round of purification was either too low to detect (not visible with silver stain) or the EMI protein was

lost in the process, possibly through aggregation. Since pure protein was not obtained, the EMI domain was not used in subsequent experiments.

The identity of each of the protein constructs was confirmed by mass spectrometry. This approach also detected a number of PTMs, primarily carbamidomethylation of the multiple cysteine residues present in each EGF domain. The large number of cysteine residues and heavy glycosylation disrupted efficient protein digestion required for mass spectrometry and therefore reduced the number of peptides recorded (Figure 48.).

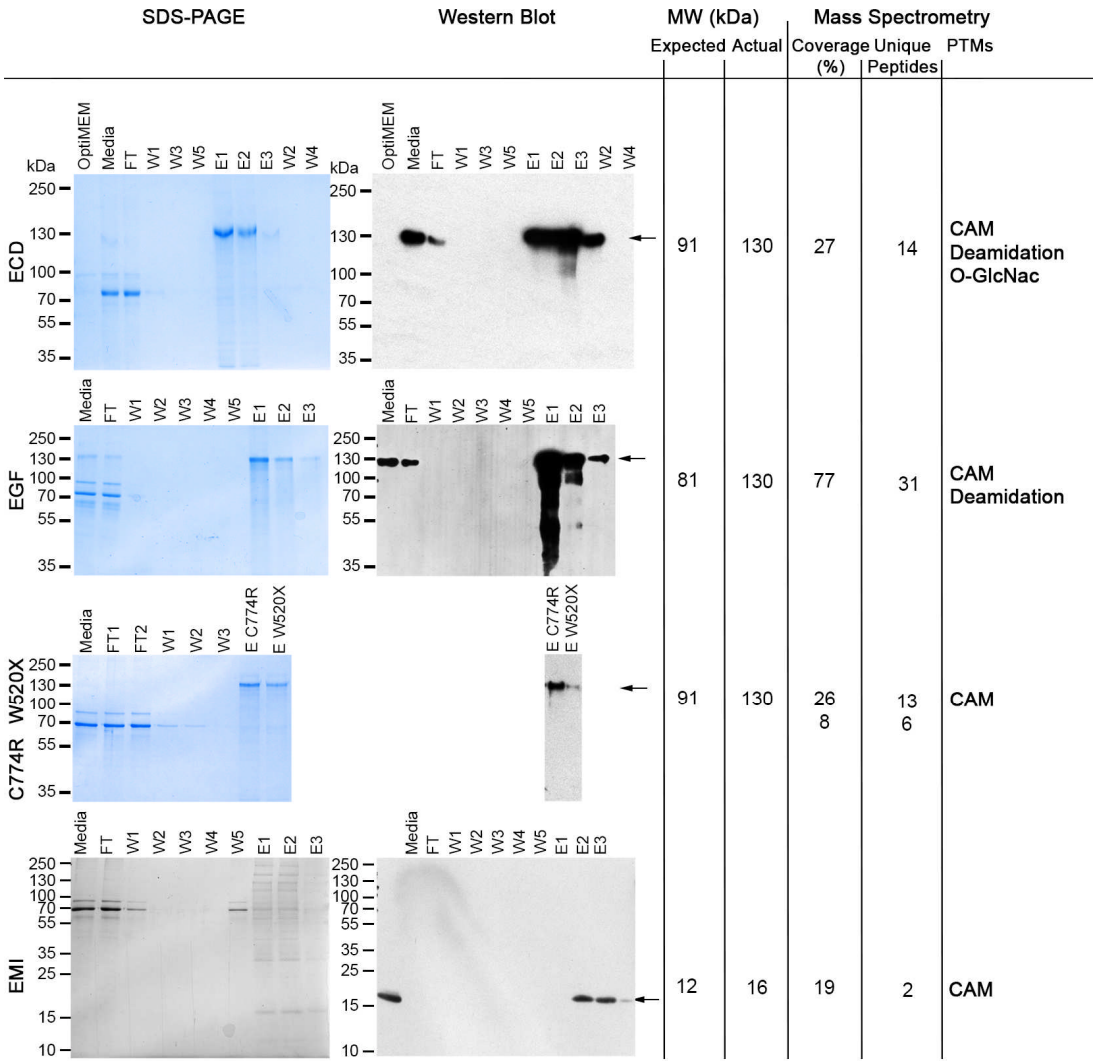

Figure 48. Purification of MEGF10 Protein Constructs

Purification of the ECD, EGF, EMI domains and mutations of the ECD C774R, W520X. SDS-PAGE gels show purified protein and any contaminating protein. Identity of protein was confirmed by western blot against the c-myc tag, and mass spectrometry. Mass spectrometry also showed potential PTMs identified for each construct. (Arrows indicate each purified MEGF10 protein construct).

5.3.4 **Lectin Blots**

To determine the nature of the PTMs on the ECD of MEGF10, a lectin blot was performed. Each lectin specifically recognises different forms of sugars attached to the protein. Each of the purified proteins were loaded onto a gel together with a sample of ovalbumin as a positive control. The ECD, EGF and C774R proteins were loaded at a relatively similar concentrations, while the mutant W520X was found to be at a slightly lower concentration, likely due to the low levels of the purified protein obtained for this mutant (Figure 49. A).

Lectin blots showed that both the ECD and the EGF domain are heavily post-translationally modified with mannose, glucose, N-acetylgalactosamine, fucose, galactose β1-3, N-acetylglucosamine and sialic acid, shown by positive interactions with each of the relevant lectins (Figure 49. B., Table 17.). However, good results were not obtained for the mutant proteins, and for W520X, this may be due to its low concentration. Therefore, I also performed a dot plot to allow sufficient protein to be loaded and probed with each lectin.

Dot blots with the various lectins showed that the mutant MEGF10 proteins are both recognised by PNA and ConA, indicating that they may have N-acetylgalactosamine, galactose β1-3, mannose and α glucose modifications. However, SBA recognised N-acetylgalactosamine on mutant C774R but not on mutant W520X and WGA recognised N-acetylglucosamine or sialic acid on mutant W520X but not on mutant C774R. This suggests that the mutations may have subtle effects on the post-translational modification of the proteins (Figure 49. C., Table 17.).

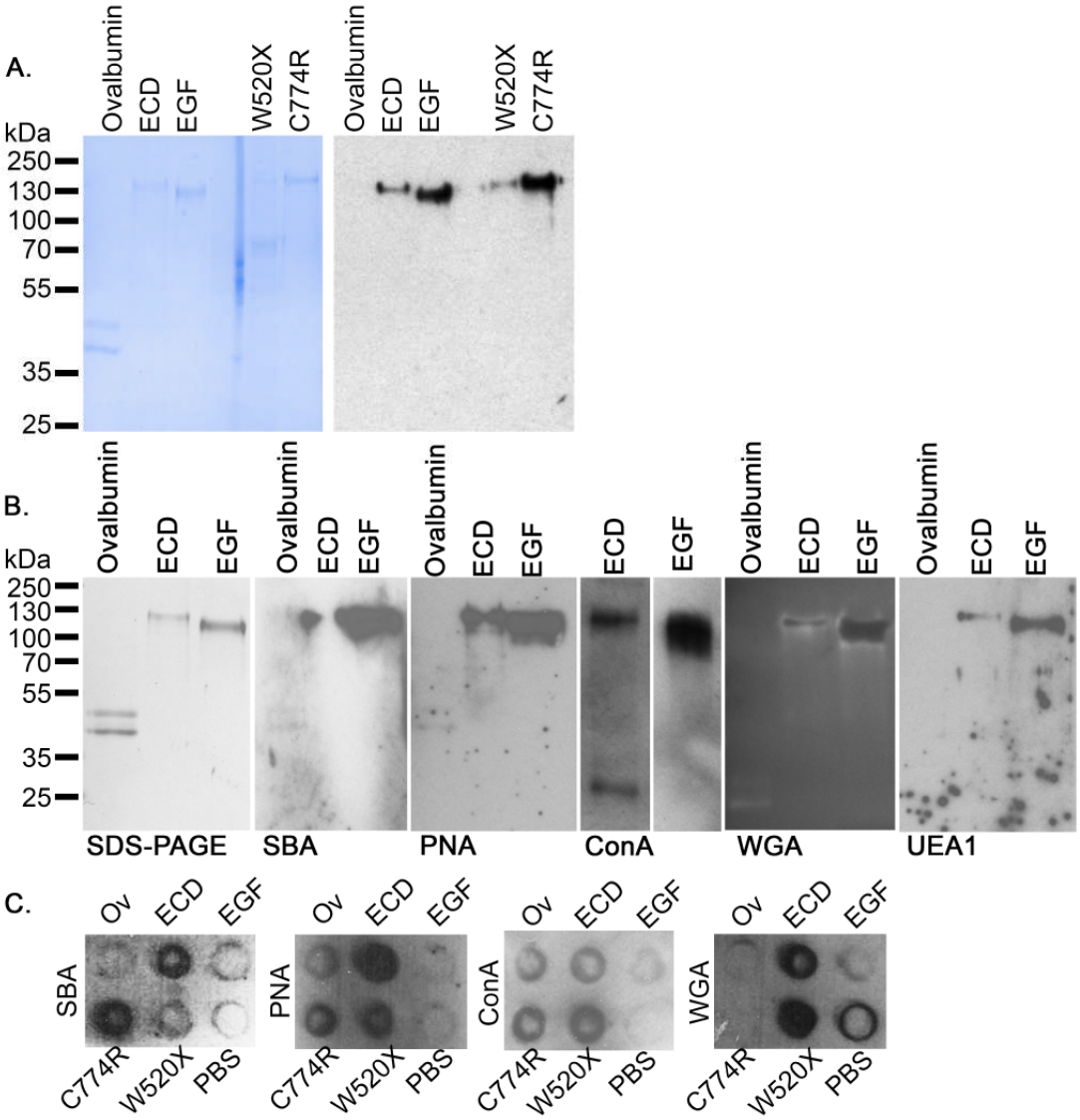

Figure 49. Lectin blots of MEGF10 proteins.

A. SDS-PAGE gel of purified MEGF10 proteins (30 µg loaded per well) and a western blot of the proteins probed with anti-cmyc. **B.** SDS-PAGE and lectin blots of lectin interactions with the ECD and EGF proteins. **C.** Dot blots showing lectin binding to each MEGF10 construct, with ovalbumin as a positive control and PBS as a negative control. (Exposure for 1 sec).

Table 17. Summary of lectin interactions with purified MEGF10 proteins.

Lectins were prepared as stock solutions at 2 mg/ml and stored at 4°C. Ovalbumin (Ov) was used as a positive control, recognised by ConA.

Lectin	Ov	ECD	EGF	C774R	W520X	Specificity
Soybean Agglutinin (SBA)		✓	✓	✓		GalNAc
Peanut Agglutinin (PNA)		✓	✓	✓	✓	GalNAc, Galβ1-3
Concanavilin A (ConA)	✓	✓	✓	✓	✓	αMan, αGlc
Wheat Germ Agglutinin (WGA)		✓	✓		✓	β-GlcNAc, Sialic Acid
Ulex europeaus agglutinin 1 (UEA1)		✓	✓	nd	nd	Fucose

5.3.5 **Protein-lipid overlay assay**

I next performed a protein-lipid overlay assay to determine if the expressed proteins bound to phospholipids, and if so, to which ones. The data (Figure 50.) suggests that both the ECD and EGF purified proteins interact strongly with several phosphatidylinositol phosphate (PI, or PtdIns) species. These include PtdIns3P, PtdIns4P, PtdInI5P, PtdIns(3,5)P_2 and PtdIns(4,5)P_2. The ECD additionally appears to interact with PtdIns(3,4)P_2, but this interaction is not seen with the EGF construct. This suggests that the EMI domain (lacking the EGF peptide) may be important for facilitating this interaction. Furthermore, removal of the EMI domain in the EGF protein appears to have enabled the interaction with phosphatidic acid (PA), a major component of the cell membrane. Both the ECD and EGF proteins interact with PS, which suggests that the EMI domain is not specifically required for this interaction. An overview of these protein lipid interactions is presented in Table 18.

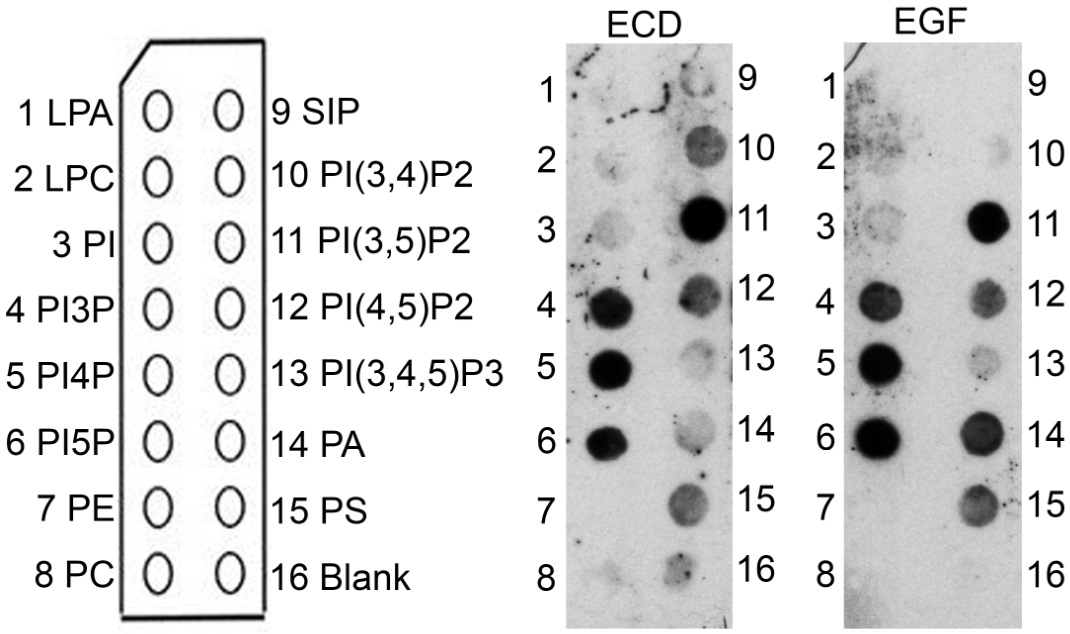

Figure 50. Protein lipid overlay assay.

The binding of the purified ECD and EGF proteins to a range of phospholipids was probed with anti-MEGF10 (Sigma Prestige). Positive interactions are seen between both proteins and a number of phospholipids. (Abbreviations listed in Table 18. with localisation and functions of each phospholipid). (PI: PtdIns).

Table 18. Phospholipid interactions with ECD and EGF proteins.

Phospholipid	ECD	EGF	Localisation / Function
Lysophosphatidic acid (LPA)			Plasma membrane, present in all examined tissues as minor membrane components and extracellular signalling (Sheng et al., 2015).
Lysophosphatidylcholine (LPC)			Biological membranes. (Tawk et al., 2010)
Phosphatidylinositol (PI)			Plasma membrane, abundant in the brain but present in all cell and tissue types.
Phosphatidylinositol 3-phosphate (PI3P)	5.3.5.1.1.1.1 ✓	5.3.5.1.1.1.2 ✓	Early endosome (Tawk et al., 2010)
Phosphatidylinositol 4-phosphate (PI4P)	5.3.5.1.1.1.3 ✓	5.3.5.1.1.1.4 ✓	Golgi apparatus (Tawk et al., 2010)
Phosphatidylinositol 5-phosphate (PI5P)	5.3.5.1.1.1.5 ✓	5.3.5.1.1.1.6 ✓	Plasma Membrane (Tawk et al., 2010)
Phosphatidylethanolamine (PE)			Present in most biological membranes, second most abundant in mammalian membranes. Role in regulating autophagy and longevity (Rockenfeller et al., 2015).
Phosphatidylcholine (PC)			Present in a high proportion of the outer leaflet of the plasma membrane. phosphatidylcholine is

			also the principal phospholipid circulating in plasma, where it is an integral component of the lipoproteins.
Sphingosine 1-phosphate (SIP)			Present in circulating plasma and the plasma membrane. Roles in vascular development, immune cell function, and inflammation. (Lipid library).
Phosphatidylinositol (3,4)-bisphosphate (PI(3,4)P2)	5.3.5.1.1.1.7 ✓		Binds pleckstrin homology (PH)-domains and it also has an important role in podosome formation near focal adhesions.
Phosphatidylinositol (3,5)-bisphosphate (PI(3,5)P2)	5.3.5.1.1.1.8 ✓	5.3.5.1.1.1.9 ✓	Late endocytic organelles (Tawk et al., 2010)
Phosphatidylinositol (4,5)-bisphosphate (PI(4,5)P2)	5.3.5.1.1.1.10 ✓	5.3.5.1.1.1.11 ✓	Present in the plasma membrane (Tawk et al., 2010) with a role in nnucleation of endocytic clathrin-coated pits (Posor et al., 2013)
Phosphatidylinositol (3,4,5)-trisphosphate (PI(3,4,5)P3)			Present in the plasma membrane. A potent membrane-bound signaling molecule that regulates a number of cellular functions including cell survival, proliferation, and cytoskeletal rearrangement (Ooms et al., 2009; Riehle et al., 2013)

Phosphatidic acid (PA)		5.3.5.1.1.1.12 ✓	Present in the plasma membrane and plays a key role in modulating membrane curvature. (Kooijman et al., 2003)
Phosphatidylserine (PS)	5.3.5.1.1.1.13 ✓	5.3.5.1.1.1.14 ✓	Inner leaflet of the plasma membrane and in endocytic membranes but is exposed on the outer leaflet of the plasma membrane in apoptotic cells. PS is required for the targeting and function of several intracellular signaling proteins(Leventis and Grinstein, 2010; Vance and Tasseva, 2013).

5.3.6 **Cell attachment assay**

MEGF10 has been suggested to play a role in mediating cell attachment (Suzuki and Nakayama, 2007a). Having confirmed that the expressed and purified MEGF10 domains were post-translationally modified, I then went on to test if these domains promoted myoblast attachment onto non-adhesive surfaces. Each of the expressed and purified domains promoted cell attachment compared to uncoated surfaces (Figure 51.). Removing the EMI domain from the ECD (EGF construct) reduced attachment compared to the full length ECD suggesting that the EMI domain contributes to cell adhesion. Both mutant MEGF10 proteins, C774R and W520X were also able to promote cell attachment, suggesting that these mutations do not disrupt cellular interactions with MEGF10 (Figure 51.).

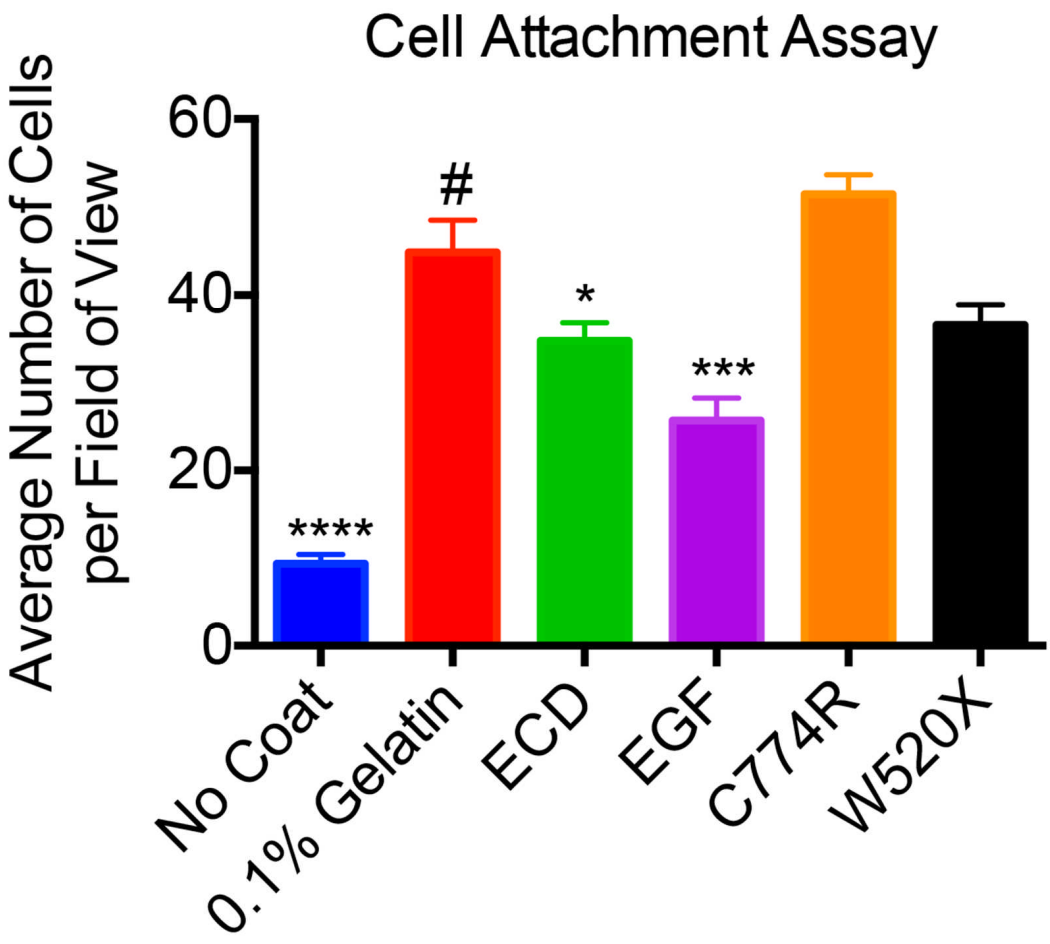

Figure 51. Myoblast attachment to MEGF10

The number of cells attaching to a non-adhesive surface coated with purified MEGF10 proteins. (* = p 0.0277, *** = p 0.0002, **** = p < 0.0001). Gelatin compared to mutants C774R and W520X showed no significant difference. (Mean values +/- S.E.M. with a minimum of five fields of view analysed for each repeat; n=3. # indicates the condition used as a comparison for t-test statistical analysis and asterisks indicate statistically significant changes.).

5.3.7 **Coated Coverslip Fusion Index Assay**

Overexpression of MEGF10 constructs in C1F myoblasts caused a significant inhibition of myoblast fusion during differentiation. Therefore, I also wanted to test if adding exogenous purified MEGF10 domains would also have an effect on fusion and differentiation. Glass coverslips were coated with these domains, and C1F myoblasts allowed to attached and differentiate.

Surfaces coated with the ECD protein significantly inhibited C1F myoblast fusion. In contrast, neither the EGF constructs nor the mutant ECD domains significantly reduced fusion, and the mutant W520X increased it. Cells fused equally well on uncoated surfaces as they did on gelatin-coated surfaces. (The fusion index was calculated as described 4.2.4) from cells stained for striated muscle myosin and nuclei (Figure 52. A.) and quantified (Figure 52. B.). These results suggest that the EMI domain may play an important role in regulating myoblast fusion during differentiation (Figure 52. B.) in the wildtype construct, but not in the mutants.

As fusion can be affected by cell density, the total number of cells (as indicated by DAPI stained nuclei) after differentiation were also counted (Figure 52. C.). The cell density was reduced for ECD, but this reduction was not significant. However a slightly lower cell density could have partly contributed to the reduction in fusion observed. However, while cell density was significantly lower for the mutant EGF domain, C774R, this reduced density was not linked to a lower fusion index.

Finally, changes to cell motility might also contribute to a reduction in fusion, as the myoblasts need to migrate towards each other in order to fuse. Test of cell motility on the different surfaces showed that C1F myoblast motility is not significantly affected by the presence of any of the ECD/EGF protein constructs compared to the 0.1% gelatin control (Figure 52. D.). Therefore, any change to fusion cannot be explained by a reduction in cell motility.

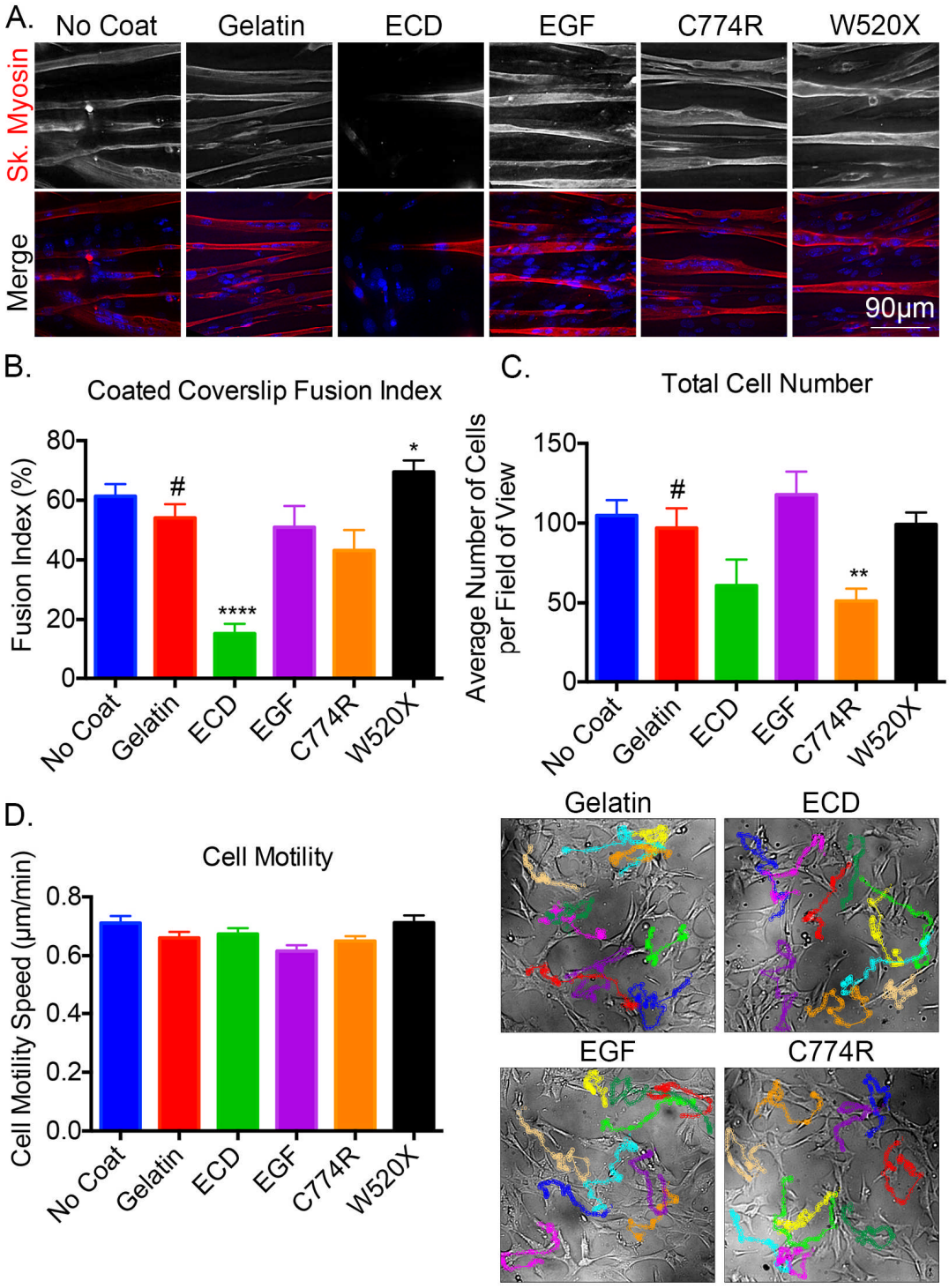

Figure 52. C1F cell activity on coated coverslips

A. C1F myoblasts differentiated on coated coverslips for seven days, stained for nuclei (blue) and skeletal myosin (red). **B.** The fusion index calculated for C1F myoblasts differentiated on coated coverslips. Five fields of view were imaged to calculate the fusion index. Fusion indices were compared to that obtained for gelatin (#). (* = p 0.0156, **** = p< 0.0001). [Gelatin vs. no coat p= 0.2524 – not significant] **C.** The total number of cells counted per field of view. [** = p 0.0037] **D.** The motility of C1F myoblasts measured over 14 hrs. 5 fields of view were imaged with 10 cells tracked per field. Sample fields of view showing the tracks recorded using ImageJ. (Mean values +/- S.E.M (n=3)).

5.4 Discussion

In this study stable mammalian cell lines were produced that express the ECD of MEGF10. Expression of the secreted protein constructs was optimal after three days incubation. Purified ECD, EGF and mutant constructs ran at a higher molecular weight than predicted on SDS-PAGE gels, consistent with post-translationally modifications of these constructs. The identity of the protein constructs was confirmed by mass spectrometry, which showed that these constructs were likely to have carbamidomethylation, and deamidation (Figure 48.). The lectin blots further indicated that a broad range of sugars are present on both ECD and EGF constructs, and that the two mutations (C774R and W520X) may subtly affect these post-translational modification. Removal of the EMI domain in the EGF construct does not seem to remove any specific PTMs. Lipid blots appear to show that the EMI domain may be important for the interaction with PtdIns(3,4)P_2 (Table 18.).

A number of different PTMs were observed for the MEGF10 ECD and EGF constructs. Mass spectrometry indicated that both carbamidomethylation and deamidation are present. Carbamidomethylation (CAM), is the alkylation of the free cysteine thiol group by iodioacetamide (IAM) and is commonly performed on cysteine residues during preparation of protein for mass spec analysis to produce cysteine residues of a known, predictable mass. Therefore the CAM modification identified by mass spectrometry is likely an artefact due to this process, and the large number of cysteine residues present in the ECD (Gundry et al., 2009; Meng et al., 2011). Deamidation is the removal of an amide group, and is a critical PTM involved in ageing and a number of conditions such as coeliac disease and neurodegenerative diseases (Li et al., 2010; Robinson and Robinson, 2001). Deamidation is dependent on the structure of the protein. *In vivo* deamidation of proteins has previously been suggested to act as a regulator of the molecular timing of biological events, in particular in protein turnover and development (Robinson, 2002). CAM is therefore most likely an artefact of mass spectrometry but deamidation of the ECD and EGF domains may play a role in myogenic development in MEGF10.

A large number of further PTMs in the MEGF10 ECD and EGF constructs were discovered from the lectin blots. Comparisons with the mutant ECD constructs showed that the C774R mutant was not recognised by wheat germ agglutinin, suggesting it may lack modification by β-GlcNAc and sialic acid. Sialic acid is part of a family of sugars composed of a 9 carbon backbone. In vertebrates the most common member of the family is N-acetylneuraminic acid is typically found at the ends of glycan branches of glycoproteins, where it increases biological diversity in PTM proteins, plays a role in maintaining the stability and turnover of glycoproteins as well as being involved in cellular functions such as intercellular interactions and signalling. In skeletal muscle, sialic acid has been identified as a marker of aging (Hanisch et al., 2013). Sialic acid is synthesised by GNE, mutations in which lead to a rare recessive myopathy characterised by distal muscle weakness and atrophy (Nishino et al., 2015).

Modification of serine and threonine residues of nucleocytoplasmic proteins with the monosaccharide β-GlcNAc is well described. *O*-linked *N*-acetylglucosamine (*O*-GlcNAc) is a PTM of serine and threonine residues of cytoplasmic and nuclear proteins. This modification has been shown to influence a range of cellular and physiological process including signal transduction, the regulation of gene expression and protein degradation, as well as neurodegenerative disease Therefore the lack of these modifications in the C774R mutant may disrupt the ability of MEGF10 the mediate signalling.

Conversely, mutant W520X was not recognised by soybean agglutinin and therefore may not have sialic acid or GalNAc modifications. The enzyme responsible for forming β-GalNAc linkages, cytotoxic T cell (CT) GalNAc transferase, influences myofibre growth, laminin expression and the neuromuscular structure in skeletal muscle (Xia et al., 2002). Therefore, mutations in the ECD of MEGF10 may affect the post-translational modification of the protein and thus influence its function.

In addition the ECD and EGF domains interact with a wide range of lipids. Their interaction with PS agrees with previous work showing that proteins containing EMI and EGF-like domains interact with PS (Park et al., 2008;

Tung et al., 2013). Intriguingly, PS is normally found on the inner leaflet of the plasma membrane, and only becomes exposed during apoptosis, or during myoblast fusion (Hochreiter-Hufford et al., 2013). This interaction with PS is consistent with the proposed role of MEGF10 in engulfing apoptotic cells, particularly its role in neuronal corpse clearance in concert with JEDI-1 and may also be important in fusion of myoblasts. The membrane receptor BAI1 is expressed in myotubes and recognises PS exposed on apoptotic cells. This interaction has been shown to mediate enhanced myoblast fusion independently of any fusion or engulfment of the apoptotic cell. This mechanism of PS recognition mediating cell fusion has been described in other tissues, including the fusion of trophoblast cells during development of the placenta. Therefore this mechanism could also be conserved in myoblast fusion (Yu and Baylies, 2013; Gauster et al., 2009)

EGF and ECD domains were also found to interact with PtdIns3P and PtdIns4P phospholipids. These lipids are associated with the early endosome and Golgi apparatus respectively (Roth, 2004; Tawk et al., 2010). As shown in Chapter 4 MEGF10_GFP localizes in vesicles and colocalises with labeled dextran internalized by endocytosis, suggesting localiation of MEGF10 within endosomes. Thus, this interaction may be important in both the secretion and internalisation of MEGF10 in cells.

The demonstration that exogenous MEGF10 ECD/EGF helps to promote myoblast attachment is consistent with a number of other previous studies that show the EGF domains of other proteins mediate cell attachment, (Kansas et al., 1994; Stacey et al., 2003).

The presence of the EMI domain in the wildtype EGF construct inhibited myoblast fusion. This suggests that the EMI domain is important in regulating fusion. The EMI domain enables multimerisation of the ECD of other proteins (Doliana et al., 2000). Loss of this domain may inhibit interactions between MEGF10 and itself, or other interacting proteins on the same cell or on adjacent cells, which may contribute to decreased fusion. Conversely, the mutant ECD proteins, which still have the EMI domain, do not affect myoblast fusion, and it is unclear why this is the case.

Overexpression of MEGF10_eGFP significantly reduced myoblast cell number over the course of differentiation (Chapter 4.), while addition of ECD protein constructs used here had little effect, except for the mutant C774R. Moreover, overexpression of MEGF10_eGFP and mutant isoforms in cultured myoblasts significantly inhibited myoblast motility, addition of the ECD protein constructs to myoblast cells does not. This may suggest the importance of the intracellular domain of MEGF10 in regulating cell activity. The intracellular domain may be crucial in enabling downstream signalling and mediating changes in fusion and cell motility. However, the correct localisation of the full length protein within the membrane may be important for mediating protein interactions, and this may not occur when the ECD is presented externally to the cells.

6 Discussion.

6.1 Robust reagents and model systems are necessary for the study of MEGF10.

One of the main findings of this research is the importance of using properly validated reagents and model systems when studying MEGF10. The contradictions and complexity of data reported in the literature concerning MEGF10 (reviewed in Chapter 1.) may arise from the intricate and dynamic nature of the skeletal muscle environment during development and regeneration. However, many of the inconsistencies may also be due to the choices of reagents and model systems that had not been fully validated for their efficacy or relevance in studying this protein.

In this study, I tested 3 commercially available antibodies, previously used in MEGF10 studies reported in the literature, to validate their ability to recognise MEGF10 in immunofluorescence and western blot. Of these three antibodies, only the Sigma Prestige antibody, which recognises the ECD of MEGF10, showed good recognition in both immunocytochemistry and to some extent western blot. I subsequently used this antibody in future experiments. The two other commercially available antibodies, both of which recognise the intracellular domain of MEGF10, from Millipore (Kay et al., 2012) and Santa Cruz (Bröhl et al., 2012) do not recognise expressed MEGF10 in our assays. This could be because protein interactions with the intracellular domain of MEGF10 (Figure 8.) may inhibit antibody binding. The inability of these commercially available antibodies to recognise the intracellular domain of MEGF10 may also suggest that the non-commercial antibody raised against the intracellular domain of MEGF10 used by (Holterman et al., 2007) may also not be effective at recognising MEGF10 and may therefore also explain some of the conflicting data presented in that study.

In contrast to the previously reported findings (Holterman et al., 2007) I found that endogenous expression levels of MEGF10 are low in cultured

myoblasts and myotubes by western blot and immunofluorescence, and RNAseq confirmed this. In satellite cells associated with isolated fibres, levels of MEGF10 are low in quiescent satellite cells, and appear to increase between 24 and 72 hrs post-isolation. Since the fibre isolation model has its limitations, in that it removes the cells (and fibres) from the native muscle environment, and therefore possible less physiological, I also investigated MEGF10 expression in an *in vivo* model system of mild hyperplasia. Again, I found that MEGF10 levels increased in response to physiological levels of fibre damage and was either non-existent or expressed at very low levels in quiescent satellite cells.

Importantly, MEGF10 does not appear to be expressed in the typical $CD34^{+}$, $Pax7^{+}$/$MyoD^{+}$ satellite cells, but in neighbouring cells that are $CD34^{+}$/$Pax7^{-}$/$MyoD^{-}$. These cells could represent another subgroup of satellite cells within the heterogeneous population of cells, arising from asymmetric cell division (Kuang et al., 2007). Alternatively, they could be myofibre associated cells such as pericytes or interstitial cells (Figure 9.). Further experiments to isolate this population of cells by FACS (Liu et al., 2015a) and to perform single cell sequencing to better characterise this population of cells would give a new insight into the role of MEGF10 (Gawad et al., 2016; Li et al., 2012; Dueck et al., 2015). Further staining of hyperplasia model fibres may give an indication into whether this model leads to the formation of new fibres. Pax7 and Pax3 play different roles in adult regenerative myogenesis and therefore determining the expression of these TFs in relation to MEGF10 expression may give an insight into this role (Kuang et al., 2007).

6.2 MEGF10 reduces myoblast fusion and motility.

This study has confirmed the work of Holterman *et al.* by showing that overexpression of MEGF10 inhibits myoblast fusion in cultured myoblasts. However, in this study, overexpression of MEGF10 did not increase cell proliferation as described previously in C2C12 cells (Holterman et al., 2007). However, the use of C1F cells to study myoblast proliferation may not have been a good model, since cell proliferation is controlled by temperature and

the presence of γ-IFN (Morgan 2002), therefore future experiments may need to be performed in primary myoblasts. In this study, overexpression of MEGF10 in C1F cells actually reduced cell number, in a manner that was independent of adenoviral infection. The overexpression of full length MEGF10 also reduced myoblast motility. Furthermore coating surfaces with the ECD of wildtype MEGF10 increased cell attachment, inhibited myoblast fusion and reduced the total number of cells after 7 days differentiation, further suggesting a role for MEGF10 in cell attachment and a role in regulating differentiation.

6.3 The extracellular domain of MEGF10 is post-translationally modified and interacts with membrane lipids.

Analysis of the purified ECD of MEGF10 showed the high level of PTMs of this protein, as expected for an ECD (Bard and Chia, 2016). It has been suggested that MEGF10 may interact with PS through its EMI domain to enable recognition of apoptotic cells (Chung et al., 2013; Scheib et al., 2012; Tung et al., 2013). However this study shows that MEGF10 may interact with PS but also recognises other lipids (including PtdIns(4)P, PtdIns(4,5)P_2 and Phosphatidic Acid) in agreement with a recent study (Iram et al., 2016). Interestingly I also found that constructs lacking the EMI domain recognised phosphatidic acid, whilst the full-length protein did not. MEGF10 has already been associated with TTR-52, which interacts with phosphatidic acid (Kang et al., 2012). Phosphatidic acid is a fusogenic lipid proposed to play a role in muscle protein accumulation (Mobley et al., 2015; Zhang et al., 2008). Removal of the EMI domain may uncover a binding site for phosphatidic acid that is blocked by the EMI domain in the full-length ECD. It is possible that when the EMI domain interacts with its binding partners, this would also expose the phosphatidic binding domain, which could be important for the function of MEGF10.

6.4 Mutagenesis of MEGF10

As part of this study, I have also tried to uncover why point mutations in the ECD of MEGF10 lead to skeletal muscle disease. Expressed mutant GFP-tagged adenoviral constructs showed a different pattern of localisation compared to the wildtype protein. In particular, the mutants did not localise to the membrane but formed aggregates surrounding the nucleus. Further staining is required to confirm whether these mutant proteins are misfolded or incorrectly processed and therefore are not transported to the membrane but retained within the ER. Contrary to expectation, the three mutations investigated produced very similar effects in myoblast cells compared to the wildtype protein. Each of the GFP-tagged mutants significantly inhibited myoblast fusion, reduced cell number after 7 days of differentiation, and severely reduced myoblast motility as found for WT GFP-tagged constructs. In addition, purified mutant MEGF10 ECD constructs coated onto cell culture surfaces enabled cell attachment in a similar manner to the wildtype ECD. However, unlike the ECD, the two mutant ECDs tested did not affect myoblast fusion or motility and had a mixed effect on the total cell number. Similarly, results were obtained for the EGF domain. The differential effect seen between overexpression of full length MEGF10 and the external presence of the ECD of MEGF10 (coated onto coverslips) may indicate that the intracellular domain of MEGF10 is crucial for mediating some of the functions of MEGF10.

Whilst this study has provided some new insights into MEGF10 there are a number of questions remaining for future study.

6.5 Are mouse models the most helpful for the study of human skeletal myopathies?

MEGF10 has been studied using a knock out mouse model, where dysregulation of retinal neuron spacing was described (Kay et al., 2012). However the mouse phenotype did not describe any myopathic symptoms. Since mouse models of MEGF10 deletion do not appear to produce an

obvious skeletal muscle phenotype determining the differences between human and mouse MEGF10 to better understand the range of phenotypes observed may enable more reliable and disease relevant model systems to be developed. Indeed it may be that mutations in MEGF10 which produce EMARDD in humans are embryonic lethal in mice and therefore these phenotypes are not described. A MEGF10 *lacZ* reporter tagged knockout mouse has been listed by the International Mouse Phenotyping Consortium, and although no phenotype has yet been described for this mouse, it may be useful in future studies to visualise localisation and changes in expression of MEGF10 over the course of development or differentiation. Mouse models of human disease have both their benefits and limitations, however more recent initiatives to characterise the function in all mouse genes and describing phenotypes through mutagenesis will likely give more accurate models of human disease in mice (Justice and Dhillon, 2016; Rosenthal and Brown, 2007).

6.6 How important might the post-translational modification of MEGF10 be for its function within skeletal muscle?

Properly folded proteins are transported form the ER to the Golgi before being transported to the cell surface. Mis-folded and poorly assembled proteins are retained in the rough ER before degradation in proteasomes (Hebert and Molinari, 2007). The post-translational modification of EGF-like domain containing proteins plays an essential role in mediating protein interactions and function, as described in Chapter 1. These protein domains are also subject to unusual forms of post-translational modification, including O-linked fucosylation. Modification of Notch has been well described as influencing signalling at the membrane as well as protein folding and trafficking to the membrane (Acar et al., 2008; Kritikou, 2008). Due to the similar structure of MEGF10 and Notch, it may be that MEGF10 is regulated in a similar manner. Further studies, perhaps using cell lines which limit branching of sugar residues may give insight into MEGF10's ability to perform its function in the absence of complete post-translational

modification. CFTR (Cystic Fibrosis TM conductance Regulator), which is mutated in cystic fibrosis, is another good example of a membrane protein where post-translational modification regulates protein synthesis, trafficking and membrane stability (reviewed (Amaral and Farinha, 2013). Therefore, further study into the effect of post-translational modification of MEGF10 may be crucial in determining the mechanisms by which it is regulated, transported and functions within the membrane.

6.7 How might the structure of MEGF10 influence its function?

Proteins with multiple EGF-like domains have been described as being relatively rigid within the membrane, such as Notch and MEGF9. Electron microscopy of MEGF9 has shown Rod-like particles (Brandt-Bohne et al., 2007), however MEGF9 has fewer EGF-like domains than MEGF10 (Chapter 1 Figure 3.) and therefore future experiments to investigate the structure of the ECD of MEGF10 by negative stain or rotary shadowing electron microscopy may be valuable in understanding MEGF10 function. Furthermore, visualising how the EMARDD mutations may affect the structure of the ECD may also give an insight into how these mutations affect MEGF10 structure and function.

6.8 Is MEGF10 regulated in a similar manner to Notch?

Notch and MEGF10 have been compared due to their similarity in structure and relationship during myoblast differentiation, where MEGF10 has been shown to activate Notch signalling and thereby suppress myoblast differentiation and fusion (Holterman et al., 2007). Notch has recently been shown to be cycled from the membrane and stored in vesicles with the intracellular domain exposed to the cytoplasm and still able to mediate downstream signalling. Two pathways have been suggested to mediate this internalisation of Notch, mediated either by Deltex or Suppressor of Deltex

(Shimizu et al., 2014). MEGF10 is also found in intracellular vesicles and therefore further experiments may be needed to determine if MEGF10 is regulated by a similar mechanism.

Like Notch, MEGF10 has been described as regulating myogenic progression. The relationship between Notch and DLL1 has been shown to regulate asymmetric stem cell division enabling renewal of the stem cell niche in neuronal stem cells (Kawaguchi et al., 2013) as well as muscle cell self-renewal (Sun et al., 2008). Indeed RT-PCR has shown that MEGF10 is upregulated in response to DLL1-dependent induction (Bröhl et al., 2012). Therefore further exploring the relationship between MEGF10 and Notch and its other interacting partners may give insights into the mechanisms by which MEGF10 acts.

6.9 How can the differences in the effect of MEGF10 on neuronal and skeletal muscle be explained?

The published literature about MEGF10 gives either a description of the roles of MEGF10 in neuronal/ brain tissue or within skeletal muscle. Reconciling the description of neurological dysfunction in mice with mutations in MEGF10 but with no description of a skeletal muscle disease and EMARDD patients with severe muscle myopathy but no neurological symptoms gives a confusing picture for the role of MEGF10 in disease.

One explanation for the different disease phenotypes observed may be due to differential expression of MEGF10 isoforms in different tissues. Two isoforms of human MEGF10 have currently been described. The second isoform lacks several 3’ exons and has an alternative C-terminal sequence. However, there is no clear data about the differential expression of these isoforms and therefore further studies into these isoforms may be helpful in determining their function.

Furthermore, cells that form the head and skeletal muscle have different developmental origins (Shi and Garry, 2006) and this may give rise to different populations of satellite cells with differential expression of MEGF10.

Characterising the, as yet, unidentified MEGF10 positive cells may give insight into their lineage from development which may help to explain the differences in expression in the brain and skeletal muscle.

6.10 Limitations of this study.

A limitation of this study, like that of previously published papers, is that part of this study has focused on the overexpression of MEGF10 to determine function This is due to the low endogenous expression of MEGF10 in cultured myoblasts. However, this method does not give a physiologically relevant insight into MEGF10 function and potential interactions.

This study has also focussed on the ECD of MEGF10, but further study into the intracellular domain of MEGF10 is also needed to better understand the downstream signalling pathways involved in myogenesis and muscle regeneration.

Satellite cells only account for 2 - 5% of nuclei beneath the basal lamina in adult muscle. Therefore studying these cells within the complex skeletal muscle environment requires a relatively large amount of material to collect sufficient satellite cells to study (Bischoff and Heintz, 1994).

6.11 How might this study impact upon research into skeletal muscle myopathies and dystrophies?

MEGF10 was highlighted as a protein of interest through its association with skeletal muscle myopathy EMARDD. Whilst this study may not directly have given any further insights into the effect of disease mutants on MEGF10 function, the identification of MEGF10 positive cells, which do not appear to be typical satellite cells, may give an insight into the disease. Further experiments to characterise this population of MEGF10 positive cells may lead to the identification of novel targets that could be exploited in the wider field of regenerative medicine. Whilst EMARDD is a very rare recessive condition, understanding the function of MEGF10 through its dysfunction in

patients may add to the current body of knowledge about muscle development, regeneration and disease. This could impact on research into and potential treatment for muscle weakness in an aging population, sports injuries and more common muscular dystrophies and myopathies.

This study has looked at mutations linked to EMARDD (W520X, C774R) and the associated myopathy with minicores disease (R71W). The R71W mutation in the EMI domain of MEGF10 disrupted expression of the protein, suggesting the importance of the EMI domain in the correct folding, processing and localisation of the whole protein. Mutations in the EGF domains of MEGF10 which cause EMARDD did not disrupt protein expression. The two mutations associated with EMARDD disrupted the localisation of the MEGF10 protein suggesting that the protein may not be able to perform its predicted role in cellular signalling. These two different mutations led to similar levels of inhibition of myoblast fusion and reduction in cell motility when exogenously expressed, which may give insight into the mechanism by which skeletal muscle is poorly formed within EMARDD patients. The mutations used in this study give an insight into both the mutations which induce a premature stop codon and the pC774R point mutation which changes a cysteine residue in an EGF domain, however in this study the effect of these different mutations did not appear to produce changes in the cellular response. Therefore further study in either primary human cells or knockout mouse models may be beneficial in exploring the spectrum of disease phenotypes described for each mutation.

EMARDD appears to fit within a spectrum of disease with variation in the onset of the disease and therefore being able to determine the prognostic factors which regulate the stage of disease onset (infantile or adult) may help to better understand the role of MEGF10 and potentially ways to treat or delay the onset of myopathic disease (Liewluck et al., 2016; Logan et al., 2011). Furthermore, understanding the factors, by which MEGF10 mutations cause either the formation of minicores or a more severe phenotype may give further insight into the complex class of minicore diseases (Boyden et al., 2012b).

6.12 Final Conclusions

This study into MEGF10 has given some new insights into MEGF10, in particular in its response to skeletal muscle hyperplasia. However, there are still a number of questions remaining for future study, some of which have been discussed here. MEGF10 is expressed within the complex environment of skeletal muscle and is likely to interact with a rage of different proteins and signalling molecules via its intracellular and ECDs. How it responds to changes in its environment under conditions of development, stress and injury remain to be fully explored.

7 Bibliography

Acar, M., Jafar-Nejad, H., Takeuchi, H., Rajan, A., Ibrani, D., Rana, N.A., Pan, H., Haltiwanger, R.S. and Bellen, H.J. 2008. Rumi is a CAP10 domain glycosyltransferase that modifies notch and is required for notch signaling. *Cell.* **132**(2), pp.247-258.

Alfaro, L.A.S., Dick, S.A., Siegel, A.L., Anonuevo, A.S., McNagny, K.M., Megeney, L.A., Cornelison, D.D.W. and Rossi, F.M.V. 2011. CD34 Promotes Satellite Cell Motility and Entry into Proliferation to Facilitate Efficient Skeletal Muscle Regeneration. *Stem Cells.* **29**(12), pp.2030-2041.

Almada, A.E. and Wagers, A.J. 2016. Molecular circuitry of stem cell fate in skeletal muscle regeneration, ageing and disease. *Nature Reviews Molecular Cell Biology.* **17**(5), pp.267-279.

Amaral, M.D. and Farinha, C.M. 2013. Rescuing Mutant CFTR: A Multi-task Approach to a Better Outcome in Treating Cystic Fibrosis. *Current Pharmaceutical Design.* **19**(19), pp.3497-3508.

Anderson, J.E. 2000. A role for nitric oxide in muscle repair: Nitric oxide-mediated activation of muscle satellite cells. *Molecular Biology of the Cell.* **11**(5), pp.1859-1874.

Appella, E., Weber, I.T. and Blasi, F. 1988. Structure and function of epidermal growth factor-like regions in proteins. *Febs Letters.* **231**(1), pp.1-4.

Ausubel, F.M., Brent, R., Kingston, R. E., Moore, D. D., Seidman, J. G. et al. 1987. *Current Protocols in Molecular Biology.* John Wiley & Sons, New York.

Bard, F. and Chia, J. 2016. Cracking the Glycome Encoder: Signaling, Trafficking and Glycosylation. *Trends in Cell Biology.* **26**(5), pp.379-388.

Baron, M. 2012. Endocytic routes to Notch activation. *Seminars in Cell & Developmental Biology.* **23**(4), pp.437-442.

Barry, E.R. and Camargo, F.D. 2013. The Hippo superhighway: signaling crossroads converging on the Hippo/Yap pathway in stem cells and development. *Curr Opin Cell Biol.* **25**(2), pp.247-253.

Barysch, S.V., Jahn, R. and Rizzoli, S.O. 2010. A fluorescence-based in vitro assay for investigating early endosome dynamics. *Nature Protocols.* **5**(6), pp.1127-1137.

Basile, J.R., Gavard, J. and Gutkind, J.S. 2007. Plexin-B1 utilizes RhoA and Rho kinase to promote the integrin-dependent activation of Akt and ERK and endothelial cell motility. *Journal of Biological Chemistry.* **282**(48), pp.34888-34895.

Beauchamp, J.R., Heslop, L., Yu, D.S.W., Tajbakhsh, S., Kelly, R.G., Wernig, A., Buckingham, M.E., Partridge, T.A. and Zammit, P.S. 2000. Expression of CD34 and Myf5 defines the majority of quiescent adult skeletal muscle satellite cells. *Journal of Cell Biology.* **151**(6), pp.1221-1233.

Benitez, B.A.S. and Komives, E.A. 2000. Disulfide bond plasticity in epidermal growth factor. *Proteins-Structure Function and Genetics.* **40**(1), pp.168-174.

Bentzinger, C.F., Wang, Y.X., Dumont, N.A. and Rudnicki, M.A. 2013. Cellular dynamics in the muscle satellite cell niche. *EMBO Rep.* **14**(12), pp.1062-1072.

Bentzinger, C.F., Wang, Y.X. and Rudnicki, M.A. 2012. Building muscle: molecular regulation of myogenesis. *Cold Spring Harbor perspectives in biology.* **4**(2).

Berkes, C.A. and Tapscott, S.J. 2005. MyoD and the transcriptional control of myogenesis. *Seminars in Cell & Developmental Biology.* **16**(4-5), pp.585-595.

Bischoff, R. and Heintz, C. 1994. Enhancement of skeletal muscle regeneration. *Developmental Dynamics.* **201**(1), pp.41-54.

Bjornson, C.R.R., Cheung, T.H., Liu, L., Tripathi, P.V., Steeper, K.M. and Rando, T.A. 2012. Notch Signaling Is Necessary to Maintain Quiescence in Adult Muscle Stem Cells. *Stem Cells.* **30**(2), pp.232-242.

Blanc, G., Font, B., Eichenberger, D., Moreau, C., Ricard-Blum, S., Hulmes, D.J.S. and Moali, C. 2007. Insights into how CUB domains can exert specific functions while sharing a common fold - Conserved and specific features of the CUB1 domain contribute to the molecular basis of procollagen C-proteinase enhancer-1 activity. *Journal of Biological Chemistry.* **282**(23), pp.16924-16933.

Blanco-Bose, W.E., Yao, C.C., Kramer, R.H. and Blau, H.M. 2001. Purification of mouse primary myoblasts based on alpha 7 integrin expression. *Experimental Cell Research.* **265**(2), pp.212-220.

Blau, H.M., Webster, C., Pavlath, G.K. and Chiu, C.P. 1985. EVIDENCE FOR DEFECTIVE MYOBLASTS IN DUCHENNE MUSCULAR-DYSTROPHY. *Advances in Experimental Medicine and Biology.* **182**, pp.85-110.

Bober, E., Franz, T., Arnold, H.H., Gruss, P. and Tremblay, P. 1994. Pax-3 is required for the development of limb muscles - a possible role for the migration of dermomyotomal muscle progenitor cells. *Development.* **120**(3), pp.603-612.

Bond, M.R. and Hanover, J.A. 2015. A little sugar goes a long way: The cell biology of O-GlcNAc. *Journal of Cell Biology.* **208**(7), pp.869-880.

Borycki, A.G., Li, J., Jin, F.Z., Emerson, C.P. and Epstein, J.A. 1999. Pax3 functions in cell survival and in pax7 regulation. *Development.* **126**(8), pp.1665-1674.

Boyden, S.E., Mahoney, L.J., Kawahara, G., Myers, J.A., Mitsuhashi, S., Estrella, E.A., Duncan, A.R., Dey, F., DeChene, E.T., Blasko-Goehringer, J.M., Bonnemann, C.G., Darras, B.T., Mendell, J.R., Lidov, H.G., Nishino, I., Beggs, A.H., Kunkel, L.M. and Kang, P.B. 2012a. Mutations in the satellite cell gene MEGF10 cause a recessive congenital myopathy with minicores. *Neurogenetics.* **13**(2), pp.115-124.

Boyden, S.E., Mahoney, L.J., Kawahara, G., Myers, J.A., Mitsuhashi, S., Estrella, E.A., Duncan, A.R., Dey, F., DeChene, E.T., Blasko-Goehringer, J.M., Bönnemann, C.G., Darras, B.T., Mendell, J.R., Lidov, H.G.W., Nishino, I., Beggs, A.H., Kunkel, L.M. and Kang, P.B.

2012b. Mutations in the satellite cell gene MEGF10 cause a recessive congenital myopathy with minicores. *neurogenetics.* **13**(2), pp.115-124.

Brandt-Bohne, U., Keene, D.R., White, F.A. and Koch, M. 2007. MEGF9: a novel transmembrane protein with a strong and developmentally regulated expression in the nervous system. *Biochemical Journal.* **401**, pp.447-457.

Bröhl, D., Vasyutina, E., Czajkowski, Maciej T., Griger, J., Rassek, C., Rahn, H.-P., Purfürst, B., Wende, H. and Birchmeier, C. 2012. Colonization of the Satellite Cell Niche by Skeletal Muscle Progenitor Cells Depends on Notch Signals. *Developmental Cell.* **23**(3), pp.469-481.

Brohl, D., Vasyutina, E., Czajkowski, M.T., Griger, J., Rassek, C., Rahn, H.P., Purfurst, B., Wende, H. and Birchmeier, C. 2012. Colonization of the satellite cell niche by skeletal muscle progenitor cells depends on Notch signals. *Dev Cell.* **23**(3), pp.469-481.

Brzoska, E., Kowalewska, M., Markowska-Zagrajek, A., Kowalski, K., Archacka, K., Zimowska, M., Grabowska, I., Czerwinska, A.M., Czarnecka-Gora, M., Streminska, W., Janczyk-Ilach, K. and Ciemerych, M.A. 2012. Sdf-1 (CXCL12) improves skeletal muscle regeneration via the mobilisation of Cxcr4 and CD34 expressing cells. *Biol Cell.* **104**(12), pp.722-737.

Buckingham, M. 2001. Skeletal muscle formation in vertebrates. *Current Opinion in Genetics & Development.* **11**(4), pp.440-448.

Callebaut, I., Mignotte, V., Souchet, M. and Mornon, J.P. 2003. EMI domains are widespread and reveal the probable orthologs of the Caenorhabditis elegans CED-1 protein. *Biochemical and Biophysical Research Communications.* **300**(3), pp.619-623.

Cardamone, M., Darras, B.T. and Ryan, M.M. 2008. Inherited myopathies and muscular dystrophies. *Semin Neurol.* **28**(2), pp.250-259.

Carlson, E.C., Mamiya, K., Liu, C.Y., Gendron, R.L., Birk, D.E., Funderburgh, J.L. and Kao, W.W.Y. 2003. Role of CyS41 in the N-terminal domain of lumican in ex vivo collagen fibrillogenesis by cultured corneal stromal cells. *Biochemical Journal.* **369**, pp.461-468.

Charge, S.B.P. and Rudnicki, M.A. 2004. Cellular and molecular regulation of muscle regeneration. *Physiological Reviews.* **84**(1), pp.209-238.

Chen, D., Jian, Y., Liu, X., Zhang, Y., Liang, J., Qi, X., Du, H., Zou, W., Chen, L., Chai, Y., Ou, G., Miao, L., Wang, Y. and Yang, C. 2013. Clathrin and AP2 Are Required for Phagocytic Receptor-Mediated Apoptotic Cell Clearance in Caenorhabditis elegans. *Plos Genetics.* **9**(5).

Chillakuri, C.R., Sheppard, D., Lea, S.M. and Handford, P.A. 2012. Notch receptor-ligand binding and activation: Insights from molecular studies. *Seminars in Cell & Developmental Biology.* **23**(4), pp.421-428.

Cho, M., Hughes, S.M., Karschmizrachi, I., Travis, M., Leinwand, L.A. and Blau, H.M. 1994. Fast myosin heavy-chains expressed in secondary mammalian muscle-fibres at the time of their inception. *Journal of Cell Science.* **107**, pp.2361-2371.

Chung, W.-S., Clarke, L.E., Wang, G.X., Stafford, B.K., Sher, A., Chakraborty, C., Joung, J., Foo, L.C., Thompson, A., Chen, C., Smith, S.J. and Barres, B.A. 2013. Astrocytes mediate synapse elimination

through MEGF10 and MERTK pathways. *Nature.* **504**(7480), pp.394-+.

Collins, C.A., Olsen, I., Zammit, P.S., Heslop, L., Petrie, A., Partridge, T.A. and Morgan, J.E. 2005. Stem cell function, self-renewal, and behavioral heterogeneity of cells from the adult muscle satellite cell niche. *Cell.* **122**(2), pp.289-301.

Collins, C.A., Zammit PS. 2009. Isolation and grafting of single muscle fibres. *Methods Mol Biol.* (482), pp.319-330.

Colombatti, A., Spessotto, P., Doliana, R., Mongiat, M., Bressan, G.M. and Esposito, G. 2012. The EMILIN/multimerin family. *Frontiers in Immunology.* **2**.

Conboy, I.M. and Rando, T.A. 2006. The regulation of Notch signaling controls satellite cell activation and cell fate determination in postnatal myogenesis (vol 3, pg 397, 2002). *Developmental Cell.* **10**(2), pp.273-273.

Cooper, R.N., Tajbakhsh, S., Mouly, V., Cossu, G., Buckingham, M. and Butler-Browne, G.S. 1999. In vivo satellite cell activation via Myf5 and MyoD in regenerating mouse skeletal muscle. *Journal of Cell Science.* **112**(17), pp.2895-2901.

Cornelison, D.D.W., Filla, M.S., Stanley, H.M., Rapraeger, A.C. and Olwin, B.B. 2001. Syndecan-3 and syndecan-4 specifically mark skeletal muscle satellite cells and are implicated in satellite cell maintenance and muscle regeneration. *Developmental Biology.* **239**(1), pp.79-94.

Cornelison, D.D.W. and Wold, B.J. 1997. Single-cell analysis of regulatory gene expression in quiescent and activated mouse skeletal muscle satellite cells. *Developmental Biology.* **191**(2), pp.270-283.

Cossu, G. and Sampaolesi, M. 2007. New therapies for Duchenne muscular dystrophy: challenges, prospects and clinical trials. *Trends Mol Med.* **13**(12), pp.520-526.

Cutting, G.R. 2015. Cystic fibrosis genetics: from molecular understanding to clinical application. *Nature Reviews Genetics.* **16**(1), pp.45-56.

Dalton, A.C. and Barton, W.A. 2014. Over-expression of secreted proteins from mammalian cell lines. *Protein Science.* **23**(5), pp.517-525.

De Angelis, L., Berghella, L., Coletta, M., Lattanzi, L., Zanchi, M., Cusella-De Angelis, M.G., Ponzetto, C. and Cossu, G. 1999. Skeletal myogenic progenitors originating from embryonic dorsal aorta coexpress endothelial and myogenic markers and contribute to postnatal muscle growth and regeneration. *Journal of Cell Biology.* **147**(4), pp.869-877.

Dellavalle, A., Sampaolesi, M., Tonlorenzi, R., Tagliafico, E., Sacchetti, B., Perani, L., Innocenzi, A., Galvez, B.G., Messina, G., Morosetti, R., Li, S., Belicchi, M., Peretti, G., Chamberlain, J.S., Wright, W.E., Torrente, Y., Ferrari, S., Bianco, P. and Cossu, G. 2007. Pericytes of human skeletal muscle are myogenic precursors distinct from satellite cells. *Nature Cell Biology.* **9**(3), pp.255-U230.

Deponti, D., Francois, S., Baesso, S., Sciorati, C., Innocenzi, A., Broccoli, V., Muscatelli, F., Meneveri, R., Clementi, E., Cossu, G. and Brunelli, S. 2007. Necdin mediates skeletal muscle regeneration by promoting myoblast survival and differentiation. *J Cell Biol.* **179**(2), pp.305-319.

Dhawan, J. and Rando, T.A. 2005. Stem cells in postnatal myogenesis: molecular mechanisms of satellite cell quiescence, activation and replenishment. *Trends Cell Biol.* **15**(12), pp.666-673.

Doliana, R., Bot, S., Bonaldo, P. and Colombatti, A. 2000. EMI, a novel cysteine-rich domain of EMILINs and other extracellular proteins, interacts with the gC1q domains and participates in multimerization. *FEBS Lett.* **484**(2), pp.164-168.

Donalies, M., Cramer, M., Ringwald, M. and Starzinskipowitz, A. 1991. Expression of M-cadherin, a member of the cadherin multigene family, correlates with differentiation of skeletal-muscle cells. *Proceedings of the National Academy of Sciences of the United States of America.* **88**(18), pp.8024-8028.

Dowler, S., Currie, R.A., Campbell, D.G., Deak, M., Kular, G., Downes, C.P. and Alessi, D.R. 2000. Identification of pleckstrin-homology-domain-containing proteins with novel phosphoinositide-binding specificities. *Biochemical Journal.* **351**, pp.19-31.

Dowler, S., Kular, G. and Alessi, D.R. 2002. Protein lipid overlay assay. *Science's STKE : signal transduction knowledge environment.* **2002**(129), pp.pl6-pl6.

Draper, I., Mahoney, L.J., Mitsuhashi, S., Pacak, C.A., Salomon, R.N. and Kang, P.B. 2014. Silencing of drpr Leads to Muscle and Brain Degeneration in Adult Drosophila. *American Journal of Pathology.* **184**(10), pp.2653-2661.

Dueck, H., Khaladkar, M., Kim, T.K., Spaethling, J.M., Francis, C., Suresh, S., Fisher, S.A., Seale, P., Beck, S.G., Bartfai, T., Kuhn, B., Eberwine, J. and Kim, J. 2015. Deep sequencing reveals cell-type-specific patterns of single-cell transcriptome variation. *Genome Biology.* **16**.

Dumont, N.A., Wang, Y.X., von Maltzahn, J., Pasut, A., Bentzinger, C.F., Brun, C.E. and Rudnicki, M.A. 2015. Dystrophin expression in muscle stem cells regulates their polarity and asymmetric division. *Nature Medicine.* **21**(12), pp.1455-+.

Dunn, K.W., Kamocka, M.M. and McDonald, J.H. 2011. A practical guide to evaluating colocalization in biological microscopy. *American Journal of Physiology-Cell Physiology.* **300**(4), pp.C723-C742.

Egginton, S., Badr, I., Williams, J., Hauton, D., Baan, G.C. and Jaspers, R.T. 2011. Physiological angiogenesis is a graded, not threshold, response. *Journal of Physiology-London.* **589**(1), pp.195-206.

Egginton, S., Hudlicka, O., Brown, M.D., Walter, H., Weiss, J.B. and Bate, A. 1998. Capillary growth in relation to blood flow and performance in overloaded rat skeletal muscle. *Journal of Applied Physiology.* **85**(6), pp.2025-2032.

Eroglu, C. and Barres, B.A. 2010. Regulation of synaptic connectivity by glia. *Nature.* **468**(7321), pp.223-231.

Fernandez-Valdivia, R., Takeuchi, H., Samarghandi, A., Lopez, M., Leonardi, J., Haltiwanger, R. and Jafar-Nejad, H. 2011. Regulation of mammalian Notch signaling and embryonic development by the protein O-glucosyltransferase Rumi. *Developmental Biology.* **356**(1), pp.128-128.

Ferrari, G., Cusella-De Angelis, G., Coletta, M., Paolucci, E., Stornaiuolo, A., Cossu, G. and Mavilio, F. 1998. Muscle regeneration by bone marrow derived myogenic progenitors. *Science.* **279**(5356), pp.1528-1530.

Fortini, M.E. and Bilder, D. 2009. Endocytic regulation of Notch signaling. *Current Opinion in Genetics & Development.* **19**(4), pp.323-328.

Freeze, B.S., McNulty, M.M. and Hanck, D.A. 2006. State-dependent verapamil block of the cloned human Ca(v)3.1 T-type Ca2+ channel. *Molecular Pharmacology.* **70**(2), pp.718-726.

Freeze, H.H. 2001. Lectin analysis of proteins blotted onto filters. *Current protocols in molecular biology / edited by Frederick M. Ausubel ... [et al.].* **Chapter 17**, pp.Unit17.17-Unit17.17.

Fukada, S., Uezumi, A., Ikemoto, M., Masuda, S., Segawa, M., Tanimura, N., Yamamoto, H., Miyagoe-Suzuki, Y. and Takeda, S. 2007. Molecular signature of quiescent satellite cells in adult skeletal muscle. *Stem Cells.* **25**(10), pp.2448-2459.

Gasteiger, E., Gattiker, A., Hoogland, C., Ivanyi, I., Appel, R.D. and Bairoch, A. 2003. ExPASy: the proteomics server for in-depth protein knowledge and analysis. *Nucleic Acids Research.* **31**(13), pp.3784-3788.

Gauster, M., Moser, G., Orendi, K. and Huppertz, B. 2009. Factors Involved in Regulating Trophoblast Fusion: Potential Role in the Development of Preeclampsia. *Placenta.* **30**, pp.S49-S54.

Gawad, C., Koh, W. and Quake, S.R. 2016. Single-cell genome sequencing: current state of the science. *Nature Reviews Genetics.* **17**(3), pp.175-188.

Gnocchi, V.F., White, R.B., Ono, Y., Ellis, J.A. and Zammit, P.S. 2009. Further Characterisation of the Molecular Signature of Quiescent and Activated Mouse Muscle Satellite Cells. *PLoS One.* **4**(4).

Graham, F.L., Smiley, J., Russell, W.C. and Nairn, R. 1977. Characterisitics of a human cell line transformed by DNA from human adenovirus type-5. *Journal of General Virology.* **36**(JUL), pp.59-72.

Gundry, R.L., White, M.Y., Murray, C.I., Kane, L.A., Fu, Q., Stanley, B.A. and Van Eyk, J.E. 2009. Preparation of proteins and peptides for mass spectrometry analysis in a bottom-up proteomics workflow. *Current protocols in molecular biology / edited by Frederick M. Ausubel ... [et al.].* **Chapter 10**, pp.Unit10.25-Unit10.25.

Gupta, R. and Brunak, S. 2002. Prediction of glycosylation across the human proteome and the correlation to protein function. *Pacific Symposium on Biocomputing. Pacific Symposium on Biocomputing.* pp.310-322.

Gutierrez, J.M. and Ownby, C.L. 2003. Skeletal muscle degeneration induced by venom phospholipases A(2): insights into the mechanisms of local and systemic myotoxicity. *Toxicon.* **42**(8), pp.915-931.

Haines, N. and Irvine, K.D. 2003. Glycosylation regulates notch signalling. *Nature Reviews Molecular Cell Biology.* **4**(10), pp.786-797.

Hamon, Y., Trompier, D., Ma, Z., Venegas, V., Pophillat, M., Mignotte, V., Zhou, Z. and Chimini, G. 2006. Cooperation between engulfment receptors: the case of ABCA1 and MEGF10. *PLoS One.* **1**, pe120.

Hanisch, F., Weidemann, W., Grossmann, M., Joshi, P.R., Holzhausen, H.-J., Stoltenburg, G., Weis, J., Zierz, S. and Horstkorte, R. 2013. Sialylation and Muscle Performance: Sialic Acid Is a Marker of Muscle Ageing. *Plos One.* **8**(12).

Hardy, D., Besnard, A., Latil, M., Jouvion, G., Briand, D., Thepenier, C., Pascal, Q., Guguin, A., Gayraud-Morel, B., Cavaillon, J.-M., Tajbakhsh, S., Rocheteau, P. and Chretien, F. 2016. Comparative

Study of Injury Models for Studying Muscle Regeneration in Mice. *Plos One.* **11**(1).

Harris, R.J. and Spellman, M.W. 1993a. O-linked fucose and other post-translational modifications unique to EGF modules. *Glycobiology.* **3**(3), pp.219-224.

Harris, R.J. and Spellman, M.W. 1993b. O-LINKED FUCOSE AND OTHER POSTTRANSLATIONAL MODIFICATIONS UNIQUE TO EGF MODULES. *Glycobiology.* **3**(3), pp.219-224.

Hase, S., Kawabata, S., Nishimura, H., Takeya, H., Sueyoshi, T., Miyata, T., Iwanaga, S., Takao, T., Shimonishi, Y. and Ikenaka, T. 1988. A new trisaccharide sugar chain linked to a serine residue in bovine blood-coagulation factor-VII and factor-IX. *Journal of Biochemistry.* **104**(6), pp.867-868.

Haskins, K.A., Russell, J.F., Gaddis, N., Dressman, H.K. and Aballay, A. 2008. Unfolded protein response genes regulated by CED-1 are required for Caenorhabditis elegans innate immunity. *Dev Cell.* **15**(1), pp.87-97.

Hawke, T.J. and Garry, D.J. 2001. Myogenic satellite cells: physiology to molecular biology. *J Appl Physiol (1985).* **91**(2), pp.534-551.

Hebert, D.N. and Molinari, M. 2007. In and out of the ER: Protein folding, quality control, degradation, and related human diseases. *Physiological Reviews.* **87**(4), pp.1377-1408.

Hedou, J., Bastide, B., Page, A., Michalski, J.-C. and Morelle, W. 2009. Mapping of O-linked beta-N-acetylglucosamine modification sites in key contractile proteins of rat skeletal muscle. *Proteomics.* **9**(8), pp.2139-2148.

Hengartner, M.O. 2001. Apoptosis: corralling the corpses. *Cell.* **104**(3), pp.325-328.

Hochreiter-Hufford, A.E., Lee, C.S., Kinchen, J.M., Sokolowski, J.D., Arandjelovic, S., Call, J.A., Klibanov, A.L., Yan, Z., Mandell, J.W. and Ravichandran, K.S. 2013. Phosphatidylserine receptor BAI1 and apoptotic cells as new promoters of myoblast fusion. *Nature.* **497**(7448), pp.263-267.

Holterman, C.E., Le Grand, F., Kuang, S., Seale, P. and Rudnicki, M.A. 2007. Megf10 regulates the progression of the satellite cell myogenic program. *Journal of Cell Biology.* **179**(5), pp.911-922.

Hoppeler, H. 2016. Molecular networks in skeletal muscle plasticity. *Journal of Experimental Biology.* **219**(2), pp.205-213.

Hori, K., Sen, A., Kirchhausen, T. and Artavanis-Tsakonas, S. 2011. Synergy between the ESCRT-III complex and Deltex defines a ligand-independent Notch signal. *Journal of Cell Biology.* **195**(6), pp.1005-1015.

Hurley, J.H. and Meyer, T. 2001. Subcellular targeting by membrane lipids. *Current Opinion in Cell Biology.* **13**(2), pp.146-152.

Ieronimakis, N., Balasundaram, G., Rainey, S., Srirangam, K., Yablonka-Reuveni, Z. and Reyes, M. 2010. Absence of CD34 on Murine Skeletal Muscle Satellite Cells Marks a Reversible State of Activation during Acute Injury. *Plos One.* **5**(6).

Iram, T., Ramirez-Ortiz, Z., Byrne, M.H., Coleman, U.A., Kingery, N.D., Means, T.K., Frenkel, D. and El Khoury, J. 2016. Megf10 Is a Receptor for C1Q That Mediates Clearance of Apoptotic Cells by

Astrocytes. *The Journal of neuroscience : the official journal of the Society for Neuroscience.* **36**(19), pp.5185-5192.

Irintchev, A., Zeschnigk, M., Starzinskipowitz, A. and Wernig, A. 1994. Expression pattern of M-cadherin in normal, denervated and regenerating mouse muscles. *Developmental Dynamics.* **199**(4), pp.326-337.

Ishibashi, J., Perry, R.L., Asakura, A. and Rudnicki, M.A. 2005. MyoD induces myogenic differentiation through cooperation of its NH2- and COOH-terminal regions. *Journal of Cell Biology.* **171**(3), pp.471-482.

Jagla, K., Dolle, P., Mattei, M.G., Jagla, T., Schuhbaur, B., Dretzen, G., Bellard, F. and Bellard, M. 1995. Mouse lbx1 and human lbx1 define a novel mammalian homeobox gene family related to the drosophila lady bird genes. *Mechanisms of Development.* **53**(3), pp.345-356.

Jat, P.S., Noble, M.D., Ataliotis, P., Tanaka, Y., Yannoutsos, N., Larsen, L. and Kioussis, D. 1991. Direct derivation of conditionally immortal cell-lines from an h-2kb-tsa58 transgenic mouse. *Proceedings of the National Academy of Sciences of the United States of America.* **88**(12), pp.5096-5100.

Jennische, E., Ekberg, S. and Matejka, G.L. 1993. Expression of hepatocyte growth-factor in growing and regenerating rat skeletal-muscle. *American Journal of Physiology.* **265**(1), pp.C122-C128.

Jesse, T.L., LaChance, R., Iademarco, M.F. and Dean, D.C. 1998. Interferon regulatory factor-2 is a transcriptional activator in muscle where it regulates expression of vascular cell adhesion molecule-1. *Journal of Cell Biology.* **140**(5), pp.1265-1276.

Johnston, A.P.W., Baker, J., Bellamy, L.M., McKay, B.R., De Lisio, M. and Parise, G. 2010. Regulation of Muscle Satellite Cell Activation and Chemotaxis by Angiotensin II. *PLoS One.* **5**(12).

Jungbluth, H. 2007. Multi-minicore disease. *Orphanet Journal of Rare Diseases.* **2**.

Justice, M.J. and Dhillon, P. 2016. Using the mouse to model human disease: increasing validity and reproducibility. *Disease Models & Mechanisms.* **9**(2), pp.101-103.

Kang, Y., Zhao, D., Liang, H., Liu, B., Zhang, Y., Liu, Q., Wang, X. and Liu, Y. 2012. Structural study of TTR-52 reveals the mechanism by which a bridging molecule mediates apoptotic cell engulfment. *Genes & Development.* **26**(12), pp.1339-1350.

Kansas, G.S., Saunders, K.B., Ley, K., Zakrzewicz, A., Gibson, R.M., Furie, B.C., Furie, B. and Tedder, T.F. 1994. A role for the epidermal growth factor-like domain of p-selectin in ligand recognition and cell-adhesion. *Journal of Cell Biology.* **124**(4), pp.609-618.

Kao, Y.H., Lee, G.F., Wang, Y., Starovasnik, M.A., Kelley, R.F., Spellman, M.W. and Lerner, L. 1999. The effect of O-fucosylation on the first EGF-like domain from human blood coagulation factor VII. *Biochemistry.* **38**(22), pp.7097-7110.

Kaszuba, K., Grzybek, M., Orlowski, A., Danne, R., Rog, T., Simons, K., Coskun, U. and Vattulainen, I. 2015. N-Glycosylation as determinant of epidermal growth factor receptor conformation in membranes. *Proceedings of the National Academy of Sciences of the United States of America.* **112**(14), pp.4334-4339.

Kauskot, A., Di Michele, M., Loyen, S., Freson, K., Verhamme, P. and Hoylaerts, M.F. 2012. A novel mechanism of sustained platelet alpha IIb beta 3 activation via PEAR1. *Blood.* **119**(17), pp.4056-4065.

Kawaguchi, D., Furutachi, S., Kawai, H., Hozumi, K. and Gotoh, Y. 2013. Dll1 maintains quiescence of adult neural stem cells and segregates asymmetrically during mitosis. *Nature Communications.* **4**.

Kay, J.N., Chu, M.W. and Sanes, J.R. 2012. MEGF10 and MEGF11 mediate homotypic interactions required for mosaic spacing of retinal neurons. *Nature.* **483**(7390), pp.465-469.

Kinchen, J.M., Cabello, J., Klingele, D., Wong, K., Feichtinger, R., Schnabel, H., Schnabel, R. and Hengartner, M.O. 2005. Two pathways converge at CED-10 to mediate actin rearrangement and corpse removal in C-elegans. *Nature.* **434**(7029), pp.93-99.

Kislinger, T., Gramolini, A.O., Pan, Y., Rahman, K., MacLennan, D.H. and Emili, A. 2005. Proteome dynamics during C2C12 myoblast differentiation. *Mol Cell Proteomics.* **4**(7), pp.887-901.

Kooijman, E.E., Chupin, V., de Kruijff, B. and Burger, K.N.J. 2003. Modulation of membrane curvature by phosphatidic acid and lysophosphatidic acid. *Traffic.* **4**(3), pp.162-174.

Kopan, R. and Ilagan, M.X.G. 2009. The Canonical Notch Signaling Pathway: Unfolding the Activation Mechanism. *Cell.* **137**(2), pp.216-233.

Kritikou, E. 2008. Sugar-coated signalling. *Nature Reviews Molecular Cell Biology.* **9**(3), pp.186-186.

Krivtsov, A.V., Rozov, F.N., Zinovyeva, M.V., Hendrikx, P.J., Jiang, Y., Visser, J.W.M. and Belyavsky, A.V. 2007. Jedi - A novel transmembrane protein expressed in early hematopoietic cells. *Journal of Cellular Biochemistry.* **101**(3), pp.767-784.

Kuang, S., Kuroda, K., Le Grand, F. and Rudnicki, M.A. 2007. Asymmetric self-renewal and commitment of satellite stem cells in muscle. *Cell.* **129**(5), pp.999-1010.

Kuang, S. and Rudnicki, M.A. 2008. The emerging biology of satellite cells and their therapeutic potential. *Trends Mol Med.* **14**(2), pp.82-91.

Kwiatkowska, K. and Sobota, A. 1999. Signaling pathways in phagocytosis. *Bioessays.* **21**(5), pp.422-431.

LaFramboise, W.A., Guthrie, R.D., Scalise, D., Elborne, V., Bombach, K.L., Armanious, C.S. and Magovern, J.A. 2003. Effect of muscle origin and phenotype on satellite cell muscle-specific gene expression. *Journal of Molecular and Cellular Cardiology.* **35**(10), pp.1307-1318.

Lamitina, T. and Cherry, S. 2008. Dangerous liaisons: the apoptotic engulfment receptor CED-1 links innate immunity to the unfolded protein response. *Dev Cell.* **15**(1), pp.3-4.

Larkin, M.A., Blackshields, G., Brown, N.P., Chenna, R., McGettigan, P.A., McWilliam, H., Valentin, F., Wallace, I.M., Wilm, A., Lopez, R., Thompson, J.D., Gibson, T.J. and Higgins, D.G. 2007. Clustal W and clustal X version 2.0. *Bioinformatics.* **23**(21), pp.2947-2948.

Lepper, C., Conway, S.J. and Fan, C.-M. 2009. Adult satellite cells and embryonic muscle progenitors have distinct genetic requirements. *Nature.* **460**(7255), pp.627-U694.

Lettre, G. and Hengartner, M.O. 2006. Developmental apoptosis in C. elegans: a complex CEDnario. *Nat Rev Mol Cell Biol.* **7**(2), pp.97-108.

Letunic, I., Doerks, T. and Bork, P. 2015. SMART: recent updates, new developments and status in 2015. *Nucleic Acids Research.* **43**(D1), pp.D257-D260.

Leventis, P.A. and Grinstein, S. 2010. The Distribution and Function of Phosphatidylserine in Cellular Membranes. In: Rees, D.C., et al. eds. *Annual Review of Biophysics, Vol 39.* pp.407-427.

Li, X., Lin, C. and O'Connor, P.B. 2010. Glutamine Deamidation: Differentiation of Glutamic Acid and gamma-Glutamic Acid in Peptides by Electron Capture Dissociation. *Analytical Chemistry.* **82**(9), pp.3606-3615.

Li, Y., Xu, X., Song, L., Hou, Y., Li, Z., Tsang, S., Li, F., Im, K.M., Wu, K., Wu, H., Ye, X., Li, G., Wang, L., Zhang, B., Liang, J., Xie, W., Wu, R., Jiang, H., Liu, X., Yu, C., Zheng, H., Jian, M., Nie, L., Wan, L., Shi, M., Sun, X., Tang, A., Guo, G., Gui, Y., Cai, Z., Li, J., Wang, W., Lu, Z., Zhang, X., Bolund, L., Kristiansen, K., Wang, J., Yang, H., Dean, M. and Wang, J. 2012. Single-cell sequencing analysis characterizes common and cell-lineage-specific mutations in a muscle-invasive bladder cancer. *Gigascience.* **1**.

Liadaki, K., Casar, J.C., Wessen, M., Luth, E.S., Jun, S., Gussoni, E. and Kunkel, L.M. 2012. beta 4 Integrin Marks Interstitial Myogenic Progenitor Cells in Adult Murine Skeletal Muscle. *Journal of Histochemistry & Cytochemistry.* **60**(1), pp.31-44.

Liewluck, T., Milone, M., Tian, X., Engel, A.G., Staff, N.P. and Wong, L.-J. 2016. Adult-onset respiratory insufficiency, scoliosis, and distal joint hyperlaxity in patients with multiminicore disease due to novel Megf10 mutations. *Muscle & nerve.* **53**(6), pp.984-988.

Liu, L., Cheung, T.H., Charville, G.W. and Rando, T.A. 2015a. Isolation of skeletal muscle stem cells by fluorescence-activated cell sorting. *Nature Protocols.* **10**(10), pp.1612-1624.

Liu, W., Wei-LaPierre, L., Klose, A., Dirksen, R.T. and Chakkalakal, J.V. 2015b. Inducible depletion of adult skeletal muscle stem cells impairs the regeneration of neuromuscular junctions. *Elife.* **4**.

Logan, C.V., Lucke, B., Pottinger, C., Abdelhamed, Z.A., Parry, D.A., Szymanska, K., Diggle, C.P., Riesen, A.v., Morgan, J.E., Markham, G., Ellis, I., Manzur, A.Y., Markham, A.F., Shires, M., Helliwell, T., Scoto, M., Hübner, C., Bonthron, D.T., Taylor, G.R., Sheridan, E., Muntoni, F., Carr, I.M., Schuelke, M. and Johnson, C.A. 2011. Mutations in MEGF10, a regulator of satellite cell myogenesis, cause early onset myopathy, areflexia, respiratory distress and dysphagia (EMARDD). *Nature Genetics.* **43**(12), pp.1189-1192.

Loov, C., Hillered, L., Ebendal, T. and Erlandsson, A. 2012. Engulfing astrocytes protect neurons from contact-induced apoptosis following injury. *PLoS One.* **7**(3), pe33090.

Loughran, G., Chou, M.-Y., Ivanov, I.P., Jungreis, I., Kellis, M., Kiran, A.M., Baranov, P.V. and Atkins, J.F. 2014. Evidence of efficient stop codon readthrough in four mammalian genes. *Nucleic Acids Research.* **42**(14), pp.8928-8938.

Love, C.A., Harlos, K., Mavaddat, N., Davis, S.J., Stuart, D.I., Jones, E.Y. and Esnouf, R.M. 2003. The ligand-binding face of the semaphorins revealed by the high-resolution crystal structure of SEMA4D. *Nature Structural Biology.* **10**(10), pp.843-848.

Luca, V.C., Jude, K.M., Pierce, N.W., Nachury, M.V., Fischer, S. and Garcia, K.C. 2015. Structural basis for Notch1 engagement of Delta-like 4. *Science.* **347**(6224), pp.847-853.

Luther, K.B. and Haltiwanger, R.S. 2009a. Role of unusual O-glycans in intercellular signaling. *International Journal of Biochemistry & Cell Biology.* **41**(5), pp.1011-1024.

Luther, K.B. and Haltiwanger, R.S. 2009b. Role of unusual O-glycans in intercellular signaling. *Int J Biochem Cell Biol.* **41**(5), pp.1011-1024.

Maggs, A.M., Taylor-Harris, P., Peckham, M. and Hughes, S.M. 2000. Evidence for differential post-translational modifications of slow myosin heavy chain during murine skeletal muscle development. *Journal of Muscle Research and Cell Motility.* **21**(2), pp.101-113.

Mangahas, P.M. and Zhou, Z. 2005. Clearance of apoptotic cells in Caenorhabditis elegans. *Semin Cell Dev Biol.* **16**(2), pp.295-306.

Maqbool, T. and Jagla, K. 2007. Genetic control of muscle development: learning from Drosophila. *Journal of Muscle Research and Cell Motility.* **28**(7-8), pp.397-407.

Mauro, A. 1961. Satellite cell of skeletal muscle fibers. *J Biophys Biochem Cytol.* **9**, pp.493-495.

McCroskery, S., Thomas, M., Maxwell, L., Sharma, M. and Kambadur, R. 2003. Myostatin negatively regulates satellite cell activation and self-renewal. *J Cell Biol.* **162**(6), pp.1135-1147.

Megeney, L.A., Kablar, B., Garrett, K., Anderson, J.E. and Rudnicki, M.A. 1996. MyoD is required for myogenic stem cell function in adult skeletal muscle. *Genes & Development.* **10**(10), pp.1173-1183.

Meilleur, K.G., Pierson, T.M., Jain, M., Donkervoort, S., Markello, T., Wolfe, L., Accardi, J., Adams, D., Sincan, M., Fuentes-Fajardo, K., Cherukuri, P.F., Cruz, P., Bajraktari, I., Lehky, T., Teer, J.K., Mullikin, J.C., Gahl, W.A., Boerkoel, C.F., Tifft, C.J. and Bonnemann, C.G. 2012. Two sibs with early onset myopathy with areflexia, respiratory distress, and dysphagia (EMARDD) due to homozygous exon 7 deletion in MEGF10. *Neuromuscular Disorders.* **22**(9-10), pp.870-871.

<Meilleur Nov 2012- MEGF10- New EMARDD Paper- 2012.pdf>.

Meng, F., Yao, D., Shi, Y., Kabakoff, J., Wu, W., Reicher, J., Ma, Y., Moosmann, B., Masliah, E., Lipton, S.A. and Gu, Z. 2011. Oxidation of the cysteine-rich regions of parkin perturbs its E3 ligase activity and contributes to protein aggregation. *Molecular Neurodegeneration.* **6**.

Mitchell, A., Chang, H.-Y., Daugherty, L., Fraser, M., Hunter, S., Lopez, R., McAnulla, C., McMenamin, C., Nuka, G., Pesseat, S., Sangrador-Vegas, A., Scheremetjew, M., Rato, C., Yong, S.-Y., Bateman, A., Punta, M., Attwood, T.K., Sigrist, C.J.A., Redaschi, N., Rivoire, C., Xenarios, I., Kahn, D., Guyot, D., Bork, P., Letunic, I., Gough, J., Oates, M., Haft, D., Huang, H., Natale, D.A., Wu, C.H., Orengo, C., Sillitoe, I., Mi, H., Thomas, P.D. and Finn, R.D. 2015. The InterPro protein families database: the classification resource after 15 years. *Nucleic Acids Research.* **43**(D1), pp.D213-D221.

Mitsuhashi, S., Mitsuhashi, H., Alexander, M.S., Sugimoto, H. and Kang, P.B. 2013. Cysteine mutations cause defective tyrosine phosphorylation in MEGF10 myopathy. *FEBS Lett.* **587**(18), pp.2952-2957.

Mobley, C.B., Hornberger, T.A., Fox, C.D., Healy, J.C., Ferguson, B.S., Lowery, R.P., McNally, R.M., Lockwood, C.M., Stout, J.R., Kavazis, A.N., Wilson, J.M. and Roberts, M.D. 2015. Effects of oral phosphatidic acid feeding with or without whey protein on muscle protein synthesis and anabolic signaling in rodent skeletal muscle. *Journal of the International Society of Sports Nutrition.* **12**.

Morgan, J.E., Beauchamp, J.R., Pagel, C.N., Peckham, M., Ataliotis, P., Jat, P.S., Noble, M.D., Farmer, K. and Partridge, T.A. 1994. Myogenic cell lines derived from transgenic mice carrying a thermolabile T antigen: a model system for the derivation of tissue-specific and mutation-specific cell lines. *Dev Biol.* **162**(2), pp.486-498.

Morgan, J.E., Gross, J.G., Pagel, C.N., Beauchamp, J.R., Fassati, A., Thrasher, A.J., Di Santo, J.P., Fisher, I.B., Xu, S.W., Abraham, D.J. and Partridge, T.A. 2002. Myogenic cell proliferation and generation of a reversible tumorigenic phenotype are triggered by preirradiation of the recipient site. *Journal of Cell Biology.* **157**(4), pp.693-702.

Morgan, J.E., Moore, S.E., Walsh, F.S. and Partridge, T.A. 1992. Formation of skeletal-muscle invivo from the mouse c2-cell line. *Journal of Cell Science.* **102**, pp.779-&.

Morgan, J.E., Pagel, C.N., Sherrratt, T. and Partridge, T.A. 1993. Long-term persistence and migration of myogenic cells injected into pre-irradiated muscles of mdx mice. *Journal of the Neurological Sciences.* **115**(2), pp.191-200.

Mullershausen, F., Russwurm, M., Friebe, A. and Koesling, D. 2004. Inhibition of phosphodiesterase type 5 by the activator of nitric oxide-sensitive guanylyl cyclase BAY 41-2272. *Circulation.* **109**(14), pp.1711-1713.

Nakayama, M., Kikuno, R. and Ohara, O. 2002. Protein-protein interactions between large proteins: two-hybrid screening using a functionally classified library composed of long cDNAs. *Genome Res.* **12**(11), pp.1773-1784.

Nalbantoglu, J., Pari, G., Karpati, G. and Holland, P.C. 1999. Expression of the primary coxsackie and adenovirus receptor is downregulated during skeletal muscle maturation and limits the efficacy of adenovirus-mediated gene delivery to muscle cells. *Human Gene Therapy.* **10**(6), pp.1009-1019.

Nanda, N., Bao, M., Lin, H., Clauser, K., Komuves, L., Quertermous, T., Conley, P.B., Phillips, D.R. and Hart, M.J. 2005. Platelet endothelial aggregation receptor 1 (PEAR1), a novel epidermal growth factor repeat-containing transmembrane receptor, participates in platelet contact-induced activation. *Journal of Biological Chemistry.* **280**(26), pp.24680-24689.

Nishino, I., Carrillo-Carrasco, N. and Argov, Z. 2015. GNE myopathy: current update and future therapy. *Journal of Neurology Neurosurgery and Psychiatry.* **86**(4), pp.385-392.

Okajima, T. and Irvine, K.D. 2002. Regulation of notch signaling by O-linked fucose. *Cell.* **111**(6), pp.893-904.

Ooms, L.M., Dyson, J.M., Kong, A.M. and Mitchell, C.A. 2009. Analysis of Phosphatidylinositol 3,4,5 Trisphosphate 5-Phosphatase Activity by in vitro and in vivo Assays. In: Larijani, B., et al. eds. *Methods in Molecular Biology.* pp.223-239.

Park, S.-Y., Kim, S.-Y., Jung, M.-Y., Bae, D.-J. and Kim, I.-S. 2008. Epidermal growth factor-like domain repeat of stabilin-2 recognizes phosphatidylserine during cell corpse clearance. *Molecular and Cellular Biology.* **28**(17), pp.5288-5298.

Park, S.Y., Yun, Y., Kim, M.J. and Kim, I.S. 2014. Myogenin is a positive regulator of MEGF10 expression in skeletal muscle. *Biochem Biophys Res Commun.*

Pasut, A., Jones, A.E. and Rudnicki, M.A. 2013. Isolation and culture of individual myofibers and their satellite cells from adult skeletal muscle. *J Vis Exp.* (73), pe50074.

Pasut, A., Oleynik, P. and Rudnicki, M.A. 2012. Isolation of muscle stem cells by fluorescence activated cell sorting cytometry. *Methods Mol Biol.* **798**, pp.53-64.

Pawlikowski, B., Lee, L., Zuo, J. and Kramer, R.H. 2009. Analysis of Human Muscle Stem Cells Reveals a Differentiation-Resistant Progenitor Cell Population Expressing Pax7 Capable of Self-renewal. *Developmental Dynamics.* **238**(1), pp.138-149.

Pawson, T. and Scott, J.D. 1997. Signaling through scaffold, anchoring, and adaptor proteins. *Science.* **278**(5346), pp.2075-2080.

Peckham, M. 2008. Engineering a multi-nucleated myotube, the role of the actin cytoskeleton. *J Microsc.* **231**(3), pp.486-493.

Peltzer, J., Colman, L., Cebrian, J., Musa, H., Peckham, M. and Keller, A. 2008. Novel murine clonal cell lines either express slow or mixed (fast and slow) muscle markers following differentiation in vitro. *Dev Dyn.* **237**(5), pp.1412-1423.

Penner, A.S., Rock, M.J., Kielty, C.M. and Shipley, J.M. 2002. Microfibril-associated glycoprotein-2 interacts with fibrillin-1 and fibrillin-2 suggesting a role for MAGP-2 in elastic fiber assembly. *Journal of Biological Chemistry.* **277**(38), pp.35044-35049.

Pierson, T.M., Markello, T., Accardi, J., Wolfe, L., Adams, D., Sincan, M., Tarazi, N.M., Fajardo, K.F., Cherukuri, P.F., Bajraktari, I., Meilleur, K.G., Donkervoort, S., Jam, M., Hu, Y., Lehky, T.J., Cruz, P., Mullikin, J.C., Bonnemann, C., Gahl, W.A., Boerkoel, C.F. and Tifft, C.J. 2013. Novel SNP array analysis and exome sequencing detect a homozygous exon 7 deletion of MEGF10 causing early onset myopathy, areflexia, respiratory distress and dysphagia (EMARDD). *Neuromuscular Disorders.* **23**(6), pp.483-488.

Pisani, D.F., Clement, N., Loubat, A., Plaisant, M., Sacconi, S., Kurzenne, J.-Y., Desnuelle, C., Dani, C. and Dechesne, C.A. 2010. Hierarchization of Myogenic and Adipogenic Progenitors Within Human Skeletal Muscle. *Stem Cells.* **28**(12), pp.2182-2194.

Posor, Y., Eichhorn-Gruenig, M., Puchkov, D., Schoeneberg, J., Ullrich, A., Lampe, A., Mueller, R., Zarbakhsh, S., Gulluni, F., Hirsch, E., Krauss, M., Schultz, C., Schmoranzer, J., Noe, F. and Haucke, V. 2013. Spatiotemporal control of endocytosis by phosphatidylinositol-3,4-bisphosphate. *Nature.* **499**(7457), pp.233-+.

Rao, Z., Handford, P., Mayhew, M., Knott, V., Brownlee, G.G. and Stuart, D. 1995. The structure of a ca2+-binding epidermal growth factor-like domain - its role in protein-protein interactions. *Cell.* **82**(1), pp.131-141.

Ratajczak, M.Z., Majka, M., Kucia, M., Drukala, J., Pietrzkowski, Z., Peiper, S. and Janowska-Wieczorek, A. 2003. Expression of functional CXCR4 by muscle satellite cells and secretion of SDF-1 by muscle-derived fibroblasts is associated with the presence of both muscle progenitors in bone marrow and hematopoietic stem/progenitor cells in muscles. *Stem Cells.* **21**(3), pp.363-371.

Riehle, R.D., Cornea, S. and Degterev, A. 2013. Role of Phosphatidylinositol 3,4,5-Trisphosphate in Cell Signaling. In: Capelluto, D.G.S. ed. *Lipid-Mediated Protein Signaling.* pp.105-139.

Robinson, N.E. 2002. Protein deamidation. *Proceedings of the National Academy of Sciences of the United States of America.* **99**(8), pp.5283-5288.

Robinson, N.E. and Robinson, A.B. 2001. Molecular clocks. *Proceedings of the National Academy of Sciences of the United States of America.* **98**(3), pp.944-949.

Rockenfeller, P., Koska, M., Pietrocola, F., Minois, N., Knittelfelder, O., Sica, V., Franz, J., Carmona-Gutierrez, D., Kroemer, G. and Madeo, F. 2015. Phosphatidylethanolamine positively regulates autophagy and longevity. *Cell Death and Differentiation.* **22**(3), pp.499-508.

Rosen, G.D., Sanes, J.R., Lachance, R., Cunningham, J.M., Roman, J. and Dean, D.C. 1992. Roles For The Integrin Vla-4 And Its Counter Receptor Vcam-1 In Myogenesis. *Cell.* **69**(7), pp.1107-1119.

Rosenblatt, J.D., Yong, D. and Parry, D.J. 1994. Satellite cell-activity is required for hypertrophy of overloaded adult-rat muscle. *Muscle & Nerve.* **17**(6), pp.608-613.

Rosenthal, N. and Brown, S. 2007. The mouse ascending: perspectives for human-disease models. *Nature Cell Biology.* **9**(9), pp.993-999.

Roth, M.G. 2004. Phosphoinositides in constitutive membrane traffic. *Physiological Reviews.* **84**(3), pp.699-730.

Rudnicki, M.A., Schnegelsberg, P.N.J., Stead, R.H., Braun, T., Arnold, H.H. and Jaenisch, R. 1993. Myod or myf-5 is required for the formation of skeletal muscle. *Cell.* **75**(7), pp.1351-1359.

Rux, J.J. and Burnett, R.M. 2004. Adenovirus structure. *Human Gene Therapy.* **15**(12), pp.1167-1176.

Sabourin, L.A., Girgis-Gabardo, A., Seale, P., Asakura, A. and Rudnicki, M.A. 1999. Reduced differentiation potential of primary MyoD-/- myogenic cells derived from adult skeletal muscle. *Journal of Cell Biology.* **144**(4), pp.631-643.

Sakamoto, K., Yamaguchi, S., Ando, R., Miyawaki, A., Kabasawa, Y., Takagi, M., Li, C.L., Perbal, B. and Katsube, K. 2002. The nephroblastoma overexpressed gene (NOV/ccn3) protein associates with Notch1 extracellular domain and inhibits myoblast differentiation via Notch signaling pathway. *Journal of Biological Chemistry.* **277**(33), pp.29399-29405.

Sato, T.K., Overduin, M. and Emr, S.D. 2001. Location, location, location: Membrane targeting directed by PX domains. *Science.* **294**(5548), pp.1881-1885.

Scheib, J.L., Sullivan, C.S. and Carter, B.D. 2012. Jedi-1 and MEGF10 signal engulfment of apoptotic neurons through the tyrosine kinase Syk. *J Neurosci.* **32**(38), pp.13022-13031.

Schultz, E. 1996. Satellite cell proliferative compartments in growing skeletal muscles. *Developmental Biology.* **175**(1), pp.84-94.

Schultz, J., Milpetz, F., Bork, P. and Ponting, C.P. 1998. SMART, a simple modular architecture research tool: Identification of signaling domains. *Proceedings of the National Academy of Sciences of the United States of America.* **95**(11), pp.5857-5864.

Schuster-Gossler, K., Cordes, R. and Gossler, A. 2007. Premature myogenic differentiation and depletion of progenitor cells cause severe muscle hypotrophy in Delta1 mutants. *Proceedings of the National Academy of Sciences of the United States of America.* **104**(2), pp.537-542.

Schwarz, F. and Aebi, M. 2011. Mechanisms and principles of N-linked protein glycosylation. *Current Opinion in Structural Biology.* **21**(5), pp.576-582.

Seale, P., Ishibashi, J., Holterman, C. and Rudnicki, M.A. 2004. Muscle satellite cell-specific genes identified by genetic profiling of MyoD-deficient myogenic cell. *Developmental Biology.* **275**(2), pp.287-300.

Seale, P., Sabourin, L.A., Girgis-Gabardo, A., Mansouri, A., Gruss, P. and Rudnicki, M.A. 2000. Pax7 is required for the specification of myogenic satellite cells. *Cell.* **102**(6), pp.777-786.

Shao, L., Luo, Y., Moloney, D.J. and Haltiwanger, R.S. 2002. O-Glycosylation of EGF repeats: identification and initial characterization of a UDP-glucose: protein O-glucosyltransferase. *Glycobiology.* **12**(11), pp.763-770.

Shao, L., Moloney, D.J. and Haltiwanger, R. 2003. Fringe modifies O-fucose on mouse Notch1 at epidermal growth factor-like repeats within the ligand-binding site and the abruptex region. *Journal of Biological Chemistry.* **278**(10), pp.7775-7782.

Sheng, X., Yung, Y.C., Chen, A. and Chun, J. 2015. Lysophosphatidic acid signalling in development. *Development.* **142**(8), pp.1390-1395.

Sherwood, R.I., Christensen, J.L., Conboy, I.M., Conboy, M.J., Rando, T.A., Weissman, I.L. and Wagers, A.J. 2004. Isolation of adult mouse myogenic progenitors: Functional heterogeneity of cells within and engrafting skeletal muscle. *Cell.* **119**(4), pp.543-554.

Shi, S.L. and Stanley, P. 2003. Protein O-fucosyltransferase 1 is an essential component of Notch signaling pathways. *Proceedings of the National Academy of Sciences of the United States of America.* **100**(9), pp.5234-5239.

Shi, X. and Garry, D.J. 2006. Muscle stem cells in development, regeneration, and disease. *Genes Dev.* **20**(13), pp.1692-1708.

Shimizu, H., Woodcock, S.A., Wilkin, M.B., Trubenova, B., Monk, N.A.M. and Baron, M. 2014. Compensatory Flux Changes within an Endocytic Trafficking Network Maintain Thermal Robustness of Notch Signaling. *Cell.* **157**(5), pp.1160-1174.

Shinin, V., Gayraud-Morel, B. and Tajbakhsh, S. 2009. Template DNA-Strand Co-Segregation and Asymmetric Cell Division in Skeletal Muscle Stem Cells. In: Audet, J. and Stanford, W.L. eds. *Methods in Molecular Biology.* pp.295-317.

Siegel, A.L., Atchison, K., Fisher, K.E., Davis, G.E. and Cornelison, D.D. 2009. 3D timelapse analysis of muscle satellite cell motility. *Stem Cells.* **27**(10), pp.2527-2538.

Singh, T.D., Park, S.Y., Bae, J.S., Yun, Y., Bae, Y.C., Park, R.W. and Kim, I.S. 2010. MEGF10 functions as a receptor for the uptake of amyloid-beta. *FEBS Lett.* **584**(18), pp.3936-3942.

Smith, M.J., Hardy, W.R., Murphy, J.M., Jones, N. and Pawson, T. 2006. Screening for PTB domain binding partners and ligand specificity using proteome-derived NPXY peptide arrays. *Mol Cell Biol.* **26**(22), pp.8461-8474.

Sorkin, A. 2001. Internalization of the epidermal growth factor receptor: role in signalling. *Biochemical Society Transactions.* **29**, pp.480-484.

Spessotto, P., Cervi, M., Mucignat, M.T., Mungiguerra, G., Sartoretto, I., Doliana, R. and Colombatti, A. 2003. beta 1 integrin-dependent cell adhesion to EMILIN-1 is mediated by the gC1q domain. *Journal of Biological Chemistry.* **278**(8), pp.6160-6167.

Stacey, M., Chang, G.W., Davies, J.Q., Kwakkenbos, M.J., Sanderson, R.D., Hamann, J., Gordon, S. and Lin, H.H. 2003. The epidermal growth factor-like domains of the human EMR2 receptor mediate cell attachment through chondroitin sulfate glycosaminoglycans. *Blood.* **102**(8), pp.2916-2924.

Stark, D.A., Karvas, R.M., Siegel, A.L. and Cornelison, D.D. 2011. Eph/ephrin interactions modulate muscle satellite cell motility and patterning. *Development.* **138**(24), pp.5279-5289.

Sun, J., Smith, L., Armento, A. and Deng, W.-M. 2008. Regulation of the endocycle/gene amplification switch by Notch and ecdysone signaling. *Journal of Cell Biology.* **182**(5), pp.885-896.

Suzuki, E. and Nakayama, M. 2007a. The mammalian Ced-1 ortholog MEGF10/KIAA1780 displays a novel adhesion pattern. *Exp Cell Res.* **313**(11), pp.2451-2464.

Suzuki, E. and Nakayama, M. 2007b. MEGF10 is a mammalian ortholog of CED-1 that interacts with clathrin assembly protein complex 2 medium chain and induces large vacuole formation. *Exp Cell Res.* **313**(17), pp.3729-3742.

Tajbakhsh, S. 2009. Skeletal muscle stem cells in developmental versus regenerative myogenesis. *Journal of Internal Medicine.* **266**(4), pp.372-389.

Tanaka, S., Terada, K. and Nohno, T. 2011. Canonical Wnt signaling is involved in switching from cell proliferation to myogenic differentiation of mouse myoblast cells. *J Mol Signal.* **6**, p12.

Tatsumi, R., Anderson, J.E., Nevoret, C.J., Halevy, O. and Allen, R.E. 1998. HGF/SF is present in normal adult skeletal muscle and is capable of activating satellite cells. *Developmental Biology.* **194**(1), pp.114-128.

Tawk, L., Chicanne, G., Dubremetz, J.-F., Richard, V., Payrastre, B., Vial, H.J., Roy, C. and Wengelnik, K. 2010. Phosphatidylinositol 3-Phosphate, an Essential Lipid in Plasmodium, Localizes to the Food Vacuole Membrane and the Apicoplast. *Eukaryotic Cell.* **9**(10), pp.1519-1530.

Thomas, P. and Smart, T.G. 2005. HEK293 cell line: A vehicle for the expression of recombinant proteins. *Journal of Pharmacological and Toxicological Methods.* **51**(3), pp.187-200.

Thompson, J.D., Higgins, D.G. and Gibson, T.J. 1994. Clustal-W - improving the sensitivity of progressive multiple sequence alignment through

sequence weighting, position-specific gap penalties and weight matrix choice. *Nucleic Acids Research.* **22**(22), pp.4673-4680.

Tomczak, K.K., Marinescu, V.D., Ramoni, M.F., Sanoudou, D., Montanaro, F., Han, M., Kunkel, L.M., Kohane, I.S. and Beggs, A.H. 2003. Expression profiling and identification of novel genes involved in myogenic differentiation. *Faseb Journal.* **17**(15), pp.403-+.

Tung, T.T., Nagaosa, K., Fujita, Y., Kita, A., Mori, H., Okada, R., Nonaka, S. and Nakanishi, Y. 2013. Phosphatidylserine recognition and induction of apoptotic cell clearance by Drosophila engulfment receptor Draper. *J Biochem.* **153**(5), pp.483-491.

Twigg, S.R.F., Lloyd, D., Jenkins, D., Elcioglu, N.E., Cooper, C.D.O., Al-Sannaa, N., Annagur, A., Gillessen-Kaesbach, G., Huening, I., Knight, S.J.L., Goodship, J.A., Keavney, B.D., Beales, P.L., Gileadi, O., McGowan, S.J. and Wilkie, A.O.M. 2012. Mutations in Multidomain Protein MEGF8 Identify a Carpenter Syndrome Subtype Associated with Defective Lateralization. *American Journal of Human Genetics.* **91**(5), pp.897-905.

Valastyan, J.S. and Lindquist, S. 2014. Mechanisms of protein-folding diseases at a glance. *Disease Models & Mechanisms.* **7**(1), pp.9-14.

Vance, J.E. and Tasseva, G. 2013. Formation and function of phosphatidylserine and phosphatidylethanolamine in mammalian cells. *Biochimica Et Biophysica Acta-Molecular and Cell Biology of Lipids.* **1831**(3), pp.543-554.

Vasyutina, E., Lenhard, D.C. and Birchmeier, C. 2007. Notch function in Myogenesis. *Cell Cycle.* **6**(12), pp.1451-1454.

Wang, N., Silver, D.L., Thiele, C. and Tall, A.R. 2001. ATP-binding cassette transporter A1 (ABCA1) functions as a cholesterol efflux regulatory protein. *Journal of Biological Chemistry.* **276**(26), pp.23742-23747.

Wang, Y.X. and Rudnicki, M.A. 2012. Satellite cells, the engines of muscle repair. *Nat Rev Mol Cell Biol.* **13**(2), pp.127-133.

Watanabe, K., Ueno, M., Kamiya, D., Nishiyama, A., Matsumura, M., Wataya, T., Takahashi, J.B., Nishikawa, S., Nishikawa, S.-i., Muguruma, K. and Sasai, Y. 2007a. A ROCK inhibitor permits survival of dissociated human embryonic stem cells. *Nature Biotechnology.* **25**(6), pp.681-686.

Watanabe, S., Kondo, S., Hayasaka, M. and Hanaoka, K. 2007b. Functional analysis of homeodomain-containing TF Lbx1 in satellite cells of mouse skeletal muscle. *Journal of Cell Science.* **120**(23), pp.4178-4187.

Webster, M.T. and Fan, C. 2014. c-MET Regulates Myoblast Motility and Myocyte Fusion during Adult Skeletal Muscle Regeneration. *Molecular Biology of the Cell.* **25**.

Wells, L., Vosseller, K. and Hart, G.W. 2001. Glycosylation of nucleocytoplasmic proteins: Signal transduction and O-GlcNAc. *Science.* **291**(5512), pp.2376-2378.

Wernig, A., Irintchev, A., Hartling, A., Stephan, G., Zimmermann, K. and Starzinskipowitz, A. 1991. Formation of new muscle-fibers and tumors after injection of cultured myogenic cells. *Journal of Neurocytology.* **20**(12), pp.982-997.

White, R.B., Bierinx, A.S., Gnocchi, V.F. and Zammit, P.S. 2010. Dynamics of muscle fibre growth during postnatal mouse development. *Bmc Developmental Biology.* **10**.

Wilkin, M., Tongngok, P., Gensch, N., Clemence, S., Motoki, M., Yamada, K., Hori, K., Taniguchi-Kanai, M., Franklin, E., Matsuno, K. and Baron, M. 2008. Drosophila HOPS and AP-3 Complex Genes Are Required for a Deltex-Regulated Activation of Notch in the Endosomal Trafficking Pathway. *Developmental Cell.* **15**(5), pp.762-772.

Wobus, M., Vogel, B., Schmucking, E., Hamann, J. and Aust, G. 2004. N-glycosylation of CD97 within the EGF domains is crucial for epitope accessibility in normal and malignant cells as well as CD55 ligand binding. *International Journal of Cancer.* **112**(5), pp.815-822.

Wouters, M.A., Rigoutsos, I., Chu, C.K., Feng, L.L., Sparrow, D.B. and Dunwoodie, S.L. 2005. Evolution of distinct EGF domains with specific functions. *Protein Sci.* **14**(4), pp.1091-1103.

Wozniak, A.C. and Anderson, J.E. 2007. Nitric oxide-dependence of satellite stem cell activation and quiescence on normal skeletal muscle fibers. *Developmental Dynamics.* **236**(1), pp.240-250.

Wu, H.H., Bellmunt, E., Scheib, J.L., Venegas, V., Burkert, C., Reichardt, L.F., Zhou, Z., Farinas, I. and Carter, B.D. 2009. Glial precursors clear sensory neuron corpses during development via Jedi-1, an engulfment receptor. *Nat Neurosci.* **12**(12), pp.1534-1541.

Xia, B., Hoyte, K., Kammesheidt, A., Deerinck, T., Ellisman, M. and Martin, P.T. 2002. Overexpression of the CT GalNAc transferase in skeletal muscle alters myofiber growth, neuromuscular structure, and laminin expression. *Developmental Biology.* **242**(1), pp.58-73.

Xiao, T., Takagi, J., Coller, B.S., Wang, J.H. and Springer, T.A. 2004. Structural basis for allostery in integrins and binding to fibrinogen-mimetic therapeutics. *Nature.* **432**(7013), pp.59-67.

Yaffe, D. and Saxel, O. 1977. Serial passing and differentiation of myogenic cells isolated from dystrophic mouse muscle. *Nature.* **270**(5639), pp.725-727.

Yamamoto, S., Charng, W.-L. and Bellen, H.J. 2010. Endocytosis and intracellular trafficking of notch and its ligands. In: Kopan, R. ed. *Notch Signaling.* pp.165-200.

Yin, J., Li, G., Ren, X. and Herrler, G. 2007. Select what you need: A comparative evaluation of the advantages and limitations of frequently used expression systems for foreign genes. *Journal of Biotechnology.* **127**(3), pp.335-347.

Yu, S.F. and Baylies, M.K. 2013. Death brings new life to muscle. *Nature.* **497**(7448), pp.196-197.

Zammit, P.S., Partridge, T.A. and Yablonka-Reuveni, Z. 2006. The skeletal muscle satellite cell: the stem cell that came in from the cold. *J Histochem Cytochem.* **54**(11), pp.1177-1191.

Zhang, L.H., Wang, X., Stoltenberg, M., Danscher, G., Huang, L. and Wang, Z.Y. 2008. Abundant expression of zinc transporters in the amyloid plaques of Alzheimer's disease brain. *Brain Res Bull.* **77**(1), pp.55-60.

Zhang, Y.M. and Bergelson, J.M. 2005. Adenovirus receptors. *Journal of Virology.* **79**(19), pp.12125-12131.

Zhou, M.M., Ravichandran, K.S., Olejniczak, E.T., Petros, A.M., Meadows, R.P., Sattler, M., Harlan, J.E., Wade, W.S., Burakoff, S.J. and Fesik,

S.W. 1995. Structure and ligand recognition of the phosphotyrosine binding domain of shc. *Nature.* **378**(6557), pp.584-592.

Zhou, Z., Hartwieg, E. and Horvitz, H.R. 2001. CED-1 is a transmembrane receptor that mediates cell corpse engulfment in C. elegans. *Cell.* **104**(1), pp.43-56.

Ziegenfuss, J.S., Biswas, R., Avery, M.A., Hong, K., Sheehan, A.E., Yeung, Y.-G., Stanley, E.R. and Freeman, M.R. 2008. Draper-dependent glial phagocytic activity is mediated by Src and Syk family kinase signalling. *Nature.* **453**(7197), pp.935-U968.